Title

THE GECMETRY AND ELECTRONIC STRUCTURE OF BIOLOGICALLY SIGNIFICANT MOLECULES AS OBSERVED BY NATURAL MAGNETIC OPTICAL ACTIVITY: I. PROTEIN CONFORMATION AND PLASTICITY, II. CHLOROPHYLL-CHLOROPHYLL INTERACTIONS, III. ELECTRONIC STRUCTURE OF METAL PORPHYR...

Author

Dratz, Edward Alexander.

Publication Date

1966-09-01

UCRL-17200

C.2

University of California

Ernest O. Lawrence Radiation Laboratory

THE GEOMETRY AND ELECTRONIC STRUCTURE OF BIOLOGICALLY SIGNIFICANT MOLECULES AS OBSERVED BY NATURAL AND MAGNETIC OPTICAL ACTIVITY:

I. Protein Conformation and Plasticity
II. Chlorophyll-Chlorophyll Interactions
III. Electronic Structure of Metal Porphyrins

Berkeley, California

DISCLAIMER

Research and Development

UCRL-17200

UNIVERSITY OF CALIFORNIA

Lawrence Radiation Laboratory
Berkeley, California

AEC Contract No. W-7405-eng-48

THE GEOMETRY AND ELECTRONIC STRUCTURE OF BIOLOGICALLY SIGNIFICANT MOLECULES AS OBSERVED BY NATURAL AND MAGNETIC OPTICAL ACTIVITY:

I I. Protein Conformation and Plasticity
II. Chlorophyll-Chlorophyll Interactions
III. Electronic Structure of Metal Porphyrins

Edward Alexander Dratz
(Ph.D. Thesis)
September 1966

THE GEOMETRY AND ELECTRONIC STRUCTURE OF BIOLOGICALLY SIGNIFICANT MOLECULES AS OBSERVED BY NATURAL AND MAGNETIC OPTICAL ACTIVITY:

I. PROTEIN CONFORMATION AND PLASTICITY

II. CHLOROPHYLL-CHLOROPHYLL INTERACTIONS

III. ELECTRONIC STRUCTURE OF METAL PORPHYRINS

Edward Alexander Dratz

Department of Chemistry
University of California
Berkeley, California

ABSTRACT

Differences in the ultraviolet optical rotatory dispersion of the allosteric enzyme aspartate transcarbamylase, produced by effectors which alter its catalytic activity, appear to reflect structural changes in the protein. These alterations of catalytic activity in response to the effectors, substrates and inhibitors, serve an important metabolic control function in the cell. The conformational changes we have detected seem to be related to the operation of the control function and may be important for an understanding of the mechanism of activity control in this enzyme. The observed changes are small but significant and can be interpreted as a 5% decrease in helix content upon maximal activation of the enzyme by substrate.

No substrate or inhibitor induced structural modifications were detected in deoxycytidine monophosphate deaminase or in carboxydismutase. By the criteria of our measurements, the oxidized and the reduced forms of cerruloplasmin have identical conformation.

The state of aggregation of chlorophylls in solution, in crystals and in photosynthetic particles is discussed in Chapter II. Evidence derived from circular dichroism (CD) and absorption spectra is used to propose a structure for the dimer of chlorophyll formed in nonbasic organic solvents. Chlorophyll a, chlorophyll b and bacteriochlorophyll *in vitro* appear to form dimers of similar structure under the conditions investigated. Aggregated chlorophyll exhibits a characteristically shaped, double CD spectrum in the long wavelength absorption band. The CD spectra of photosynthetic membrane fractions isolated from higher plants and photosynthetic bacteria suggest that some of the *in vivo* chlorophyll is aggregated. Investigations of membrane lamellae isolated from a mutant barley which contains no chlorophyll b reveal that chlorophyll a - chlorophyll a interactions are essentially independent of the presence of chlorophyll b, and that chlorophyll b - chlorophyll b interactions are present in the lamellae of normal barley.

The CD spectrometer constructed for these measurements is described. The range of the instrument extends from 220 millimicrons to 1200 millimicrons. Multiple spectrum averaging increases the ultimate sensitivity of CD measurements to 10^{-6} optical density units.

A study of the magnetic circular dichroism (MCD) of porphyrins is presented in Chapter III. The physical basis of MCD is explained by a simple classical derivation. A semiclassical two-state model is developed to describe MCD quantitatively and to treat the influence of electron spin. The polarization of the electronic transitions in metal free protoporphyrin are assigned from the MCD spectrum. The MCD and absorption properties of zinc(II) porphyrins approach those expected for a free

electron in a circular box. The magnetic field splits orbitally degenerate porphyrin excited states: For the zinc porphyrins, an orbital angular momentum of 6.5 is found in the lowest energy absorption band and 0.8 in the Soret band, whereas 9 and 1 are predicted by the free electron model. There is a more pronounced departure from the free electron model for other transition metal porphyrins. The orbital angular momenta of the lowest energy bands are: copper(II), 6.0; silver(II), 5.3; nickel(II), 4.7; cobalt(II), 4.6 and iron(II), 4.0. A detailed interpretation of the metal porphyrin MCD is accomplished by the use of molecular orbital theory. MCD experiments on iron porphyrins and heme proteins indicate that the magnetic orbital splitting is sensitive to ligand coordination above and below the iron porphyrin plane.

A brief evaluation of the possible future usefulness of MCD in chemistry and biology is included.

FOREWORD

The first shots have been fired in the revolution that is encompassing modern biology. Information on the structure and function of cell components is becoming available which indicates that the cell can be explained entirely in chemical and physical terms — the vitalists are retreating. The broad outlines of the DNA-RNA-protein mechanism of cellular information storage and retrieval seem well established. However, it is obvious that there are numerous unsolved or untouched problems in every area of biology. A few outstanding examples of these problems are: the control of metabolism, the mechanism of differentiation, membrane phenomena, learning, memory, the immune reaction, the light reactions in photosynthesis and vision.

Clearly, one of the future directions for chemistry lies in attempts at achieving a molecular understanding of these biological problems. The chemist who is so bold as to study such complex biological systems can proceed in one of two ways. He can, through cell fractionation, break a complex cellular system into simpler parts (physically or by specific inhibition). Or, by building simple model systems, he can attempt to mimic interactions present in the cell.

The study of the structure of the results of cell fractionation or model building can be approached with the help of certain types of physical tools. These physical tools fall into three general

types: scattering, hydrodynamic and spectroscopic methods.

Scattering methods, such as x-ray diffraction of electron microscopy, require solid samples in nonphysiological conditions. Despite this disadvantage, scattering methods have been responsible for much of the hard information that we now have about the cell and cell components. Some outstanding examples are the x-ray structures of DNA (Watson, Crick, 19533) and of myoglobin (e.g. Kendrew, 1962). The detailed pictures that result from these techniques will undoubtedly continue to add immeasurably to the study of cell components.

Hydrodynamic methods, such as sedimentation and diffusion, can proceed under more physiological conditions and are sensitive to gross shape, size and density of molecules and cell particles. A proof of the semiconservative replication of DNA (Meselson and Stahl, 1958) is an example of the important results that have come from sedimentation methods. Hydrodynamic methods, together with chromatography, are the basic separation tools used in cell fractionation.

Spectroscopic methods measure absorption, emission and refraction of light (where light is taken to mean electromagnetic radiation from radio waves to x-rays). Generally, these measurements can be done in solution reasonably close to physiological conditions. Spectroscopic methods tend to be sensitive to short range interactions, such as nearest neighbor interactions in polymers.

Spectroscopic methods usually are more difficult to understand intuitively or to interpret quantitatively than scattering or hydro-

dynamics. The spectroscopic phenomena are basically quantum mechanical in nature while scattering and hydrodynamic phenomena are classical. The theoretical groundwork for interpreting the spectroscopic properties of large molecules is only partially developed. However, in most cases, the theoretical basis is sound enough to serve as a guide to an empirical approach. Spectroscopic methods have a tremendous untapped potential and are affording more and more detailed structural information on materials in solution (e.g. Cantor, 1966).

The chemist studying a complex biological structure must use any and all of the tools mentioned above when they are helpful. Each general class of tools requires certain special knowledge and experience, and it is a rare individual who is truly expert in all. We have chosen to concentrate on the spectroscopic approach to the study of materials extracted from the cell (Chapters I and II) and to study models of biological materials (Chapters II and III).

REFERENCES

Cantor, C. R. (1966). PhD. Thesis, University of California, Berkeley. University of California Lawrence Radiation Laboratory Report 16701.

Kendrew, J. C. (1962). Brookhaven Symposium in Biology, 15, 216-228.

Meselson, M. and F. W. Stahl (1958). Proc. Nat. Acad. Sci. 44, 671.

Watson, J. D. and F.H.C. Crick (1953). Cold Spring Harb. Symp. in Quant. Biol. 18, 123-131.

ACKNOWLEDGEMENTS

The experiments and the interpretation of same described in this thesis were aided immeasurably by the contributions of many people. Some of the most prominent contributors are acknowledged below, but many shall remain nameless.

Professor Melvin Calvin, as my research director, has made this work possible. Initially his boundless enthusiasm instilled interest in me for the physical approach to the study of biology, and later his wide knowledge and critical insight were extremely helpful. Professor Calvin provides a uniquely stimulating laboratory where one is exposed to all things biological.

Dr. M. Klein for imparting to me a wealth of knowledge of every sort, and for a very beautiful, enthusiastic view of inventive scientific work.

Professor M. Gouterman for numerous long and helpful discussions. Professor Gouterman's ideas are the basis for the detailed understanding of much of the porphyrin work, and his assistance with the classical derivation of magnetic circular dichroism is greatfully acknowledged.

Professor K. Sauer who workedvery closely on all phases of the chlorophyll problem. Mr. R. Thompson for extensive instrumental development and construction assistance. Mr. G. Litton who wrote or helped to debug most of the computer programs used herein. Dr. R. Biltonen for discussions of curve fitting, exciton calculations and a general

critical view. Dr. J. Thorne, an inventive and industrious colleague. Miss C. Miller for technical assistance.

Mrs. Evie Litton who prepared nearly all of the drawings for this thesis and Mrs. Jo Onffroy who typed the final draft. My wife, Peggy, who typed several drafts, attempted to teach me some grammar, spelling and punctuation, and struggled to keep scientific work in perspective.

TABLE OF CONTENTS

INTRODUCTION

This thesis describes experiments using absorption and refraction of light to study some aspects of biological structure and function. More particularly, we place emphasis on optical activity techniques.

Louis Pasteur first realized that biological specificity resides at the same level of molecular structure which gives rise to rotation of plane polarized light. Pasteur found that certain substances could exist in isomeric forms that differed only in their effect on polarized light and were indistinguishable in chemical composition and other physical properties. Some isomers rotated polarized light to the right, some to the left, and some rotated not at all. Synthetic organic chemicals were formed as a mixture of these isomers and had no optical activity while the natural products were usually formed as a single isomer. Pasteur found that molecules had a three-dimensional structure and that the optically active isomers were nonsuperimposable mirror images of one another:

> "All artificial products of the laboratory . . . . and all mineral species are superposable on their images. On the other hand, most natural organic products . . . . the essential products of life, are dissymmetric in such a way that their images cannot be superposed upon them."
>
> (Louis Pasteur, Alembic Club Reprint, 14, 41, 1860)

One of Pasteur's most striking experiments on the biological implications of molecular dissymmetry was the fermentation of a mixture of left and right tartrate with yeast. The yeast ate only the right-handed tartrate and growth stopped when the right tartrate was depleted, leaving a solution of the left tartrate.

Pasteur's molecular dissymmetry work laid the foundation for stereochemistry—the concept and study of the three-dimensional structure of molecules. Le Bel and van't Hoff soon proposed (1874) the tetrahedral carbon atom on the basis of optical activity considerations. Werner's brilliant work on the stereochemistry of metal complexes was not widely accepted until optically active complexes were predicted and prepared (Werner, 1912). However, after this spectacular beginning, optical activity methods fell into disuse except in the field of sugar chemistry.

One other major contribution to the beginnings of optical activity research was the work of Cotton (1896), who anticipated the close relationship between absorption and optical activity. Cotton observed a change of sign in rotation at the absorption peak of certain compounds and discovered the phenomena of circular dichroism (the differential absorption of left and right circular light) in the absorption region of the same compounds. Both of these phenomena, circular dichroism and the change in sign of rotation at an absorption peak, have been called "Cotton effects." Optical activity measurements in absorption regions are relatively difficult and were not pursued experimentally to any great extent until quite recently. Now, measurements in absorption regions are the basis of optical activity research and are largely responsible for the rebirth of optical activity as a useful tool (Djerassi, 1960; Mason, 1963; Velluz, Legrand and Grosjean, 1965). The early work briefly described above is very beautifully and thoroughly recounted by Lowry (1964).

Most cell components are found to exhibit optical activity. Progress in biochemistry has brought us new isolation procedures for complex,

sensitive biological molecules and particles. And the availability of relatively pure cell components has in turn made a detailed attack on the challenging problems of biological structure and function possible. Optical activity methods are taking an increasingly larger role in the study of the conformation of proteins (e.g., Urnes and Doty, 1961), nucleic acids (e.g., Cantor, 1966) and metal complexes (e.g., Mason, 1963).

In Chapter I we present a study of model polypeptides and isolated proteins with respect to the importance of protein flexibility in catalytic activity and metabolic control. Chapter II is a study of the state of aggregation of chlorophyll in solution and in isolated photosynthetic particles. This chapter also includes a detailed discussion of the instrumentation required for circular dichroism measurements.

The basic requirement for optical activity is that the molecule or aggregate of symmetrical molecules have no point or plane of symmetry. Unsymmetrically substituted tetrahedral carbon, a helix of one sense, a symmetric chromophore in an asymmetric field, are examples of optically active structures. A relatively small class of asymmetric compounds can be studied by conventional optical activity methods. However, it has been known since Faraday that a magnetic field induces optical activity in all matter. Chapter III attempts to determine whether useful structural information can be found by the study of magnetic optical activity. The problem is treated on a simplified theoretical basis and magnetic circular dichroism experiments are presented with particular emphasis on the study of metal porphyrin spectra.

REFERENCES

Cotton, M. , Ann. de Chimie et de Physique 8, 347 (1896).

Djerassi, C. (1960), Optical Rotatory Dispersion (McGraw-Hill Co., N. Y.).

Lowry, T. M. (1935), Optical Rotatory Power (Longmans, Green and Co., London), or (1964), Optical Rotatory Power (Dover Publications, Inc., N. Y.).

Mason, S. F., Quarterly Reviews (London) 17, 20 (1963).

Urnes, P., and P. Doty, Adv. Protein Chem. 16, 401 (1961)..

Velluz, L., M. Legrand and M. Grosjean (1965), Optical Circular Dichroism (Academic Press, Inc., N. Y.).

Werner, A., Bull. Soc. Chem. IV, 1, (1912).

I. PROTEIN CONFORMATION AND PLASTICITY

A. Introduction

The thermodynamic hypothesis that the three-dimensional structure of a protein is determined by the amino acid sequence seems well established (Epstein, Goldberger and Anfinsen, 1963; Whitney and Tanford, 1965; Schachman, 1963). The particular configuration that a protein assumes appears to be the configuration that is thermodynamically the most stable. However, the thermodynamic hypothesis does not exclude the possibility that there may be many three-dimensional forms of a protein which differ only slightly in free energy. Within thermodynamic and energetic limitations, a protein may have considerable freedom to reversibly deform into many configurations under the influence of slight environmental changes.

In recent years several workers have proposed that proteins do not function as envisioned by the classic rigid template (lock and key) model of Fischer, and that protein plasticity may be important for biological activity. The concept of protein "configurational adaptability" was proposed by Karush, in 1950, to explain the binding of small molecules by serum albumin. In the presence of a specific small molecule, a particular conformation of the protein was assumed to be stabilized by virtue of the interaction between the bound molecule and certain groups on the protein. Koshland (1958) proposed protein plasticity as an explanation for anomalous kinetic and binding data found with certain enzymes. This "induced fit" of the substrate into the protein might be useful, Koshland suggested, if the binding groups were initially on the "outside" of the protein and accessible to the environment, and that upon binding of small

molecules the protein refolded, protecting reactive intermediates in the enzyme reaction from the environment (Koshland, 1962).

It was first observed in studies of hemoglobin that the binding of a ligand at one site affected the ligand binding at other sites (Wyman, 1948). And the idea that the binding site interaction was mediated by a protein conformational change was proposed (Wyman and Allen, 1951). Recently, many other proteins have been shown to exhibit binding site interactions of a similar type and Monod has generalized these observations in the concept of the "allosteric protein" (Monod, Changeux and Jacob, 1963). In this view, the binding of a ligand brings about a protein conformational change which leads to altered chemical properties (ligand affinity, catalytic activity). Feedback inhibition (Umbarger, 1956; Yates and Pardee, 1956), which occurs when the first enzyme of a biosynthetic pathway is inhibited by the ultimate product of the pathway, is explained quite nicely by the allosteric protein concept. The unique kinetic behavior of feedback inhibited enzymes, the observation that the control function could be impaired without loss of catalytic activity, and the fact that the inhibitors were often sterically quite different than the substrate (e.g., Gerhart and Pardee, 1963), suggests that a protein conformational change mediates the substrate-inhibitor site interactions (Monod, Wyman and Changeux, 1965).

The substantial number of enzymes which have clearly been shown to have feedback inhibition and acceleration properties seem to be largely responsible for the short term control of cell metabolism, catabolism and synthetic reactions (Atkinson, 1965; Monod, Wyman and Changeux, 1965). The allosteric protein has also been implicated in the control of genetic

transcription (Lwoff, 1966). The repressors controlling induced enzyme synthesis, that are supposed to be responsible for long term control of the cell, have many of the characteristics ascribed to an allosteric enzyme. Obviously, the concept of the allosteric enzyme is very important and the detailed mechanism of its control operation deserves further study.

The theory of the flexibility of the allosteric enzyme is based largely on kinetic and other indirect evidence. Further, the majority of enzymes do not show multiple site interactions, but may possess "induced fit" types of plasticity. The goal of this work was to seek some direct physical changes in peptide structural interactions which were correlated with changes in catalytic activity and substrate binding. The first requirement of this work was to do these investigations on dilute water solutions under conditions where subtle effects of environment could be varied easily. Optical rotatory dispersion (ORD) studies of polypeptides and proteins have been shown to be sensitive to the conformation of polypeptide chains (Urnes and Doty, 1961). ORD work can proceed in dilute solution and seemed the method of choice for these studies.

Visible and near ultraviolet ORD studies of polypeptides, reviewed by Urnes and Doty (1961), indicate that the ORD depends primarily on peptide conformation and is largely independent of amino acid side chain constitution, except for the steric limitations presented by some side chains (Blout, 1962). More recent experimental work of Blout, Schmier and Simmons (1962), Holzwarth and Doty (1965), and theoretical work of Woody (1962) and Schellman and Oriel (1962), have put the understanding

of polypeptide and protein optical activity on comparatively firm empirical and theoretical ground. With this encouragement, we may proceed with some care to use ORD to investigate plasticity in protein structure.

One main limitation of this work was the rather strict requirements of enzyme purity and stability. Crude homogenates or partially purified enzymes suffice for kinetic studies but are not suitable for optical work. At the time this investigation was done, there was really only one allosteric enzyme with sufficient purity for study. We were able to obtain some of this material, aspartate transcarbamylase (Gerhart and Pardee, 1963).

We also attempted experiments with deoxycytidine monophosphate deaminase, which shows some spectacular kinetic effects (Scarano, Geraci, Polzella and Campanile, 1963), but it was too impure and unstable in our hands for reliable study by these methods. We studied carboxydismutase, a multisubstrate enzyme that was available in a high state of purity (Trown, 1965). The kinetics of carboxydismutase seemed quite normal, and we wanted to investigate the possibility of induced fit effects in this case. The copper transport protein, cerruloplasmin, was studied because of independent physical evidence that it changed its conformation when the copper was reduced (Blumberg, Eisinger, Aisen, Morell and Scheinberg, 1963).

Physical changes induced in aspartate transcarbamylase by allosteric inhibitor and substrate are considered first in some detail. Next, we treat more briefly the other proteins in which no positive effects on conformation alteration were found.

B. Aspartate Transcarbamylase

Enzyme properties

Aspartate transcarbamylase (ATCase) (Gerhart and Pardee, 1963) is the first enzyme in the pyrimidine biosynthetic pathway and is one of the best characterized examples of an allosteric enzyme. Aspartic acid and carbamyl phosphate are coupled by ATCase to form carbamylaspartate, which is transformed by a series of enzymatic reactions to the pyrimidine nucleotides, uridine triphopshate (UTP) and cytidine triphosphate (CTP). As first shown by Yates and Pardee (1956), cytidine derivatives exert a regulatory influence upon the activity of the enzyme in whole cells and in cell extracts. Kinetic measurements on purified ATCase show that CTP binds reversibly at a site distinct from the catalytic site, and inhibits the enzyme by reducing its affinity for the substrate aspartate (Gerhart and Pardee, 1963). The level of the ultimate product, CTP, is controlled by feedback inhibition of ATCase.

At pH's lower than 6.1 ATCase shows a normal hyperbolic dependence of reaction velocity on substrate concentration (Figure I-1a). However, ATCase has a sigmoidal substrate saturation curve for aspartate at pH's greater than 6.1 (shown in Figure I-1a), indicating a cooperative interaction between catalytic sites—i.e., ATCase increases its aspartate affinity with increasing aspartate concentration. CTP and pH modify the substrate site interaction as evidenced by their effect on the substrate saturation curve of ATCase, shown in Figure I-1a. Cooperative interactions between catalytic sites and the modification of this interaction by CTP are examples of indirect interactions between binding sites that are characteristic of allosteric enzymes (Monod, Wyman, and Changeux, 1965). It is quite striking that the cooperative substrate site

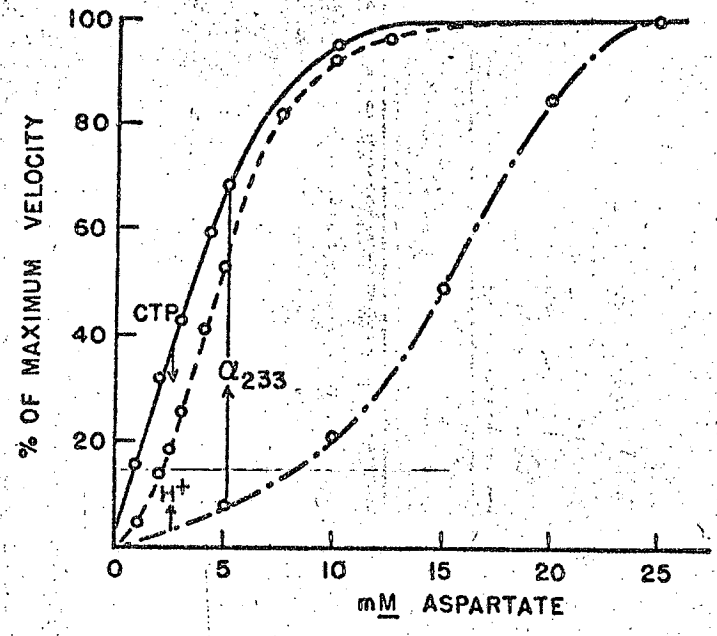
100
80
60
40
20
% OF MAXIMUM VELOCITY
CTP
α_{233}
H^+
0
5
10
15
20
25
mM ASPARTATE

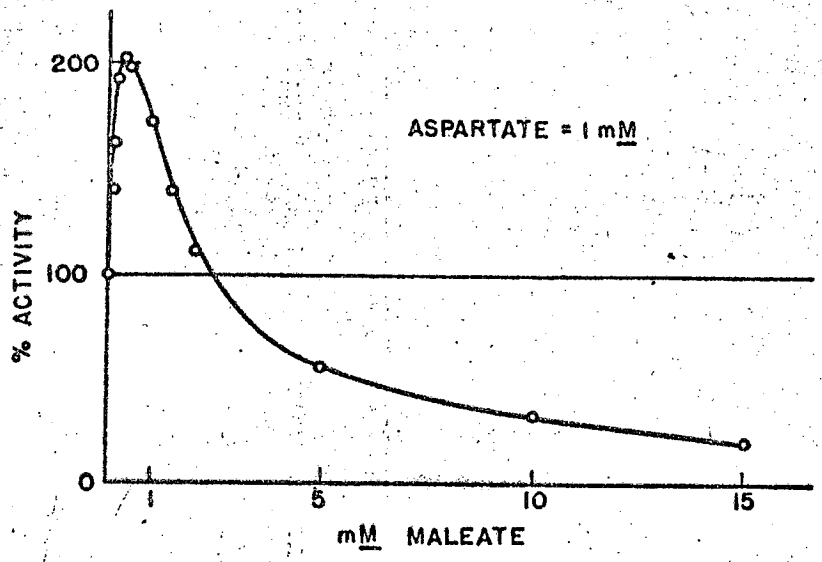
200
100
0
% ACTIVITY
ASPARTATE = 1 mM
1
5
10
15
mM MALEATE

MUB-6086

Figure I-1a. The effect of CTP and pH on the reaction velocity substrate dependence of ATCase. 3.6 mM carbamyl phosphate and 40 mM buffer present in all samples. pH 6.1, ———; pH 7 or pH 6.1 plus 2.10^{-4} M CTP, - - - -; pH 8.6 __ . __ . . All of the curves (except the pH 6.1 plus the 2.10^{-4} M CTP curve) are taken from Gerhart and Pardee (1963). The arrows on the graph are explained in the text.

Figure I-1b. The effect of the substrate analog, maleate, on the reaction velocity of ATCase. 1 mM aspartate, 3.6 mM carbamyl phosphate and 40 mM potassium phosphate; pH 7. (Curve taken from Gerhart and Pardee, 1963.).

interaction allows nonreactive substrate analogs that are simple competitive inhibitors at high concentrations to activate the enzyme at low concentrations. Figure I-1b shows the activation of ATCase by a nonreactive substrate analog at low concentrations and the competitive inhibition at high concentrations. Several substrate analogs show this effect.

The kinetic effects, in summary, are as follows: CTP promotes a decrease in ATCase's affinity for aspartate while substrates, substrate analogs, and protons increase enzyme affinity for aspartate. At a given aspartate concentration, the aspartate affinity of the enzyme determines the catalytic activity (reaction velocity) of ATCase. The activity changes at a fixed aspartate concentration are represented in Figure I-1a by the arrows showing the direction of the activity shift upon addition of CTP and H^+.

Materials and methods

All chemicals were obtained commercially. The sodium salt of poly-L-glutamic acid, supplied by Mann Research, Inc., had an average degree of polymerization of about 180, estimated by the intrinsic viscosity in 0.1 M NaCl. The poly-L-glutamic acid concentration was estimated from the dry weight, assuming one water of hydration per residue. ATCase was a gift from Dr. John Gerhart. The enzyme assay (Gerhart and Pardee, 1962) and method of preparation (Gerhart and Schachman, 1965) were previously described. All enzyme solutions contained 2 mM mercaptoethanol and 0.2 mM EDTA. Potassium phosphate was used for the pH 7.0 and pH 6.1 buffers, while Tris HCl was used for pH 8.6. The buffers were 40 mM for the kinetic measurements and 4 mM for the optical measurements below 240 mμ. The enzyme concentrations were determined from the absorption

at 279 mμ, using $A^{1\ cm}_{1\ mg/ml} = 0.59$. The average residue weight ($\bar{M}$) of ATCase was estimated, from a preliminary amino acid analysis (Gerhart and Schachman, 1965b) to be 120.

Optical rotatory dispersion measurements utilized a Cary Model 60 recording spectropolarimeter. The rotations were independent of slit width and the specific rotations were independent of the (concentration) (Path length) product over a ten-fold range. Lamp position adjustment and slit width adjustment were made for minimum noise level at the wavelength region of interest. When the Cary 60 spectropolarimeter is properly adjusted and warmed up, the limiting factor in reliable observation of small rotatory effects is usually cell quality and cleanness. The cells made by Pyrocell, Inc., were selected for minimum birefringence and were cleaned inside and out by soaking in concentrated HNO_3-H_2SO_4 (50/50 by volume) and by a one-minute exposure to MeOH-3 M KOH (50/50 by volume). When properly cleaned, the cells could be removed and replaced in the polarimeter with no observable change in the rotation (< 0.3 millidegree at most wavelengths of interest). Cells of 0.1, 1.0 and 10 mm pathlength were used.

All measurements were performed at 4.5 ± 1.0°C to retard the decomposition of carbamyl phosphate. A special thermostated cell holder was built for the Cary 60. Copies of this very simple device have successfully been used in several laboratories because it affords satisfactory temperature control and excellent reproducibility in cell positioning. An aluminum block is bored with a 22 mm hole along the light path and reamed to smoothly accept standard 22 mm O.D. cells of up to 10 cm pathlength. Water channels are drilled in such a way that the water passes

completely around the sample well 3-5 times. The details of these channels are not critical. Three rounded feet fit into the kinematic mounting points on the Cary 60 when the sample elevator is lowered. A water-antifreeze mixture is circulated through the water channels from a refrigerated bath at about o°C, and the sample temperature is measured in the solution with a glass covered thermocouple. The thermocouple wires pass out through a Bendix connector in the top of the sample elevator.

The specific rotation measurements for different samples at the same solution conditions varied 1 to 2% due to volumetric errors in sample preparation. This variation of specific rotation from sample to sample was too large to permit a satisfactory determination of the absolute specific rotations of the enzyme in the presence and absence of effectors. However, we could determine the relative rotation in the presence and absence of effector by a titration method. For the titration experiments, 2 to 3 ml of enzyme solution was pipetted into a 0.1 or 1.0 mm cell and the ORD spectrum measured. Five to 20-lambda aliquots of concentrated effector solutions, previously adjusted to the appropriate pH, were added with a micropipet. The enzyme solution was mixed by slow inversion of the cell and the ORD spectrum measured. Corrections for dilution and CTP rotation were applied. The magnitude of rotation at selected wavelengths was most precisely determined by chart recording of the rotation at each fixed wavelength for extended periods (ca. 10 min) with a 10 or 30-second pen time constant. After running a spectrum the peak and trough wavelength points were repeated and the rotations were unchanged within the noise level in all cases. The specific residue

rotation (R') was calculated according to the relation:

$$(R') = \frac{3}{n^2 + 2} \quad \frac{\alpha(\lambda)}{l\ c} \quad \frac{\bar{M}}{100}$$, where

$\alpha(\lambda)$ = observed rotation in degrees, l = pathlength in decimeters, c = concentration in grams/ml, $\bar{M}$ = average residue weight, and n = refractive index of the solution at wavelength of measurement. The refractive index of water at 231 mμ (International Critical Tables, 1930) and 20°C was used for all wavelengths. The Lorentz factor, $3/(n^2 + 2)$, for H_2O at 231 mμ is 0.7635.

Absorption measurements utilized a N_2-purged Cary Model 15 spectrophotometer. Absorption spectra were taken relative to a buffer solution of identical concentration. The phosphate buffer used for the far UV absorption measurements had a maximum absorption of one at 180 mμ in a 0.1 mm cell.

Helix content of ATCase

ORD has been shown to be sensitive to protein and polypeptide secondary structure (Urnes and Doty, 1961). Helices, coils (Blout, Schmier and Simmons, 1962) and β linkages (Iizuka and Yang, 1966) give distinct dispersion curves in the region of peptide bond absorption from 180-240 mμ. At the present time ORD is largely an empirical tool, and simple polypeptides of known conformations are used as models to compare to proteins of unknown conformation.

Figure I-2a shows the ORD of poly-L-glutamic acid (PLGA) in the helical and coil conformations in the region of peptide bond absorption. The ORD spectra are strikingly different. At low pH ($\lesssim$ 4.5) the carboxylate groups on the glutamic acid side chains are largely uncharged and the helix form is stable (Urnes and Doty, 1961). At higher pH, the

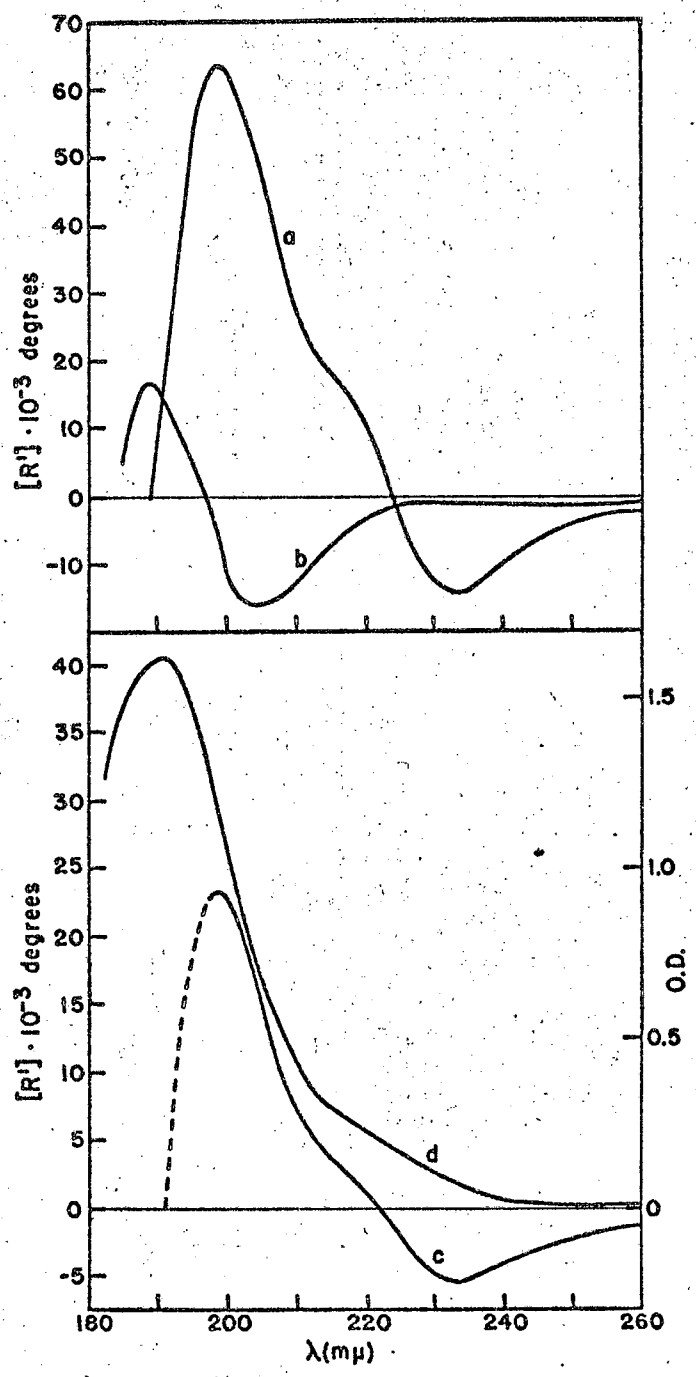
70
60
50
40
30
20
10
0
-10
[R'] · 10⁻³ degrees
a
b
40
35
30
25
20
15
10
5
0
-5
1.5
1.0
0.5
0
O.D.
d
c
180
200
220
240
260
λ(mμ)

MUB-6088

Figure I-2. Optical rotatory dispersion (ORD) and absorption.

a) ORD of Poly-L-Glutamic Acid, pH 4.3, helix form (no added salt).

b) ORD of Poly-L-Glutamic Acid, pH 7, random coil form.

c) ORD of ATCase, pH 6.1; the average residue weight is taken as 120 g/mole. The dotted portion of the curve is in a region of very high noise level and is much less reliable than the other data.

d) Absorption of ATCase, 2.08 mg/ml, pH 6.1 in a 0.1 mm cell measured vs. buffer.

carboxylate groups on the glutamic acid side chains become negatively charged and the charge repulsions break the helix and form a coil. Similar PLGA ORD curves, differing slightly in magnitude, have previously been published by other workers (Blout, et al., 1962).

Figure 2c shows the UV ORD of ATCase. The spectrum is very similar in shape to that of helical PLGA, but the magnitude/residue is much smaller. The ORD curve of ATCase is fit very well with about 37% of the PLGA helix specific residue rotation with no contribution from the nonhelical residues. Figure I-3 shows a plot comparing the ORD of ATCase with 0.37 times the PLGA specific residue rotation. The only appreciable deviation between the two curves is in the region between 225 and 205 mu. This small deviation is thought to be due to an almost complete cancellation of opposing contributions of the Cotton effects of the various nonhelical residues. Some nonhelical residues may contribute positive rotation and others negative rotation, leading to a cancellation. Unfortunately, there is almost no data on the UV ORD of uncharged peptide derivatives. Amino acid derivatives like:

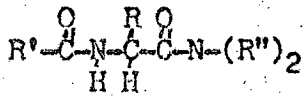

(where R is the amino acid side chain and R" and R' are methyl groups or derivatives of methyl groups that enhance water solubility) would be useful models for nonhelical amino acids in proteins. In a study of the far UV optical activity of myoglobin, using circular dichroism, Holzwarth and Doty (1965) have found a similar cancellation of the contributions of the nonhelical residues. In the case of myoglobin, the circular dichroism can best be fit by 70% model polypeptide helix dichroism with

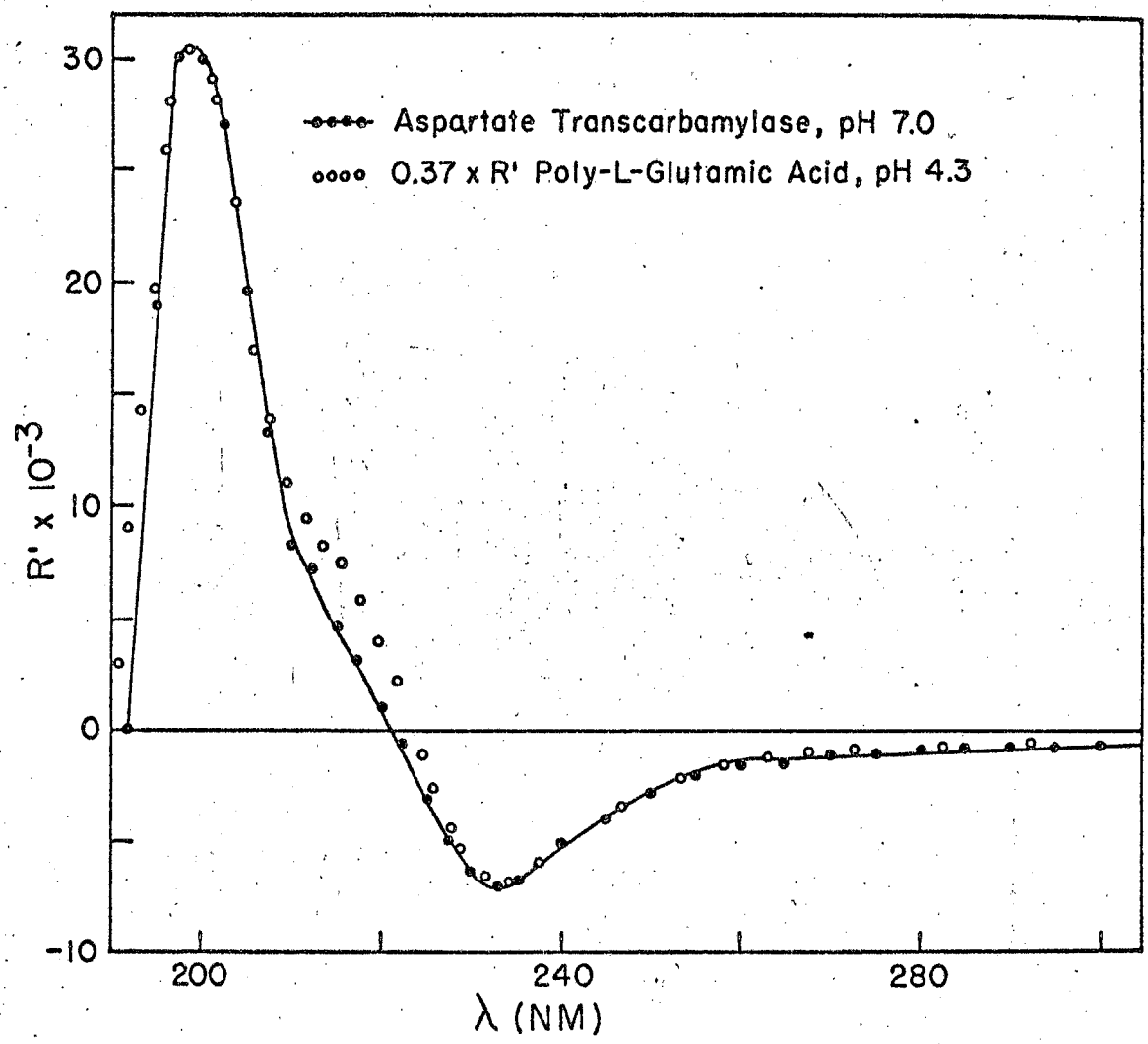

Figure I-3. Comparison of the reduced residue rotation of ATCase with 37% of the reduced residue rotation of helical poly-L-glutamic acid.

no contribution from the nonhelical residues (Holzwarth, 1965). We conclude that, to a first approximation, 37% of the residues of ATCase are in the helical conformation.

Several other methods are available for helix content estimation from ORD data (Schechter, Carva and Blout, 1964; Sogami, Leonard and Foster, 1963). The other treatments of this problem rely on the monotonic visible and near UV data, and we feel that the most reliable method should be the direct observation of the peptide helix Cotton effects as done here. The exact absolute value of helix content of ATCase is not of prime importance in our work, and, furthermore, we did not want to use the large amounts of material required for precise visible measurements. None of the methods of helix content estimation are really satisfactory for proteins with low helix content, since local charge and dipole fields (Tinoco, 1962) from regions of the protein wrapped around the helical segments are not present in the reference polypeptides. It should be mentioned that PLGA may not be the ideal reference material for helix content estimation, and these problems have been discussed by Yang and McCabe (1965).

The helix content of proteins can also be estimated from the hypochromic effect that the helical conformation exerts on the ultraviolet peptide bond absorption (Rosenheck and Doty, 1961). This method agrees well with ORD in the case of simple polypeptides and some proteins. The use of this method for proteins is complicated by the contribution of aromatic amino acid side chains, as well as arginine, methionine, cystine, amide and carboxylate groups, to the absorption in the region of peptide bond absorption. However, this approach is attractive because it requires

very small amounts of material, and we felt that more cases should be tried to fully explore its possible usefulness. The side chain contribution to the absorption of ATCase was estimated from an amino acid analysis (Gerhart and Schachman, 1965b) and the amino acid side chain extinction coefficients given by Rosenheck and Doty (1961). A tabulation of mole fractions of amino acids and their extinction coefficients is given in Table I. The absorption spectrum of ATCase is given in Figure I-2d. The helix content of ATCase was estimated by the peptide hypochromicity to be 95% at 190 mμ, 51% at 197 mμ, and 48% at 205 mμ. The 190 mμ point has the largest relative correction for side chain absorption and is least trustworthy. The 197 mμ point has the smallest relative correction, and Rosenheck and Doty (1961) believe 197 mμ to be the most reliable.

The peptide hypochromicity gives a value of helix content for ATCase larger than that predicted by ORD. If the 190 mμ point is neglected, the peptide bond hypochromism indicates about 50% helix. This is acceptable agreement with the ORD value of 37%. We consider the hypochromism value as the less reliable since the side chain as well as the peptide bond absorption may be considerably perturbed by the environment inside the protein.

Substrate and inhibitor-induced changes in ORD

The entire ORD curve of ATCase changes in magnitude when CTP, substrate analogs, or protons are added to the enzyme. The observed changes are small (about 5-6% maximum) but can be measured over most of the wavelength range of interest. Table II shows the specific rotation per residue of ATCase at the trough of the 233 mμ Cotton effect in the presence of various substances that affect its kinetic behavior. We use

Table I. Peptide bond hypochromicity calculation - ATCase

Correction for ATCase side chain absorption. n_i = moles amino acid/mole protein [$3.1 \cdot 10^5$ g/mole protein assumed from Gerhart and Schachman (1965b)]. χ_i = mole fraction amino acid (2780 amino acids/mole protein). $\varepsilon_i(\lambda)$ = side chain molar extinction coefficient at wavelength indicated, taken from Rosenheck and Doty (1961).

Amino acid (i)	n_i	$\chi_i \cdot 10^2$	$\varepsilon_i(190) \cdot 10^{-3}$	$\chi_i\varepsilon_i(190)$	$\varepsilon_i(197) \cdot 10^{-3}$	$\chi_i\varepsilon_i(197)$	$\varepsilon_i(205 \cdot 10^{-3}$	$\chi_i\varepsilon_i(205)$
phenylalanine	103	3.71	44.	1630.	16.0	594.	9.6	356.
tyrosine	68	2.45	36.	882.	33.0	807.	8.5	208.
tryptophane	17	0.61	17.	104.	20.0	122.	19.5	119.
arginine	141	5.07	12.5	633.	6.0	304.	1.2	608.
amide	314	11.30	6.2	700.	1.4	158.	0.45	50.9
histidine	90	3.24	5.3	172.	3.6	117.	4.20	136.
cystine	26	0.94	2.5	23.	1.5	14.	1.0	9.4
methionine	56	2.02	1.6	32.	1.6	32.	1.6	32.2
carboxylate	301	10.84	0.9	97.5	0.3	32.5	0.1	10.8
$\varepsilon_{\text{side chain}}(\lambda) = \sum_i \chi_i\varepsilon_i$				4274		2181		983
$\varepsilon_{\text{protein/peptide}}$				8640		6940		3450
$\varepsilon_{\text{protein}} - \varepsilon_{\text{side chain}} = \varepsilon_{\text{peptide}}$				4366		4759		2467
$\varepsilon_{\text{peptide}}$ (100% helix)				4100		3200		2000
$\varepsilon_{\text{peptide}}$ (0% helix)				6900		6350		3200
% Helix				90%		50.8%		48.2%

Table II. Values of specific residue rotation of ATCase at 233 mμ in various solutions from a typical experiment. The Δ values are the differences caused by solution alteration. All experiments show the same trends of effector-induced changes in the rotation. The errors shown in the table are the observed noise level in the ORD spectrum.

Sample	$[R']_{233\ m\mu}$		
pH = 6.1	5,240 ± 20	Δ = 90	Δ = 350
pH = 6.1 + 10^{-4} M CTP	5,330 ± 20		
pH = 8.5	5,590 ± 20	Δ = 220	
pH = 8.5 + 5 mM succinate and 3 mM carb. PO_4	5,380 ± 20		

233 mμ is a convenient wavelength for tabulating the ORD change because the relative errors are lowest at this wavelength. These measurements were repeated several times and always showed the trends indicated in Table II; however, the variations in the observed differences were large enough to make the magnitude of the change uncertain. We found that titration of the change in optical rotation shows the rotational changes clearly (see the Materials and Methods section).

Figure I-3a shows the change in ATCase rotation observed upon addition of small aliquots of a concentrated mixture of carbamyl phosphate and succinate, a nonreactive substrate analog that is bound to the enzyme. The rotation decreases with increasing substrate analog concentration, while the catalytic activity increases (see Figure I-1b) under these conditions. The role of carbamyl phosphate is important to note here, in that carbamyl phosphate is required for the rotatory

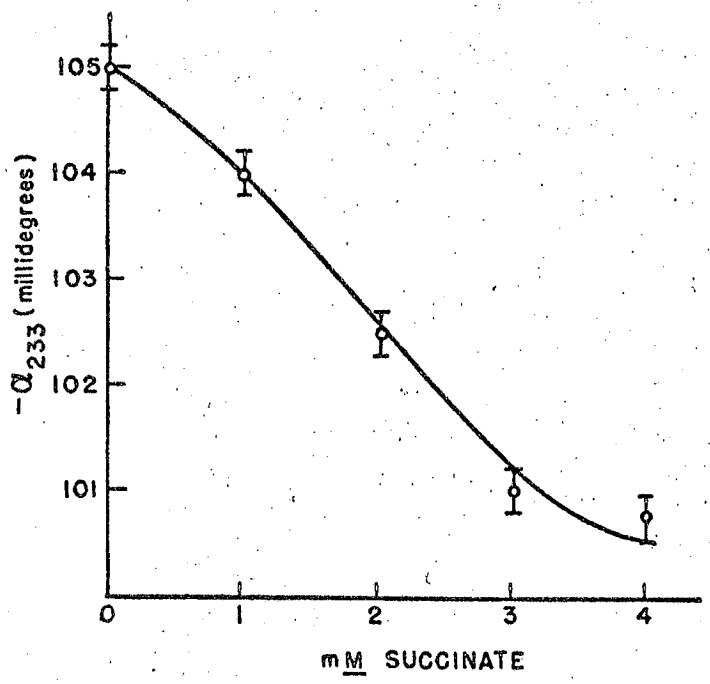

3a

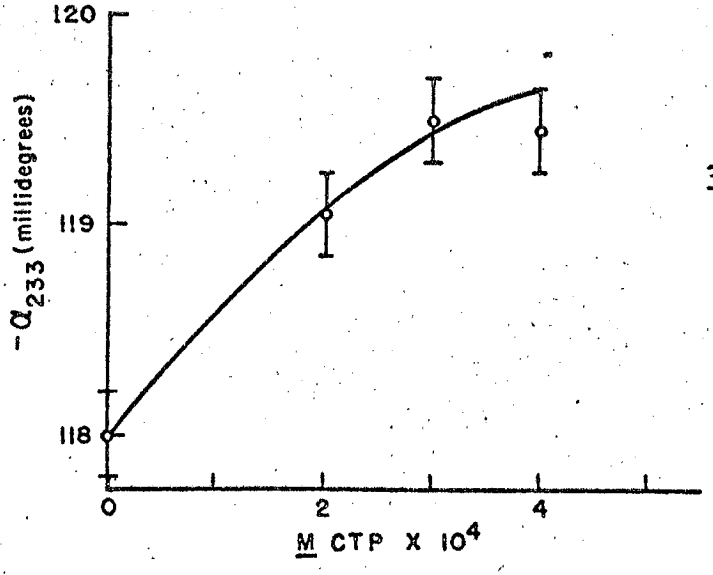

3b

MUB-6087

Figure I-3' The dependence of the rotation of ATCase, at the trough of the 233 mμ Cotton effect, on the concentration of CTP and substrate analog, succinate.

a) Enzyme (1.75 mg/ml) at pH 8.6, and aliquots of a mixture of 150 mM potassium succinate and 130 mM carbamyl phosphate (pH 8.6) added.

b) Enzyme (2.08 mg/ml) at pH 6.1 and aliquots of 20 mM CTP (pH 6.1) added.

change, yet causes no change in protein rotation by itself (within experimental error). Perhaps carbamyl phosphate is necessary for the binding of succinate. Figure I-3b shows the increase in rotation of ATCase as the CTP concentration increases. The catalytic activity decreases with increasing CTP concentration (as can be seen in Figure I-1a). The effect of added protons on the enzyme shows increased rotation (Table I) with decreased activity (Figure I-1a). The effects of the various added materials on ATCase rotation and catalytic activity are summarized in Table III. All measurements consistently show an inverse correlation between the magnitude of the rotation and catalytic activity of ATCase.

Table III. Summary of the catalytic and rotatory effects of adding various materials to solutions of ATCase. The change in absolute value of the rotation is given in the table.

Material added	Catalytic Activity	|Rotation|
Substrate analog (succinate)	+	-
CTP	-	+
H^+	-	+

The changes in rotation clearly show that there is a change in the relationships of amide residues in the protein accompanying changes in the catalytic activity. Figure I-4 shows the maximum change in the ORD of ATCase caused by the addition of substrate analog. The shape of the difference ORD curve is very close to that of the polypeptide helix, indicating that, on the face of it, some residues of the protein have

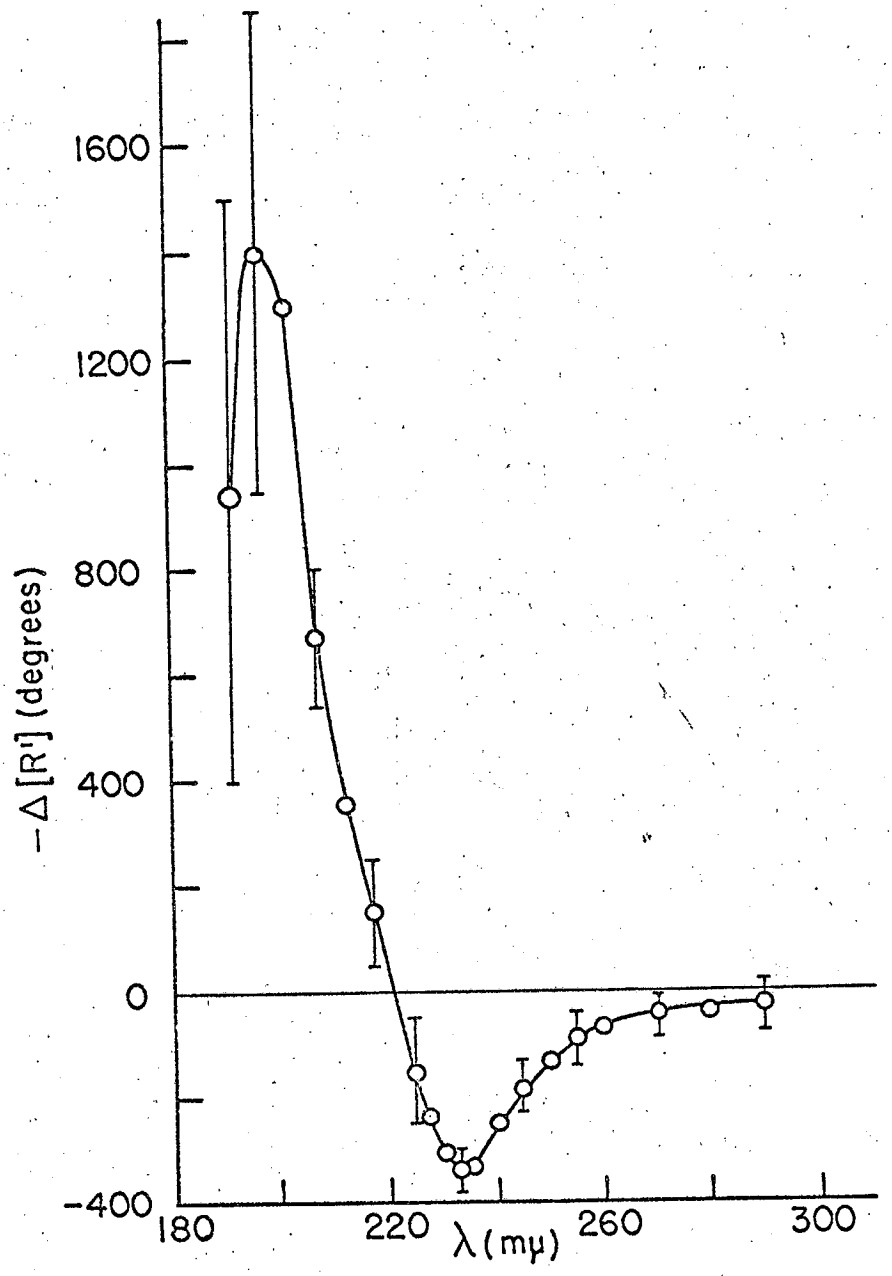

MUB-11124

Figure I-4. The change in specific residue rotation of ATCase at pH 8.6 brought about by 4 mM potassium succinate and 4 mM carbamyl phosphate. The difference is presented as (enzyme + effector) - (free enzyme).

undergone a coil-to-helix transition. The noise level is relatively high in the region of 200 mμ and below, and it is difficult to follow the details of the change; however, it is clear that the maximum change in the 200 mμ region relative to the maximum change at 233 mμ is consistent with a change in helix content.

Care must be taken in assigning such small differences to any particular structural change, and we must examine alternative explanations carefully.

(1) Small molecules can acquire optical activity when bound to an optically active large molecule (Stryer and Blout, 1961, Li, Ulmer and Vallee, 1962). If the ORD changes observed were due to induced optical activity in the bound effectors, specific rotations in excess of 10^6 degrees per mole of bound substrate analog would be required to explain the observed change in rotation (even if as many as 10 substrate analogs per mole of enzyme were bound, while the current evidence indicates 4/enzyme [Changeux, 1966]). Specific rotations of this magnitude are much larger than can reasonably be expected. Furthermore, induced Cotton effects will be centered very close to the absorption maxima of the bound molecules. CTP has a weak ORD spectrum with a Cotton effect centered at 270 mμ. An induced Cotton effect in CTP would show up in the 270 mμ region and could not give rise to an ORD change with the wavelength dependence observed. Substrate analogs, succinate and malate, have somewhat different absorption spectra, and both appear to produce an ORD spectrum change of the same shape. Since the same ORD changes are caused by substances with different absorption spectra (CTP, succinate, malate), we can rule out Cotton effects induced in the bound molecules as the source of the changes.

(2) Effector-induced alterations in the nonhelical regions of the protein structure could change the charge and dipole environment around the helix and give rise to an altered helix ORD. Changes in the charge and dipole fields would be expected to have the largest effect on the helix ORD in the electronically forbidden $n - \pi^*$ region around 225 mμ (Woody, 1962; Schellman and Oriel, 1962; Tinoco, 1962) and to be less important in the electronically allowed N - V peptide bond transition around 190 mμ (Woody, 1962; Tinoco, 1962; Holzwarth and Doty, 1965). It is very unlikely that alterations in the static fields would produce the same percentage change in the ORD at 200 mμ and at 233 mμ as is observed. We can conclude that the change in ORD is probably not due to alterations in the nonhelical regions of the protein. (The nonhelical regions may well change under the influence of the allosteric effectors, but this is not the source of the ORD changes we observe.)

(3) In principle, one other possible explanation for a change in ORD with the wavelength dependence of the helix-coil type is a change in the local refractive index due to swelling or shrinking (change in internal hydration), thereby altering the local electric field of the light inside the protein and leading to an altered ORD amplitude. If we assume a Lorentz local field, a very large change in refractive increment for the protein (of the order of 6% maximum) would be required to explain the observed effect. A change in refractive increment of this magnitude is extremely unlikely.

In summary, the addition of allosteric effectors causes a physical change in the protein structure. The interrelationships of the amide residues clearly change, and, although static field and hydration effects

are not strictly excluded, the allosteric transition is most probably accompanied by a change in helix content of the enzyme.

ATCase appears to be composed of 6 subunits, 4 regulatory and 2 catalytic, the interaction of which controls the catalytic activity (Gerhart, 1964; Gerhart and Schachman, 1965). The helix-coil transition that has been found could change the geometry of the subunits and thereby affect the subunit interaction. It has been observed that substrate analogs induce a change in the sedimentation coefficient of ATCase (Gerhart and Schachman, 1965b). However, the magnitude of the change in ORD and sedimentation are both very small. The molecular weight of ATCase (Gerhart and Schachman, 1965a) is about 3×10^5, which corresponds to about 2.6×10^3 residues, approximately 8.3×10^2 (37%) of which are in a helical environment. The number of residues involved in the allosteric helix-coil transition can be estimated to be about 40-50 residues from the maximum change in rotation of about 5 to 6%. This small alteration of the enzyme structure occurs during a change of substrate affinity of two orders of magnitude or more. It is not surprising, however, that small alterations of enzyme structure could lead to large changes in activity by affecting the shape, polar environment, or charge on the catalytic site. The allosteric enzyme acts like a biochemical amplifier (Atkinson, 1965) in that a small signal causes a large effect.

The estimate of the number of residues involved is a lower limit. The net observed effect could be the result of opposite transitions, one helix-to-coil and the other coil-to-helix; the difference in the number of residues would be seen by our experiments. It is also possible

that a large number of residues modify their helix dimensions as compared to a smaller number undergoing a complete helix-to-coil transition. The former point of view is unfavorable because helix-coil transitions tend to be cooperative. It would be desirable to separate the rotatory contribution of the isolated regulatory and catalytic subunits (Gerhart and Schachman, 1965a), although the isolated subunits may respond differently to allosteric effectors compared to the intact complex. The theory of the allosteric enzymes (Monod, Wyman and Changeux, 1965) predicts that binding of an effector shifts an equilibrium between an active and an inactive form of the enzyme. It seems reasonable to take the ORD results as a measure of the position of this equilibrium. Correlations of the equilibrium shift with independent studies of effector binding under the same conditions should allow a sensitive test of the mechanism of the allosteric enzyme.

C. Other Proteins

Deoxycytidine monophosphate deaminase

This enzyme has extremely interesting kinetics, showing inhibition and acceleration by several nucleotides (Scarano, Geraci, Polzella and Campanile, 1963; Monod, Wyman and Changeux, 1965). A sample of the enzyme was obtained from Dr. E. Scarano, who sent it by air from Naples, Italy, in frozen solution. The enzyme had lost much of its original specific activity by the time it arrived and the ORD and specific activity were not constant in our hands. Measurements of effector induced ORD alteration were attempted, but none of the results were considered reliable. Deoxycytidine monophosphate deaminase is very hard to purify and is known to be very tricky to handle (Scarano, 1964), so this work was not pursued.

Carboxydismutase

Carboxydismutase couples carbon dioxide (bicarbonate) and ribulose diphosphate (RuDP) in the presence of magnesium ion (Pon, 1962) to initiate the photosynthetic carbon reduction cycle. This enzyme has recently been prepared in a high state of purity (Trown, 1965). The induced fit hypothesis of Koshland applies to multisubstrate and cofactor-requiring enzymes such as this. Magnesium may be required for the binding of RuDP or bicarbonate and we wanted to see if a combination of one, two, or all three of the bound materials would detectably affect carboxydismutase conformation.

Experimental

The carboxydismutase (isolated from spinach) solutions and ribulose diphosphate were obtained from Dr. P. Trown. The method of purification and assay of the enzyme have been described (Trown, 1965). The enzyme solutions were at pH 7.5 in 0.05 M Tris HCl buffer, and the specific activity of the enzyme was 88 units/mg. Potassium RuDP solutions were adjusted to pH 7.5 with the same Tris buffer. The magnesium chloride stock solution was 1.0 M and was also buffered at pH 7.5 with Tris. The solutions were all prepared with ion free water that was deionized by ion exchange until it gave no color with dithizone. All glassware was cleaned in HNO_3/H_2SO_4 and rinsed with ion free water. The ORD measurements were done as previously described in the ATCase section (p. 12) and were carried out at approximately 4°C.

Results and discussion

Ribulose diphosphate has considerable rotational strength with a Cotton effect centered at about 280 mμ (see Figure I-5a). The ORD of carboxydismutase is shown in Figures I-5b and I-6. The rotation is

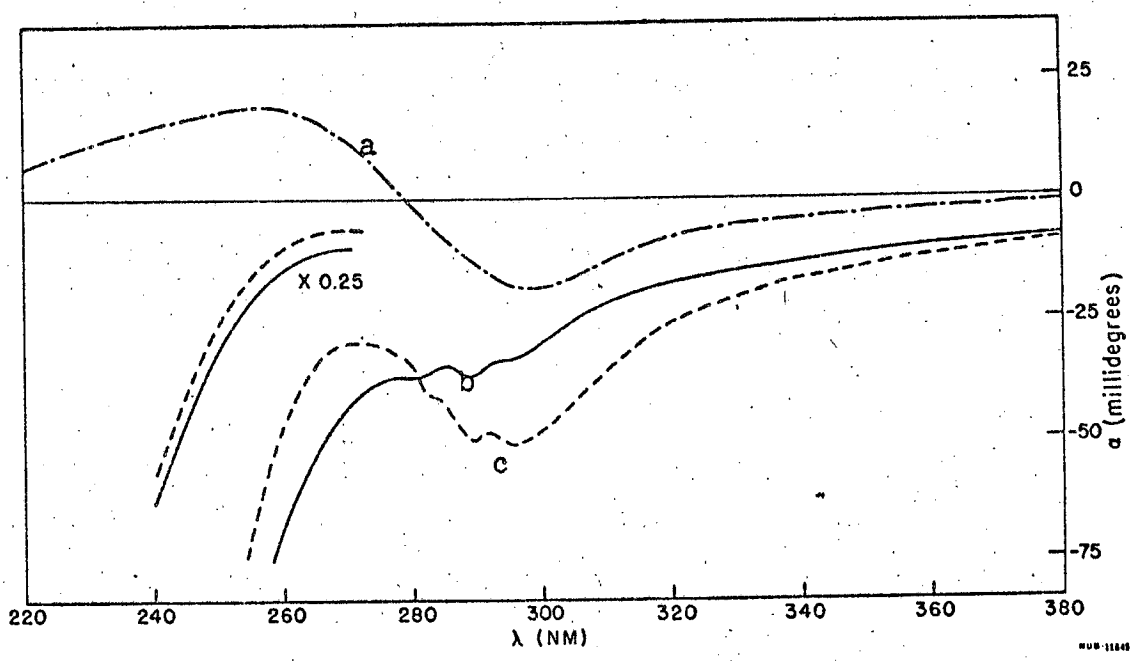

Figure I-5. ORD of spinach carboxydismutase (1.20 mg/ml, in 50 mM tris HCl pH 8.0). _____, 1 cm path; plus 0.93 mM potassium ribulose diphosphate and 10 mM magnesium chloride, - - - -. ORD of potassium ribulose diphosphate (0.93 mM, 50 mM Tris HCl pH 8.0, 10 mM magnesium chloride, 1 cm cell), __ · __ ·. The wavelength axis is labeled in NM (nanometers) which are equivalent to mμ (millimicrons).

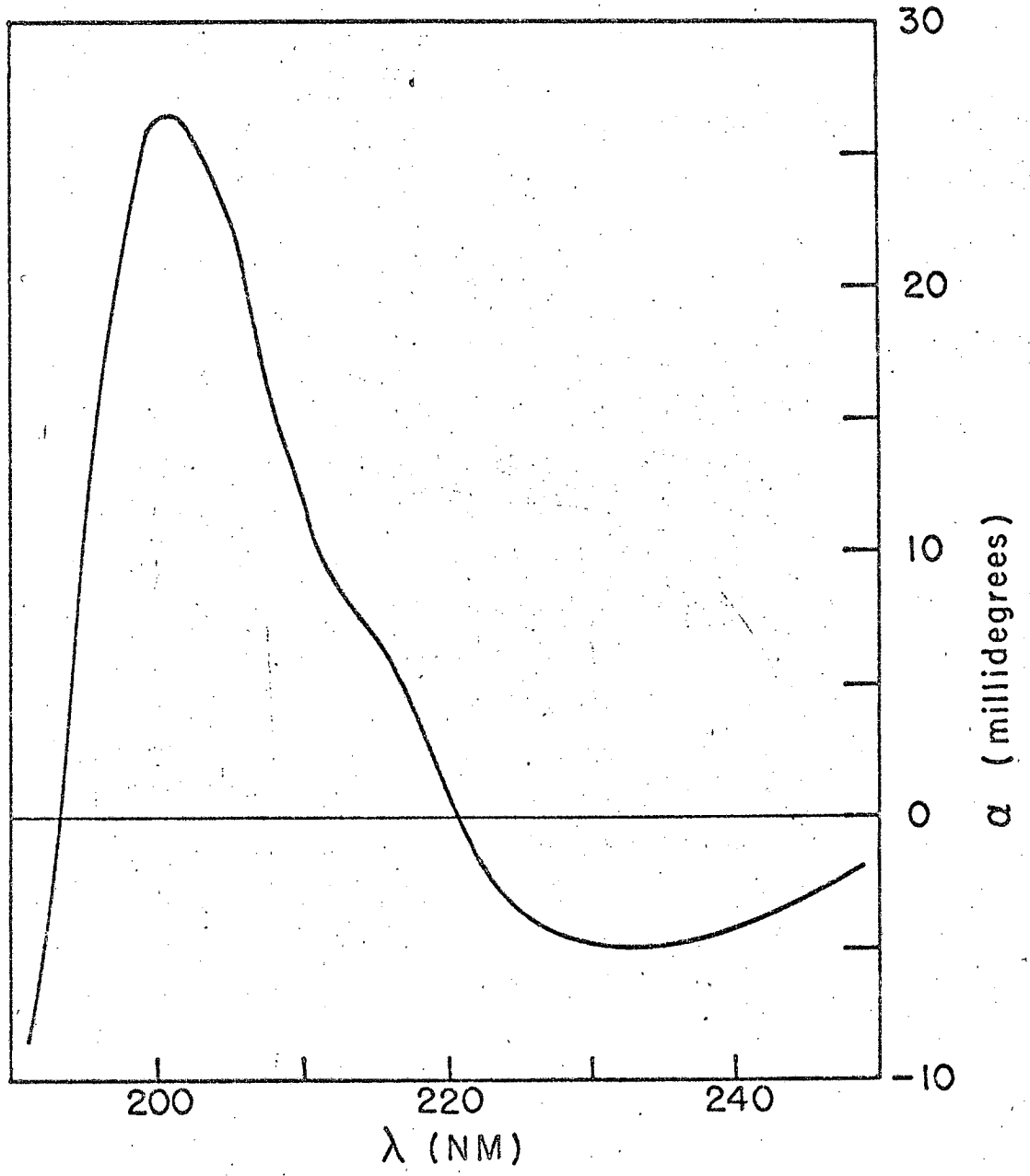

MUB 11640

Figure I-6. ORD of carboxydismutase, 1.52 mg/ml, 1 mM Tris HCl pH 8.0, 0.1 mm path. The peak absorbance of the protein at 191 mμ is 1.48. Addition of 0.93 mM ribulose diphosphate, 10 mM magnesium chloride and 2 mM sodium bicarbonate do not change the curve (root mean square noise level is about ± 0.5 millidegree). The wavelength axis is labeled in NM (nanometers) which is equivalent to mμ (millimicrons).

quite similar in shape to helical PLGA with some small inflections near 280-295 mμ, the regions of aromatic amino acid absorption.

The protein is about 25% helix as judged by the magnitude of the rotation in the peptide absorption region of 190-240 mμ. Mg^{++}, bicarbonate or Mg^{++} and bicarbonate together have no detectable effect on the protein rotation (< 0.5%). RuDP added to the enzyme shows approximately additive rotation as is shown in Figure I-5c. Addition of Mg^{++} or bicarbonate to the RuDP-enzyme solution does not initially affect the rotation. A large excess of Mg^{++} or bicarbonate leads to a slow decrease of the contribution of the RuDP to the rotation. This is probably due to a small amount of dissolved bicarbonate or Mg^{++} impurity respectively, allowing the enzymatic destruction of RuDP.

Under all of these conditions, there is no change in rotation attributable to the protein. The protein rotation can be measured over the entire wavelength range by subtracting the RuDP rotation. However, in the region below 235 mμ there is a very small contribution of the RuDP relative to that of the protein. So in the 230 mμ region, we can measure the protein rotation with only a small correction for the presence of RuDP. Addition of RuDP plus Mg^{++} bicarbonate leads to rapid destruction of RuDP but no apparent change in protein rotation.

We conclude that any conformational change undergone by carboxydismutase in the presence of its substrates and cofactor must be extremely small or is not of a type detected by ORD. The conformation alteration of a few residues in the region of the active site would not be a large enough effect to be seen with present sensitivity.

Cerruloplasmin

Cerruloplasmin is a copper transport protein with 8 coppers/protein molecule. This material was interesting for our work because previous experiments suggested that a conformation change occurs in the protein when the copper is reduced (Blumberg, et al., 1963). It was found that the effect of the copper on the nuclear magnetic resonance (line width) of the bulk water protons had a discontinuity when about one-half of the copper was reduced. This observation suggested that the access of the solvent water to the copper had changed and thus that the protein conformation changed upon copper reduction.

Solutions of human cerruloplasmin were obtained from Dr. H. Schienberg. The oxidized protein has a deep blue color due to visible copper absorption. The ORD of the cerruloplasmin was measured before and after complete reduction by solid dithionite. The copper was bleached by dithionite and small Cotton effects due to the copper bands in the visible disappeared; but the protein showed no evidence for conformation change by the criteria of our experiments. The contribution of the copper bands to the rotation was negligible below 300 mμ, where the protein rotation is quite strong.

It should be mentioned that some interesting and unique information did result from these studies. Dr. W. Blumberg (1965), using the visible rotatory strength data in combination with electron spin resonance and optical absorption data was able to determine the detailed electronic structure around the copper site in the protein. The circular dichroism and ORD of cerruloplasmin in the visible is presented in the next chapter (p. 53).

A more wide ranging study of more proteins was not attempted because of the negative experiments in most cases and the very small effects which could be seen with the one case, ATCase, that showed positive results. If additional pure allosteric proteins become available, this study should be extended.

REFERENCES

Atkinson, D. E., Science 150, 851 (1965).

Blout, E. R. (1962), in Polyamino Acids, Polypeptides and Proteins, M. A. Stahmann, ed. (University of Wisconsin Press, Madison, Wis.).

Blout, E. R., I. Schmier and N. S. Simmons, J. Am. Chem. Soc. 84, 3193 (1962).

Blumberg, W. E. (1965), International Symposium on the Biochemistry of Copper (in the press).

Blumberg, W. E., J. Eisinger, P. Aisen, A. G. Morell and I. H. Scheinberg, J. Biol. Chem. 238, 1675 (1963).

Changeux, J. P. (1966), unpublished.

Epstein, C. J., R. F. Goldberger and C. B. Anfinsen, Cold Spring Harbor Symp. 28, 439 (1963).

Gerhart, J. C., Brookhaven Symposium in Biology 17, 222 (1964).

Gerhart, J. C., and A. B. Pardee, J. Biol. Chem. 237, 891 (1962).

Gerhart, J. C., and A. B. Pardee, Cold Spring Harbor Symp. 28, 491 (1963).

Gerhart, J. C., and H. J. Schachman, Biochemistry 4, 1054 (1965a).

Gerhart, J. C., and H. J. Schachman (1965b), unpublished work.

Holzwarth, G. (1965), personal communication.

Holzwarth, G., and P. Doty, J. Am. Chem. Soc. 87, 218 (1965).

International Critical Tables (1930), McGraw Hill Book Co., New York, VII, 13.

Iizuka, E., and J. T. Yang, Proc. Nat. Acad. Sci. 55, 1175 (1966).

Karush, F., J. Am. Chem. Soc. 72, 2705 (1950).

Koshland, D. E., Jr., Proc. Nat. Acad. Sci. 44, 98 (1958).

Koshland, D. E., Jr. (1962), in Horizons in Biochemistry, M. Kasha and B. Pullman, eds. (Academic Press, N. Y., 1962), p. 265.

I ..ff, A., Science 152, 1216 (1966).

L , T., D. D. Ulmer and B. L. Vallee, Biochemistry 1, 114 (1962).

Monod, J., J. P. Changeux and F. Jacob, J. Mol. Biol. 6, 306 (1963).

Monod, J., J. Wyman and J. P. Changeux, J. Mol. Biol. 12, 88 (1965).

Pon, N. G. (1962), Ph.D. Thesis, University of California, Berkeley.

Rosenheck, K., and P. Doty, Proc. Nat. Acad. Sci. 47, 1775 (1961).

Scarano, E. (1964), personal communication.

Scarano, E., G. Geraci, A. Polzella and E. Campanile, J. Biol. Chem. 238, 1556 (1963).

Schachman, H. K., Cold Spring Harbor Symp. 28, 409 (1963).

Schechter, E., and E. R. Blout, Proc. Nat. Acad. Sci. 51, 794 (1964); Schechter, E., J. P. Carva and E. R. Blout, ibid. 51, 1029 (1964.

Schellman, J. A., and P. Oriel, J. Chem. Phys. 37, 2114 (1962).

Sogami, M., W. V. Leonard, Jr. and J. F. Foster, Arch. Biochem. Biophys. 100, 260 (1963).

Stryer, L., and E. R. Blout, J. Am. Chem. Soc. 83, 1411 (1961).

Tinoco, I., Jr., Adv. Chem. Phys. 14, 113 (1962).

Trown, P. W., Biochemistry 4, 908 (1965).

Umbarger, H. E., Science 123, 848 (1956).

Urnes, P., and P. Doty, Adv. Protein Chem. 16, 401 (1961).

Whitney, P. L., and C. Tanford, Proc. Nat. Acad. Sci. 53, 524 (1965).

Woody, R. W. (1962), Ph.D. Thesis, University of California, Berkeley.

Wyman, J. (1948), in "Heme Proteins" in Adv. in Protein Chemistry, M. L. Anson and J. T. Edsal, eds., 4, 407-531.

Wyman, J., and D. W. Allen, J. Polymer Sci. 7, 499 (1951).

Yang, J. T., and W. J. McCabe, Biopolymers 3, 209 (1965).

Yates, R. A., and A. B. Pardee, J. Biol. Chem. 221, 757 (1956).

II. CHLOROPHYLL-CHLOROPHYLL INTERACTIONS

A. Introduction

The basic carbon fixation reactions of photosynthesis have been understood for some time (Bassham and Calvin, 1957). These reactions occur in the dark using ATP and reduced pyridine nucleotides resulting from energy converting light reactions. The mechanisms of the photoreactions themselves are still poorly understood.

The light reactions seem to require a highly specific organization of chlorophylls, carotenoids and some redox cofactors arranged in lipoprotein membranes (chloroplast lamella and bacterial chromatophores). Any treatment such as solvent extraction, mild heating or treatment with most detergents almost invariably leads to complete loss of the photosynthetic activity. Isolated chlorophyll molecules in solution are incapable of the energy converting reactions characteristic of photosynthetic organisms.

The evidence at hand points to an important role for the particular way in which the pigments and cofactors are arranged spatially. The pigment molecules, for example, cannot be considered to be isolated from one another even as a good first approximation. Typical lamellar fractions contain 6 to 8% chlorophyll by weight and pigment concentrations run in excess of 0.1 mole/liter.

Evidence from absorption spectra of chloroplasts from higher plants and algae, as well as of photosynthetic bacteria, suggests that *in vivo* the chlorophyll is at least partially aggregated. For example, low temperature spectroscopy of plant material resolves several absorption maxima in the long wavelength region, but the extracted chlorophyll *a*

has only a single peak (e.g., Butler, 1966). Fluorescence excitation spectra of these samples suggest that a part of the chlorophyll a, absorbing on the short wavelength side of the main band, is unaggregated and highly fluorescent, while the chlorophyll a absorbing on the long wavelength side of the main band is weakly fluorescent and is supposed to be aggregated (Butler, 1966; Clayton, 1966).

Studies aimed at elucidating the nature of the pigment associations and their environments have met with only partial success. Oriented chloroplasts or fragments from them show little or no dichroism for most of the pigment absorption (Goedheer, 1955; Olson, Butler and Jennings, 1962; Sauer and Calvin, 1962). The fluorescence of the chlorophyll in these organelles is found to be almost completely depolarized. A long wavelength form of chlorophyll a which is dichroic and gives rise to polarized fluorescence involves only a small fraction of the total chlorophyll in chloroplasts (Olson et al., 1962; Sauer and Calvin, 1962). This fraction may, however, be of utmost importance to the energy conversion process.

Studies of nuclear magnetic resonance, infrared and visible absorption spectra, and of apparent molecular weights of purified chlorophylls in solution show that dimers and higher aggregates form readily under some conditions (e.g., Katz, Dougherty and Boucher, 1966; Sauer, Lindsay Smith and Schultz, 1966). These aggregates have greatly enhanced optical activity compared to the monomers and have been studied by optical rotatory dispersion (ORD) in the case of chlorophyll a (Sauer, 1965). The chlorophyll in chloroplast subunits also shows optical activity which is large compared to that of the extracted chlorophyll (Sauer, 1965;

Ke, 1965), and this has been used as additional evidence for the presence of aggregated chlorophyll *in vivo*. It has been recognized, however, that the large optical activity of the chloroplast lamellar fragments (quantasomes) could be due to chlorophyll-protein or chlorophyll-lipid interactions, as well as to chlorophyll-chlorophyll interactions.

We present a study of the circular dichroism (CD) of chlorophyll dimers, chlorophyll crystals and chlorophyll containing membrane fractions of chloroplasts and photosynthetic bacteria. Our analysis of the dimer CD and absorption data leads us to propose a structure for the chlorophyll dimer in solution. Our experiments also give a direct (but more qualitative) indication that strong chlorophyll-chlorophyll interactions are present in the photosynthetic material examined. We show that CD measurements reveal chlorophyll-chlorophyll interactions in a much more obvious way than ORD and open the possibility that further CD and absorption experiments could potentially reveal the detailed geometry of the chlorophyll interactions *in vivo*.

The first section is a detailed description of the CD instrument we constructed. Subsequent sections relate the dimer absorption and CD experiments and analysis of dimer structure. The crystal CD and absorption experiments, quantasome experiments, analysis of quantasome results, and a study of CD and absorption of the chromatophores from photosynthetic bacteria follow.

B. Instrumentation

The circular dichroism instrument constructed has a useful wavelength range, from 220 NM in the ultraviolet to 1100 NM in the near infrared, and extremely high sensitivity (measurements of a circular

dichroism of one part in 10^6 are possible through most of the wavelength range). The heart of the instrument is an electrically variable optical retardation plate or Pockels' cell (Billings, 1949, 1952), which is used to modulate the light beam polarization from right to left circular at 400 Hz. If the sample under investigation differentially absorbs right and left circular light (circular dichroism) 400 Hz modulation of the light intensity results, which is detected with a photomultiplier tube, amplified and measured with a phase sensitive detector. The theory and practice of the optical retardation device has been described in great detail in a series of papers by Billings (1949, 1952) and Carpenter (1950). Babcock (1953) first used the device for circular dichroism measurements. Similarly conceived circular dichrographs, which are less sensitive than the instrument described here, are described by Grosjean and Legrand (1960) and Holzwarth (1965). Other types of circular dichroism instruments are reviewed by Lowry (1964) and Velluz, Legrand and Grosjean (1965). The book by Velluz et al. (1965) should be consulted for many useful instrumental considerations.

Appendix I contains a treatment of the theoretical limitation on signal/noise of circular dichroism and optical rotatory dispersion. Our instrument approached the theoretical limitations to within a factor of 2. The main theoretical noise limitation of a well designed instrument is the statistical fluctuation in light intensity due to the quantal nature of light (e.g., Davidson, 1962). To minimize this source of noise, usually called the Schottky effect or shot noise, high light intensity is required and high efficiency of detection of that light. There are several factors which can degrade the performance below this theoretical

limit, and our methods of coping with these problems will be discussed in the course of the development.

Optics

A schematic diagram of the optical part of the instrument is shown in Figure II-1. Light from the xenon arc lamp falls on an elliptical mirror E and is focused on the entrance slit of the prism (M1)-grating (M2) double monochromator. The light from the exit slit of the monochromator is approximately collimated by cylindrical mirror C and spherical mirror Sp. The light is plane polarized by prism P and is modulated between right and left circular light by the Pockels' cell labeled Mod. The extraordinary polarized beam is masked off at M while the ordinary beam passes through the sample at S or S' and on to the end window photomultiplier, PM. The instrument is mounted on a sturdy optical bench made of 2-inch diameter stainless steel rails, affording stable alignment of the optical components.

The high pressure xenon arc (X in Figure 1) is the brightest source available for the region of the spectrum of interest (Baum and Dunkelman, 1950). The main problem with this arc is its notorious instability. We found that the 450-watt Osram[1] unit XBO 450 is far superior in brightness and stability to Hanovia or PEK lamps. Most of the instability was due to arc flutter rather than overall intensity variations. The arc flutter could be minimized by keeping the lamp in still air rather than blowing large volumes of cool air over it as is usually done. Apparently the high velocity air stream unequally cools the lamp envelope and causes

---

[1]Obtainable from Macbeth Sales, Little Britain Road, Newberg, N. Y.

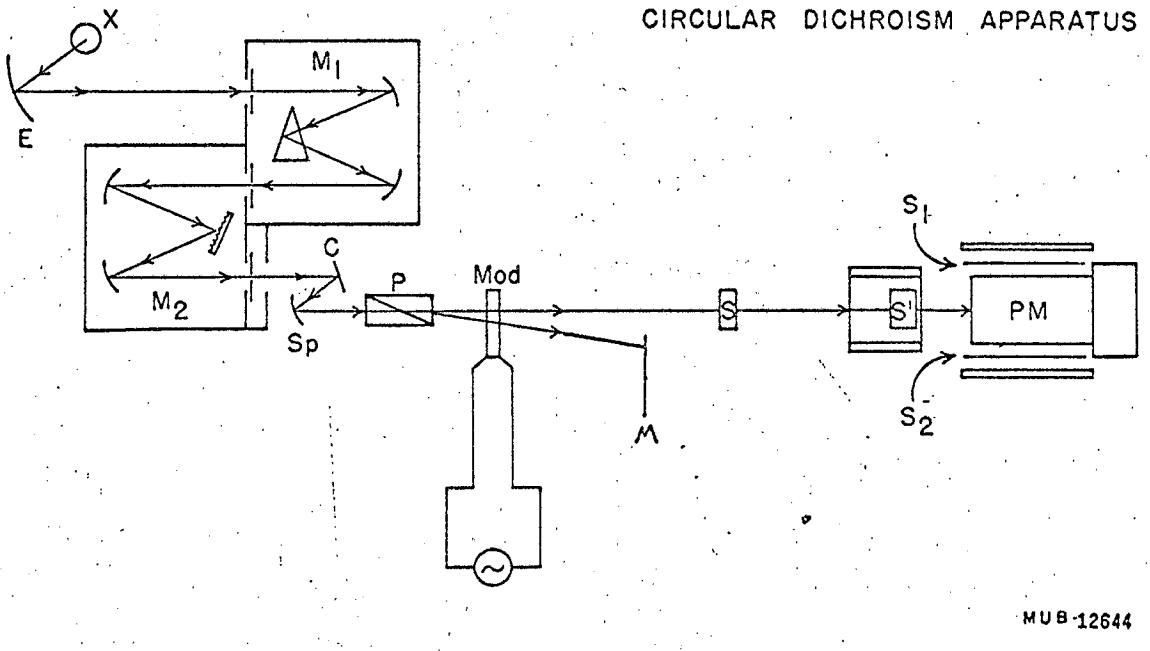

Figure II-1. Diagram of the optical components of the circular dichroism apparatus, the components are explained in the text.

convection currents in the gas inside the lamp. The lamp house is simply constructed from a 4-inch diameter brass tube wrapped with copper cold water cooling coils. The lamp house is closed on the top and bottom and purged with dry N_2 gas to prevent ozone formation. The light exit window was made of suprasil quartz (Engelhardt-Hanovia). The suprasil window did not discolor under far UV irradiation, as did more impure quartz. The lamp operates satisfactorily in this environment, showing no noticeable drop in intensity after 1000 hours. Older lamps are somewhat less stable than fresh ones, however. The problem of the remaining arc flutter is further reduced by the simple expedient of magnifying the arc and overfilling the entrance slit to the monochromator. In this way, the light from the edges of the arc is discarded. A magnification which reduces the light intensity by a factor of 3 leads to a factor of 10 increase in light stability (compared to exactly filling the slit). The lamp is powered by a Belman-Invar TC-100 power supply in the current regulated mode with a 0.1 Ω series resistance. The lamp position was made continuously adjustable in three perpendicular directions by suspending the whole lamp house on three perpendicular Gilman light-duty slide assemblies. The gibs on the slides may be locked when the best lamp position is found as judged by maximum light intensity through the system.

The image of the xenon arc source is magnified and focused on the monochromator slit by means of an off-axis ellipsoidal mirror (E in Figure II-1). The arc is placed at the near focal point of the ellipse and the monochromator slit at the far focal point. The off-axis design allows the light to pass to the side of the lamp envelope on the way to

the slit. The mirrors were made from a Bausch & Lomb 11-3/4 inch diameter on-axis elliptical mirror by cutting four 4-1/2 inch diameter off-axis circular mirrors from the outside edges. The short axis focal point at 4-1/4 inches and long axis focal point at 30 inches provide a 7X magnified image of the arc at the monochromator slit. These mirrors were first surface aluminized under high vacuum and then magnesium fluoride overcoated. When tested on an optical bench with a tungsten Point-o-Light lamp at one focal point these mirrors gave relatively poor images at the second focal point; however, the quality of the image could be markedly improved by a slight straining of the mirror in a trial and error fashion.

A Cary 14 prism-grating double monochromator (Applied Physics Corp., Monrovia, Calif.) is used to provide light of high spectral purity. The Cary 14 is fairly fast optically (f/8), has exceptionally low stray light levels, and the dispersion exceeds 35 Å/millimeter of slit width over the entire wavelength range. The monochromator exit light is approximately collimated with a concave cylindrical mirror (C) and a concave spherical mirror (Sp). The light is plane polarized at P with an optically contacted synthetic crystal quartz (10°) Rochon prism (Karl Lambrecht, Chicago, Ill.) with a 1-cm clear aperture. This 10° prism gave sufficient deviation of the extraordinary beam so that it was well separated from the ordinary beam in 6 inches and was masked off at M before the ordinary beam entered the sample.

The Pockels' cell (Mod) was a custom design built by Baird-Atomic, Inc. The Pockels' cell was a potassium dihydrogen phosphate unit of 8-mm thickness, with indium foil ring electrodes and ultrasil quartz

windows (Hanovia). This arrangement has excellent transparency (> 90% transmission including reflection losses) and gives approximately 75% peak circular polarization. The circular polarization was measured at optimum sinusoidal driving voltage by placing either a Polaroid 590 NM circular polarizer or a Glan-Thompson polarizer oriented perpendicular to P in the sample space and measuring the DC and AC components of light intensity with a PM and an oscilloscope. The circular polarization was not perfect because: (1) the Pockels' cell depolarizes the imperfectly collimated light somewhat (Billings, 1952) and, (2) the electric field between the circular ring electrodes is not homogeneous. The optimum operation of the Pockels' cell is quite sensitive to exact orientation with respect to beam direction and polarization. A mounting device was built with three micrometer controlled degrees of freedom. The Pockels' cell orientation could be adjusted, while it was in operation, for rotation about the light propagation axis (z) and for tilt in two orthogonal directions (x,y) relative to the light propagation axis.

The last optical component is the photomultiplier tube (PM). We used 2-inch end window type PM's because they are insensitive to light polarization. An EMI 9558QA (S-20) was used for most of the work. This tube has a peak quantum efficiency in excess of 25% and gives outstanding performance from 185 to 800 NM. For experiments in the near infrared, a Dumont 6911 S-1 tube was employed.

The optics were alighed with a 0.5 milliwatt Helium-Neon gas laser (Spectra-Physics) by autocollimation.

Measurement of circular dichroism

The voltage on the Pockels' cell is sin wave modulated:

$$V_{pc} = V_o \sin \omega t \qquad \text{II-(1)}$$

The resulting retardation of the light (Billings, 1952) is:

$$\delta = \delta_o \sin \omega t \qquad \text{II-(2)}$$

The light passing through the system is treated as the sum of right and left circular light intensities I_r, I_l respectively. The right and left components in the presence of a dichroic material are:

$$I_r = I_{o/2} (1 + \sin \delta)\, e^{-\varepsilon_r \ell c/2.3} \qquad \text{II-(3)}$$

$$I_l = I_{o/2} (1 - \sin \delta)\, e^{-\varepsilon_l \ell c/2.3} \qquad \text{II-(4)}$$

where ε_r, ε_l are decadic molar extinction coefficients of the dichroic material for right and left circular light respectively, C is the concentration in moles/liter, ℓ is the pathlength in cm and I_o is the incident light intensity.

The total light intensity, I, can be found by adding equations II-(3) and (4) to yield:

$$I = I_r + I_l = \frac{I_o}{2} \left[(e^{-\varepsilon_r \ell c/2.3} + e^{-\varepsilon_l \ell c/2.3}) + \sin \delta (e^{-\varepsilon_r \ell c/2.3} - e^{-\varepsilon_l \ell c/2.3}) \right] \qquad \text{II-(5)}$$

We define an average decadic molar extinction coefficient, ε:

$$\varepsilon \equiv (\varepsilon_r + \varepsilon_l)/2 \qquad \text{II-(6)}$$

Multiplying eq. II-(5) by $e^{-\varepsilon \ell c/2.3} \times e^{\varepsilon \ell c/2.3} = 1$,

the light intensity is:

$$I = \frac{I_o e^{-\varepsilon \ell c/2.3}}{2} \left[(e^{-(\varepsilon_l - \varepsilon)\ell c/2.3} + e^{-(\varepsilon_r - \varepsilon)\ell c/2.3}) + \sin \delta (e^{-(\varepsilon_r - \varepsilon)\ell c/2.3} - e^{-(\varepsilon_l - \varepsilon)\ell c/2.3}) \right] \qquad \text{II-(7)}$$

Now $(\varepsilon_l-\varepsilon)\ell c$ and $(\varepsilon_r-\varepsilon)\ell c$ are always small compared to unity and the exponentials containing these factors can be approximated: $e^{-x} \approx 1-x$ to better than 1% in the worst case. With this excellent approximation, eq. II-(7) becomes with substitution of eq. II-(2):

$$I = I_o e^{-\varepsilon\ell c/2.3} + \frac{I_o e^{-\varepsilon\ell c/2.3}}{4.6} (\varepsilon_l-\varepsilon_r)\ell c \sin(\delta_o \sin \omega t) \qquad \text{II-(8)}$$

We see that the first term is a D.C. term and the second term is an A.C. term at ω, the modulation frequency. The ratio of the A.C. term to the D.C. term is linearly proportional to: $(\varepsilon_l-\varepsilon_r)\ell c = OD_l - OD_r$ = optical density in left light minus optical density in right light = circular dichroism. We hold the DC term constant by feedback control of the photomultiplier gain so the circular dichroism is linearly related to the magnitude of the A.C. signal. This A.C. signal is predominantly a sin wave at ω, but also contains small higher odd harmonics of ω (Velluz, et al., 1965). The A.C. voltage is synchronously rectified (e.g., Andrew, 1955) and filtered. The resulting voltage, V_{sig}, is linearly related to the circular dichroism:

$$V_{sig} = K (\varepsilon_l-\varepsilon_r)\ell c \qquad \text{II-(9)}$$

where K is an instrument constant to be determined.

Electronics

A block diagram of the D.C. control circuit and A.C. detection circuit is shown in Figure II-2. The signal voltage from the PM tube is opposed by a 1.3 volt mercury battery suppression bridge. This arrangement minimizes 60 Hz. power line pick up. The A.C. signal is split off at this point and its fate will be discussed after the D.C. control loop. The difference between the mercury battery voltage and

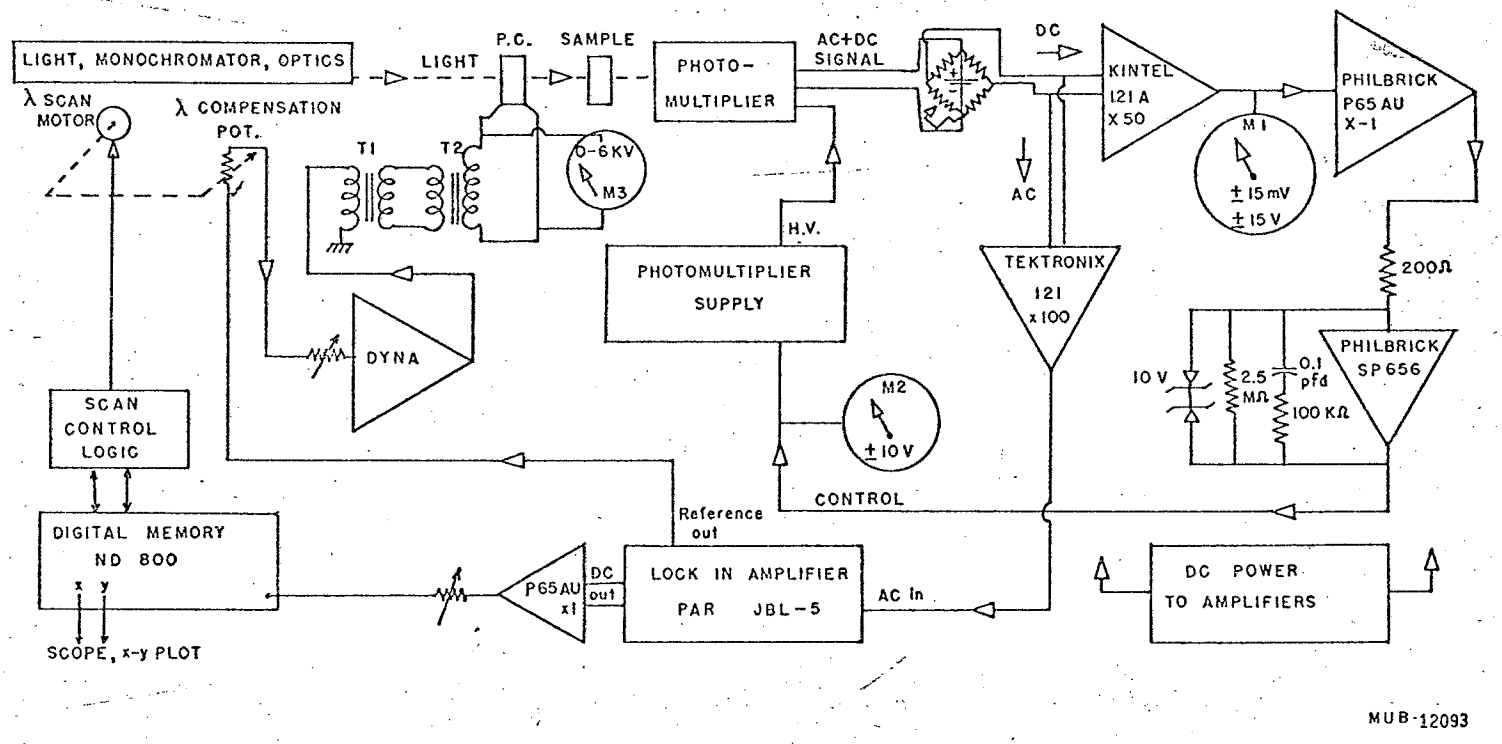

Figure II-2. Block diagram of the electronic components of the circular dichroism apparatus. The components are explained in the text.

the PM voltage the D.C. control loop error signal is amplified (20X) by the first D.C. amplifier, a Kintel A120, and the second D.C. amplifier, a Philbrick P65AU, which is used as a gain of 1 inverting amplifier. The last D.C. amplifier is a Philbrick SP656, which is a high gain (10^4) stage, whose response is strongly attenuated at 400 Hz, the modulation frequency, by an R-C network. Ten-volt Zener diodes back-to-back across the feedback resistor of A-3 keep the amplifier from saturating if the loop is opened accidentally. The D.C. error voltage is monitored at meter M-1 as well as the control voltage to the PM supply (M-2). The PM supply is a Power Designs 1544, 0-3KV unit. The control point in this supply is near ground potential and the control current is fed into the power supply summing point through a 10K resistor. A ± 10-volt control signal will swing the supply in excess of ± 1000 volts. The control loop has a gain in excess of one million and operates very satisfactorily. The Power Designs supply discriminates strongly against the modulator frequency, and the loop gain at the modulator frequency is < .01.

The A.C. detection leg of the circuit is based on a Princeton Applied Research (PAR) JBL-5 lock-in amplifier. The Pockels' cell is sine wave modulated with the amplified PAR reference voltage. The peak modulation voltage must be made linearly proportional to wavelength. A 5-V. 400 Hz reference voltage taken from the PAR is placed across a linear potentiometer which is in turn geared to the wavelength drive of the monochromator. A portion of the reference voltage, proportional to wavelength, is amplified by a Dyna 30-watt audio amplifier. The amplified output is coupled by an impedance matching transformer T1

(Stancor, RT-202) to a high voltage step-up transformer, T2 (Hill Magnetic Products, Menlo Park, Calif., H-1013D). This transformer (T2) supplies the Pockels' cell and a Sensitive Research electrostatic voltmeter, M3. The modulation voltage is directly proportional to wavelength to about 1%.

The 400 Hz A.C. signal from the photomultiplier, which is produced by a dichroic sample, is amplified by a Techtronix 122 low-level A.C. preamplifier (100X) directly preceding the PAR lock-in amplifier. The PAR D.C. output is linearly related to the circular dichroism of the sample of interest. The PAR phase and frequency trim and the Pockels' cell modulation voltage are optimized by the use of a sample with a large CD signal. The calibration of the instrument is discussed in the next section.

The standard Cary 14 monochromator scan is driven by a synchronous motor, so CD spectra can be recorded on a synchronously driven pen recorder. For more flexible operation, the wavelength is sensed by a second potentiometer, and a D.C. signal proportional to wavelength is used to drive the x axis of an x-y recorder.

Calibration

Absolute calibration of circular dichroism is difficult and is one of the main drawbacks of this method. We have made use of several calibration methods: (1) Published values of circular dichroism (e.g., Velluz et al., 1965); (2) measured amplifier gain and % circular polarization; (3) mathematical transformation of measured CD to ORD and subsequent comparison with measured ORD. All three methods gave substantial agreement; however, the third method is most satisfactory and will be described in detail.

The Kronig-Kramers relations (Moffitt and Moscowitz, 1959; Moscowitz, 1960, 1961) offer an exact means of calculating the rotatory dispersion arising from the observed CD spectrum. This calculation requires no assumptions about CD band shape or position. The calculated ORD due to the measured CD can be compared to the ORD measured in a recording polarimeter. A Cary 60 polarimeter was calibrated absolutely with the use of National Bureau of Standards sucrose. The calculated ORD was scaled to agree as closely as possible with the measured ORD; the scaling factor then was used as a calibration constant for subsequent CD measurements.

The molecular rotation $[\phi_\lambda]$ at a wavelength λ is related to the molecular ellipticity $[\theta_\lambda]$ by the following relation (Moscowitz, 1960):

$$[\phi_\lambda] = 2/\pi \int_0^\infty [\theta_{\lambda'}] \frac{\lambda'}{\lambda^2 - \lambda'^2} \, d\lambda' \qquad \text{II-(10)}$$

where: $$[\phi_\lambda] = \frac{\alpha_\lambda(\text{degrees}) \cdot 100}{\ell(\text{cm})\ c(\text{moles/liter})} = \text{molecular rotation} \qquad \text{II-(11)}$$

and $$[\theta_\lambda] = 3.3 \cdot 10^3 \, \Delta\varepsilon_\lambda = \frac{3.3 \cdot 10^3 \cdot \Delta OD(\lambda)}{\ell(\text{cm})\ c(\text{moles/liter})} =$$

$$\text{molecular ellipticity} \qquad \text{II-(12)}$$

and $\Delta OD(\lambda) = OD_\ell(\lambda) - OD_r(\lambda) =$ observed circular dichroism at λ.

It can be seen that the contribution of the measured CD to the rotation at wavelength λ is the integral overall of the measured CD values. In principle, the values of ellipticity substituted into the above eq. II-(10) and the resulting rotation should be corrected to their vacuum values by the Lorentz factor, $3/(n(\lambda)^2 + 2)$, where $n(\lambda)$ is the refractive index of the solvent at λ. J. M. Thiery (1966) has shown, however, that neglect of this Lorentz correction introduces negligible error (< 0.1%) for

common solvents if the CD data is taken at least 50 nm away from the solvent absorption edge. The solvent refractive index has a small dispersion far from the absorption edge. Eq. II-(10) was evaluated with a digital computer, and a FORTRAN IV subroutine for this purpose (KKTRAN) is given in Appendix II.

The main problem with the calibration of CD by comparison with ORD/rotation is that the ORD/rotation of most compounds is not entirely due to instrumentally accessible CD bands. Drüde tails from inaccessible far UV dichroism bands give monotonic contributions to the near UV rotation data for most optically active materials. In most cases we cannot know the exact magnitude of the Drüde tail, but only its approximate, $1/(\lambda^2-c)$, shape (where c is a constant). The Drüde tail uncertainty introduces the largest error into this ORD comparison method of CD calibration.

This problem can best be illustrated by an example. The steroid, isoandrosterone, is useful for calibration of CD because it has a large signal and is easy to obtain. The experimental CD of isoandrosterone and the calculated ORD are shown in Figure II-3. The observed ORD, as well as the observed minus calculated ORD, is shown in Figure II-4. The difference has a smooth Drüde shape throughout the wavelength range of interest. The calibration of the CD instrument with isoandrosterone is precise only to about ± 5% due to the Drüde tail uncertainty. The steroid samples give a conveniently large signal, but cover only a restricted wavelength range in the near UV. One would like to have samples that could be used for calibration in the visible and near IR region of the spectrum to check to constancy of sensitivity with wavelength. No ideal comparison samples were found, although the CD of many

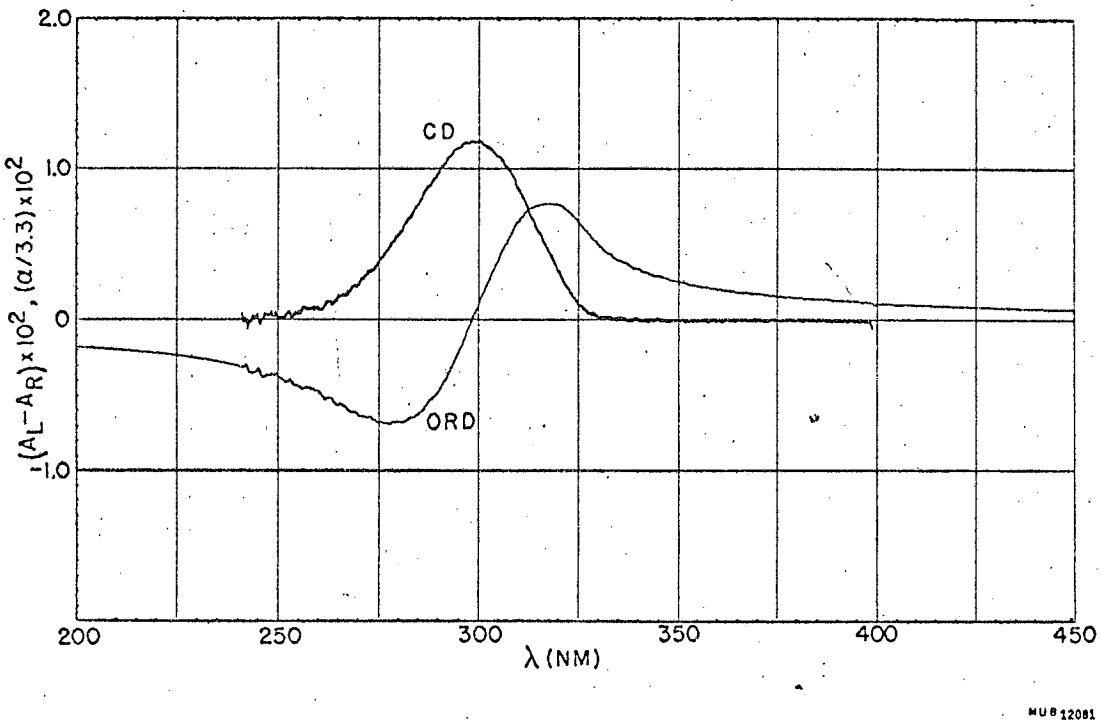

Figure II-3. Measured circular dichroism (CD) of isoandrosterone, 1.05 mg/ml, 100% ethanol, 1 cm cell, darker line (in observed optical density units). Calculated optical rotatory dispersion (ORD) due to the CD band shown, lighter line (in degrees).

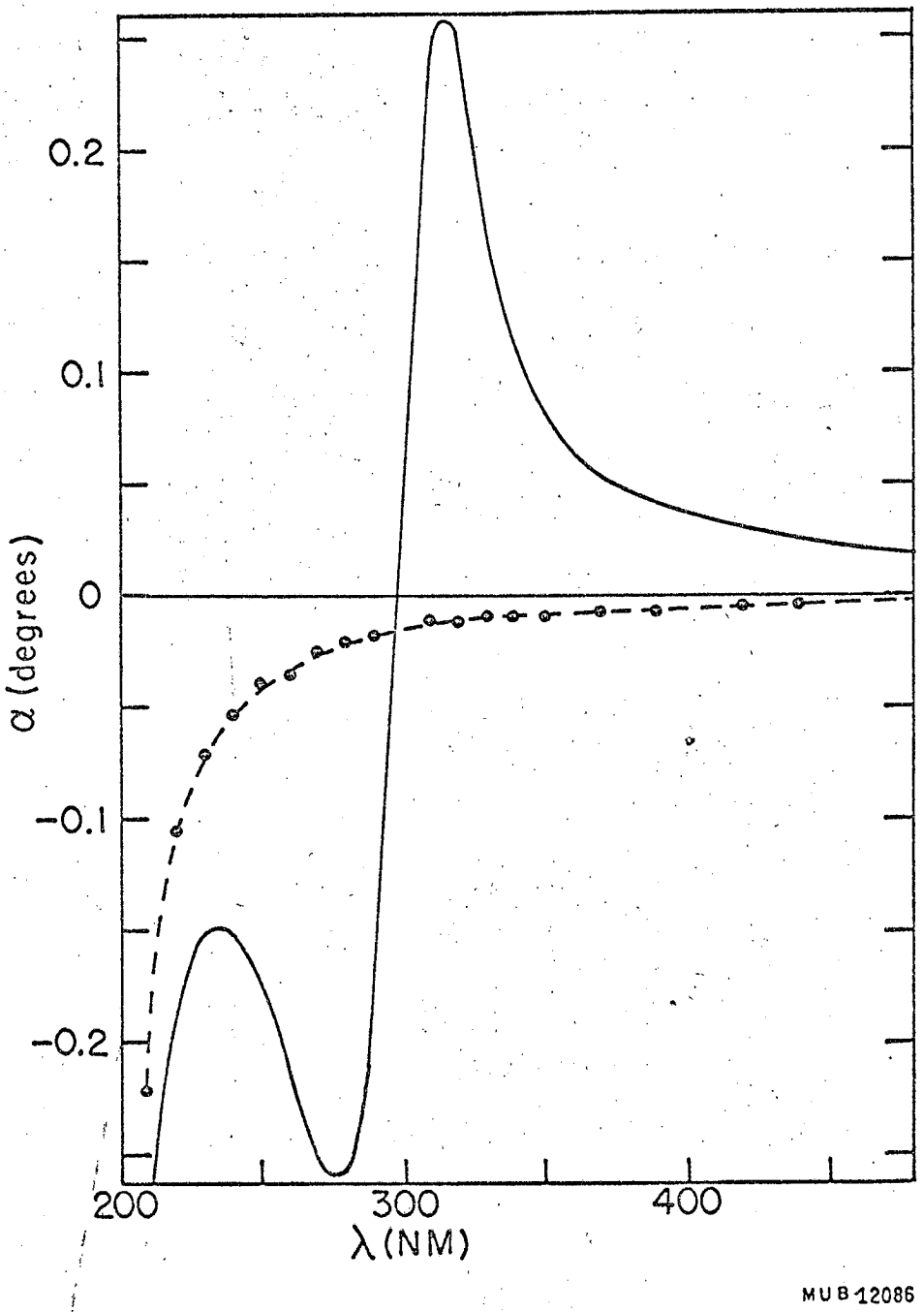

Figure II-4. Measured ORD of isoandrosterone, 1.05 mg/ml, 100% ethanol, 1 cm cell, solid line ____. Measured minus calculated ORD (due to 295 NM CD band, shown in Figure II-3), ● - - - ● - - - .

different samples were transformed to ORD and gave very good agreement with the measured ORD at all wavelengths using the steroid calibration from the 300 nm region.

A sample that shows CD signals from approximately 1000 nm to the far UV is the copper protein, cerruloplasmin, that was mentioned in Chapter I (p. 33). The visible and near IR portion of the CD and absorption are shown in Figure II-5. Cerruloplasmin has a relatively small CD and ORD in the visible and near IR, so measurement uncertainties are relatively large (± 5%). There is a very strong UV ORD tail from the protein, similar in shape to poly-L-glutamic acid helix (Chapter I, p. 15), but somewhat smaller on a rotation per residue basis. However, the strong UV ORD tail can, in this case, be independently measured on the decolorized protein (the copper is reduced with, e.g., dithionite) that has no visible and near IR absorption or CD. The difference between the decolorized protein ORD and the colored protein ORD gives the contribution of the visible and near IR copper bands to the ORD. (It was shown in Chapter I, p. 33, that the protein ORD does not change when the copper is reduced.) If this were a larger signal it would be an ideal case where all the CD bands that contribute to an observed ORD curve can be measured. The Kronig-Kramers transform of the measured CD (Figure II-5) is shown in Figure II-6 compared to the measured ORD. The agreement is very good since the curves match to well within the noise level of the measurements (ORD known to about ± 1 millidegree). The relatively large discrepancy in the 350 nm region is due to the large protein rotation in this region and the very small difference between the colored and decolorized protein (the well known small difference in two large numbers problem).

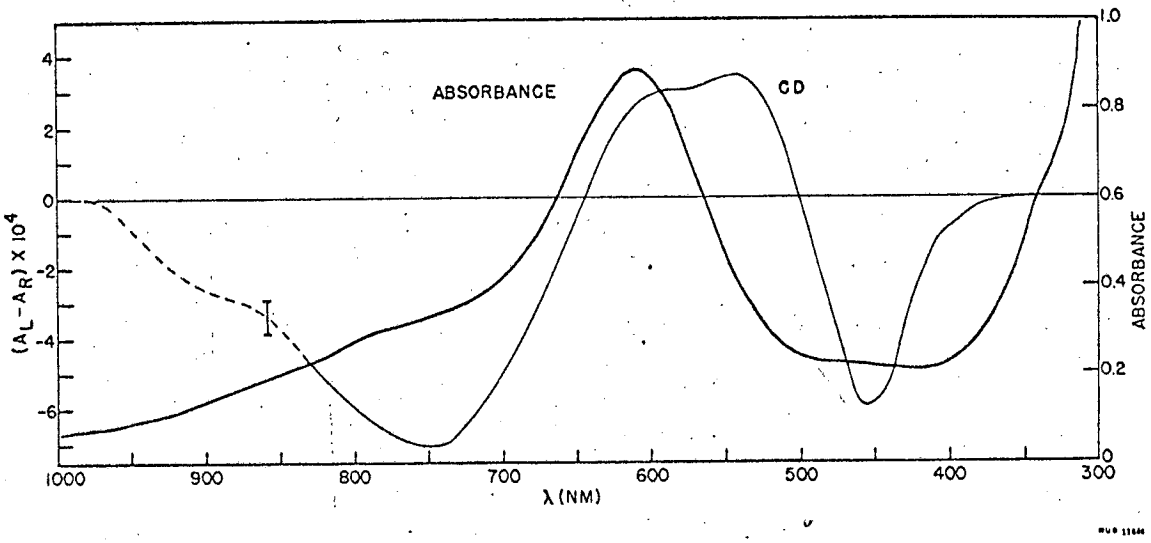

Figure II-5. Absorption (dark curve) and CD (light curve) of oxidized human cerruloplasmin, 41 µg Cu/ml, pH 7.0 (0.061 M sodium phosphate), 1% sodium chloride, 1 cm cell.

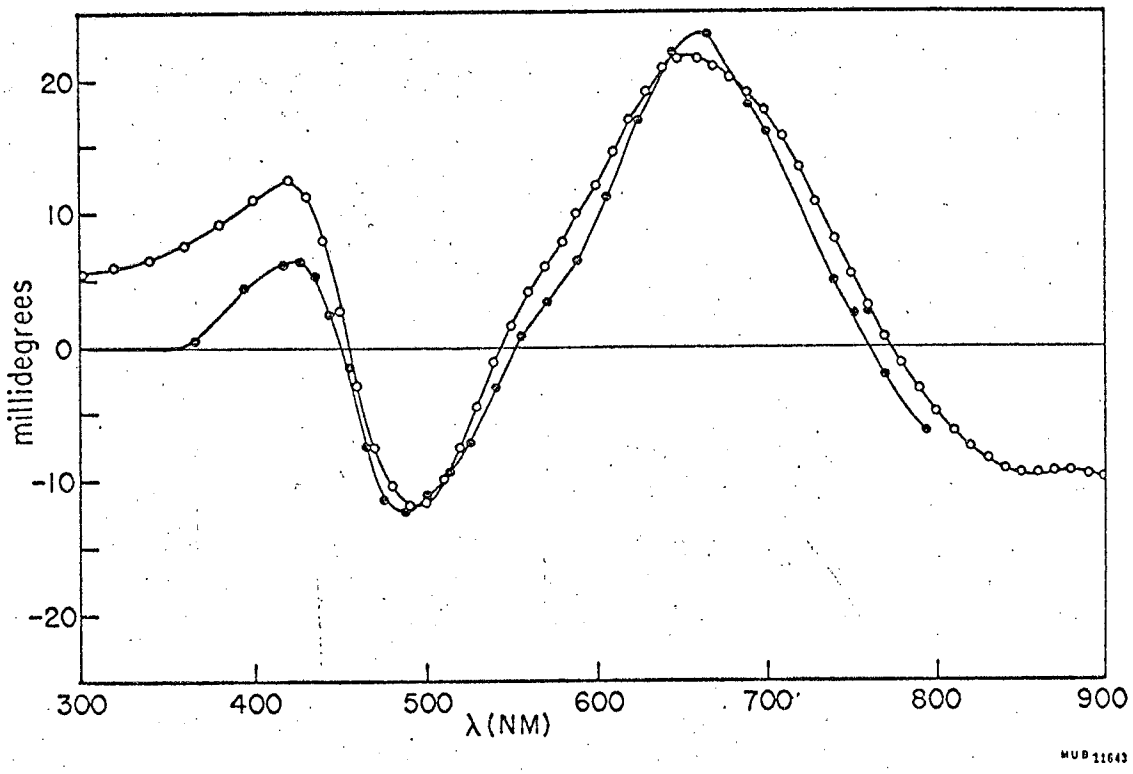

Figure II-6. ORD of(oxidized-reduced) human cerruloplasmin, 41 µg Cu/ml, pH 7.0 (0.061 M sodium phosphate, 1% sodium chloride) 1 cm cell, o—o—o—o . ORD of same solution calculated from the CD of Figure II-5 o— o — o— .

Many other experimental ORD curves were compared to the calculated ORD curves derived from the CD in this way. All comparisons agreed to within experimental error; some of the stronger signals gave beautiful fits, but none covered such a wide wavelength range as the cerruloplasmin example. All the experimental evidence taken together indicates that CD sensitivity is constant with wavelength, although no single satisfactory test of this question was found.

Multiple spectrum averaging

As we mentioned at the outset, the useful range of the instrument is about 220 nm to 1100 nm. The noise level varies with wavelength at constant spectral band width and is about $\pm 1 \cdot 1^{5}$ OD units from 250 nm to 750 nm at 1 nm spectral band width and a 1-second time constant. The noise level increases toward the outer wavelength limits because of decreasing light source intensity in the ultraviolet and decreasing detector efficiency in the near infrared.

An increase in signal/noise was required for some of the measurements, and it was found that simply increasing the time constant was not entirely satisfactory. For white noise (constant noise level vs. frequency) the root mean square noise level is expected to decrease as $1/\sqrt{\tau}$, where τ is the filter time constant. An increase in time constant did not attenuate the noise as strongly as expected for white noise. Apparently the noise amplitude in the system increases strongly at low frequency (so-called 1/f noise or "pink" noise). A large sensitivity increase was obtained, however, by averaging many fairly rapid scans (0.5-2 min) of the CD spectrum using an on-line digital measuring device. This approach is useful because the signal adds in with each

scan of the spectrum, but the average value of the random noise is zero and the noise tends to average out (Klein and Barton, 1963). For white (constant amplitude vs. frequency) noise, the signal to noise increases as the square root of the number of spectra averaged. We actually found a somewhat more rapid increase in signal to noise up to an improvement of 10:1; presumably the rapid increase in signal/noise is due to the peculiar noise spectrum of the xenon arc. The signal/noise improvement rate dropped after 10:1, and 20:1 improvement seems to be nearly the practical limit. Multiple scans reduce the 250-750 nm noise level to about $\pm 1 \cdot 10^{6}$ OD units in 1 to 2 hours, and a correspondingly large improvement is found at the extremes of wavelength where the noise was higher.

The averaging device employed was a 1024 channel Nuclear Data ND 800 Enhancetron. A feature of this device is its ability to digitize spectra in both the forward and backward direction. The Cary 14 monochrometer used had only a few Å backlash in the wavelength drive mechanism, which is completely negligible for most spectra. Spectra were recorded "forward" from long wavelength to short and then "backward" from short to long wavelength. The Enhancetron time base and logic signals were used to control the Cary 14 scan motor. The control circuit is shown in Figure II-7. Two relays normally control the Cary 14 scan motor. A double pole triple throw switch (labeled transfer switch in Figure II-7) was added in the scan control box of the Cary 14 to bypass the normal scan relays and the relevant connections were brought out to a similar set of external relays. These external relays could be controlled by the Enhancetron (Etron) logic signals through the buffer circuits (up/down control, scan/stop

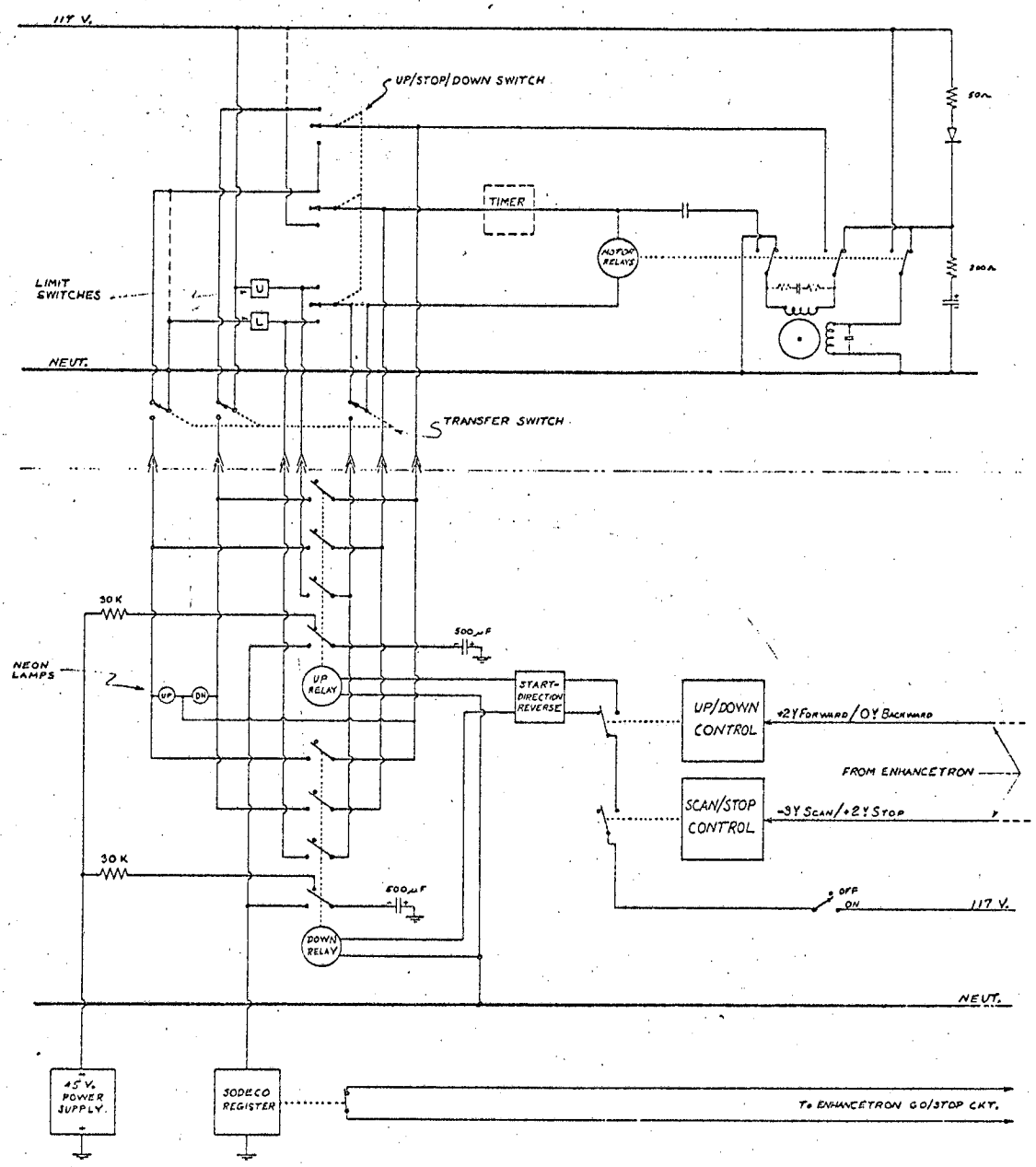

Figure II-7. Schematic diagram of the Cary monochromator external scan control. The parts above the —— -- —— — line are internal to the standard Cary 14 scan control, internal wires marked with a long dashed line, - - - , were removed. The short dashed lines represent ganged throws of switches or relays.

control) detailed in Figure II-8. When the Etron was put in the measure mode, a signal called "go" went positive. The "go" signal was used to drive a small (Sigma 4F - 8000 LG-S-1) relay through a transistor buffer (see Figure II-8). The small relay closed one of the larger scan control relays if a manual enable switch (scan) was on. The initial scan direction could be selected by an up/down switch. The monochromator would scan in the initial direction until the Enhancetron reached the last channel (512 or 1024). At the last channel (CHI) an Etron buss (forward-backward buss) would change; this buss (through a similar buffer transistor and relay shown in Figure II-8) was used to enable the other scan control relay, reversing the scan. This process is repeated, scanning the same region of the spectrum many times. At the beginning of each scan one pole of the external scan relay was used to subtract a count from a preset Sodeco (see Figure II-7) counter. When the preset number of scans was reached, the Sodeco counter closed a set of contacts which stops the scanning process by dropping the Stop SW buss of the Enhancetron. After several hundred scans (more than normal) the "turn around" wavelengths were the same to a few Angstroms. The narrowest CD spectra normally studied were about 100 Å wide at Half-height. For the narrowest spectra many passes were done, scanning down in wavelength only and winding wavelength back manually to the same starting point for every scan. No difference was found comparing spectra recorded in one direction to those done by the forward-backward procedure.

A Philbrick P65AU amplifier was used as a gain of one differential amplifier to convert the floating, double-ended output of the PAR to a single-ended input of the ND 800 Enhancetron as shown in Figure II-2.

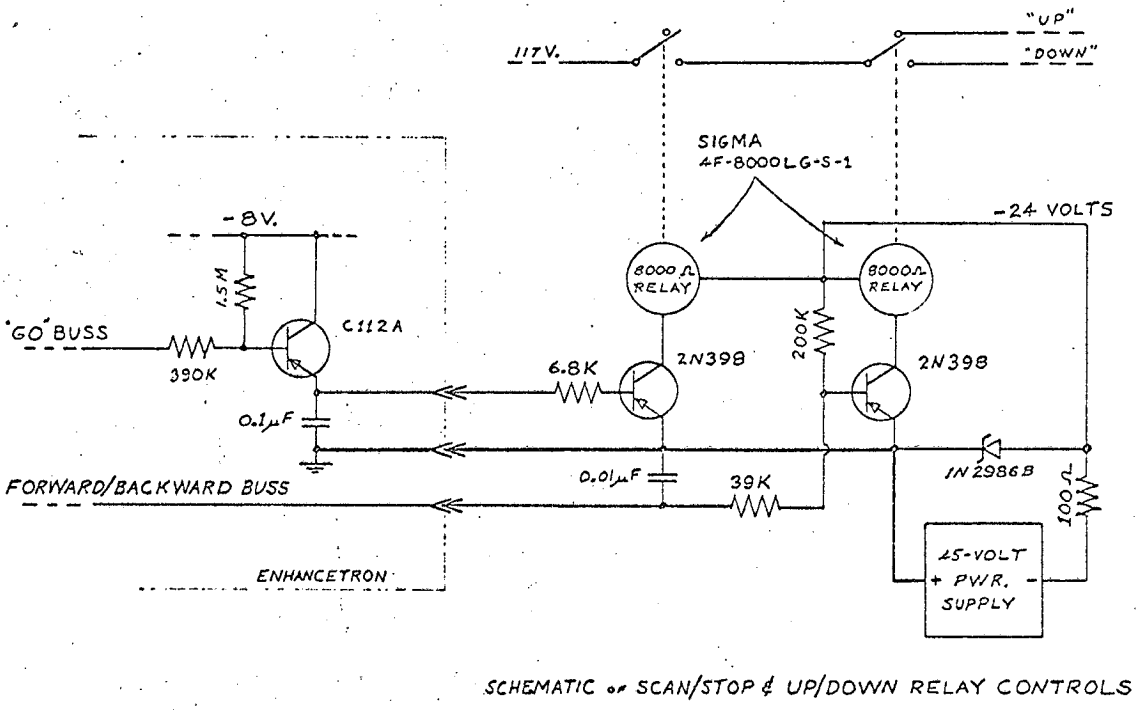

SCHEMATIC OF SCAN/STOP & UP/DOWN RELAY CONTROLS

MUB-11222

Figure II-8. Buffer circuits used between the Nuclear Data ND 800 Enhancetron logic and the external monochromator scan control shown in Figure II-7.

The analog to frequency converter in the Enhancetron is quite sensitive and memory capacity is limited to $2^{14} - 1$ counts, so a 10:1 attenuation was used before the Enhancetron input. The averaged spectra could be displayed on an oscilloscope and plotted on an x-y plotter.

Absorption spectra were recorded using a Cary 14 spectrophotometer. In the case of scattering samples the Model 1462 Scattered-Transmission Accessory was used. Optical rotatory dispersion spectra were obtained using a Cary 60 instrument modified with an R-136 Hamamatsu red-sensitive photomultiplier.

Materials

The preparation of chlorophyll a, chlorophyll b and bacteriochlorophyll are described elsewhere (Sauer, Lindsay Smith and Schultz, 1966). Carbon tetrachloride was reagent grade and was used without purification.

The suspension of microcrystalline chlorophyll a was prepared by adding isooctane to a small sample of the solid chlorophyll. After vigorous stirring, the suspension was spun in a clinical centrifuge at top speed for 5 min., and the supernatant suspension was used directly. No noticeable settling occurred during the half-hour period of measurement.

Chromatophores from Rhodospirillum rubrum and Rhodopseudomonas spheroides were obtained by washing 5-day old cultures free of growth medium, followed by sonication for 3 min. at 0°C with a Biosonik oscillator. Fragments sedimenting between 40,000 g (30 min) and 180,000 g (50 min) were washed and resuspended in 0.05 M phosphate buffer, pH 7.5.

Barley was grown from seed in a phytotron under controlled illumination and temperature and was harvested about 3 weeks after germination. The normal (Lyon) and the mutant strain (Chlorina 2), which is missing

chlorophyll b (Highkin and Frenkel, 1962) were grown under identical conditions and harvested at the same time. Chloroplasts were isolated from the homogenized leaves essentially by the procedure of Park and Pon (1961). Sonication of the chloroplast suspension was followed by isolation of a fraction sedimenting between 9000 g (10 min) and 110,000 g (30 min), resuspension in 10^{-3} M phosphate buffer, pH 7.5, and clarification at 9000 g (10 min).

C. Chlorophyll Dimers in Solution

The apparent molecular weight of chlorophyll a (Aronoff, 1962), chlorophyll b (Katz, Closs, Pennington, Thomas and Strain, 1963) and bacteriochlorophyll (Sauer and Lindsay Smith, 1965) increases with concentration in nonpolar solvents. Lavorel (1957) and Weber and Teale (1958) first reported chlorophyll a dimerization in hydrocarbon solvents based on fluorescence measurements on concentrated solutions. Chlorophyll a, chlorophyll b and bacteriochlorophyll appear to obey Beer's law very closely in most solvents. However, in nonpolar hydrocarbon and halocarbon solvents the absorption spectra are strongly concentration dependent.

Analysis of the absorption data of the three chlorophylls in the concentration range of 10^{-6} M to 5.10^{-4} M in carbon tetrachloride supports a simple monomer-dimer equilibrium (Sauer, Lindsay Smith and Schultz, 1966). Figure II-9 shows a concentrated minus dilute solution difference spectrum for bacteriochlorophyll and the calculated monomer and dimer absorption spectra. The monomer spectra in dilute carbon tetrachloride solutions are very similar to those in ether or acetone at all concentrations. The dimer absorption spectra of all three chlorophylls show a splitting of the long wavelength absorption band

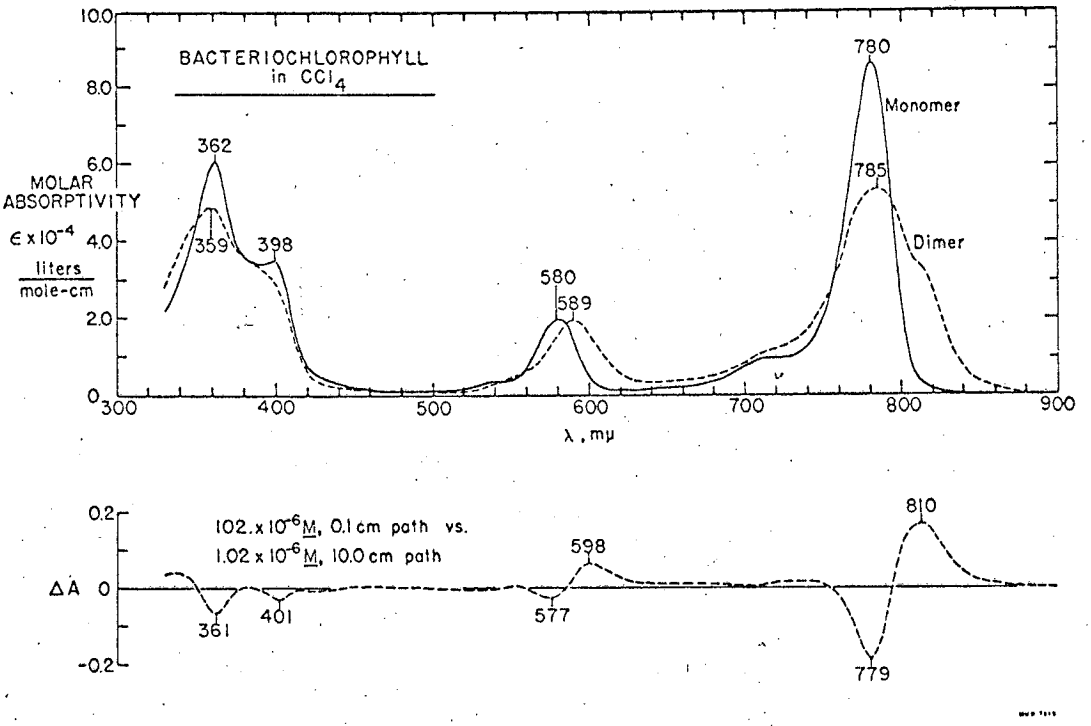

Figure II-9. Absorption spectra of bacteriochlorophyll in carbon tetrachloride. The lower dashed curve is a difference spectrum measured between solutions at different concentrations with the pathlength inversely proportional to concentration. Upper curves calculated for pure monomer (solid) and pure dimer (dashed). After Sauer, et al. (1966).

(at about 780 mμ in bacteriochlorophyll in Figure II-9) with appearance of a long wavelength shoulder (Sauer et al., 1966). All three chlorophylls have dimerization constants ($K_d = D/M^2$) near 10^4 M^{-1} in carbon tetrachloride.

We will be concerned with the CD spectra of the dimers found by Sauer et al. (1966), so we will summarize some of the properties of these aggregates. The chlorophyll species involved in the monomer-dimer equilibrium under the conditions of the Sauer et al. (1966) experiments are almost certainly the chlorophyll monohydrate:

$$2\ \text{Chl} \cdot H_2O \rightleftharpoons (\text{Chl} \cdot H_2O)_2$$

The presence of water has not been directly shown as yet, but it seems to rationalize many observations. Water must be present during preparation of crystalline chlorophyll (Jacobs, Vatter and Holt, 1954), and these "wet" crystals are used to prepare solutions for optical work. Infrared measurements (Katz et al., 1963; Sidarov and Terenin, 1960) give evidence for bound water (to the central magnesium) in similar solvents. A previously unassigned NMR peak near 0 cps (from TMS) in bacteriochlorophyll (Sauer et al., 1966) appears where water bound to the central magnesium would be expected. In rigorously dried solvents (e.g., benzene), the aggregation appears to occur at much lower concentrations. Livingston, Watson and McArdle (1949) found essentially complete aggregations of chlorophyll a at 10^{-6} M in rigorously dry benzene. Aronoff's (1962) measurements of chlorophyll a in benzene (with no rigorous drying) indicates essentially no aggregation at the low concentrations used by Livingston et al. (1949).

Livingston et al. (1949) found that small amounts of water or other nucleophiles broke up the aggregates in the rigorously dry benzene and

that the equilibrium of the dry aggregate with these nucleophiles is complex, involving higher aggregates than dimers. Aggregate spectra in rigorously dry hydrocarbons at low concentrations have been reported by Fernandez and Becker (1959), although these authors made a different interpretation of their data.

Figure II-10 shows the chemical structure of bacteriochlorophyll, with the atoms labeled in a standard way. IR measurements in chlorocarbon solvents can best be interpreted on the basis of dimers formed between a carbonyl of one molecule (primarily the ketone on carbon 9 in Figure II-10) with the central magnesium of the second (Katz et al., 1963; Anderson and Calvin, 1964). This interpretation has been confirmed by the direct observation of the Mg - O bond vibration in the aggregate in the far infrared at 310 cm^{-1} (Boucher, Strain and Katz, 1966). NMR measurements also show aggregations of the three chlorophylls and indicate that the ring V carbonyl region is involved. The molecular weight and NMR work indicate that the chlorophyll b carbonyl on ring II (at position 3 in Figure II-10) is involved in trimer formation at higher concentrations (Closs, Katz, Pennington, Thomas and Strain, 1963). The NMR on bacteriochlorophyll also seems to indicate some trimer at the highest concentration (Sauer et al., 1966) involving the acetyl group in ring I (position 2 in Figure II-10).

The aggregations observed by Livingston et al. (1949), by Katz et al. (1963) and Closs et al. (1963) all require the presence of magnesium in the center of the chlorophyll ring. It can be seen by inspection of the data of Closs et al. (1963) that the aggregation in the absence of the magnesium is at least 100-fold less than for the magnesium complexes.

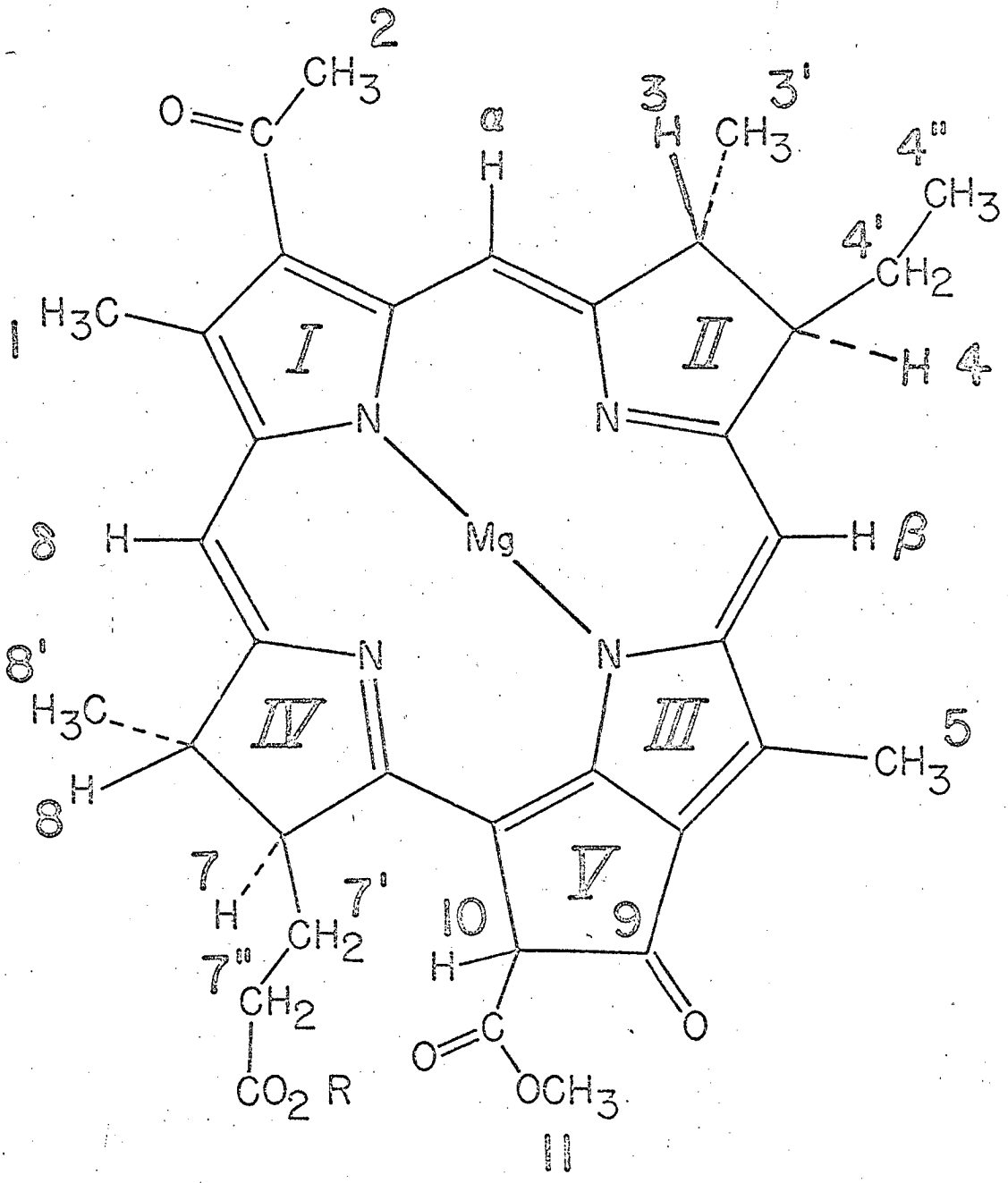

Figure II-10. Bacteriochlorophyll structure. Chlorophyll a and b have ring II unsaturated and are missing hydrogens 3 and 4. Chlorophyll a has a vinyl group at position 2, replacing the acetyl and chlorophyll b further replaces the methyl at 3' with an aldehyde.

A tentative picture emerges from the previous work on the in vitro aggregation of the three chlorophylls: (1) All three chlorophylls seem to form similar dimers (Sauer et al., 1966)(with $K_d \approx 10^4$ M^{-1}) involving a bond between the central magnesium and the ring V carbonyl (Katz et al., 1966). (2) Trimers may form in very concentrated solutions of chlorophyll b (Katz et al., 1963, and Closs et al., 1963) and bacteriochlorophyll (Sauer et al., 1966). (3) The above conclusions apparently obtain only with the chlorophyll monohydrates and that rigorous drying of solvents leads to higher aggregation at low concentrations (Livingston et al., 1949). (4) Addition of nucleophiles such as alcohol, water or pyridine competes for magnesium with the chlorophyll carbonyl and breaks the dimer (or trimer) (Sauer et al., 1966; Closs et al., 1963). Sauer and Ku (1966) have shown that the dimer-nucleophile titration for chlorophyll a in carbon tetrachloride can be described by a simple equilibrium involving dimers, monomers and chlorophyll nucleophile complexes. (5) These aggregation effects are independent of the phytyl group (a 20-carbon side chain labeled R in Figure II-10) (Closs et al., 1963).

Optical properties of chlorophyll dimers

Chlorophyll a, chlorophyll b and bacteriochlorophyll in polar solvents show an unmeasurably small circular dichroism. An extremely weak monomer optical activity can be measured by the more sensitive ORD method (see Appendix I), although the signals are close to limit of ORD sensitivity and reproducibility. In carbon tetrachloride, a solvent that favors dimers, increasing concentration results in enhanced ORD (Sauer, 1965) and CD. Figure II-11 shows the ORD and absorption of a fairly concentrated chlorophyll a solution (about 65% dimer) and the ORD and

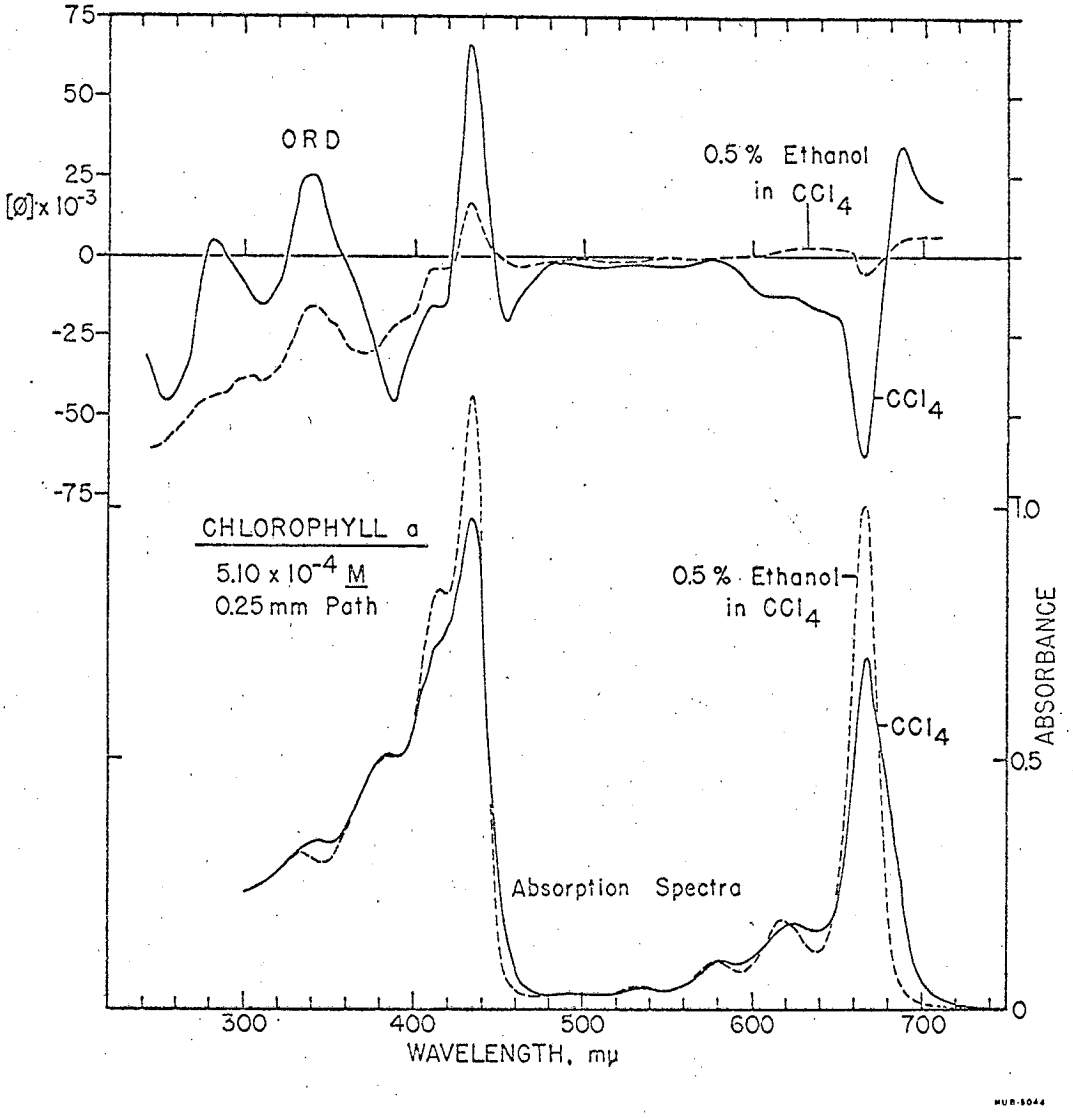

Figure II-11. Absorption and ORD spectra of chlorophyll a in carbon tetrachloride, 5.1×10^{-4} M, 0.25 mm path and of the same solution after addition of 0.5% (v/v) ethanol. After Sauer (1965).

absorption that results when the dimer is broken up with ethanol. The monomer has very small ORD (the dimer is not quite 100% absent in Figure II-11) and the long wavelength shoulder on the absorption disappears. All three chlorophylls behave similarly.

The circular dichroism and absorption spectra of chlorophyll a, chlorophyll b and bacteriochlorophyll solutions in carbon tetrachloride containing about 85% dimer are shown in Figures II-12, 13 and 14. Precise CD measurements on dilute solutions, free of aggregates, have not yet been possible in carbon tetrachloride because of decomposition of the dilute chlorophyll solutions during the prolonged time of measurement. Measurements on dilute solutions can be made rapidly, to avoid decomposition, but with a resulting increase in noise level. The dilute solutions show essentially no dichroism, with an upper limit of about 5% of the concentrated (dimer) signals. This observation is consistent with ORD measurement in dilute carbon tetrachloride that the monomer ORD is at most 5% of the dimer (Sauer, 1965). For our purposes, the CD of all the chlorophylls in carbon tetrachloride is entirely due to chlorophyll-chlorophyll interactions with a negligible contribution from monomers.

We can, with this simplification, calculate the molar circular dichroism of the dimers from the concentration of the solution, the known dimerization constant (Sauer et al., 1966), and the observed circular dichroism. We must be careful that there is not significant contribution from trimers in the chlorophyll b and bacteriochlorophyll case. More recent measurements, shown later, show that the bacteriochlorophyll CD in Figure II-14 is distorted appreciably by trimers,

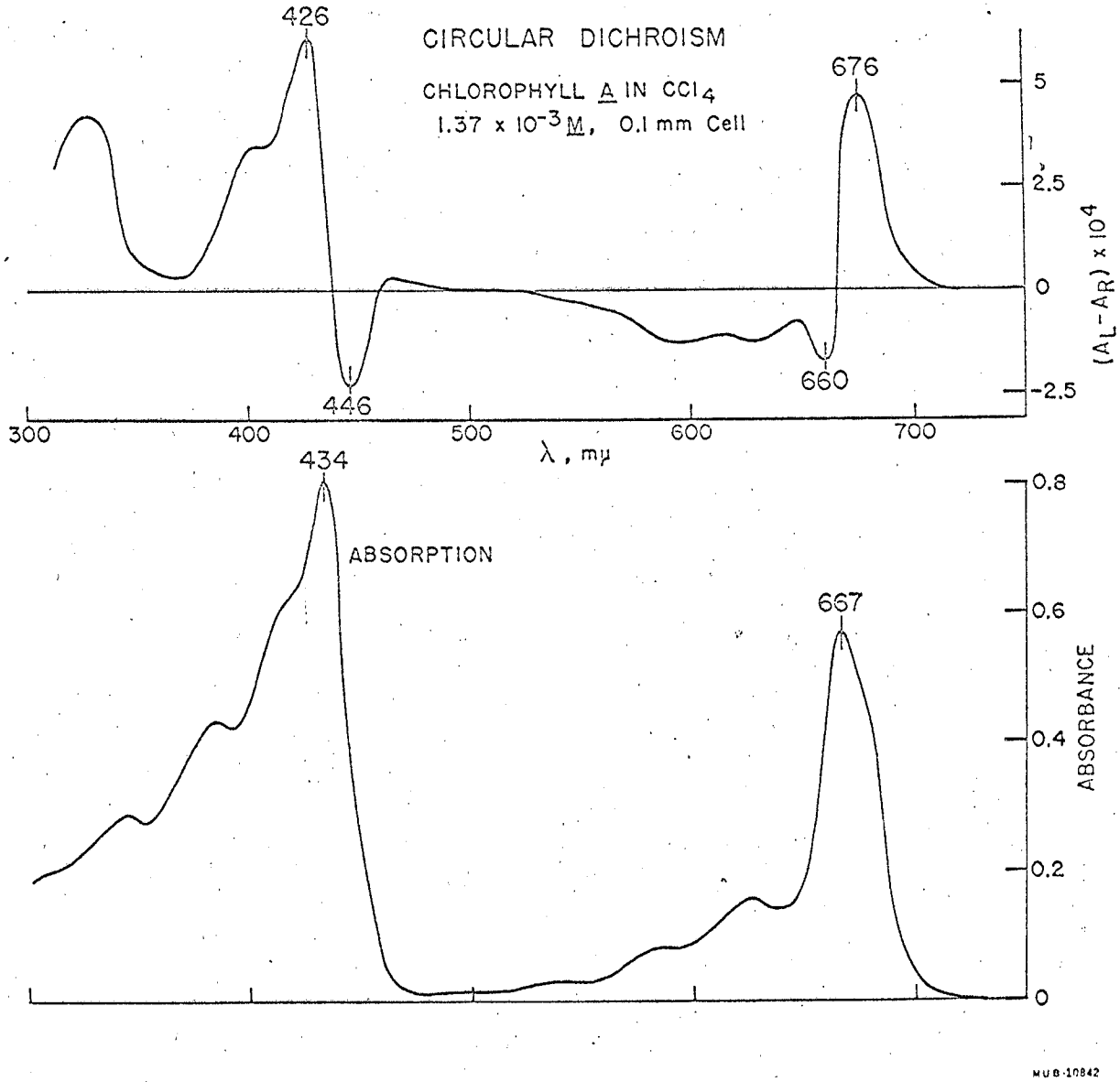

Figure II-12. Absorption and CD spectra of chlorophyll a dimers in carbon tetrachloride.

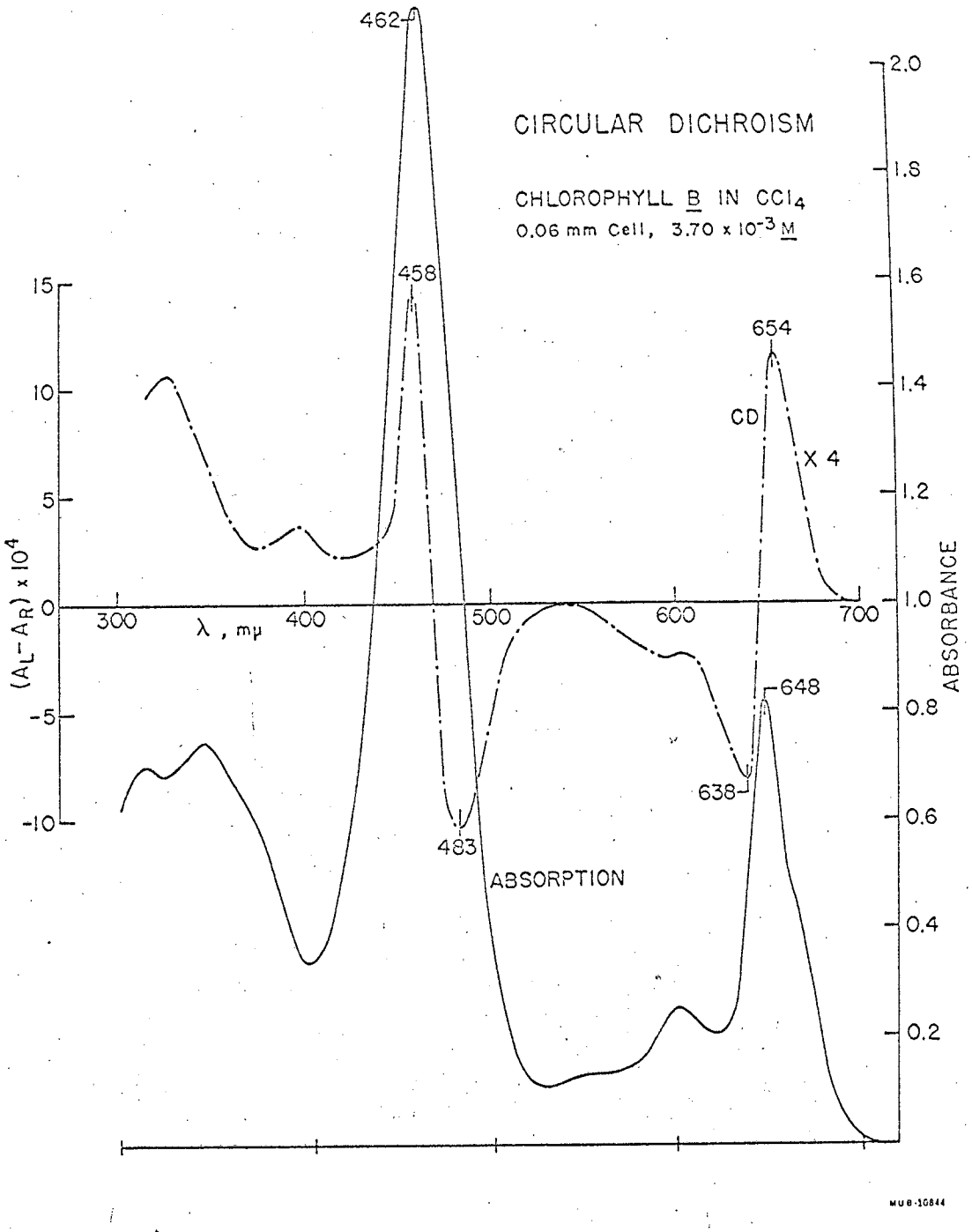

Figure II-13. Absorption and CD spectra of chlorophyll b dimers in carbon tetrachloride. The CD spectrum show at wavelengths longer than 530 mμ has been multiplied by 4.0.

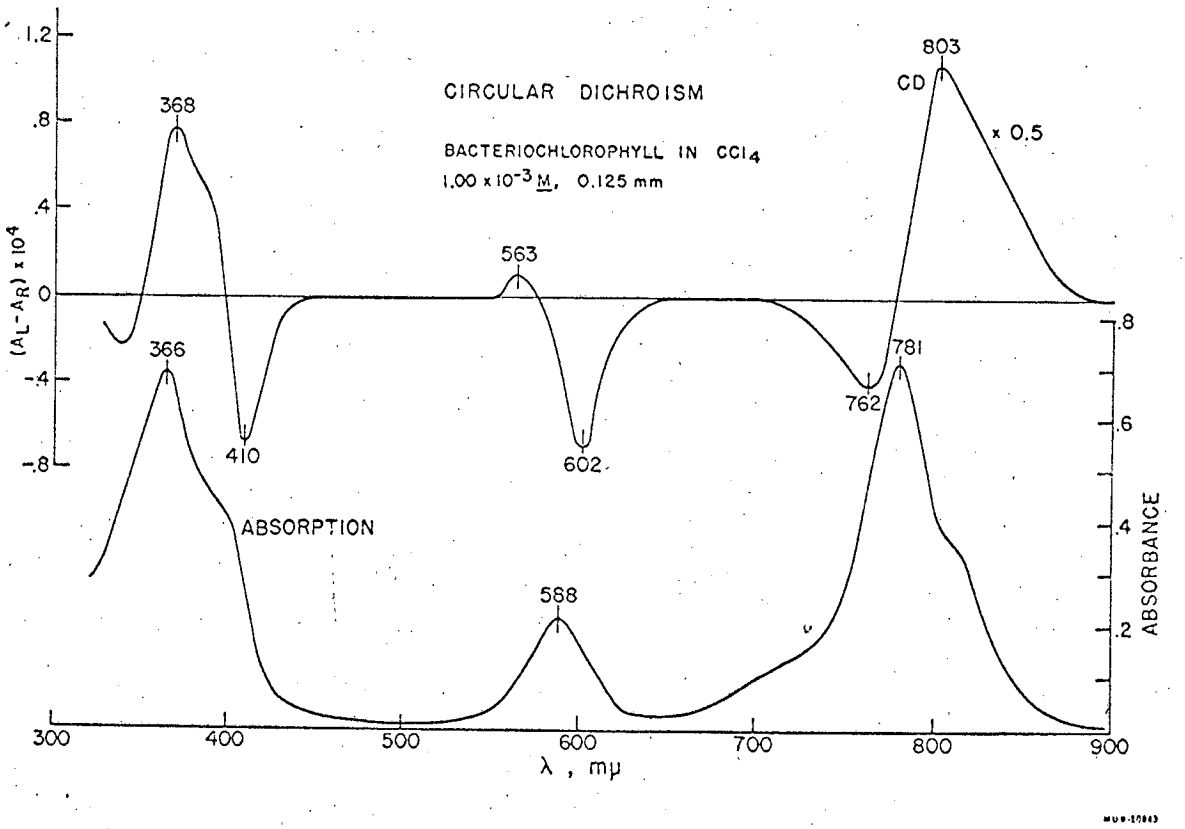

Figure II-14. Absorption and CD spectra of bacteriochlorophyll dimers in carbon tetrachloride. The CD spectrum shown at wavelengths longer than 700 mμ has been multiplied by 0.5.

which contributes on the long wavelength side of the 803 mμ positive CD peak and the 602 mμ negative CD peak.

The chlorophyll dimers give large circular dichroism signals in the relatively isolated far red band (at 650 mμ for chlorophyll b, 680 mμ for chlorophyll a and 780 mμ for bacteriochlorophyll), as well as in the more complex Soret band (in the 400 mμ region), which is a composite of two nearby electronic transitions. We shall concentrate, initially, on interpreting the CD of the far red bands of these compounds. All three chlorophyll dimers show qualitatively very similar CD spectra. This is consistent with all the evidence, from NMR, IR, and absorption measurements quoted earlier, that the three dimers have very similar structure. All three chlorophyll dimers show a double circular dichroism spectrum that is positive on long wavelengths and reverses sign close to the center of the absorption band.

Discussion of dimer optical properties

The splitting of the absorption and double CD spectra of the dimers can be understood in terms of the resonance exciton interaction between the identical monomers in the dimers (Levinson, Simpson and Curtis, 1957; Tinoco, 1964; Tinoco, Woody and Bradley, 1963). Similar exciton interactions have been seen in aggregates of organic dyes (Bergman and O'Konski, 1963), molecular crystals (Davydov, 1962; McClure, 1959), helical polypeptides (Tinoco, Halpern and Simpson, 1962), and stacked polynucleotides (Warshaw, Bush and Tinoco, 1965). The optical properties of the aggregates depend upon the optical properties of the monomers in the aggregate and to the geometry of the aggregate (Tinoco, 1963). We will see that analysis of the absorption and CD spectra of the chlorophyll dimers, in principle,

will allow determination of the geometry of the dimer in solution. This is an interesting possibility from a physical chemistry point of view, and is all the more useful in regard to the chlorophyll interactions in plants and photosynthetic bacteria. The treatment of dimer structure that follows makes several simplifying assumptions and is necessarily preliminary. Most of these assumptions are not fundamental but merely convenient for practical calculations. The simplified theory allows us to propose a structure for the chlorophyll dimer, and at the end we will discuss tests of the assumptions used.

General theoretical approach to dimer structure

The theory of molecular electronic absorption is well known and is treated in many books on the subject (e.g., Sandorfy, 1964; Kauzman, 1957). The detailed theory of optical activity is more recent and is perhaps best treated by Moffitt and Moscowitz (1959). The most useful theoretical development for our purpose is a body of work by Tinoco and coworkers on the optical properties of polymers of identical subunits (e.g., Tinoco, Woody and Bradley, 1963; Bush, 1965). The theory has been summarized in a form specifically for dimers by Tinoco (1963).

The absorption and circular dichroism of molecules can be expressed in terms of the electric dipole transition moment, $\underset{\sim}{\mu}_{oa}$, and the magnetic dipole transition moment, $\underset{\sim}{m}_{oa}$ (e.g., Kauzman, 1957). The electric dipole transition moment $\underset{\sim}{\mu}_{oa}$, is a vector that describes the direction and magnitude of electronic charge distribution change during a transition from electronic state o to state a. The magnetic dipole transition moment, $\underset{\sim}{m}_{oa}$, similarly describes the direction and magnitude of the magnetic moment change during the o to a transition. The absorption

intensity of the o to a transition is proportional to the dipole strength D_{oa}, which is defined:

$$D_{oa} = (\mu_{oa})^2 = 9.16 \cdot 10^{-39} (\text{cgs}) \int_{\nu_1}^{\nu_2} \frac{\varepsilon(\nu)}{\nu} \, d\nu \qquad \text{II-(13)}$$

where $\varepsilon(\nu)$ is the observed extinction coefficient at frequency ν, and ν_1 and ν_2 are the limits of the region where the o → a transition has measurable absorption. The sign and magnitude of the CD (or ORD) due to the o to a transition is proportional to the rotational strength R_{oa}, which is defined as:

$$R_{oa} = \text{Im} \, (\underset{\sim}{\mu}_{oa} \cdot \underset{\sim}{m}_{oa}) = 0.696 \cdot 10^{-42} (\text{cgs}) \int_{\nu_1}^{\nu_2} \frac{\Delta\varepsilon(\nu)}{\nu} \, d\nu \qquad \text{II-(14)}$$

where Im means the imaginary part of the scalar product of the two vectors and $\Delta\varepsilon$ is the observed CD (difference in extinction coefficient in left and right circular light).

The combination of the two monomers into a dimer perturbs the electronic distribution during the electronic transition and thus affects the absorption and circular dichroism. The general approach is to express the absorption and CD of the dimer in terms of the measured absorption and CD of the monomer and the geometry of the dimer. The first approximation to the perturbation caused by dimerization is the resonance (exciton) interaction of the monomer electronic transitions of equal energy.

Consider monomers 1 and 2 with unperturbed wavefunctions ϕ_{io} and ϕ_{ia} for monomer i (i=1,2) in the ground (o) and excited state (a) respectively. For the first approximation we neglect molecular vibrations (which can be included later, Young, 1966). The ground state of the dimer is approximately given by: $\psi_o = \phi_{10}\phi_{20}$. From simple degenerate

perturbation theory (e.g., Bohm, 1951) the excited state is the symmetric (+) and antisymmetric (-) combination of the degenerate states with excitation on monomer 1, $\phi_{1a}\phi_{2o}$, and with the excitation on monomer 2, $\phi_{1o}\phi_{2a}$.

$$\psi_{A\pm} = 1/\sqrt{2}\ (\phi_{1a}\phi_{2o} \pm \phi_{1o}\phi_{2a}) \qquad \text{II-(15)}$$

The $\pm$ states will, in general, have different energies due to the coulomb interactions between the electrons on the two monomers. If we think simply of the transition as creating a dipole in the monomer of interest the $\pm$ combinations are the additions and subtractions of these two dipoles to form a higher energy state and a lower energy state:

$E_{\pm} = E_a \pm V_{12}$

where E_a is the energy of the unperturbed state and V_{12} is the coulomb potential energy between the two excited monomers.

$$V_{12} = (\phi_{1a}\phi_{2o} \mid \sum_{i,j} \frac{e^2}{r_{ij}} \mid \phi_{1o}\phi_{2a}) \qquad \text{II-(16)}$$

where the sum is over i and j, the electrons of monomer 1 and monomer 2, respectively, r_{ij} is the distance between the electrons and e is the electronic charge. If we treat the charge distribution change during the electronic transition simply as a point dipole, neglecting the higher terms in a multipole expansion (not essential, but a useful starting point), then V_{12} is just the dipole interaction potential between the two monomer transition dipoles.

$$V_{12} = 1/R^3(\underset{\sim}{\mu}_{1oa}\cdot\underset{\sim}{\mu}_{2oa} - 3(\underset{\sim}{R}_{12}\cdot\underset{\sim}{\mu}_{1oa})(\underset{\sim}{R}_{12}\cdot\underset{\sim}{\mu}_{2oa})/R^2) \qquad \text{II-(17)}$$

where $\underset{\sim}{R}_{12} = \underset{\sim}{R}_1 - \underset{\sim}{R}_2$, the vector distance between the center of monomer 1 and monomer 2, and $R = |\underset{\sim}{R}_{12}|$.

As a first approximation, we neglect the magnetic dipole moment of the chlorophyll monomer. This simplifies the expression for the rotational strength considerably. This approximation is justified because the basic chlorin or tetrahydroporphyrin skeleton has zero magnetic transition dipole moment for the allowed electronic transitions (Eyring, Walter and Kimball, 1944). The asymmetric carbon atoms that destroy the molecular plane as a symmetry plane are aliphatic substituents and only weakly affect the pi orbital system of the chlorophylls. Thus, the magnetic dipole transition moment that they induce is very small. For our purpose the chlorophyll molecule is considered as being optically inactive to a first approximation. We will give a slightly more detailed argument on this point later. With this approximation the exciton contribution to the rotational strength of the dimer may be written in terms of the electric dipole transition moments of the monomer (Tinoco, 1963):

$$R_{\pm} = \mp(\pi \nu_o/2c)(\underset{\sim}{R}_{12} \cdot \underset{\sim}{\mu}_{1oa} \times \underset{\sim}{\mu}_{2oa}) \qquad \text{II-(18)}$$

where ν_o is the unperturbed absorption frequency at the absorption band maximum and $\underset{\sim}{R}_{12}$ is defined above. The dipole strength can be written:

$$D_{\pm} = D_o \pm \underset{\sim}{\mu}_{1oa} \cdot \underset{\sim}{\mu}_{2oa} \qquad \text{II-(19)}$$

where D_o is the unperturbed monomer dipole strength. If we define an angle, β, between the transition moments, the dipole strength can be written:

$$D_{\pm} = D_o(1 \pm \cos \beta) \qquad \text{II-(20)}$$

The transition frequencies in cm^{-1} are:

$$\nu_{\pm} = \nu_o \pm V_{12}/hc \qquad \text{II-(21)}$$

where h is Plank's constant and c is the velocity of light. Some consequences of these zero order equations are that the total intensity of

the dimer absorption is equal to twice the monomer absorption, $D_+ + D_- = 2D_o$ and the exciton contribution to the CD is symmetrical above and below zero, $R_+ + R_- = 0$.

In fact, Sauer et al. (1966) found that the intensity of the absorption is not conserved in going from the chlorophyll monomers to the dimers in a single absorption band (e.g., a 14.5% increase in absorption of the red band in the bacteriochlorophyll dimer compared to the sum of the monomers). The CD is not symmetrical above and below zero (Figures II-12, 13 and 14) for the chlorophyll dimers. The transition of interest of one monomer interacts not only through the degenerate resonance exciton effect discussed above, but also with the anisotropic polarizability and charge density presented by the neighboring monomer (Devoe and Tinoco, 1962; Tinoco, 1960). We call these interactions with the anisotropic polarizability and charge density nondegenerate, because they can be represented as interactions between transition moments off resonance. We do not wish to treat these higher order effects theoretically, but rather to correct for them, so that the most important zero order resonance effects can be sorted out of the data.

Optical data analysis

The observed dimer spectrum can be decomposed into the two exciton components by computer analysis (Sauer et al., 1966). Figure II-15 shows the decomposition of the red absorption band of the bacteriochlorophyll dimer into two components. Gaussian shaped absorption components fit the spectrum satisfactorily if the Gaussian components are allowed to have different widths on the low and high energy side.

The two exciton components are required to have the same low energy

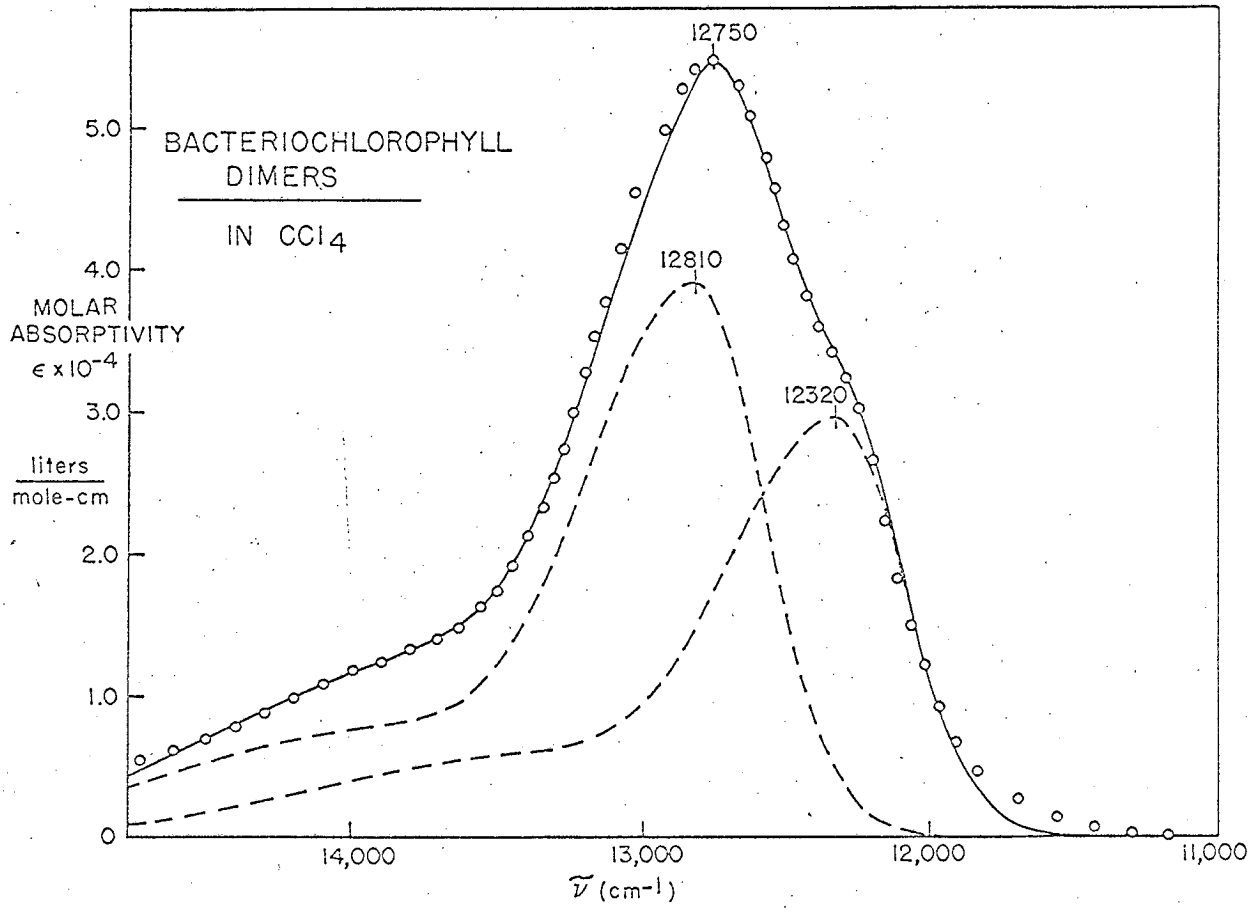

Figure II-15. Decomposition of the long wavelength electronic transition of the bacteriochlorophyll dimer into two asymmetric Gaussian components (dashed curves). The components differ only in position and amplitude. The solid curve is the sum of the dashed components and is compared to the experimental absorptivities/mole monomer (after Sauer, et al., 1966) which are represented by the open circles.

width and the same high energy width but may have different amplitudes. The energy splitting, the relative amplitude of the components and the two width parameters give four independent parameters. Separate bands for the higher energy vibrational components which make small contributions in the peak absorption region are included. The absorption fitting proceeds by trial and error adjustment of the absorption band parameters using a digital computor to calculate the curve. The fit to the spectrum is seen to be quite good and seems to be unique within the limitations imposed above. The change in intensity of a band (hypo- or hyperchromism) upon forming the dimer can be neglected by simply taking the ratio of the two dipole strengths from the absorption spectrum, D_+/D_-.

The CD spectrum is a slightly different problem. The nondegenerate, off resonance, interactions give single dichroism bands, while the resonance, exciton interactions give double CD bands (Tinoco, 1962). The situation is illustrated in Figure II-16 for both ORD and CD spectra. The example given is similar to the actual situations for the chlorophyll dimers, where the amplitude of the double CD component, I in Figure II-16, is about equal to the single CD component, II in Figure II-16, to give a typical observed curve similar to III in Figure II-16. We wish to extract the double CD component (e.g., I in Figure II-16) from the observed CD spectrum (e.g., III in Figure II-16).

For strongly allowed transitions, as in the chlorophylls, the single CD peaks are expected to have the same shape as the absorption (Moffitt and Moscowitz, 1961). For exciton splittings smaller than the band width of the transition (and electric dipole allowed transitions) the degenerate CD component has the shape of the derivative of the absorption

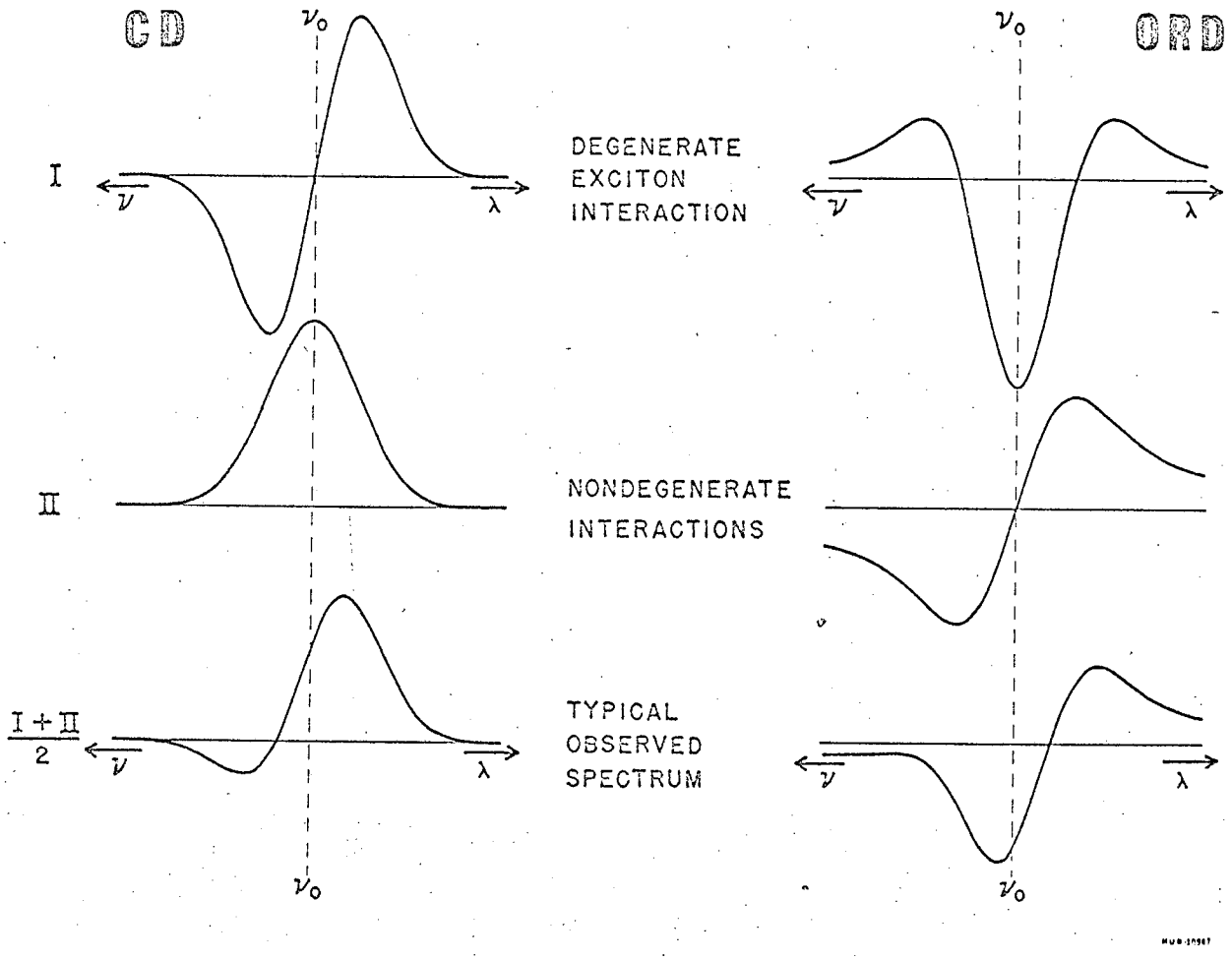

Figure II-16. Typical CD and ORD curves resulting from degenerate (I) and non-degenerate (II) interactions. These curves are obtained by decomposing the corresponding lower curves (I + II)/2, which approximate those observed for chlorophyll dimers.

curve (Biltonen, 1966). We use the shape of the asymmetric Gaussian exciton component, found from the absorption spectrum, to fit the CD spectrum of the dimer rather than the monomer absorption shape. The observed dimer CD can be fit satisfactorily if a single asymmetric Gaussian (centered at the mean frequency of the absorption exciton components) is taken as the single CD shape and the derivative of this Gaussian is taken as the double CD shape. However, for the chlorophylls the exciton splitting is very close to the absorption band width, so the shape of the double CD component is not exactly given by the derivative of the absorption.

A better procedure for such a large exciton splitting is to use the full dimer spectrum for the single CD component shape. The double CD shape is derived by taking the two exciton component shapes and positions from the absorption spectrum but with unit amplitude. The sign of the high energy exciton component is reversed and the two exciton components are added to derive the double CD shape. This procedure yields a curve which is similar to that shown as R in Figure II-17, where R_+ and R_- represent the observed exciton components (which are asymmetric in the chlorophylls).

The long wavelength CD spectrum of bacteriochlorophyll fit in this way, is shown in Figure II-18. (This CD data was taken from a solution with 60% dimer and essentially no trimer, so it looks slightly different from Figure II-14, where some trimer was present.) The double CD component shape derived by the above procedure is shown as curve I in Figure II-18. The open points and curve III are the experimental CD and the solid points are the sum of the I and II component curves. The

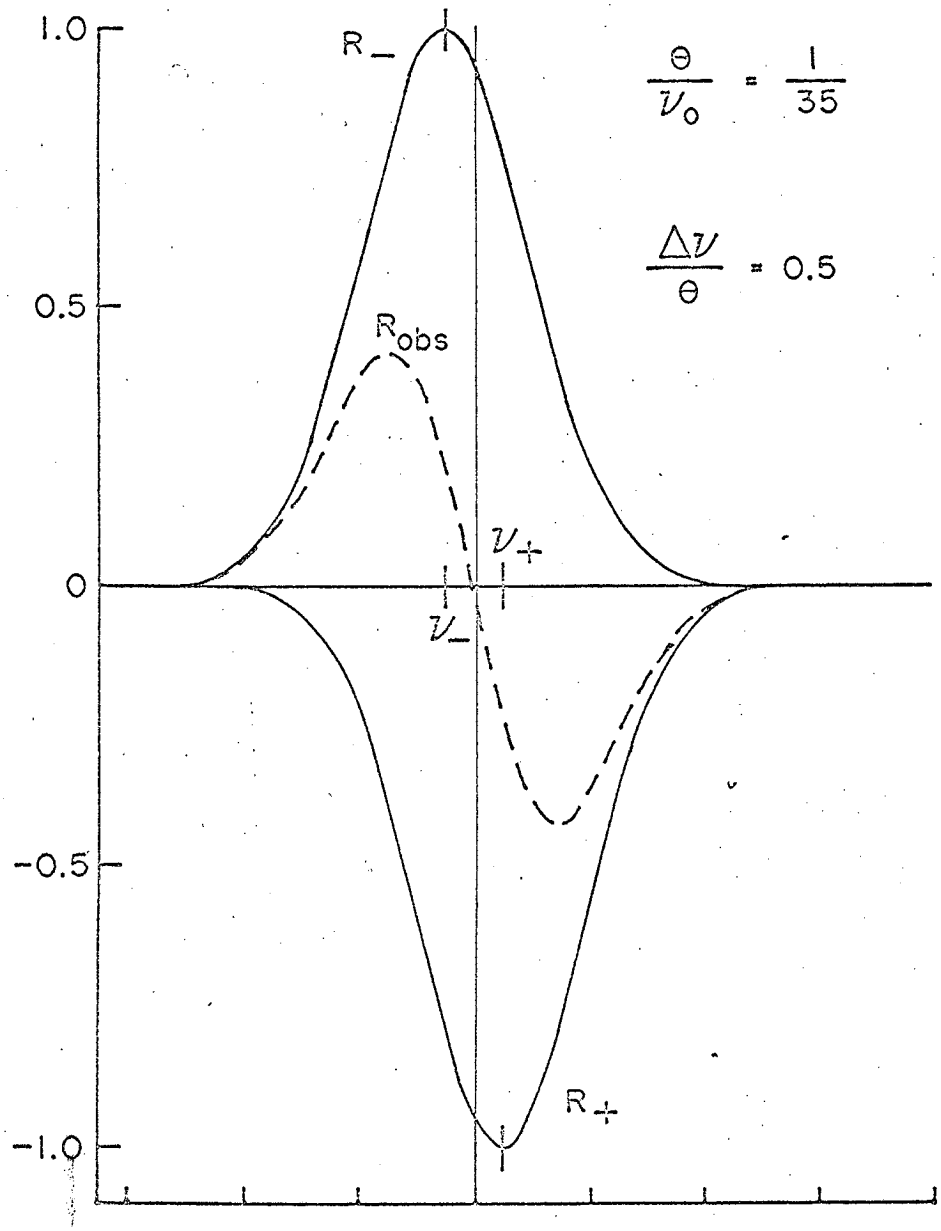

MUB-10962

Figure II-17. Typical double CD component for an exciton split transition where the splitting is small compared to the band width. The cancellation of rotational strength in the center of the band is illustrated. Both R_+ and R_- have Gaussian shapes with halfwidth Θ, and they are separated by $\Delta\nu$.

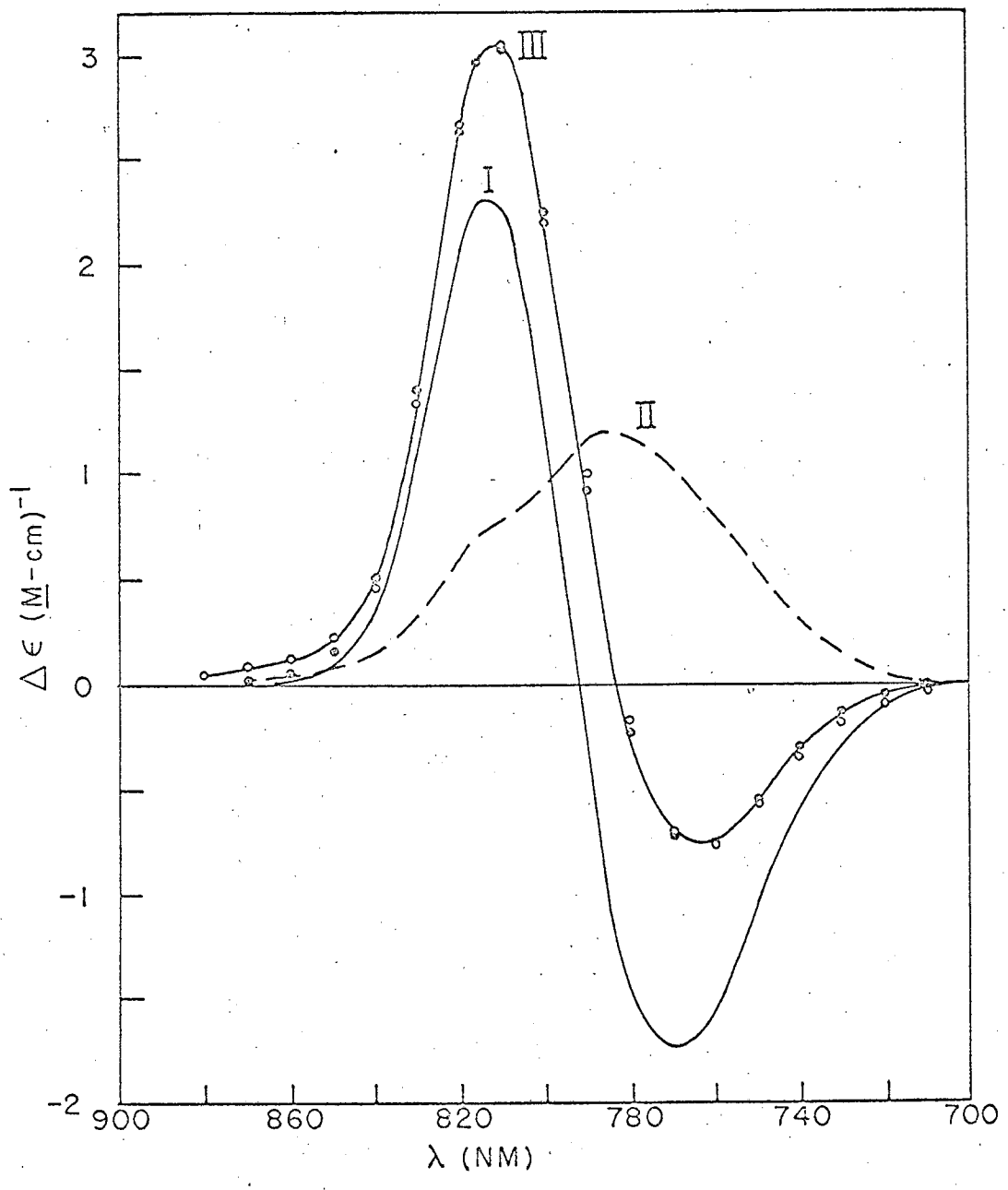

MUB-12091

Figure II-18. Decomposition of long wavelength circular dichroism of bacteriochlorophyll dimer into degenerate (solid curve labeled I) and non-degenerate (dashed curve labeled II) components. The origin of the I and II curve shapes are described in the text. The experimental points are represented by the open circles, ○, and the sum of the I and II components are the solid points, ●.

fit is extremely good, only two adjustable parameters are used, the amplitude of the double component (I) and the amplitude of the single component (II). The fitting is accomplished by a linear, least squares criteria procedure (Wilson, 1952; Deming, 1943) using a computer program written by Dr. R. Biltonen (1966).

The double CD component (I in Figure II-18) does not yield the desired exciton rotational strength $R_{\pm}$ quantity directly, as can be seen from Figure II-17, where the cancellation of rotational strength in the middle of the band can be seen. The amplitude of the individual $R_{\pm}$ components can be found from the double CD component I in Figure II-18 by knowing the exciton splitting V_{12}. Fortunately, an experimental value for the exciton splitting has been found from the chlorophyll dimer absorption spectrum, so rotational strength values, $R_{\pm}$, can be obtained. Table I gives the dipole strength ratios, D_+/D_-, rotational strengths, $R_{\pm}$, and exciton splittings, $\Delta\nu = (\nu_+ - \nu_-) = 2V_{12}/hc$, resulting from the monomer transitions at ν_o for the three chlorophylls. The exciton splitting is assumed positive for the purposes of this table.

Dimer geometry

The most detailed structural information that we might expect to derive from the data of Table I is dependent on the choice of a particular theoretical model. However, some conclusions can be made that are relatively independent of the choice of model. If a degenerate CD component is found experimentally, the general theory (Tinoco, 1962) requires that the chromophores are not coplanar and that, further, if we assume that the monomer magnetic dipole transition moment is essentially zero (a good assumption in this case) we can state that the monomer transition moments are not parallel or exactly perpendicular in the dimer.

Table I. Spectral Properties of the Exciton Split Components of the Dimers of Three Chlorophylls in Carbon Tetrachloride. [λ_o and ν_o refer to the average of the two exciton band positions, e.g., $\nu_o = (\nu_+ + \nu_-)/2$].

Molecule	λ_o(mμ)	ν_o(cm^{-1})	$\Delta\nu$(cm^{-1})	D_+/D_-	$R_\pm \cdot 10^{40}$ cgs	$\frac{R_\pm}{D_o\nu_o} \cdot 10^8$ cgs
Chlorophyll a	674	14848	363	1.48	± 20	± 0.74
Chlorophyll b	655	15259	398	1.81	± 18	± 0.79
Bacteriochlorophyll	796	12565	490	1.32	± 44.5	± 0.92
	590	16940	470	0.9	∓ 6.9	∓ 0.32

The point dipole approximation results in the expression for the optical properties (Tinoco, 1963):

$$D_{\pm} = D_o \pm \underset{\sim}{\mu_1} \cdot \underset{\sim}{\mu_2} \qquad \text{II-(22)}$$

$$R_{\pm} = \mp(\pi/2)(\nu_o/c)(\underset{\sim}{R_{12}} \cdot \underset{\sim}{\mu_1} \times \underset{\sim}{\mu_2}) \qquad \text{II-(23)}$$

$$\nu_{\pm} = \nu_o \pm V_{12}/hc \qquad \text{II-(24)}$$

$$V_{12} = 1/R^3 \left[\underset{\sim}{\mu_1} \cdot \underset{\sim}{\mu_2} - \frac{3(\underset{\sim}{R_{12}} \cdot \underset{\sim}{\mu_1})(\underset{\sim}{R_{12}} \cdot \underset{\sim}{\mu_2})}{R^2}\right] \qquad \text{II-(25)}$$

The quantities D_+/D_- and $R_{\pm}/D_o\nu_o$ in Table I depend only on the geometry of the dimers and not on the intensities or positions of the absorption bands. The similarities of these quantities for the three chlorophylls quantitatively supports the earlier more qualitative suggestion that the structure of all three dimers is similar.

The D_+/D_- ratio depends only on the angle between the monomer transition moments, within the dipole approximation. If β = intertransition moment angle; $D_+/D_- = (1 + \cos\beta)/(1 - \cos\beta)$ II-(26)

The absorption measurements imply an angle of about 80 degrees between the red transition moments for all three dimers (eq. II-(26)) from the data in Table I. Planar aromatic molecules tend to stack with parallel planes when aggregated. For parallel planes, the point dipole rotational strength is:

$$R_{\pm} = \mp \frac{\pi \nu_o d}{hc} D_o \sin\beta \qquad \text{II-(27)}$$

where d is the distance between the planes and β is the angle between transition moments as before. For aromatic systems, the interplanar distance is 3.4 - 3.6 Å (e.g., Pauling, 1960). The CD spectra yield an intertransition moment angle of β = 12 — 10° for an interplanar distance of 3.4 - 3.6 Å. The distance can certainly be no smaller than 3.4 Å and larger distances give smaller angles.

Within the limitations of the point dipole model, the angle between the transition moments of 80 degrees found from the absorption spectra is not dependent on any assumption about the parallelism of the monomer planes. The large discrepancy between the intertransition moment angle found from the absorption spectra (80°) and the angle found from the CD spectra assuming parallel planes (12°) seems much too large to ascribe completely to inadequacies in the point dipole model since the exciton splitting is experimentally observed. We are forced to the conclusion that the chlorophyll planes are not parallel in the dimer.

The above conclusion about non-parallelism of planes in the dimer is completely independent of the assumption that the magnetic dipole transition moment ($\underset{\sim}{m}_{oa}$) of the monomer is zero. The monomer CD depends on the component of $\underset{\sim}{m}_{oa}$ in the molecular plane ($CD \propto \underset{\sim}{m}_{oa} \cdot \underset{\sim}{\mu}_{oa}$) since $\underset{\sim}{\mu}_{oa}$ is in plane. We can see from the small CD of the monomer that the component of the magnetic transition moment $\underset{\sim}{m}_{oa}$, in the plane of the molecule is extremely small. The terms that we neglected were of the form $\underset{\sim}{\mu}_{1oa} \cdot \underset{\sim}{m}_{2oa}$. If the planes were parallel, these terms would be no larger than the monomer CD which is completely negligible for our purpose.

It is encouraging that we have reached the conclusion that the chlorophyll planes are not parallel. The previously related evidence (e.g., reviewed by Katz et al., 1966) convincingly shows that the dimer is held together by a C-9 carbonyl ····· magnesium bond (see Figure II-10). A study with space-filling molecular models (Cortauld, Corey-Pauling-Koltun)[1] indicates that any reasonable approach between the C-9 carbonyl and the central magnesium requires a substantial angle ($\gtrsim$ 30°) between chlorophyll planes. Katz et al. (1963) reach similar conclusions.

---

[1]Ealing Corp., 2225 Massachusetts Ave., Cambridge, Mass.

Since we can conclude with some confidence that the planes are not parallel, the problem of dimer geometry becomes somewhat more complex. If we center a coordinate system at monomer one, two angles and a distance are needed to specify a vector from its center to the center of the other monomer. Three additional angles are needed to specify the orientation of the second monomer in space about its center. Therefore, six parameters, five angles and a distance, are needed to specify the dimer geometry in the general case. The observable parameters available for each absorption band with a reasonably large exciton splitting are the degenerate rotational strength, $R_{\pm}$, the ratio of dipole strengths, D_+/D_-, and the exciton splitting itself, V_{12}. Thus, there are three interaction parameters for each absorption band that exhibits a large exciton interaction. At least six independent pieces of data are needed to determine the five unknown angles and a distance required for specifying the dimer geometry. The exciton interaction parameters for two independent transitions, polarized along different directions in the molecular plane yield the required six pieces of data.

Bacteriochlorophyll has two distinct transitions at 780 mμ and 590 mμ. These transitions are both strong and are in-plane pi - pi transitions (Goedheer, 1955). Fluorescence polarization measurements (Goedheer, 1957) show that these transitions are perpendicularly polarized. Both bands show double CD components indicating exciton splitting. The splitting of the 590 mμ band is not as obvious as in the 780 mμ band because the 590 mμ band is wider. However, the 590 mμ band is very much wider in the dimer compared to the monomer, and this dimer peak can be fit to two exciton components satisfactorily. The six exciton interaction parameters for these two bacteriochlorophyll transitions

are given in Table I. The 590 mμ transition moments are oriented at approximately 100 degrees in the dimer by the dipole approximation.

We must now reconsider the approximate magnitudes of the magnetic dipole transition moments for these two bacteriochlorophyll transitions, since the out of plane components of the magnetic dipole transition moment of one monomer can interact with the electronic dipole transition moment of the other monomer if the planes are not parallel in the dimer (Tinoco, 1962).

Consider a hypothetical optically inactive bacteriochlorophyll derivative which is symmetrically (dihydrogen or dimethyl) substituted at C-3, 4, 7, 8 and 10 (see Figure II-10). The main electronic perturbations from full rectangular symmetry are the carbonyl groups at positions 2 and 9. Aside from aliphatic substitution, the carbonyls leave a C_2 axis of symmetry perpendicular to the molecular plane of symmetry. For this hypothetical molecule (which is considered to be C_{2h} in group theoretical notation) the magnetic dipole transition moments are identically zero by symmetry for allowed electric dipole transitions such as we are considering. The aliphatic substituents which induce the optical activity in bacteriochlorophyll are very weak perturbations on our hypothetical molecule and therefore must induce only a very small magnetic dipole transition moment, and this can reasonably be neglected.

The general orientation of the dimer can conveniently be described by the coordinate system shown in Figure II-19. Molecule one is placed in the xy plane centered at the origin of a right-handed cartesian coordinate system (x,y,z). Molecule one transition moments are directed along the x,y axes. The center of the second molecule is located by a vector

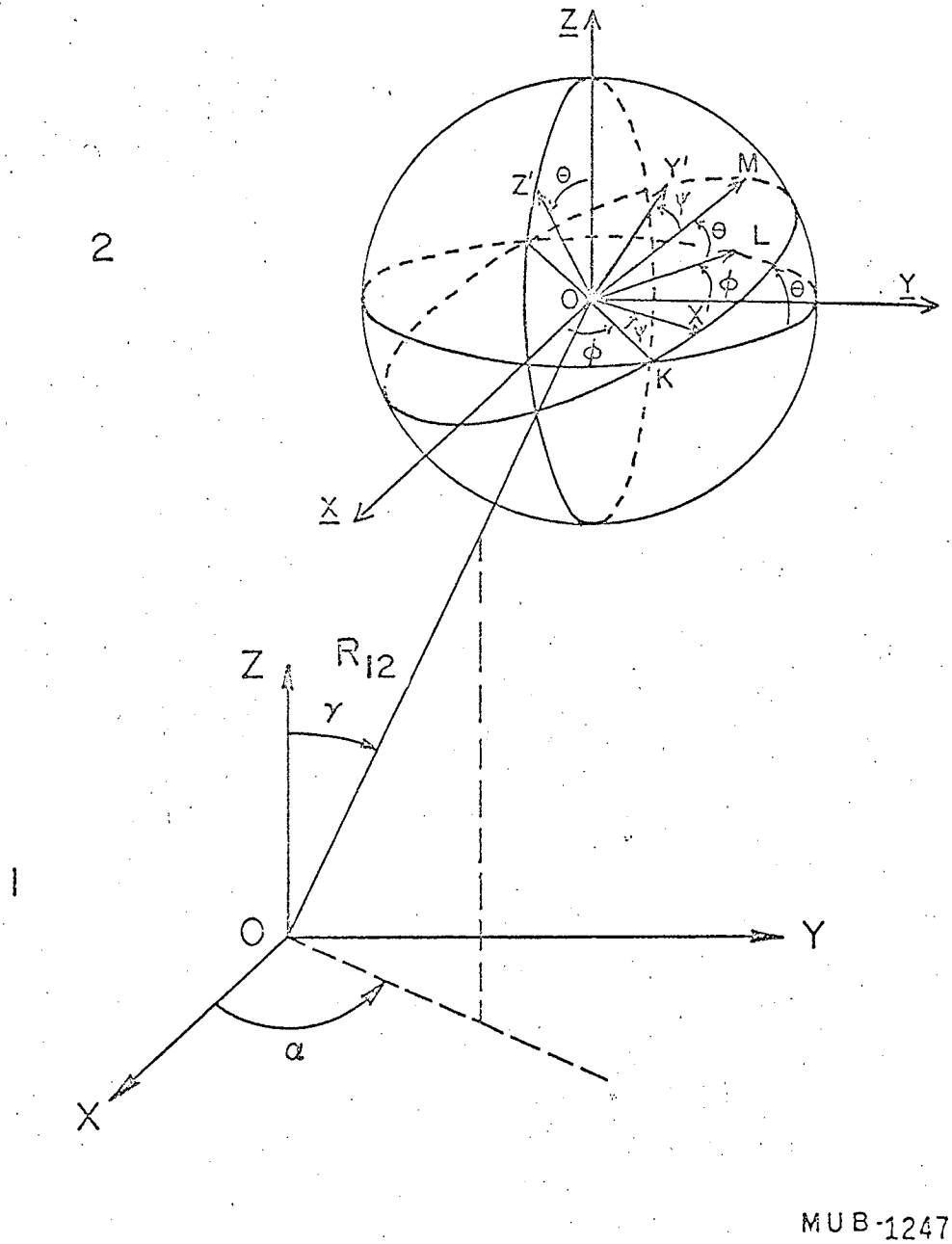

MUB-12473

Figure II-19. The coordinate system used to describe the dimer structure. The angles are defined in the text.

from the origin of the first coordinate system specified by the cylindrical polar coordinates R, γ and α. The second molecule is placed in the x'y' plane centered at the origin of a right-handed cartesian coordinate system (x',y',z'). And the transition moments of the second molecule are directed along the x',y' axes. The x y z system at the center of molecule two is parallel to the xyz system. The angles, ϕ,θ,ψ, which orient the x'y'z' system relative to the x y z system are the Eulerian angles as defined by Wilson, Decius and Cross (1953).

The last piece of information we need to carry through the point dipole analysis of the dimer structure is the direction of the dipole transition moments in the molecular plane. We remarked earlier that bacteriochlorophyll is only slightly perturbed from a very symmetrical rectangular molecule. For the symmetrical parent molecule, magnesium opposite tetrahydroporphyrin, unambiguous theoretical arguments assign the long wavelength transition moment along the long conjugation axis of the molecule (Platt, 1949; Gouterman, 1961; Gouterman, Wagniere and Snyder, 1963). An axis along the long conjugation direction bisects the bond between carbons 1 and 2 and the bond between carbons 5 and 6 in Figure II-10. Gouterman (1961) calls this long axis the Y axis, but we inadvertently assigned the long conjugation axis to the x axis early in this work, and we stuck to our convention throughout. The only bacteriochlorophyll substituents which can appreciably perturb the electronic structure of the basic magnesium opposite tetrahydroporphyrin skeleton are the carbonyl groups on positions 2 and 9 (see Figure II-10). The tetrahydroporphyrin has a typical "long field" (Platt, 1956) spectrum which is empirically and theoretically expected to be insensitive to conjugated substituents.

Molecular orbital calculations, using parameters determined by a self-consistent field configuration interaction calculation (Weiss et al., 1965), indicate that the carbonyls only very slightly affect the directions of the 780 and 590 mμ bands of tetrahydroporphyrin (Sauer, 1966). The transition moment directions of bacteriochlorophyll are essentially determined by the geometry of the molecules and we will neglect the effects of carbonyl substituents. This is not a fundamental approximation and apparently not a serious one, but it is convenient. To summarize, the long conjugation axis (1/2 - 5/6) of the monomers which correspond to the 780 mμ transition are placed along the x, x' axes, and the short conjugation axis (3/4 - 7/8) which corresponds to the 590 mμ transition are placed along the y, y' axes in Figure II-19.

For the point dipole approximation the following geometrical expressions are found for the exciton contribution to the rotational strength ($R_\pm$), the exciton splitting (V_{12}) and the dipole strength ratio (D_+/D_-).

$$X_1 = DRX = (D_+/D_-)_x = \frac{1 + (\cos\phi\cos\psi - \sin\phi\sin\psi\cos\theta)}{1 - (\cos\phi\cos\psi - \sin\phi\sin\psi\cos\theta)} \qquad \text{II-(28)}$$

$$X_2 = DRY = (D_+/D_-)_y = \frac{1 - (\sin\phi\sin\psi - \cos\phi\cos\psi\cos\theta)}{1 + (\sin\phi\sin\psi - \cos\phi\cos\psi\cos\theta)} \qquad \text{II-(29)}$$

$$X_3 = ROTX = \frac{2(R_\pm)_x c}{\pi\nu_x\mu_x^2} = \mp R[\sin\alpha\sin\theta\sin\psi - \cos\gamma(\sin\phi\cos\psi + \cos\phi\sin\psi\cos\theta)] \qquad \text{II-(30)}$$

$$X_4 = ROTY = \frac{2(R_\pm)_y c}{\pi\nu_y\mu_y^2} = \mp R[\cos\alpha\sin\theta\sin\psi + \cos\gamma(\cos\phi\sin\psi + \sin\phi\cos\psi\cos\theta)] \qquad \text{II-(31)}$$

$$X_5 = VKX = \frac{(V_{12})_x}{\mu_x^2} = \frac{1}{R^3}\{(\cos\phi\cos\psi - \sin\phi\sin\psi\cos\theta) - 3\cos\alpha[\cos\alpha(\cos\phi\cos\psi - \sin\phi\sin\psi\cos\theta) + \sin\alpha(\sin\phi\cos\psi + \cos\phi\sin\psi\cos\theta) + \cos\gamma\sin\theta\sin\psi]\} \qquad \text{II-(32)}$$

$$X_6=VKY=\frac{(V_{12})_y}{\mu_y^2}=-\frac{1}{R^3}\{(\sin\phi\sin\psi-\cos\phi\cos\psi\cos\theta)-3\sin\alpha[\cos\alpha(\cos\phi\sin\psi+\sin\phi\cos\psi\cos\theta)+\sin\alpha(\sin\phi\sin\psi-\cos\phi\cos\psi\cos\theta-\cos\gamma\sin\theta\cos\psi]\}\qquad\text{II-(33)}$$

where μ_x^2, μ_y^2, ν_x, ν_y are derived from the experimental values of the absorption intensity and wavelength of maximum absorption (found by Sauer et al., 1966). The experimental values of the exciton splitting, rotational strength and dipole strength ratios are given in Table I. The X_i, eqs. II-28 - 33, relate the experimental observables and geometrical factors of interest.

We have not been able to solve these simultaneous equations in closed form for the angles of interest, so we used a numerical computer method for the solution. The method adopted is analogous to the method of steepest descents. The observed value of X_i was subtracted from each of the X_i equations to get a new set of functions X'_i which must all equal zero for a solution. The six equations were added and squared to get a function F that is also zero for a solution. The method uses the partial derivatives of F with respect to each of the six unknowns, α, γ, θ, ϕ, ψ, and R. Trial values of the unknowns are supplied, and the function F and its partial derivatives with respect to the unknowns are calculated. The unknowns are altered a small amount in the direction the partial derivatives indicate will bring F closer to zero. This process is repeated until a minimum in F is reached. A typical solution gives a value of $F = 10^{-25}$ for the system of equations and each component X_i is about 10^{-14} (while each X_i is of the order of unity). The master fitting program VARMIT is available as share routine (Zo Eo VARM). Several different solutions are found for different sets of trial values of the

Page 95 follows

six unknowns. Two procedures were used for getting the trial values. (1) The observable X_i quantities were calculated by the computer for a set of angles varied systematically, in 15 degree steps, from $0 - 2\pi$ for α, ψ, ϕ and from $0 - \pi$ for γ and θ, at several R values from 3.5 - 10 Å in 0.5 Å steps. This procedure required a large number of computations, but only a small amount of computer time. The program (DIMER, given in Appendix II) was written so that the X_i values were printed out together with the angles used for the calculation only if all the X_i's were within a factor of two of the experimental numbers. Only a small number (0.5%) of the combination of unknowns met this criteria and only a few regions of angles and R values gave X_i values close (20%) to the experimental values. The angles and R values found in this way were used as trial values for the unknowns in solving the F equation. (2) The trial values which were required to solve the F equation were varied in a systematic manner over a large range of values with no attempt at selecting trial values which agreed closely with experiment.

We found no way to determine the number of linearly independent solutions for this set of equations, and we can never be absolutely sure that all of them have been found. There is also the further ambiguity in our experimental data, that we do not measure the sign of the exciton splitting, only its magnitude. For this reason we tried calculation with four combinations of sign of exciton splitting:

Set	V_x	V_y
A	+	+
B	-	-
C	+	-
D	-	+

A very large number of mathematical solutions are found for the six simultaneous equations and our experimental data, approximately 15 for each set of exciton splittings. However, the solutions occurred at only three values of the center to center distance: R = 8.22, 7.51, 6.54 Å. Changing the values of the observable quantities by 5 - 10%, to simulate experimental error, alters the solutions by a correspondingly small amount, so the solutions found are stable. It is often the case that there are many more mathematical solutions to a problem than there are physically acceptable solutions. We required that any physically reasonable solution must not bring the chlorophyll molecules too close; in other words, steric repulsion made many of the structures physically unreasonable. Many of the R = 8.22 Å solutions, some of the R = 7.56 Å, but none of the R = 6.54 Å solutions met the steric requirements. The bacteriochlorophyll molecular shape was approximated by adding a ring V and bacteriochlorophyll substituents (Fig. II-10) to the Ni etioporphyrin structure (Fleischer, 1962) using standard van der Waals radi (e.g., Pauling, 1960). Consideration of the distortions suggested by Corwin, Water and Singh (1962) did not substantially change the results, because only marginal solutions were affected and these had been kept earlier anyway. Some of the further ambiguity that remains was built into our approach earlier. We have represented the chlorophyll molecule with a pair of perpendicular transition moments that have a center of symmetry as well as the plane of symmetry. This means that if we have found a correct solution we will also have mathematically equivalent solutions in other quadrants. This need not concern us because we have several other physical criteria that we can use to select the proper quadrant for the structure.

We noted earlier that the chlorophyll dimerization requires the central magnesium and an inact ring V (Figure II-10) and that the evidence for an essential magnesium to C-9 carbonyl bond in the dimer was conclusive. Five or six of our solutions gave a C-9 carbonyl ····· magnesium bond principally in parameter set A and D, and these were judged to be the physically reasonable solutions. Two of the solutions, one from set A where molecule 2 was on top and the other from set D where molecule 2 was on the bottom were equivalent geometrically and several attractive features of this structure led us to propose it as the structure for the chlorophyll dimer in solution.

A drawing of this structure is shown in Figure II-20. The chlorophyll planes meet at a 35 degree angle with the bulky ends of the molecules together. Of course, the C-9 carbonyl of the top molecule coordinates the central magnesium of the bottom one. This is not a true projection drawing as the top molecule is merely overlayed onto the bottom one, but will be sufficient to illustrate features of the proposed structure. The chlorophylls have a large "ring current" and the protons that are close in the dimer are strongly shifted in the NMR when the dimer is broken up with methanol (Closs et al., 1963). The NMR experiments are done at high concentration where trimer is present in chlorophyll b and bacteriochlorophyll. We are only interested in the dimer here so the chemical shifts will be given for chlorophyll a which only forms a dimer. The proton shifts (for assigned protons) due to breaking the methyl chlorophyllide a dimer given by Closs et al. are summarized in Table III.

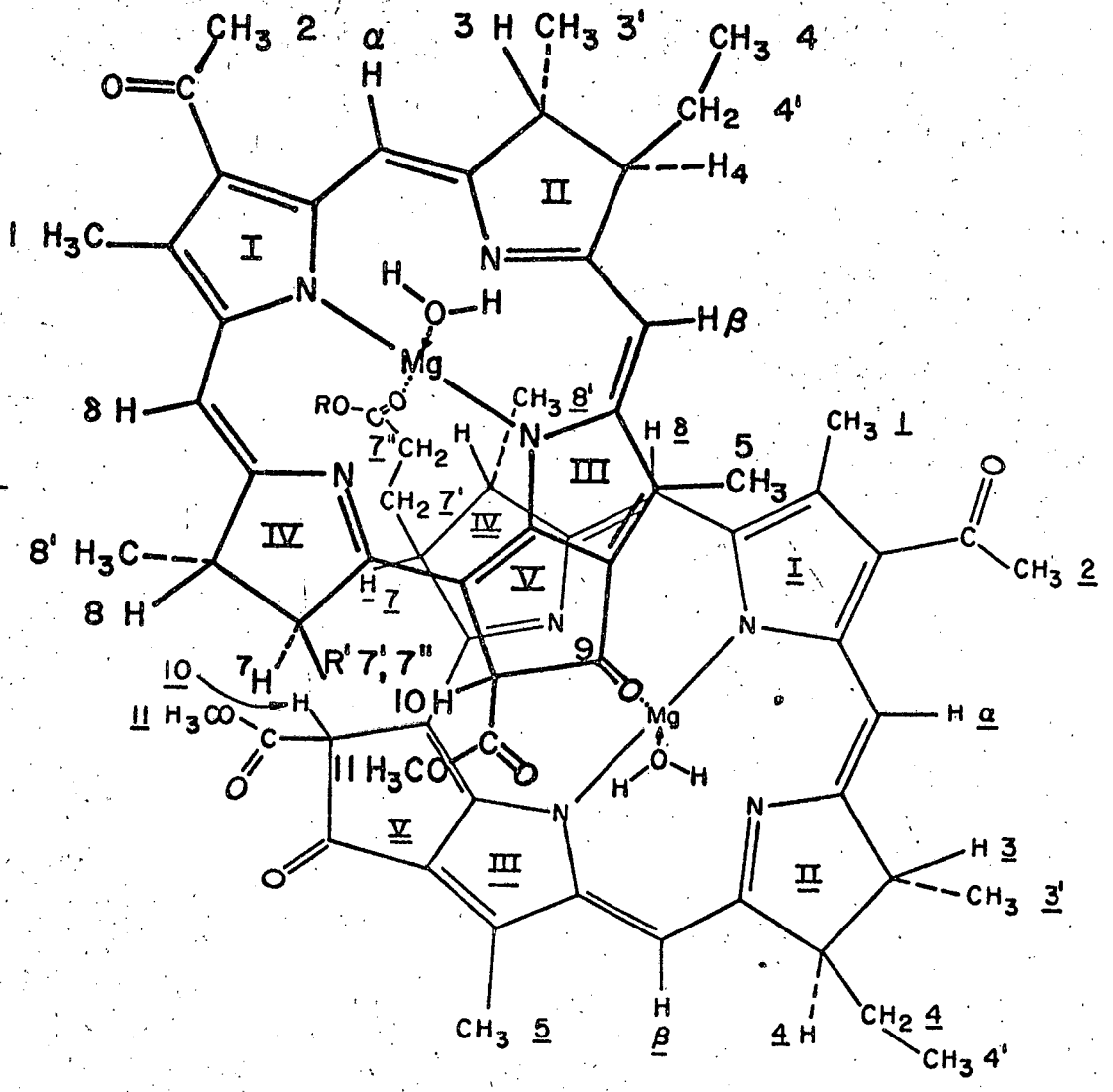

Figure II-20. Proposed structure for the chlorophyll dimer. The molecule drawn with darker lines is on top, inclined at 35° to the lighter drawn molecule which is the plane of the page. The substituent members of the lower molecule are underlined. The R on the top molecule is either methyl or phytyl. This R group is referred to as 7''' in Table III for the methyl chlorophyllide. The R' on the bottom molecule is a propionic acid methyl or phytyl ester.

Table III. Proton NMR shifts caused by breaking up the methyl chlorophyllide a dimer with methanol (shifts are given in Hz, spectra measured at 60 M Hz) after Closs et al., 1963.

Position	Group	Shift (Hz)
10	H	111
5	CH_3	51
7'''	ester CH_3	50
11	CH_3	43
8'	CH_3	25
β	H	11
δ	H	8
4	CH_2	5
4'	CH_3	2
3	CH_3	4
α	H	5
1	CH_3	2
2	Vinyl	-1

Note: The 7''' hydrogens refer to the methyl group on the propionic acid methyl ester attached to the 7 position (see Fig. II-10 or Fig. II-20) of the chlorophyll ring.

It can be seen that the protons that are in the ring overlap region of our proposed structure are the ones that are most perturbed upon breaking the dimer.

A particular feature of our proposed structure is that the C-7 propionic ester carbonyl of the bottom molecule coordinates the magnesium

of the top molecule. After discovering that this bond was possible sterically, we reviewed the other evidence on dimer structure. In the methyl chlorophyllides, the methyl group on the propionic ester shows one of the strongest perturbations in the NMR when the dimer is broken up (see 7''' methyl in Table III). Inspection of the carbonyl infrared data of Katz et al. (1963) suggested that the two component ester carbonyl peak (at about 1730 cm^{-1}) may split in the dimer. One of the relevant infrared spectra of methyl chlorophyllide a is reproduced in Figure II-21. The well known 1653 cm^{-1} aggregation peak is apparent in the top spectrum A in chloroform. The middle spectrum B has 0.5% ethanol added and about 25% dimer. The bottom spectrum in tetrahydrofuran shows the monomer spectrum with complete absence of the 1653 cm^{-1} aggregation peak. The C-7 and C-10 ester carbonyl infrared absorption peaks overlap in the monomer at about 1740 cm^{-1} (see Figure II-21C). However, a definite low energy shoulder at about 1715 cm^{-1} is apparent on the dimer ester peak in A and less so in B of Figure II-21.* The direction of the ester carbonyl shift (to lower frequency) is consistent with a bond formed to magnesium. The chlorophyll a spectrum given by Katz et al. (1963) suggests that in the dimer the propionic ester carbonyl may shift into the 1700 cm^{-1} ketone peak, the ester peak at 1740 cm^{-1} is unusually sharp and the "ketone" peak at 1700 cm^{-1} is quite broad.

The dimer structure is, of course, determined by steric and non-covalent interactions. The importance of the C-9 carbonyl ····· magnesium bond has been mentioned several times. In our proposed structure the C-7 propionic ester bond to magnesium is one of the main factors which gives a unique optically active dimer. The asymmetric center at C-7 puts the

* The 1715 cm^{-1} shoulder is apparently of small amplitude. This is consistent with our proposed structure since only one of the four ester carbonyls of the dimer is expected to shift.

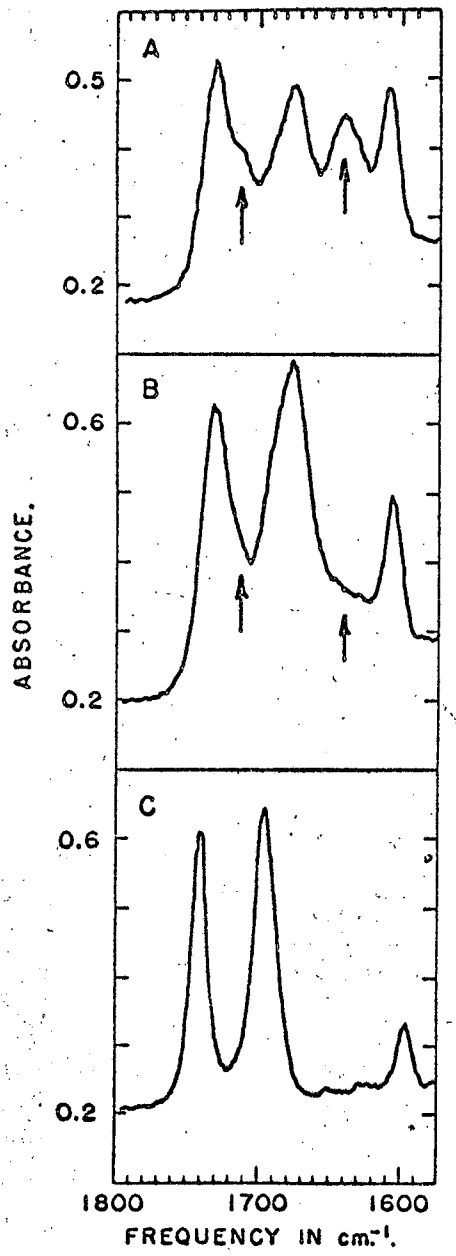

Figure II-21. Infrared spectra of methyl chlorophyllide a in aggregating (A. ethanol free chloroform-destablilized), partially aggregating (B. chloroform containing 0.5% ethanol), and aggregate free (C, tetrahydrofuran) solvents. The arrows on figures A and B at ca. 1653 cm^{-1} mark the well known carbonyl aggregation peak. The arrows at ca. 1715 cm^{-1} on figures A and B mark the proposed ester aggregation peak (after Katz et al., 1963).

propionic ester carbonyl above the plane of the bottom monomer in Figure II-20, and the second monomer must be on top if the ester carbonyl ····· magnesium bond is to form. In contrast, the asymmetric center at C-10 seems not to be an important determinant of our dimer structure. These aspects of the proposed structure may be tested by study of altered chlorophylls. For example, pyrochlorophyll is dihydrogen substituted at the C-10 carbon and so this asymmetric center is removed. Our proposed structure would predict that the pyrochlorophyll dimer would be essentially identical to the dimer formed from the parent chlorophyll. Further, if the C-7 asymmetric center were racemized in pyrochlorophyll, the dimer CD would be expected to vanish, but the dimer absorption would be unchanged. It is thought that chlorophyll a' is enantiomorphic to chlorophyll a at the C-7, C-8 and C-10 positions. Our proposed dimer structure would predict that the reflection at C-7 in chlorophyll a' would produce a dimer with identical absorption, but opposite CD compared to the chlorophyll a dimer. And, of course, pyrochlorophyll a' and chlorophyll a' would be expected to form essentially identical dimers.

Note that we have placed water above and below the magnesium in the top and bottom molecules respectively, so that magnesium is six coordinated (a well known coordination number for magnesium complexes). The water molecules inhibit higher aggregate formation; rigorous drying of solvents leads to higher aggregates.

Figure II-22 shows a picture of the proposed structure of the chlorophyll dimer built from the space filling Corey-Pauling-Koltun[1] models. The molecules are methyl chlorophyllides; the phytol chains

---

[1]Ealing Corp., 2225 Massachusetts Ave., Cambridge, Mass.

Figure II-22. A Corey-Pauling-Koltun model of the proposed chlorophyll dimer structure. Bacteriochlorophyll is on top and chlorophyll a is on the bottom. However, this is immaterial because all the dimers are thought to have the same structure. The molecules shown here are methyl chlorophyllides, i.e., the long phytyl tails have been replaced by methyl groups. The bottom molecule has ring I right-forward and ring II left-forward, while the top molecule has ring V forward, in contact with the magnesium of the lower molecule. The water molecule attached to the magnesium of the tpp molecule has a spurious hydrogen between the oxygen and the magnesium merely for convenience of attachment with these particular models. The coordinates of the top molecule are: R = 8.22 Angstroms, γ = 42°, α = 78°, ϕ = 0°, θ = 35°, ψ = 90° (see Figure II-19).

ZN-5980

have been omitted as they do not add steric restrictions to the structure and they make the picture considerably more complicated. One chlorophyll plane is lying on the plane of the table and the chlorophyll planes meet at 35 - 40 degrees. The bulky ring four and ring five regions of both monomers are toward the back. The bottom molecule has ring I on the right forward and ring II on the left forward. The top molecule has ring V forward with the C-9 carbonyl in contact with the magnesium of the lower plane. The top molecule has a water shown coordinating the magnesium. A spurious extra hydrogen is between the magnesium and the water oxygen merely because this is the only way we could attach the water with the Corey-Pauling-Koltun models, short of glue.

This dimer structure has been proposed on the basis of bacteriochlorophyll optical data, but dimers of all three chlorophylls are thought to have this structure. In summary, we found several sterically reasonable mathematical solutions to the structure of the chlorophyll dimer. We invoked other physical evidence to select structures that had a carbonyl magnesium bond. Chemical reasoning led us to the final proposed structure. It is astonishing that our simple theoretical model leads to such good agreement with many other types of data from infrared and NMR.

Less approximate theoretical models may be applied to test the proposed structure. This problem is analogous to a crystal structure determination, where finding a trial structure is most of the battle. Once a trial structure is found, more data can be used (e.g., Soret region optical data in chlorophyll dimers) and more refined interpretation may be possible. For example, we used the point dipole approximation in our interpretation. The chlorophyll centers are about 8 Å apart, and

the dipole length of the optical transitions are 2 - 3 Å. The point dipole approximation is probably qualitatively correct, but may be somewhat inaccurate quantitatively.

Calculation of the exciton splitting is particularly sensitive to the details of the electronic charge distribution during the transition. A better approximation for the exciton splitting is the monopole-monopole method which considers the energy of interaction between the transition charge density on each atom of monomer 1 with the transition charge density on each atom of monomer 2 (see eq. II-(16)) (Bush, 1965). The problem with this approach is that the atomic transition charge densities (monopoles) are not experimentally observable and must be calculated. This puts one more bit of theory into the analysis. Sophisticated pi electron calculations on the chlorophylls (Weiss and Gouterman, 1965) may yield good values for these transition charge densities. The chlorophyll molecules are only slightly perturbed from very symmetrical systems and this makes the calculations considerably more reliable. Other more detailed considerations, such as the effect of vibrations on dimer band shape might also be useful in the analysis (Young, 1965; Fulton and Gouterman, 1964; Weigang, 1965).

D. Crystalline Chlorophyll a

Figure II-22' shows the absorption and CD spectra for chlorophyll a microcrystals in suspension. The crystal structure is not yet known for any of the chlorophylls; however, the CD measurement has definite qualitative interest in relation to the observed quantasome chlorophyll CD. There is a slight solubility of chlorophyll a in isooctane, the suspension medium, so there is a small monomer peak at 666 mμ. In the crystal absorption spectrum this peak is shifted to 745 mμ. This large red shift

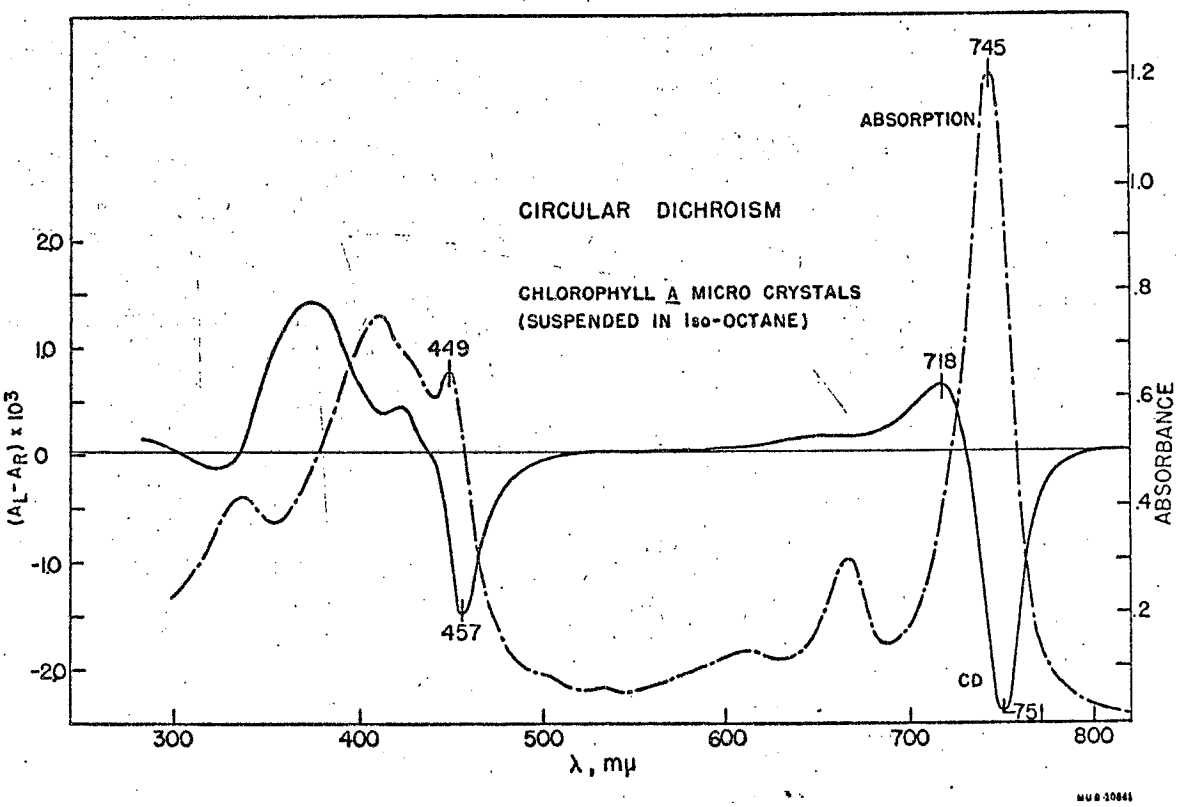

Figure II-22'. Absorption and CD spectra of a suspension of chlorophyll a microcrystals in iso-octane. The path length is 1.0 cm.

of the crystal over the monomer is probably due to the enormous polarizability of the crystalline environment compared to the solvent surrounding the monomer. It is a general observation that transitions of molecules in polarizable solvents are red-shifted relative to those in solvents of low polarizability (Robinson, 1961). These red shifts are experimentally observed for the chlorophyll transitions. Increasing chlorophyll aggregation leads to increasing red shift of the absorption. A 10 - 15 mμ red shift for the dimer relative to the monomer is observed in carbon tetrachloride. At very high concentrations in carbon tetrachloride the bacteriochlorophyll absorption and CD show evidence of higher aggregates, red shifted 30 mμ relative to the monomer. The molecule in the crystal is essentially dissolved in chlorophyll, a very polarizable medium, and the large red shift (80 mμ for chlorophyll a) results.

An analysis of the crystal CD shows that the degenerate CD component (e.g., I in Figure II-16) crosses zero within 1 mμ of the observed absorption peak. Therefore, the weak short wavelength shoulder observed in the crystal absorption spectrum (ca. 720 mμ) is not an exciton split peak and must be vibrational in origin. The gaussian half width is only about 25 cm^{-1} larger than for the monomer in CCl_4, so the exciton splitting in the crystal is probably very small.

E. Quantasome from Barley Chloroplasts and from a Mutant Deficient in Chlorophyll b

Analysis of the optical properties of a preparation from higher plant chloroplasts is complicated by the presence of chlorophyll a, chiefly responsible for the absorption maxima at 678 and 436 mμ, and chlorophyll b, which gives rise to the distinct shoulder near 650 mμ

and another at about 470 mμ. The carotenoids present have absorption maxima at 458, 455 and 428 mμ (Sauer and Calvin, 1962). Figure II-23 shows the ORD and absorption spectra of suspensions of lamellar fragments (quantasomes) of chloroplasts from normal barley as well as from a mutant that is completely missing chlorophyll b (Highkin and Frenkel, 1962). In the visible region of the spectrum, the mutant and normal quantasomes have identical ORD and absorption spectra except for the chlorophyll b regions near 650 and 470 mμ, where there are large differences. Figure II-24 shows the CD spectra of these same materials. The chlorophyll a part of the CD spectrum in the mutant appears to be identical to the chlorophyll a region in the normal barley.

The chlorophyll a in the quantasomes shows a large double CD component as we saw in the dimers and crystals. Presence of the double CD component in the chlorophyll a absorption region is good direct evidence for chlorophyll a-chlorophyll a interaction in quantasomes. Chlorophyll-protein or chlorophyll-lipid interactions would lead only to single CD bands and, if present, would only increase or decrease the asymmetry of the observed double CD component. The presence of a double CD implies that the interacting chlorophylls are not coplanar in the quantasomes. The double CD component crosses zero at about 685 mμ. This is the average frequency of the exciton bands, $\nu_0 = (\nu_+ + \nu_-)/2$, that give rise to the double CD. Thus, the interacting chlorophyll a molecules absorb on the long wavelength side of the quantasome absorption peak at 678 mμ. The chlorophyll that absorbs on the short wavelength side of the main peak is thought to be unaggregated, because it has relatively high fluorescence efficiency (Butler, 1966; Clayton, 1966). Photochemical work with

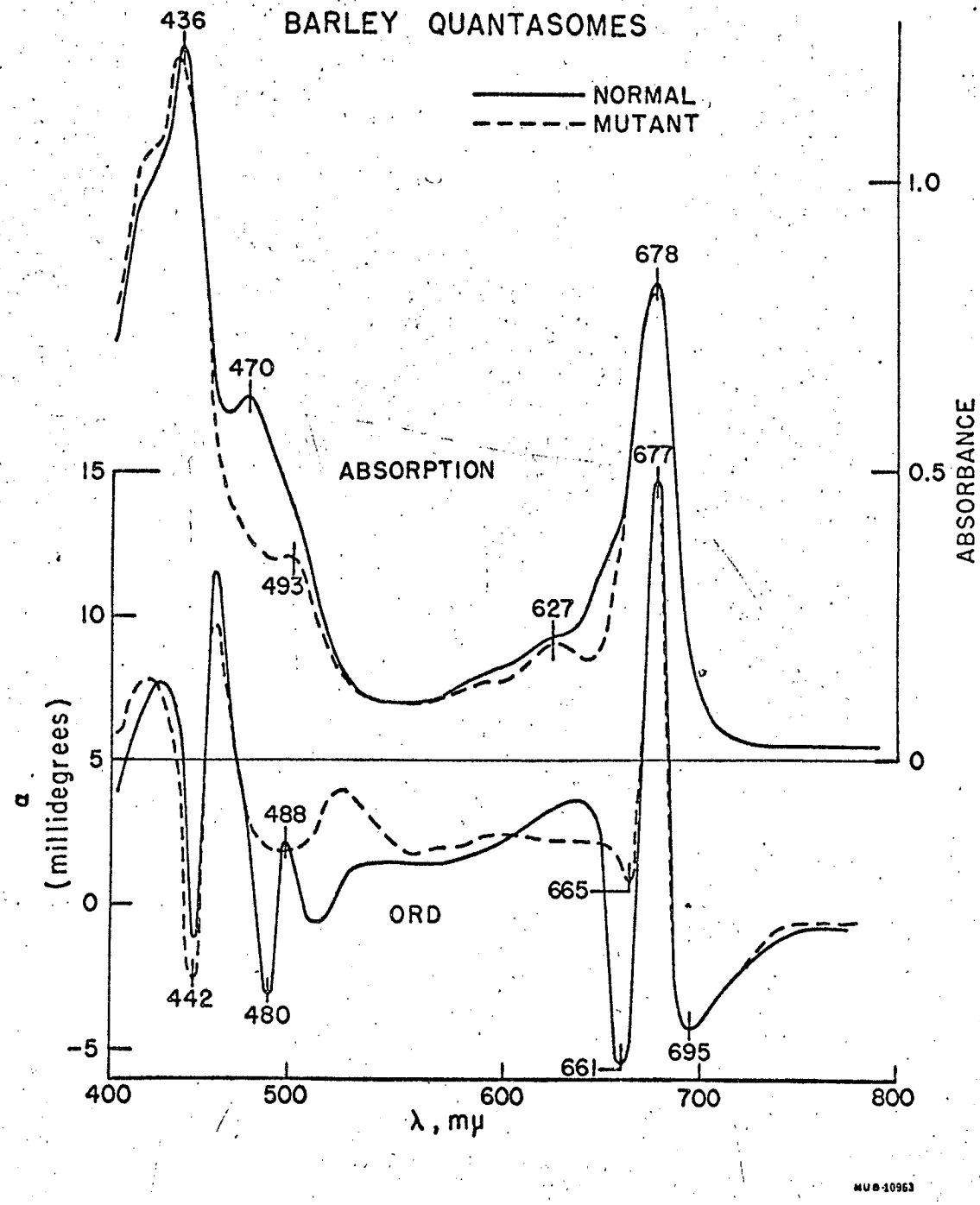

Figure II-23. Absorption and ORD spectra of quantasomes from normal barley (solid curves) and from a mutant lacking chlorophyll b (dashed curves).

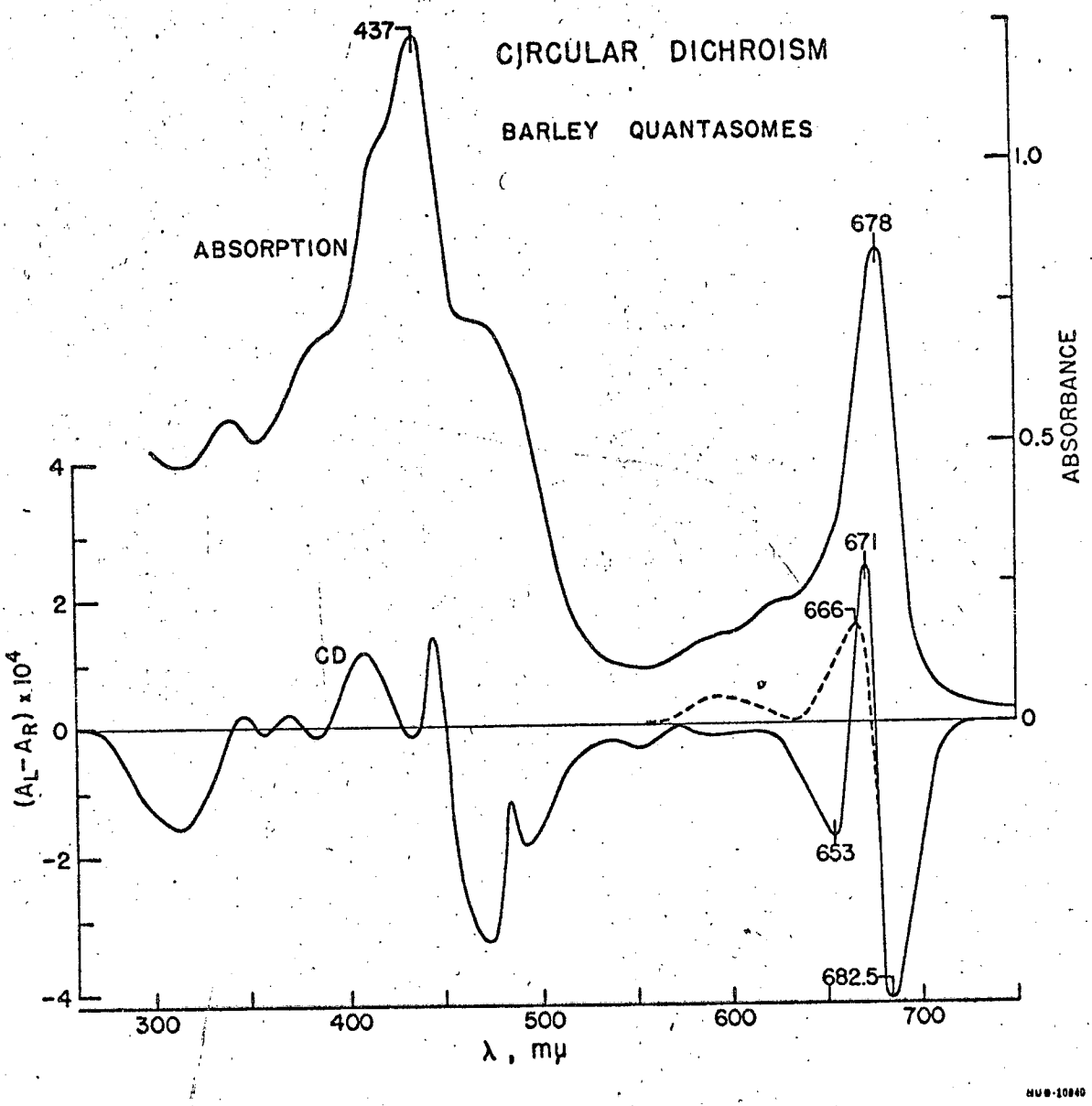

Figure II-24. Absorption and CD spectra of quantasomes from normal barley (solid curves) and CD spectrum of quantasomes from a mutant lacking chlorophyll b (dashed curve).

isolated chloroplasts show that a short wavelength class of chlorophyll molecules with peak absorption at ca. 673 mμ catalyze different reactions than a long wavelength class of chlorophyll molecules absorbing at ca. 683 mμ (Kelly and Sauer, 1965).

The shape of the chlorophyll CD in quantasomes is reminiscent of the shape of the crystalline chlorophyll CD, which suggests that the chlorophyll a molecules in quantasomes and in the crystal have similar geometries. However, the interacting chlorophyll a in quantasomes is not aggregated exactly like a three-dimensional crystal because the absorption is not red shifted as far as is the three-dimensional crystal. Chlorophyll a monolayers have their absorption shifted to 680 mμ (Bellamy, Gains and Tweet, 1963). The red shift of the chlorophyll that gives rise to the double CD in the quantasomes is about the same as the red shift in the monolayer. It may be, therefore, that the aggregated chlorophyll in the quantasomes is only one molecule thick, corresponding to a geometry similar to a two-dimensional chlorophyll a crystal.

The CD amplitude is small for quantasomes compared to that for a crystal suspension with equal peak absorption. A decrease in CD amplitude in a one- or two-dimensional crystal is expected relative to a three-dimensional crystal of otherwise identical geometry. The exciton forces giving rise to the CD effects are relatively long range (Hochstrasser and Kasha, 1964), and therefore depend on the extent of the aggregate.

The quantasome chlorophyll a CD (Figure II-24) has about the same amplitude as that of the chlorophyll a dimer CD (Figure II-12) for equivalent total red absorption. It would be useful to subtract the absorption

of the nonaggregated chlorophyll in the quantasome to determine the aggregate CD amplitude per unit of aggregate absorption. However, we have no direct evidence on the fraction of the total chlorophyll a that is aggregated in the quantasome. The exciton splitting evidenced by the CD is not resolved in the crystal or quantasome absorption at normal temperatures. However, the liquid nitrogen temperature derivative spectra of plant material resolves peaks at 673 mμ, 683 mμ and about 695 mμ (Butler, 1966). The double CD component crosses zero at about 685 mμ, and the observed absorption peak in the 673 mμ region is too far away to contribute to the double CD of the aggregate. The 673 mμ peak, estimated by Brown and French (1959) to be about 50% of the total chlorophyll a absorption, is a reasonable approximation to the amount of unaggregated chlorophyll a. It is consistent with the CD evidence to propose that both the chlorophyll a 683 and 695 mμ are exciton peaks resulting from the same aggregate. If this were true, about one-half of the chlorophyll a is in the aggregate. Assuming that at most one-half of the chlorophyll a in the quantasome is aggregated, the specific CD amplitude of the aggregated chlorophyll a is at least twice that of the solution dimer.

The chlorophyll a dimer CD has a shape similar to the quantasome chlorophyll a CD, although the dimer CD has opposite sign. The opposite sign is not an indication of any great difference in the two geometrical structures, for it could result from a mirror image relationship. We take the similarity in shape of the dimer and quantasome CD to mean that the two geometrical structures may be similar. A long wavelength shoulder is clearly seen in the dimer spectrum, but a long wavelength

shoulder does not appear clearly in the spectrum of the plant material. The relatively large amplitude of the quantasome chlorophyll a CD suggests a more extensive aggregate than a dimer. Helices, which are analogues of a one-dimensional crystal, are predicted to have a relatively large dependence of the rotational strength on chain length (Tinoco, Woody and Bradley, 1963). Two-dimensional systems might be expected to have an even stronger dependence on aggregate size. On the other hand, it is possible that the quantasome aggregates are dimers with a geometry that leads to larger rotational strength than the solution dimer. We conclude that the aggregated chlorophyll a in the quantasomes absorbs on the long wavelength side of the main peak and is at least a dimer, and is most probably a more extensive aggregate in one or two dimensions.

Plants can be grown with altered amounts of the different chlorophyll components. From the CD of these materials we may be able to find out how much of the chlorophyll a is aggregated, determine the absorption and CD of the aggregated components, and, in principle, determine the geometry of the aggregate.

The predominant interaction of chlorophyll a is with itself, since the CD in the chlorophyll a region is identical in the normal and chlorophyll b-free mutant. The chlorophyll b region also has a degenerate component in the quantasome CD that is seen in the difference between the normal and the b-free mutant CD curves. This double CD in the chlorophyll b region indicates that in the normal barley at least some of the chlorophyll b is interacting with other chlorophyll b molecules.

One must not ignore the possibility that the observed CD in quantasomes is not due to degenerate interaction between chlorophylls, but rather due to more than one type of independent non-interacting chlorophyll. This explanation would require at least two types of chlorophyll environment, one absorbing at long wavelength with negative CD and the other at short wavelength with smaller positive CD. The close relation between the chlorophyll a dimer and the crystal CD, where only chlorophyll-chlorophyll interactions are present, and the quantasome chlorophyll a tends to favor the chlorophyll-chlorophyll interaction as the origin of the CD in quantasomes. Experimental investigation of plant material having altered amounts of the different chlorophyll components should answer this question directly.

F. Chromatophores from Photosynthetic Bacteria

Figure II-25 shows the CD spectrum and absorption spectrum of Rhodospirillum rubrum chromatophores, and Figure II-26 shows the absorption spectrum of chromatophores of Rhodopseudomonas spheroides, together with portions of the ORD and CD spectra. The near infrared peaks of chromatophores from both species of bacteria show pronounced double CD components, indicating strong bacteriochlorophyll interactions. It is interesting that while the solution dimers of all three chlorophylls have positive CD at long wavelength, all the in vivo material examined has a negative long wavelength CD component. It may be that grossly similar chlorophyll-chlorophyll interactions occur in all the in vivo material, whether plant or bacteria.

R. rubrum chromatophores exhibit a double CD band (Figure II-9) that crosses zero very close to the main absorption peak at 880 mμ.

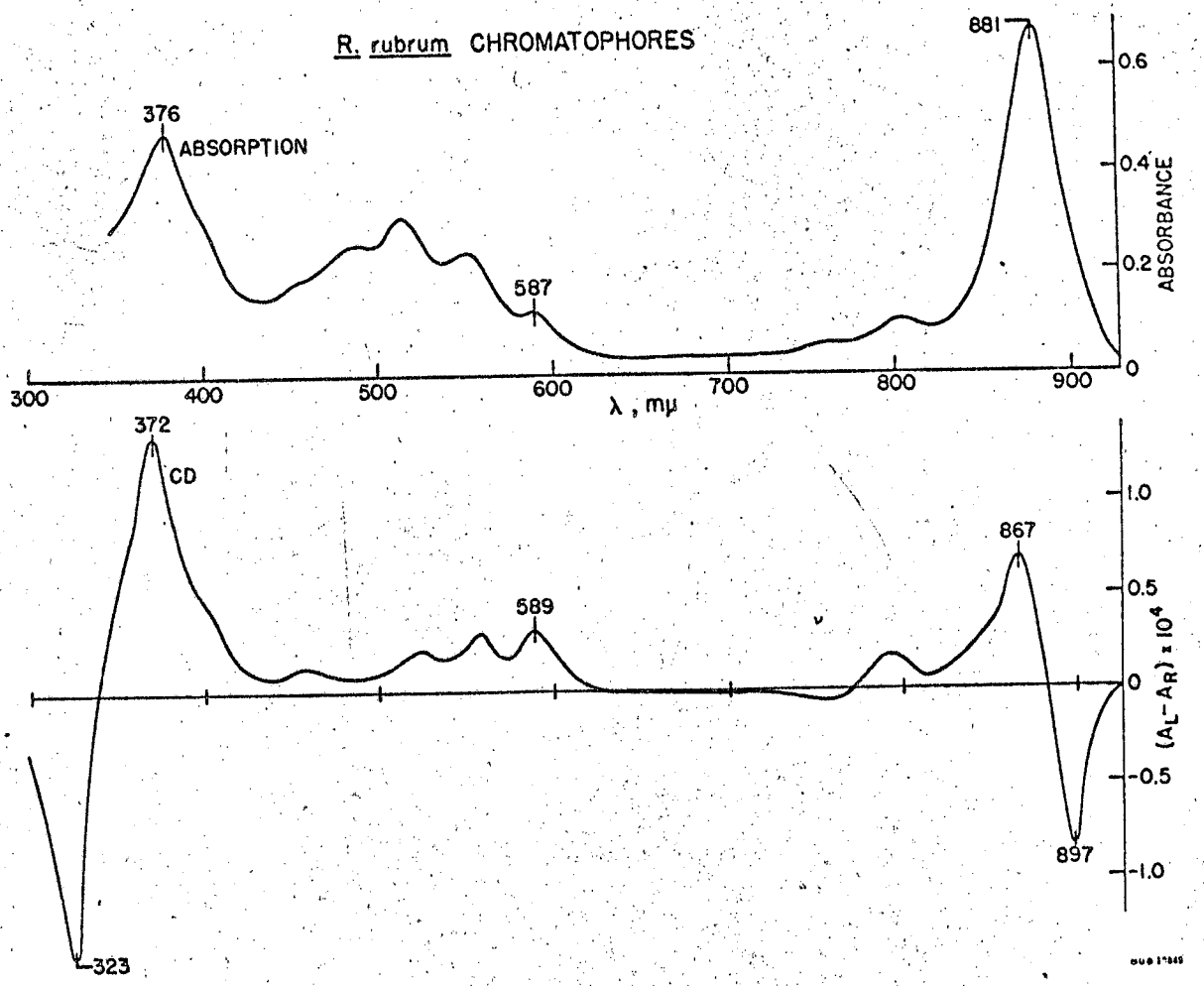

Figure II-25. Absorption and CD spectra of chromatophores from Rhodospirillum rubrum.

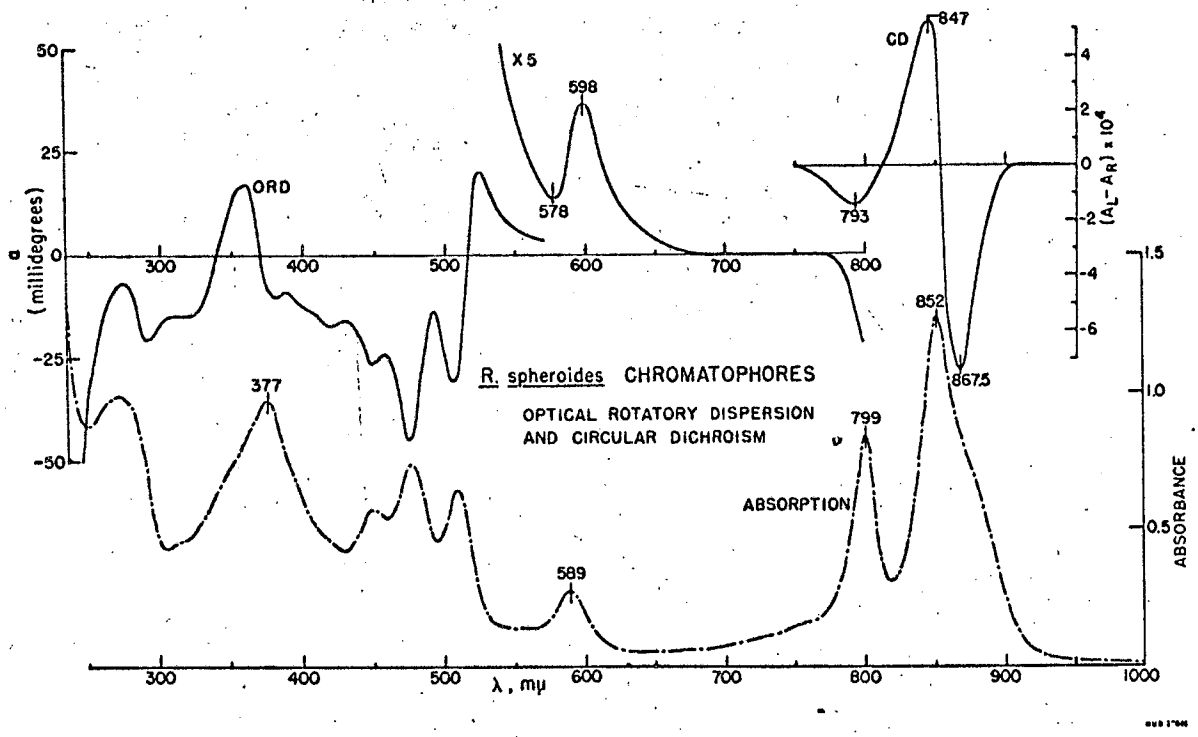

Figure II-26. Absorption, CD and ORD spectra of chromatophores from Rhodospirillum rubrum.

This indicates that at least some of the bacteriochlorophyll with absorption centered at the main peak is aggregated with an exciton splitting small compared to the band width. Little unaggregated bacteriochlorophyll seems to be present, as this peak in the chromatophore spectrum is sharp and not spread out, as it would have to be if both isolated and aggregated molecules were present together. The bacteriochlorophyll long wavelength peak is slightly wider for the chromatophores than for the monomer absorption in carbon tetrachloride. If we assume a band shape like that in the monomer spectrum, the exciton splitting is of the order of 30 - 60 cm^{-1}.

In R. rubrum, the 590 mμ bacteriochlorophyll CD peak has no obvious double CD component. However, the CD peak is red shifted from the absorption peak. Since this is an allowed electronic transition, one would not expect vibrational effects to shift the CD maximum from the absorption maximum (Moffitt and Moscowitz, 1959). A negative component of the bacteriochlorophyll CD on the short wavelength side of the 590 mμ peak may be obscured by the positive carotenoid CD. This could be the origin of the 2.5 mμ red shift of the positive bacteriochlorophyll CD peak. The CD curve at the bottom of Figure II-16 shows an example of the shift of a single CD peak centered at the absorption maximum by the addition of a double CD component. R. rubrum can be grown carotenoidless under the proper conditions (Cohen-Bazire and Stanier, 1958). Carotenoidless chromatophores would allow us to see the 590 mμ bacteriochlorophyll CD and absorption free of interference.

R. spheroides chromatophores (Figure II-26) show a particularly strong double CD in the longest wavelength absorption band, indicating

aggregation of the bacteriochlorophyll. The sharp peak on the short wavelength side at 799 mμ seems to have a comparatively weak double CD component, judged by the shift to 793 mμ in the CD spectrum, with a magnitude approximately equal to that of the solution dimer. The 799 mμ band absorbs about where the solution dimers do, but shows no obvious splitting in the chromatophore absorption spectrum. The positions of the double CD and absorption indicate that the band may be due to dimers of bacteriochlorophyll. The small exciton splitting requires that the dimers have a different geometry from that of the solution dimers.

The R. spheroides bacteriochlorophyll long wavelength absorption band at 852 mμ is red shifted much farther than the bacteriochlorophyll solution dimer and, since the double CD indicates an aggregate, the bacteriochlorophyll absorbing here is undoubtedly an aggregate higher than a dimer. There is an obvious long wavelength shoulder (ca. 880 mμ) on the main absorption band (852 mμ). The double CD component crosses zero slightly to the long wavelength side of the main absorption peak. Similar behavior is observed in all of the chlorophyll dimers in solution. The long wavelength shoulder may well be an exciton component split off from the main peak. Many photosynthetic bacteria show this long wavelength shoulder, sometimes to an extent that varies with growth conditions (Clayton, 1963). Under these conditions, either the bacteriochlorophyll aggregate geometry is altered or two different aggregated forms are present in variable amounts. Low temperature absorption and CD measurements may distinguish between these alternatives.

REFERENCES

Anderson, A. F. H., and M. Calvin, Arch. Biochem. Biophys. 107, 251 (1964).

Andrew, E. R. (1955), Nuclear Magnetic Resonance (Cambridge University Press, New York).

Aronoff, S., Arch. Biochem. Biophys. 98, 344 (1962).

Babcock, H. W., Astrophysical Journal 118, 387 (1953).

Bassham, J. A., and M. Calvin (1957), The Path of Carbon in Photosynthesis (Prentice Hall, Inc., Englewood Cliffs, N. J.).

Baum, W. A., and L. Dunkelman, J. Opt. Soc. Am. 40, 782 (1950).

Bellamy, W. D., G. L. Gaines, Jr. and A. G. Tweet, J. Chem. Phys. 39, 2528 (1963).

Bergman, K., and C. T. O'Konski, J. Phys. Chem. 67, 2169 (1963).

Billings, B. H., J. Opt. Soc. Amer. 39, 797 (1949); ibid. 39, 802 (1949); ibid. 47, 12 (1952).

Biltonen, R., to be published.

Boucher, L. J., H. H. Strain and J. J. Katz, J. Am. Chem. Soc. 88 (1966), in press.

Brown, J. S., and C. S. French, Plant Physiol. 34, 305 (1959).

Bush, C. A. (1965), Ph.D. Thesis, University of California, Berkeley.

Butler, W. L. (1966), The Chlorophylls, L. P. Vernon and G. R. Seely, eds. (Academic Press, N. Y.), p. 343.

Carpenter, R. O'B., J. Opt. Soc. Amer. 40, 255 (1950).

Clayton, R. K. (1963), in Bacterial Photosynthesis, H. Gest, A. San Pietro and L. P. Vernon, eds. (Antioch Press, Yellow Springs, Ohio), p. 495.

Clayton, R. L. (1966), The Chlorophylls, L. P. Vernon and G. R. Seely, eds. (Academic Press, N. Y.), p. 610.

Closs, G. L., J. J. Katz, F. C. Pennington, M. R. Thomas and H. H. Strain, J. Am. Chem. Soc. 85, 3809 (1963).

Cohen-Bazire, G., and R. Y. Stanier, Nature 181, 250 (1958).

Corwin, A. H., J. A. Water and R. Singh, J. Org. Chem. 27, 4280 (1962).

Davidson, N. (1962), Statistical Mechanics (McGraw-Hill Book Company, Inc., N. Y.), p. 299.

Davydov, A. S. (1962), Theory of Molecular Excitations (McGraw-Hill Book Company, Inc., N. Y.).

Deming, W. E. (1943), Statistical Adjustment of Data (John Wiley, N. Y.).

Devoe, H., and I. Tinoco, Jr., J. Mol. Biol. 4, 518 (1962).

Eyring, H., J. Walter and G. E. Kimball (1944), Quantum Chemistry (John Wiley & Sons, Inc., N. Y.).

Fernandez, J., and R. S. Becker, J. Chem. Phys. 31, 467 (1959).

Fleischer, E. B., J. Am. Chem. Soc. 85, 146 (1962).

Fulton, R. L., and M. Gouterman, J. Chem. Phys. 41, 2280 (1964).

Goedheer, J. C., Nature 176, 928 (1955).

Goedheer, J. C., Biochim. Biophys. Acta 16, 471 (1955).

Goedheer, J. C. (1957), Thesis, Utrecht.

Gouterman, M., J. Mol. Spectry. 6, 138 (1961).

Gouterman, M., G. Wagniere and L. C. Snyder, J. Mol. Spectry. 11, 108 (1963).

Grosjean, M., and M. Legrand, Compt. Rend. 251, 2150 (1960).

Highkin, H. R., and A. W. Frenkel, Plant Physiol. 37, 814 (1962).

Hochstrasser, R. M., and M. Kasha, Photochem. Photobiol. 3, 317 (1964).

Holzwarth, G., Rev. of Scientific Instr. 36, 59 (1965).

Jacobs, E. E., A. E. Vatter and A. S. Holt, Arch. Biochem. Biophys. 53, 228 (1954).

Katz, J. J., G. L. Closs, F. C. Pennington, M. R. Thomas and H. H. Strain, J. Am. Chem. Soc. 85, 3801 (1963).

Katz, J. J., R. C. Dougherty and L. J. Boucher (1966), in The Chlorophylls, L. P. Vernon and G. R. Seely, eds. (Academic Press, N. Y.), p. 186.

Kauzman, W. (1957), Quantum Chemistry (Academic Press, Inc., N. Y.).

Ke, B., Nature 208, 573 (1965).

Kelly, J., and K. Sauer, Biochemistry 4, 2798 (1965).

Klein, M. P., and G. W. Barton, Rev. Sci. Instr. 34, 754 (1963).

Lavorel, J., J. Phys. Chem. 61, 1600 (1957).

Levinson, G. S., W. T. Simpson and W. Curtis, J. Am. Chem. Soc. 79, 4314 (1957).

Livingston, R., W. F. Watson and M. McArdle, J. Am. Chem. Soc. 71, 1542 (1949).

Lowry, T. M. (1935), Optical Rotatory Power (Longmans, Green and Co., London); or (1964), Optical Rotatory Power (Dover Publications, Inc., N. Y.).

McClure, D. S., Solid State Phys. 8, 1 (1959).

Moffitt, W., and A. Moscowitz, J. Chem. Phys. 30, 648 (1959).

Moscowitz, A. (1960), in Optical Rotatory Dispersion, C. Djerassi, ed. (McGraw-Hill Book Company, Inc., N. Y.), p. 150.

Moscowitz, A., Adv. in Chem. Phys. 4, 1 (1962).

Olson, R. A., W. L. Butler and W. H. Jennings, Biochim. Biophys. Acta 58, 144 (1962).

Park, R. B., and N. G. Pon, J. Mol. Biol. 3, 1 (1961).

Platt, J. R., J. Chem. Phys. 17, 484 (1949).

Platt, J. R. (1956), in Radiation Biology, A. Hollaender, ed. (McGraw-Hill, N. Y.), Vol. III, Ch. 2.

Pauling, L. (1960), The Nature of the Chemical Bond (Cornell University Press, Ithaca, N. Y.), 3rd Ed.

Robinson, G. W. (1961), in Light and Life, W. D. McElroy and B. Glass, eds. (Johns Hopkins Press, Baltimore), p. 11.

Sandorfy, C. (1964), Electronic Spectra and Quantum Chemistry (Prentice-Hall, Inc., Englewood Cliffs, N. J.).

Sauer, K., Proc. Nat. Acad. Sci. 53, 716 (1965).

Sauer, K. S. (1966), unpublished work.

Sauer, K., and M. Calvin, Biochim. Biophys. Acta 64, 324 (1962).

Sauer, K., and M. Calvin, J. Mol. Biol. 4, 451 (1962).

Sauer, K., and J. Ku (1966), to be published.

Sauer, K., J. R. Lindsay Smith and A. J. Schultz, J. Am. Chem. Soc. 88, 2681 (1966).

Sidorov, A. N., and A. N. Terenin, Optics i Spectroscopy (USSR) 8, 254 (1960).

Thiery, J. M. (1965), private communication.

Tinoco, I., Jr., J. Chem. Phys. 33, 1332 (1960).

Tinoco, I., Jr., Adv. in Chem. Phys. 4, 113 (1962).

Tinoco, I., Jr., Radiation Res. 20, 133 (1963).

Tinoco, I., Jr., J. Am. Chem. Soc. 86, 297 (1964).

Tinoco, I., Jr., A. Halpern and W. T. Simpson (1962), Polyamino Acids, Polypeptides and Proteins, M. A. Stahmann, ed. (University of Wisconsin Press, Madison), p. 147.

Tinoco, I., Jr., R. W. Woody and D. F. Bradley, J. Chem. Phys. 38, 1317 (1963).

Velluz, L., M. Legrand and M. Grosjean (1965), Optical Circular Dichroism (Academic Press, Inc., New York).

Warshaw, M. M., C. A. Bush and I. Tinoco, Jr., Biochem. Biophys. Res. Commun. 18, 633 (1965).

Weber, G., and F. W. J. Teale, Trans. Faraday Soc. 54, 640 (1958).

Weigang, O. E., Jr., J. Chem. Phys. 43, 71 (1965).

Weiss, C., and M. Gouterman (1965), unpublished work.

Weiss, C., H. Kobayashi, and M. Gouterman, J. Mol. Spectry. 16, 415 (1965).

Wilson, E. B. (1952), Introduction to Scientific Research (McGraw-Hill Book Company, Inc., N. Y.).

Wilson, E. B., Jr., J. C. Decius and P. C. Cross (1955), Molecular Vibrations (McGraw-Hill Book Company, Inc., N. Y.), p. 286.

Young, J. (1966), Ph.D. Thesis, University of California, Berkeley.

III. ELECTRONIC STRUCTURE OF PORPHYRINS

General Introduction to Magnetic Optical Activity

The large majority of molecules do not have natural optical activity and cannot be studied by the methods of Chapters I and II. Michael Faraday discovered that optically inactive materials rotate the plane of polarized light in the presence of a magnetic field (Faraday, 1845, 1846). This phenomenon was called Faraday rotation, and it soon became clear that magnetic optical activity was a general phenomenon exhibited by all materials. A great deal of experimental work was done on magnetic optical rotation in the latter part of the 19th Century (Verdet, 1863; Perkin, 1896) and the early part of the 20th Century. Several reviews of the early work are available (Lowry, 1935; Partington, 1954; Waring and Custer, 1960; Buckingham and Stephens, 1966). I believe it is fair to say that with one or two exceptions (e.g., Van Vleck and Penny, 1936) the early magnetic optical activity work did not provide useful information.

Most of the magnetic optical activity experiments were done in transparent regions (but see: Cotton and Schérer, 1930). Natural optical activity has become the most useful when measuring in absorbing regions so that the contributions of single absorption bands to the optical activity can be separated (Djerassi, 1960; Mason, 1963; Velluz, Legrand and Grosjean, 1965; Holzwarth and Doty, 1965). Magnetic optical activity must be measured in absorption regions for any hope of interpreting the results. Recent instrumental advances have allowed magnetic optical activity measurements in absorbing regions. Both

magnetic optical rotatory dispersion (MORD) and magnetic circular dichroism (MCD) measurements of molecules in solution have been reported (Shashoua, 1964, 1965; Foss and McCarville, 1965; Schooley, Bunnenberg and Djerassi, 1965). However, most of the experimental work has been published with no attempt at interpretation. The recent theoretical analysis of MORD data by Stephens, Suetaka and Schatz, 1966, has begun to yield useful information on the electronic structure of molecules. There has also been some recent magnetic optical activity work done in the solid state which has been interpreted very nicely (Henry, Schnatterly and Slichter, 1965). A hundred years of experimental and theoretical groundwork is finally beginning to bear fruit.

Soon after the advent of quantum mechanics, Rosenfeld (1929) derived the basic quantum mechanical equations for magnetic optical activity. This derivation was expanded to paramagnetic ions by Kramers (1930) and to molecules by Serber (1932). These derivations have been modified by Tobias and Kauzman (1961) and Groenewege (1962). Bush and Tinoco (1964) extended the theory to polymers and Stephens has recently made some useful additions to the theory in the region of absorption (Stephens, 1966). The quantum mechanical theory seems to be in a satisfactory state to compare with experiment. Several early workers derived classical theories of MORD and these are reviewed by Partington (1956); most of the classical theories were not successful. Drude's classical theory of MORD (Drude, 1900) is basically sound, but it is incomplete in many important ways and is almost unbelievably opaque.

We derive a classical theory for MCD in order to clarify the physical basis of the phenomenon. We also present a simple semiclassical two-state

derivation to bridge the gap to the more general quantum mechanical theory (e.g., Stephens, 1966). Some special theoretical topics such as multiplicity-forbidden transitions and the effect of unpaired spin are discussed. The experimental section discusses instrumentation briefly. We present detailed experimental results on various metal porphyrins and heme proteins, cytochrome c and hemoglobin derivatives. The experiments are interpreted by free electron theory and molecular orbital theory. These results give information on porphyrin electronic structure, metal-porphyrin interactions and ligand interactions. Many other types of molecules were investigated and these are mentioned at the end in a general assessment and evaluation of the probable usefulness of MCD in chemistry and biology.

A. Classical Theory of MCD

The systematic quantum mechanical theories of magnetic optical activity, even when presented lucidly (e.g., Stephens, 1966), are exceedingly complicated. Furthermore, the physical basis for the phenomenon is obscured in a morass of notation and formalism in the quantum mechanical theories. The measurement of magnetic optical activity is becoming more common in chemistry and biology and a more intuitively appealing derivation is needed. It is important to note that the classical model, coupled with a very simple semi-classical derivation, reproduces the results of the general quantum mechanical theory exactly. We hope that the "theory" presented here will add insight at the expense of a little rigor and that it will be a useful guide to the experimentalist.

General method, background and preliminaries

The MCD will be derived by considering the power absorbed by a pair of classical oscillators in a magnetic field. Consider a molecule, initially fixed in space with an optically excitable electron bound (by "springs") so that it can oscillate in the x and y directions. Circularly polarized light is propagated along the z axis: $E = E_x \cos \omega t \pm E_y \sin \omega t$ (where ω is the frequency of the light) and a magnetic field is directed along the z axis $H = H_z$. Electron spin will be neglected initially and will be treated in the semi-classical part later.

The essential point is that the previously independent x and y oscillators are coupled in the magnetic field by the Lorentz force:

$$F_x = (e/c)\, \dot{r}_y\, H_z = (e/c)\, v_y\, H_z \qquad \text{III-(1)}$$

$$F_y = (e/c)\, \dot{r}_x\, H_z = (e/c)\, v_x\, H_z \qquad \text{III-(2)}$$

where r_x and r_y are the coordinates of the electron and v_x and v_y are the x and y components of the instantaneous velocity, e is the charge on the electron and c is the speed of light. In the presence of the magnetic field, motion in the x direction results in a y directed force. This is analogous to a molecular Hall effect in that a current (charge motion, $dr/dt = \dot{r}$) in the presence of a magnetic field gives rise to a force on the charge perpendicular to both the current and the field.

The forces on the electron in the presence of the light and the field are:

inertia + viscosity + restoring force = driving force

mass·acceleration + damping · velocity + displacement · spring constant = driving force

Spring constants k_x, k_y are related to the oscillator resonant frequencies;

$k_x = m\omega_x^2$, $k_y = m\omega_y^2$, and we define damping constants: damping = $m\gamma_x$ where m is the electron mass. The equations for the forces on the electron in the presence of the magnetic field and the circular light can be written for the x and y directions:

$$x: m(\ddot{r}_x + \gamma_x\dot{r}_x + \omega_x^2 r_x) = (e/c)\,\dot{r}_y H_z + (eE_x/m)\cos\omega t \qquad \text{III-(3)}$$

$$y: m(\ddot{r}_y + \gamma_y\dot{r}_y + \omega_y^2 r_y) = (e/c)\,\dot{r}_x H_z \pm (eE_y/m)\sin\omega t \qquad \text{III-(4)}$$

The response of the system can be considered linear for small fields and we define in-phase response coefficients, A_x and A_y, and out-of-phase response coefficients, B_x and B_y:

$$r_x = A_x \cos\omega t + B_x \sin\omega t \qquad \text{III-(5)}$$

$$r_y = A_y \sin\omega t + B_y \cos\omega t \qquad \text{III-(6)}$$

The A coefficients characterize the displacement of the electron in-phase with the exciting light and can be shown to be responsible for the refractive index and magnetic optical rotation. The response out-of-phase with the driving light corresponds to absorption and magnetic circular dichroism as will become clear below.

In the absence of the H field, the perpendicular oscillators are independent. We will digress to review the well known results for independent oscillators to make clear the significance of the A and B coefficients without the complication of the coupling. If $H_z = 0$, equations III-(3) and (4) are identical apart from the different resonant frequencies, ω_1 and damping constants. We need consider one equation only, e.g., the x equation. The results at the end will be the same for the y equation. Substituting the response equations, III-(5), (6) into III-(3) with $H_z = 0$, we get the following:

$$(-\omega^2 A_x + \gamma_x\omega B_x + \omega_x^2 A_x)\cos\omega t + (\omega^2 B_x - \gamma_x\omega A_x + \omega_x^2 B_x)\sin\omega t = (eE/m)(\cos\omega t) \qquad \text{III-(7)}$$

The coefficients of the cosine terms on the right and left hand sides must be equal and independent of the sine terms, so two equations result:

$$A_x = \frac{(eE/m)(\omega_x^2 - \omega^2)}{(\omega_x^2 - \omega^2)^2 + \gamma_x^2\omega^2} \qquad \text{III-(10)}$$

$$B_x = \frac{(eE/m)\,\gamma_x\omega}{(\omega_x^2 - \omega^2)^2 + \gamma_x^2\omega^2} \qquad \text{III-(11)}$$

A dipole moment μ is induced by the displacement of the charge. The in-phase moment is $\mu_x = eA_x$ and the out-of-phase moment is $\mu_x' = eB_x$. The polarizability is the induced moment divided by the field producing the moment. The in-phase polarizability α_x is therefore:

$$\alpha_x = \frac{\mu_x}{|E_x|} = \frac{e^2}{m}\,\frac{(\omega_x^2 - \omega^2)}{(\omega_x^2 - \omega^2)^2 + \gamma_x^2\omega^2} \qquad \text{III-(12)}$$

while the out-of-phase polarizability α_x' is:

$$\alpha_x' = \frac{\mu_x'}{|E_x|} = \frac{e^2}{m}\,\frac{\gamma_x\,\omega}{(\omega_x^2 - \omega^2)^2 + \gamma_x^2\omega^2} \qquad \text{III-(13)}$$

This last term will be shown to give absorption. The work done on the system (electron) by the light is the force displacement: $W = \vec{F}\cdot\vec{r}$. The rate of work done is the power absorbed: $P = dW/dt$: $= \vec{F}\cdot d\vec{r}/dt = e\vec{E}\cdot\vec{v}$. The velocity in the x direction can be expressed as the derivative of eq. III-(5).

$$r_x = A_x \cos\omega t + B_x \sin\omega t \qquad \text{III-(5)}$$

$$\dot{r}_x = v_x = \omega(-A_x \sin\omega t + B_x \cos\omega t) \qquad \text{III-(14)}$$

The power absorbed by the x oscillator can be found using eqs. III-(14), (12), (13):

$$P_x = (dW/dt)_x = e(\vec{E}\cdot\vec{v})_x = \omega eE_x(-A_x \sin \omega t \cos \omega t + B_x \cos^2 \omega t) \qquad \text{III-(15)}$$

The average value of the power absorbed over one cycle of the light can be found by integrating over ωt.

$$\bar{P}_x = (\overline{dW/dt})_x = eE_x \int_0^{2\pi} (-A_x \sin \omega t \cos \omega t + B_x \cos^2 \omega t)\, d(\omega t) \qquad \text{III-(16)}$$

This is where it becomes clear that the in-phase response (A_x) term contributes zero to the average absorption, while the out-of-phase response (B_x) term gives the average power absorbed per molecule (integration of $\int_0^{2\pi} \sin x \cos x\, dx = 0$, $\int_0^{2\pi} \cos^2 x\, dx = 1/2$):

$$\bar{P}_x = (\overline{dW/dt})_x = eE_xB_x/2 = \frac{e^2E_x^2\,\omega\,\gamma_x}{m[(\omega_x^2 - \omega^2)^2 + \gamma_x^2\omega^2]} \qquad \text{III-(17)}$$

The change in intensity caused by passage of light across dz cm of a volume with N molecules/cm^3 is:

$$-dI = \bar{P}N\, dz \qquad \text{III-(18)}$$

Both sides of eq. III-(18) are divided by the x polarized light intensity, $I = cE_x^2/4\pi$ and the resulting expression is integrated to determine the absorption:

$$\ln(I/I_o) = 4\pi N\bar{P} z/c \equiv \sigma_x Nz \qquad \text{III-(19)}$$

where σ_x is an absorption cross section[1] which is defined by the above relation. The absorption is only significant when ω is near ω_x so we may simplify the cross section equation using the resonance approximation: $(\omega_x^2 - \omega^2) \approx 2\omega(\omega_x - \omega)$. With this approximation the cross section can be written:

$$\sigma_x = (4\pi e^2/mc) \frac{\gamma_x/4}{(\omega_x - \omega)^2 + \gamma_x^2/4} \propto B_x \qquad \text{III-(20)}$$

Equation III-(20) describes the well known damped oscillator or Lorentzian absorption line.

---

[1]The absorption cross section can be related to the more familiar decadic molar extinction coefficient, ε, by: $\varepsilon = \sigma N_o/2303$, where N_o is Avogadro's number.

We see that the absorption depends on the response of the oscillator out-of-phase to the light and in a similar manner that the polarizability depends on the in-phase response of the oscillator. As the frequency approaches ω_x, the polarizability due to the x oscillator and the absorption of the x oscillator vary as shown below.

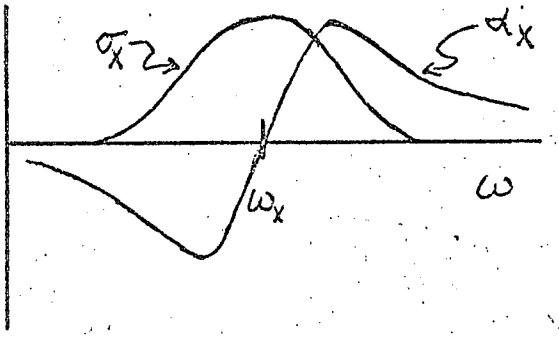

The y oscillator will show a similar curve at some other frequency, ω_y, or if $\omega_x = \omega_y = \omega_o$ the absorption and polarizability amplitude would be twice as big at ω_o.

The magnetic field may now be added to couple the two oscillators. Three cases will be of interest: nondegenerate oscillators $\omega_x << \omega_y$, degeneracy $\omega_x = \omega_y = \omega_o$, and near degeneracy $\omega_x \approx \omega_y$. Each of these cases will be treated separately for added clarity; however, the near degenerate problem requires a general solution which contains the other two as special cases.

Nondegenerate oscillators

The nondegenerate limiting case corresponds to the situation where the two oscillators absorb at widely separated frequencies so that when the region of absorption of one oscillator is investigated there is negligible absorption from the other oscillator. If we investigate the ω_x region the y oscillator will respond in phase with the driving

light frequency, ω. Since we are investigating x, we can neglect the effect of the field on y. These simplifications reduce eq. III-(4) to:

$$\ddot{r}_y + \omega_y^2 r_y = \pm \frac{eE_y}{m} \sin \omega t \qquad \text{III-(21)}$$

As we remarked above, the y displacement is entirely in-phase with the driving light, so eq. III-(6) is:

$$r_y = A_y \sin \omega t \qquad \text{III-(22)}$$

Thus, the in-phase y displacement coefficient, A_y, is simply:

$$A_y = \pm \frac{eE_y}{m(\omega_y^2 - \omega^2)} \qquad \text{III-(23)}$$

The velocity in the y direction can be found by substitution of eq. III-(23) into the time derivative of eq. III-(22):

$$v_y = \dot{r}_y = \pm \frac{eE_y}{m(\omega_y^2 - \omega^2)} \cos \omega t \qquad \text{III-(24)}$$

Now the forces on the x oscillator can be written including the effect of the y oscillator by substituting eq. III-(24) into eq. III-(3):

$$\ddot{r}_x + \gamma_x \dot{r}_x + \omega_x^2 r_x = \frac{eE}{m}\left(1 \pm \frac{eH}{mc}\frac{\omega}{\omega_y^2 - \omega^2}\right) \cos \omega t \qquad \text{III-(25)}$$

where $E = E_x = E_y$ for circularly polarized light and the $\pm$ signs refer to right and left circularly polarized light.

It should be emphasized at this point that eq. III-(25) shows the physical basis of nondegenerate MCD. The presence of the y oscillator in the field gives the x oscillator a boosting force in the right circular light which leads to an increase in absorption by the x oscillator in right circular light. The y oscillator drags the x oscillator in left circular light, which will lead to a decrease in absorption by the x oscillator in left circular light. The x and y oscillator interaction

depends linearly on the H field and is the molecular Hall effect basis of the nondegenerate MCD mentioned earlier. The x-directed force due to the y oscillator will depend on how close ω_y is, because of the $\pm\, 1/(\omega_y^2 - \omega^2)$ term in eq. III-(25). To further develop this case we substitute eq. III-(5) into III-(25) to get the following:

$$(\omega_x^2 - \omega^2)(A_x \cos \omega t + B \sin \omega t) + \omega\gamma_x(-A_x \sin \omega t + B_x \cos \omega t) = \frac{eE}{m}\left[\pm \frac{eH}{mc} \frac{\omega}{(\omega_y^2 - \omega^2)} + 1\right] \cos \omega t \qquad \text{III-(26)}$$

where $E_x = E_y = E$ for circular light. The cos and sin terms are separately equal as before so we get two equations.

$$(\omega_x^2 - \omega^2)\, B_x - \omega\gamma_x A_x = 0 \qquad \text{III-(27)}$$

$$(\omega_x^2 - \omega^2)\, A_x + \omega\gamma_x B_x = \frac{eE}{m}\left[\pm \frac{eH}{mc} \frac{\omega}{(\omega_y^2 - \omega^2)} + 1\right] \qquad \text{III-(28)}$$

which are easily solved for the unknowns A_x and B_x to obtain:

$$A_x = \frac{(eE/m)(\omega_x^2 - \omega^2)\left[1 \pm \left(\frac{eH}{mc}\right)\frac{\omega}{(\omega_y^2 - \omega^2)}\right]}{(\omega_x^2 - \omega^2)^2 + \omega^2\gamma_x^2} \qquad \text{III-(29)}$$

$$B_x = \frac{(eE/m)\,\omega\gamma_x\left[1 \pm \left(\frac{eH}{mc}\right)\frac{\omega}{(\omega_y^2 - \omega^2)}\right]}{(\omega_x^2 - \omega^2)^2 + \omega^2\gamma_x^2}. \qquad \text{III-(30)}$$

The average power absorbed is found from the B_x coefficient as in eq. III-(17).

$$P_x = \left(\frac{dW}{dt}\right)_x = \frac{eE_x B_x \omega}{2} = \frac{e^2 E_x^2}{2m} \frac{\omega\gamma_x\left[1 \pm \left(\frac{eH}{mc}\right)\frac{\omega}{(\omega_y^2 - \omega^2)}\right]}{(\omega_x^2 - \omega^2)^2 + \omega^2\gamma_x^2} \qquad \text{III-(31)}$$

The power absorbed by the x oscillator is different for right (+) and left (-) circular light. The power absorbed is related to the absorption cross section, σ, in the usual way (eq. III-(19).

$$\sigma_{x\pm} = \frac{2\pi e^2 \omega^2 \gamma_x}{mc} \frac{\left[1 \pm \left(\frac{He}{mc}\right)\frac{\omega}{(\omega_y^2-\omega^2)}\right]}{(\omega_x^2-\omega^2)^2 + \omega^2\gamma_x^2} \qquad \text{III-(32)}$$

The absorption cross sections for right (σ_{x+}) and left (σ_{x-}) are shown below as well as the MCD, $\Delta\sigma$, which is the difference in absorption in right and left light:

$$\text{MCD} = \Delta\sigma_x = \sigma_{x+} - \sigma_{x-}$$

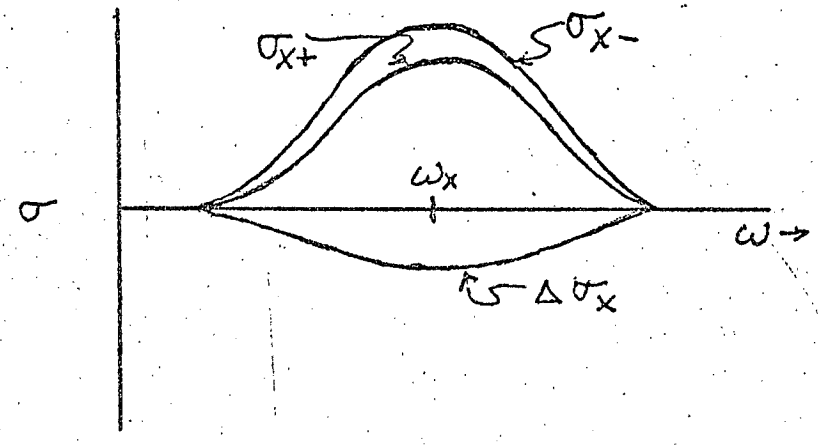

An expression for the MCD is given by:

$$\Delta\sigma_x = \sigma_{x+} - \sigma_{x-} = \frac{4\pi e^3 H \omega^3}{m^2 c^2} \frac{\gamma_x}{\left[(\omega_x^2-\omega^2)^2 + \omega^2\gamma_x^2\right](\omega_y^2-\omega^2)} \qquad \text{III-(33)}$$

For the nondegenerate case, we see that the MCD near ω_x is a single dichroism band with the same shape as the absorption; it can be positive or negative depending on the sign of $(\omega_y^2 - \omega^2)$, that is, whether ω_y is greater or less than ω_x. The formula for the MCD at ω_y is the same, except ω_x and ω_y are interchanged and γ_y replaces γ_x. If $\gamma_x = \gamma_y$ the MCD at ω_y is the same amplitude as that at ω_x but of opposite sign. The maximum value of the frequency (shape) term is $1/\gamma$ as written in III-(34), so if γ_x differs from γ_y the MCD bands at ω_x and ω_y have equal but oppositely signed areas (Area = height x width). The MCD for two widely

separated transitions is shown below.

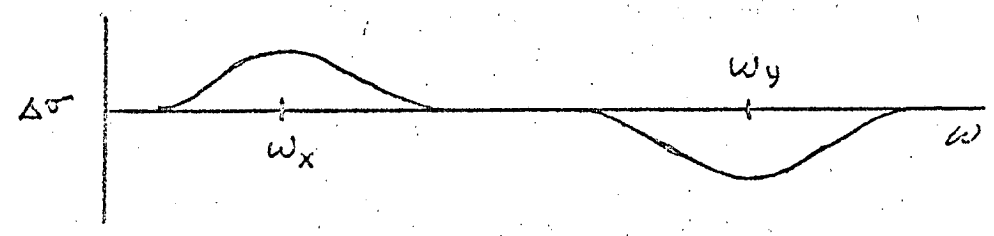

This is an important general result: The x-y nondegenerate interactions cancel in pairs, and it follows that nondegenerate MCD, $\Delta\sigma$, summed over all frequencies is zero. Of course an actual molecule has many x, y transitions that can interact in a magnetic field, and few molecules would be expected to be as simple as the above example. The external magnetic field does not couple y polarized with other y polarized transitions, but only with x polarized transitions. If we take a slightly more complicated case of two y polarized oscillators and one x oscillator we can schematically represent the MCD as:

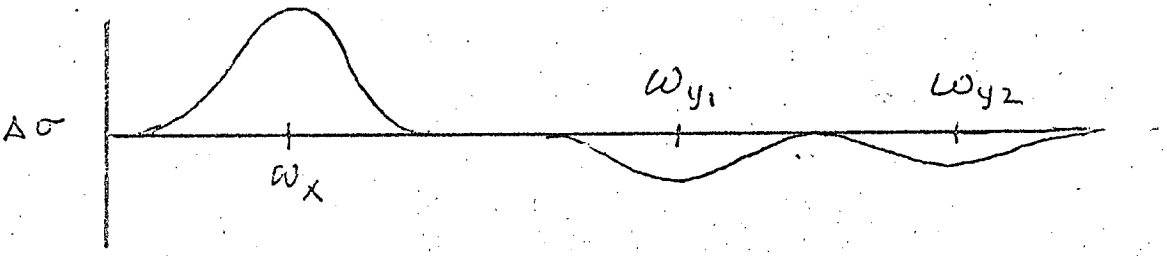

A slightly more detailed argument (which will be given later) shows that the strength of interaction between x and y oscillators depends on the product of their absorption strength (which would be clear if oscillator strengths were put into the classical model as is usually done). For molecules of low symmetry where transitions cannot be classified as x and y, the MCD resulting from non-parallel transitions is proportional to $\sqrt{f_1 \; f_2 \cos \theta_{12}}$, where θ_{12} is the angle between transition 1 and 2 and f_1, f_2 are the oscillator strengths of the transitions.

Degenerate Oscillators

The degenerate case corresponds to $\omega_x = \omega_y = \omega_o$, so that displacements in the x and y directions are equivalent. The oscillations can have a circular component, the sense of the circulation depends upon the particular combination of x and y displacements. We can define a right and a left hand circulation as:

$$r_+ \equiv r_x + ir_y$$
$$r_- \equiv r_x - ir_y \qquad \text{III-(35)}$$

where the molecular plane is now the complex plane and $i = \sqrt{-1}$. The circular displacements have equivalent energy in the absence of the magnetic field, but the magnetic field causes an increase in the energy (frequency) of r_+ and a decrease in the energy (frequency) of r_-. The circular charge motion is like an electronic orbital motion (in the molecular x,y plane) and the presence of the magnetic field causes an orbital Zeeman splitting. This degenerate MCD case has been treated satisfactorily in nearly every book on physical optics (e.g., Stone, 1963), so we will be brief here. In the complex plane, circularly polarized light can be represented, $E = E_o e^{\pm i\omega t}$. If we add and subtract eqs. III-(3), (4) in the following way, (3) + i (4) and (3) - i (4), we get an expression for the forces on the circular oscillator (in the presence of a magnetic field).

$$\left(\frac{d^2}{dt^2} + \gamma\frac{d}{dt} + \omega_o^2\right) r_\pm = \pm i\frac{eH}{mc} r_\pm + \frac{eE}{m}\begin{Bmatrix} e^{\pm i\omega t} \\ e^{\mp i\omega t} \end{Bmatrix} \qquad \text{III-(36)}$$

where the top equation is for r_+ and the bottom for r_-. To derive the MCD we again require the power absorbed by the circular oscillator.

$$P = dW/dt = e\vec{v}\cdot\vec{E} = e(v_x E_x + v_y E_y) \qquad \text{III-(37)}$$

and since $v_x = (v_+ + v_-)/2$, $v_y = (v_+ - v_-)/2$, $E_x = (E_+ + E_-)/2$ and $E_y = (E_+ - E_-)/2$, the power absorbed by the circular oscillator is:

$$P = e/2(v_+ E_- + v_- E_+) \qquad \text{III-(38)}$$

Note that the (+) motion absorbs (-) light and vice versa.

We define complex response coefficients, $A_\pm$ as:

$$v_\pm \equiv A_\pm \left\{ \begin{matrix} e^{\mp i\omega t} \\ e^{\mp i\omega t} \end{matrix} \right\} \qquad \text{III-(39)}$$

Equation III-(39) is substituted into eq. III-(36) and the resulting simultaneous equations are solved for A_+ and A_- yielding:

$$A_+ = \frac{eE/m}{(\omega^2 - \omega_o^2) \mp \frac{eH\omega}{mc} \pm i\omega\gamma} \qquad \text{III-(40a)}$$

$$A_- = \frac{eE/m}{(\omega^2 - \omega_o^2) \mp \frac{eH\omega}{mc} \mp i\omega\gamma} \qquad \text{III-(40b)}$$

A_- is the complex conjugate of A_+.

We need the time average of the power absorbed, which is found by substitution of eqs. III-(39) and III-(40) into III-(38) and integrating with respect to d(ωt) from 0 to 2π. The result is:

$$\overline{P}_\pm = \frac{e^2E^2}{m} \frac{\gamma/4}{\left(\omega - \omega_o \mp \frac{eH}{2mc}\right)^2 + \gamma^2/4} \qquad \text{III-(41)}$$

where the resonance approximation, $\omega_o^2 - \omega^2 \approx 2\omega\ (\omega_o - \omega)$, has been applied.

Using the definition of absorption cross section, III-(19), we can write the cross section in left and right light, $\sigma_\pm$ as:

$$\sigma_\pm = \frac{4\pi e^2}{mc} \frac{\gamma/4}{\left[\omega - \left(\omega_o \pm \frac{eH}{2mc}\right)\right]^2 + \gamma^2/4} \qquad \text{III-(42)}$$

In the absence of the field, the normal absorption formula results:

$$\sigma_+ = \sigma_- = \frac{4\pi e^2}{mc} \frac{\gamma/4}{(\omega-\omega_0)^2 + \gamma^2/4} \qquad \text{III-(20)}$$

However, in the presence of the field the absorption is split into two components, one absorbing right circular light at $\omega_0 + eH/2mc$ and one absorbing left circular light at $\omega_0 - eH/2mc$. The MCD experiment measures the difference in these two cross sections, as is shown below.

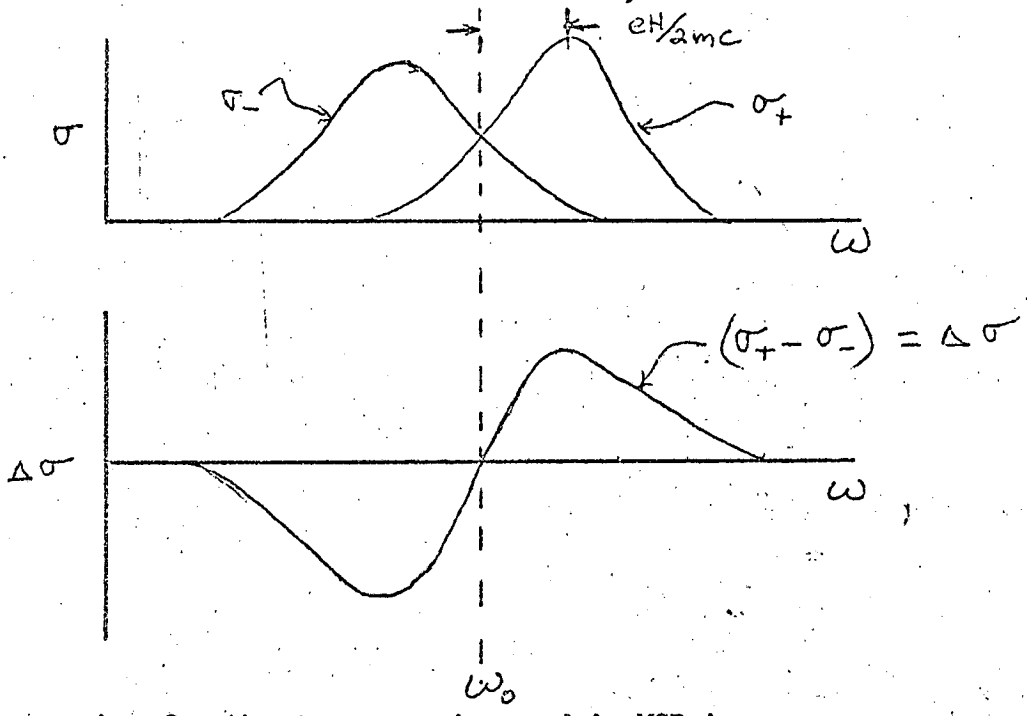

An expression for the $\Delta\sigma$ curve observed in MCD is:

$$\Delta\sigma = \sigma_+ - \sigma_- = \frac{4\pi e^2}{mc}\left[\frac{\gamma/4}{\left(\omega-\omega_0+\frac{eH}{2mc}\right)^2+\gamma^2/4} - \frac{\gamma/4}{\left(\omega-\omega_0-\frac{eH}{2mc}\right)^2+\frac{\gamma^2}{4}}\right] \qquad \text{III-(43)}$$

There are several simple ways of putting the above into a more compact form, but this is an opportunity to point out a more general result that will be useful later.

In practice, molecular absorption lines depart considerably from the damped oscillator, Lorentzian, shape that results from this treatment. One can always say that the absorption depends upon some constant

times a shape function, $f(\omega, \omega_o, \gamma)$, where this may be a Lorentzian, Gaussian or some other shape: $\sigma = C\, f(\omega, \omega_o, \gamma)$. In the presence of the field, the two absorption curves are:

$$\sigma_+ = C\, f(\omega, \omega_o + \delta, \gamma)$$
$$\sigma_- = C\, f(\omega, \omega_o - \delta, \gamma) \qquad \text{III-(44)}$$

where $\delta = eH/2mc$, is the Zeeman splitting. The difference between σ_+ and σ_- can be found from a Taylor series expansion about ω_o:

$$\sigma_+ - \sigma_- = \Delta\sigma \approx C\delta f'(\omega, \omega_o, \gamma) + C\delta^3/6\, f'''(\omega, \omega_o, \gamma) + ... \qquad \text{III-(45)}$$

Where the ' and ''' refer to the first and third derivative of the function with respect to frequency If the splitting, δ, is much less than the line width, γ, the first term is sufficient to very good accuracy. The maximum value of the nth derivative of any reasonable shape functions is proportional to $1/\gamma^n$, so the second term in III-(45) is reduced, relative to the first term, by the Zeeman splitting over the line width squared. The value of the second term is extremely small (< 0.01%), compared to the first term, in most cases of interest.

For the Lorentzian, damped oscillator case the MCD resulting from the first term of eq. III-(45) is:

$$\Delta\sigma = \frac{8\pi e^3}{m^2c^2} H \frac{(\omega-\omega_o)\ \gamma^4/4}{[(\omega-\omega_o)^2 + \gamma^2/4]^2} \qquad \text{III-(46)}$$

This form can also be derived from eq. III-(42) or III-(43) by other more direct approximations, but the more general treatment above will be useful later.

We see, in a fairly simple way, how degenerate x and y oscillators give rise to an orbital motion which is subject to a Zeeman splitting in the presence of the magnetic field. One Zeeman component absorbs the left circular light and the other Zeeman component absorbs the

right light. Zeeman splitting of a degeneracy gives a double MCD curve. The maximum value of the signal will depend on the ratio of the splitting, δ, to the line width, γ, and will, of course, be largest for narrow lines. Even so, the MCD approach allows study of Zeeman splittings which are as small as 10^{-4} of the absorption line width. The existence of an x - y degeneracy requires that a molecule have a 3-fold or higher axis of symmetry and this restricts the possible cases. It will be shown later that near degeneracy gives similar effects, however, and in molecules which depart only slightly from x - y degeneracy, the double MCD curves will result.

Comparison of eq. III-(46) and III-(34) indicates that the relative magnitudes of the nondegenerate and degenerate MCD effects scale as:

$$\frac{\Delta\sigma \text{ nondeg}}{\Delta\sigma \text{ deg}} \approx \frac{\gamma\omega}{2(\omega_y^2 - \omega_x^2)} \qquad \text{III-(47)}$$

where the same γ is assumed for both cases. Compared to the degenerate case, the nondegenerate MCD signal drops off rapidly as the x and y transitions become far apart.

After a few more classical arguments, a semi-classical treatment will allow consideration of the effects of electron spin and multiplicity forbidden transitions on the orbital Zeeman effect.

In general, we can relate the observed MCD to two terms, one term (nondegenerate) with the shape of the absorption, eq. III-(34), and one term (degenerate) with the shape of the derivative of the absorption, eq. III-(46). A more general classical derivation, which follows, includes oscillator strengths, treats the intermediate near-degeneracy case, and includes the effect of random orientation of molecules as occurs in a solution of isotropic glass.

General Classical MCD

From a molecular orbital point of view, as the electrons in a molecule change their distribution during an electronic transition (analogous to a classical oscillation) the net charge displacement along a particular molecular axis may be much less than a unit electronic charge. We are guided by this idea in the following classical model, where an effective charge of the oscillating electron, e_x and e_y is introduced. It will become clear that the square of the ratio of the effective charge to the electronic charge is the well known oscillator strength, i.e., $(e_x/e)^2 = f_x$. Also, we consider the problem of space fixed fields, E_X, E_Y, and H_Z, and randomly oriented, molecule fixed oscillators x and y such as would obtain in solution. This problem is handled in a general, if a slightly cumbersome, way by projecting the space fixed fields onto the molecule fixed axes with use of the direction cosines (Margenau and Murphy, 1956). The space fixed coordinate system (X,Y,Z) is defined with unit vectors $\hat{i}$, $\hat{j}$, $\hat{k}$ respectively. The circularly polarized light is in the X, Y plane and is denoted $E(\hat{i} \cos \omega t \pm \hat{j} \sin \omega t)$ and the magnetic field is along the Z axis and is denoted $\hat{k}H$. The projections of the space fixed fields on the molecular axes are found from the matrix of the direction cosines A_{ij}:

$$\begin{matrix} \text{Molecular} \\ \text{Components} \end{matrix} \qquad \begin{matrix} \\ \text{Space fixed} \\ \text{fields} \end{matrix}$$

$$\begin{pmatrix} x \\ y \\ z \end{pmatrix} = \begin{pmatrix} A_{11} & A_{12} & A_{13} \\ A_{21} & A_{22} & A_{23} \\ A_{31} & A_{32} & A_{33} \end{pmatrix} \begin{pmatrix} E \cos \omega t \\ \pm E \sin \omega t \\ H \end{pmatrix} \qquad \text{III-(48)}$$

The projections of the external fields on the molecular axes are:

$$\begin{aligned} x&: \; A_{11} E \cos \omega t \pm A_{12} E \sin \omega t + A_{13} H \\ y&: \; A_{21} E \cos \omega t \pm A_{22} E \sin \omega t + A_{23} H \\ z&: \; A_{31} E \cos \omega t \pm A_{32} E \sin \omega t + A_{33} H \end{aligned} \qquad \text{III-(49)}$$

The forces of the pair of oscillators can be conveniently described in terms of a displacement $\vec{r} = \hat{i}\, r_x + \hat{j}\, r_y$ in the following equation:

$$\ddot{\vec{r}} + \underset{\sim}{\gamma} \cdot \dot{\vec{r}} + \underset{\sim}{\omega}^2 \cdot \vec{r} = \frac{\underset{\sim}{e}}{mc} \dot{\vec{r}} \times \vec{H} + \frac{\underset{\sim}{e} \vec{E}}{m} \qquad \text{III-(50)}$$

where $\underset{\sim}{e}$, $\underset{\sim}{\gamma}$ and $\underset{\sim}{\omega}$ stand for the x and y components of the effective charge, damping constant and resonant frequency respectively. $H_x = H_y = 0$, so the $\dot{\vec{r}} \times \vec{H}$ terms of interest are $\hat{i}\, \dot{r}_y H_z - \hat{j} \dot{r}_x H_z$. The x and y components of displacement can be written (where the effective charges e_x and e_y have been incorporated):

$$\ddot{r}_x + \gamma_x \dot{r}_x + \omega_x^2 r_x = A_{33} \frac{e_x}{mc} \dot{r}_y H_z + \frac{e_x E}{m} (A_{11} \cos \omega t \pm A_{12} \sin \omega t) \qquad \text{III-(51)}$$

$$\ddot{r}_y + \gamma_y \dot{r}_y + \omega_y^2 r_y = -A_{33} \frac{e_y}{mc} \dot{r}_x H_z + \frac{e_y E}{m} (A_{21} \cos \omega t \pm A_{22} \sin \omega t) \qquad \text{III-(52)}$$

The derivation proceeds as before by defining the displacement coefficients:

$$\begin{aligned} r_x &\equiv A_x \cos \omega t + B_x \sin \omega t \\ r_y &\equiv A_y \sin \omega t + B_y \cos \omega t \end{aligned} \qquad \text{III-(5),(6)}$$

Equations III-(5) and (6) are substituted into II-(51) and (52) and four equations result since the coefficients of the sin and cos terms must be independently equal:

$$\begin{aligned} &(1) \cos \omega t: \; -\omega^2 A_x + \gamma_x \omega B_x + \omega_x^2 A_x = \frac{e_x H_z \omega}{mc} A_{33} A_y + \frac{e_x E}{m} A_{11} \\ &(2) \sin \omega t: \; -\omega^2 B_x - \gamma_x \omega A_x + \omega_x^2 B_x = -\frac{e_x H_z \omega}{mc} A_{33} B_y \pm \frac{e_x E}{m} A_{12} \end{aligned} \qquad \text{III-(53) (Cont.)}$$

$$(3)\ \sin\omega t:\quad -\omega^2 A_y - \gamma_y\omega B_y + \omega_y^2 A_y = \frac{e_y H_z \omega}{mc} A_{33}A_x \pm \frac{e_y E}{m} A_{22}$$

$$(4)\ \cos\omega t:\quad -\omega^2 B_y + \gamma_y\omega A_y + \omega_y^2 B_y = -\frac{e_y H_z \omega}{mc} A_{33}B_x + \frac{e_y E}{m} A_{21} \qquad \text{III-(53)}$$

These equations can be solved for the unknown response coefficients, A_x, B_x, A_y and B_y. First, however, we anticipate that we will be interested in the average power absorbed by the oscillators, $\overline{P} = \int_0^{2\pi} (dW/dt)d(\omega t)$. This can be found as before from the instantaneous power absorbed:

$$dW/dt = \underset{\sim}{e}\,\dot{\vec{r}} \cdot \vec{E} = e_x\dot{r}_x E_x + e_y\dot{r}_y E_y = E[e_x\dot{r}_x(A_{11}\cos\omega t \pm A_{12}\sin\omega t) + e_y\dot{r}_y(A_{21}\cos\omega t \pm A_{22}\sin\omega t)] \qquad \text{III-(54)}$$

The average power is found by averaging the instantaneous power over $d(\omega t)$:

$$\overline{P} = E\int_0^{2\pi} e_x(-A_x\sin\omega t + B_x\cos\omega t)(A_{11}\cos\omega t \pm A_{12}\sin\omega t)\,d(\omega t) + E\int_0^{2\pi} e_y(A_y\cos\omega t - B_y\sin\omega t)(A_{21}\cos\omega t \pm A_{22}\sin\omega t)\,d(\omega t) \qquad \text{III-(55)}$$

Terms in the products of sin and cos average to zero and terms in squares of sin or cos contribute 1/2. The power absorbed from the randomly oriented oscillators depends on the A and B response coefficients in the following way:

$$\overline{P} = (E/2)e_x(A_{11}B_x \mp A_{12}A_x) + Ee_y/2(A_{21}A_y \mp A_{22}B_y) \qquad \text{III-(56)}$$

The A's and B's will be seen to contain direction cosine functions, A_{ij}, as in eq. III-(56), so the final averaged result for the random oriented oscillators will be found from the products of the direction cosine functions integrated over space. The system of four inhomogeneous linear equations, III-(53), can systematically be solved by considering the four homogeneous equations which can be written as the determinant of the

coefficients of the A's and the B's. This determinant is:

$$\begin{vmatrix} A_x & B_x & A_y & B_y \\ \omega_x^2 - \omega^2 & \gamma_x\omega & -\beta_x & 0 \\ -\gamma_x\omega & \omega_x^2 - \omega^2 & 0 & +\beta_x \\ -\beta_y & 0 & \omega_y^2 - \omega^2 & -\gamma_y\omega \\ 0 & \beta_y & \gamma_y\omega & \omega_y^2 - \omega^2 \end{vmatrix} \quad \begin{matrix} \text{R.H.S.} \\ \frac{e_x A_{11}}{m} E \\ \pm \frac{e_x A_{12}}{m} E \\ \pm \frac{e_y A_{22}}{m} E \\ \frac{e_y A_{21}}{m} E \end{matrix} \qquad \text{III-(57)}$$

together with the R.H.S. which is the inhomogeneous part of the four equations, III-(53). $e_xH\omega A_{33}/mc$ has been written as β_x, and similarly $\beta_y = e_yH\omega A_{33}/mc$. All four coefficients A_x, B_x, etc., have the same denominator, which is the value of the above determinant.

$$D = [(\omega_x^2 - \omega^2)^2 + \omega^2\gamma_x^2][(\omega_y^2 - \omega^2)^2 + \omega^2\gamma_y^2] \qquad \text{III-(58)}$$

The numerators can be found by substituting the coefficients of the unknown of interest by the right hand side and evaluating the resulting determinants. Terms in the magnetic field higher than the first power are dropped because they are very small for any attainable field. The numerators of the response coefficients, N_1, are:

$$N_{A_x} = \frac{e_xE}{m}\Big\{\Big[A_{11}(\omega_x^2-\omega^2) \mp A_{12}\gamma_x\omega\Big]\Big[(\omega_y^2-\omega^2)^2+\omega^2\gamma_y^2\Big] \pm \beta_y A_{22}\Big[(\omega_x^2-\omega^2)(\omega_y^2-\omega^2) - \gamma_x\gamma_y\omega^2\Big] + \beta_y A_{21}\Big[\gamma_x\omega(\omega_y^2-\omega^2) + \gamma_y\omega(\omega_x^2-\omega^2)\Big]\Big\} \qquad \text{III-(59)}$$

$$N_{B_x} = \frac{e_xE}{m}\Big\{\Big[A_{11}\gamma_x\omega \pm A_{12}(\omega_x^2-\omega^2)\Big]\Big[(\omega_y^2-\omega^2)+\gamma_y^2\omega^2\Big] + \beta_y A_{21}\Big[\gamma_x\gamma_y\omega^2 - (\omega_x^2-\omega^2)(\omega_y^2-\omega^2)\Big] \pm \beta_y A_{22}\Big[\gamma_y\omega(\omega_x^2-\omega^2) + \gamma_x\omega(\omega_y^2-\omega^2)\Big]\Big\} \qquad \text{III-(60)}$$

$$N_{A_y} = \frac{e_y E}{m}\Big\{\left[A_{21}\gamma_y\omega \pm A_{22}(\omega_y^2-\omega^2)\right]\left[(\omega_x^2-\omega^2)^2+\gamma_x^2\omega^2\right]$$
$$\mp\beta_x A_{12}\left[\gamma_x\omega(\omega_y^2-\omega^2)+\gamma_y\omega(\omega_x^2-\omega^2)\right] \qquad \text{III-(61)}$$
$$+\beta_x A_{11}\left[(\omega_x^2-\omega^2)(\omega_y^2-\omega^2)+\gamma_x\gamma_y\omega^2\right]\Big\}$$

$$N_{B_y} = \frac{e_y E}{m}\Big\{\left[A_{21}(\omega_y^2-\omega^2) \mp A_{22}\gamma_y\omega\right]\left[(\omega_x^2-\omega^2)^2+\gamma_x^2\omega^2\right]$$
$$\pm\beta_x A_{12}\left[\gamma_x\gamma_y\omega^2-(\omega_x^2-\omega^2)(\omega_y^2-\omega^2)\right] \qquad \text{III-(62)}$$
$$-\beta_x A_{11}\left[\gamma_y\omega(\omega_x^2-\omega^2)+\gamma_x\omega(\omega_y^2-\omega^2)\right]\Big\}$$

The average power absorbed is found by substituting the above coefficients into eq. III-(56) and averaging the resulting direction cosine products over the Eulerian angles, $0 < \phi < 2\pi$, $0 < \psi < 2\pi$ and $0 < \theta < \pi$, as defined by Wilson, Decius and Cross (1955), who also have a convenient table of the direction cosines. The direction cosine product integrals must be normalized by the Eulerian angle volume element: $8\pi^2 = \int_0^{\pi}\int_0^{2\pi}\int_0^{2\pi} \sin\theta\, d\theta\, d\phi\, d\psi$. These products can all be worked out with some effort and most of them are zero. This process allows us to arrive at the average power absorbed for the randomly oriented x and y oscillators in circular light in the presence of the magnetic field.

$$\bar{P} = \frac{E^2}{m}\Big\{\frac{2}{3}\,\frac{e_x^2\gamma_x\omega}{(\omega_x^2-\omega^2)+\gamma_x^2\omega^2} + \frac{2}{3}\,\frac{e_y^2\gamma_y\omega}{(\omega_y^2-\omega^2)+\gamma_y^2\omega^2}$$
$$\pm\frac{2}{3}\,\frac{e_x e_y H\omega}{mc}\left[\frac{(\omega_y^2-\omega^2)\gamma_x\omega+(\omega_x^2-\omega^2)\gamma_y\omega}{\left[(\omega_x^2-\omega^2)^2+\gamma_x^2\omega^2\right]\left[(\omega_y^2-\omega^2)^2+\gamma_y^2\omega^2\right]}\right]\Big\} \qquad \text{III-(63)}$$

If we make the identification: $e_x^2 = e^2 f_x$ and $e_y^2 = e^2 f_y$, the absorption formula will be seen to agree with the normal classical and quantum mechanical absorption formula, and will allow us to see how the field dependent part depends on the x and y oscillator strength. The absorption cross section is defined as before by eq. III-(19), and the average absorption (in unpolarized light) is:

$$\bar{\sigma} = \frac{\sigma_+ + \sigma_-}{2} = 4/3\pi \frac{e^2\omega}{mc}\left\{ \frac{f_x \gamma_x \omega}{(\omega_x^2-\omega^2)^2+\gamma_x^2\omega^2} + \frac{f_y \gamma_y \omega}{(\omega_y^2-\omega^2)^2+\gamma_y^2\omega^2}\right\} \quad \text{III-(64)}$$

The MCD is given by the relation:

$$\overline{\Delta\sigma} = \sigma_+ - \sigma_- = 4/3\pi\left(\frac{e^2\omega}{mc}\right)\left(\frac{e\omega H}{mc}\right)\sqrt{f_x f_y}\left\{\frac{(\omega_y^2-\omega^2)\gamma_x\omega + (\omega_x^2-\omega^2)\gamma_y^2\omega}{[(\omega_y^2-\omega^2)^2+\gamma_y^2\omega^2][(\omega_x^2-\omega^2)^2+\gamma_x^2\omega^2]}\right\}$$

III-(65)

Further arguments allow us to derive similar formulas for the MORD, but this derivation is long enough as it is, and the MCD part is usually the most difficult to understand. The two limiting cases previously treated can easily be written from the general relations, III-(65), (64) above, and the results have now been averaged for random orientation of the molecules. For the degenerate case, where $\omega_x = \omega_y = \omega_o$ and $\gamma_x = \gamma_y = \gamma$, the averaged result is:

$$\bar{\sigma} = 8/3\pi \frac{e^2\omega^2}{mc}\left\{\frac{f\gamma\omega}{(\omega_o^2-\omega^2)^2+\gamma^2\omega^2}\right\} \approx \frac{8}{3}\frac{\pi e^2}{mc}\left\{\frac{f\,\gamma/4}{(\omega_o-\omega)^2+\gamma^2/4}\right\} \quad \text{III-(66)}$$

$$\overline{\Delta\sigma} = 8/3\pi\left(\frac{e^2\omega}{mc}\right)\left(\frac{e\omega H}{mc}\right)\frac{f\gamma\omega(\omega_o^2-\omega^2)}{[(\omega_o^2-\omega^2)^2+\gamma^2\omega^2]} \approx \frac{4}{3}\frac{\pi e^3 H}{m^2c^2}\frac{f(\omega_o-\omega)\gamma/4}{[(\omega_o-\omega)^2+\gamma^2/4]^2} \quad \text{III-(67)}$$

where f is the oscillator strength of the transition. The result of applying the resonance approximation has been written as the second equation on each line. The resonance approximation is applicable in almost every circumstance of interest. For the nondegenerate case ($\omega_x << \omega_y$), the averaged result can be written in the resonance approximation:

$$\text{Absn:}\quad \bar{\sigma}_x = 4/3(\pi/mc)\frac{e^2 f_x \gamma_x/4}{(\omega_x-\omega)^2+\gamma_x^2/4} \quad \text{III-(68)}$$

$$\text{MCD:}\quad \Delta\bar{\sigma}_x = 2/3\pi\frac{e^3 H}{m^2c^2}\sqrt{f_x f_y}\frac{\gamma_x/4}{[(\omega_x-\omega)^2+\gamma_x^2/4](\omega_y^2-\omega^2)} \quad \text{III-(69)}$$

We see clearly here that the nondegenerate MCD depends on the product

of the oscillator strengths of the x and y bands which are coupled by the field, as had been stated earlier. From this consideration, one would expect large MCD relative to the absorption from a weak band that was close to a strong perpendicularly polarized band.

The result for the optimally oriented degenerate pair of oscillators, eqs. III-(42), III-(20) and III-(46), can be compared to the result for the randomly oriented degenerate oscillators, III-(66) and (67), to determine the effect of random orientation. It can be seen that random orientation decreases the average absorption to 2/3 of the maximum for optimum orientation, and that the MCD decreases to 1/3 of the maximum for optimum orientation. If the randomly oriented nondegenerate results, eqs. III-(68) and (69), are compared to the optimally oriented equations, III-(32) and (34), it is seen that the average absorption is 1/3 and average MCD is 1/6 of the maximum for optimum orientation of the molecules along the external fields. We see that for both the degenerate and nondegenerate cases, the ratio of the MCD to absorption is reduced by a factor of two by the random orientation of the oscillators:

$$\frac{\Delta\sigma_{max}}{\sigma_{max}} = 2\,\frac{\overline{\Delta\sigma}}{\overline{\sigma}} \qquad \text{III-(70)}$$

This result will be very important in analyzing the experimental data which is presented later. This same conclusion can be reached by other arguments, as a check on this procedure, but they will not be given here.

The problem of near degeneracy, $\omega_x \approx \omega_y$, has not been considered explicitly by other workers. The classical formula, III-(65), can be used to derive a form for the shape of the intermediate case of near degeneracy. If we let $\gamma_x \cong \gamma_y$ and $f_x \approx f_y$ and define $2\Delta\omega \equiv \omega_x - \omega_y$

and $(\omega_x + \omega_y)/2 \equiv \bar{\omega}$, the near degeneracy MCD formula is:

$$\Delta\sigma = \left(4/3\right)\frac{\pi e^2 H}{mc} \frac{\gamma f \bar{\omega}(\bar{\omega}-\omega)}{\left[(\bar{\omega}-\omega)^2 + \Delta\omega^2 + \gamma^2/4\right] - (4\Delta\omega^2)(\bar{\omega}-\omega)^2} \qquad \text{III-(72)}$$

This equation allows us to estimate when nondegeneracy will be distinguishable from degeneracy. The absorption and MCD for various values of separation between ω_x and ω_y at a fixed γ are plotted in Figure III-1. For values of $\Delta\omega < \gamma/4$, essentially no effect of near degeneracy is observed. The MCD and absorption bands are only very slightly wider than the degenerate curves. For $\Delta\omega$ increasing from $\gamma/4$ to $\gamma/2$ the observed width of the absorption and MCD increases until two separate peaks become resolved in absorption. The surprising result is that for nearly equal absorption intensity for the two components ($f_x \tilde{\approx} f_y$), the near degeneracy shows up first in the absorption as two separate peaks and the MCD is insensitive to the near degeneracy. The $f_x \tilde{\approx} f_y$ situation would be valid for slightly perturbed degenerate systems.

If, however, the x and y oscillators had a very different strength, only one transition would be observed in absorption (at ω_y if $f_x << f_y$). The MCD would still be described by eq. III-(72) if $f = \sqrt{f_x f_y}$ and $\gamma_x = \gamma_y$, and the MCD curves in Figure III-1 are unchanged. The MCD crosses zero at $\bar{\omega}$, which is now $\Delta\omega$ from the absorption peak at ω_y. The absorption would look like the A curve in Figure III-1, but would move away from the $\bar{\omega}$ MCD crossover as $\Delta\omega$ increases. This circumstance applies to near accidental degeneracy, and we reach the important conclusion that the MCD shows the near degeneracy quite markedly for $\Delta\omega \gtrsim \gamma/10$.

Figure III-1. Calculated absorbance and MCD for near degenerate transitions of equal width and strength. The component lines are Lorentzian in shape, and have 500 cm^{-1} full width at half height. The energy difference, $\Delta\omega$, between components are: in A, $\Delta\omega = 0$, in B, $\Delta\omega = 62.5$ cm^{-1}, in C, $\Delta\omega = 125$ cm^{-1}, in D, $\Delta\omega = 250$ cm^{-1}, in E, $\Delta\omega = 375$ cm^{-1}, and in F, $\Delta\omega = 500$ cm^{-1}.

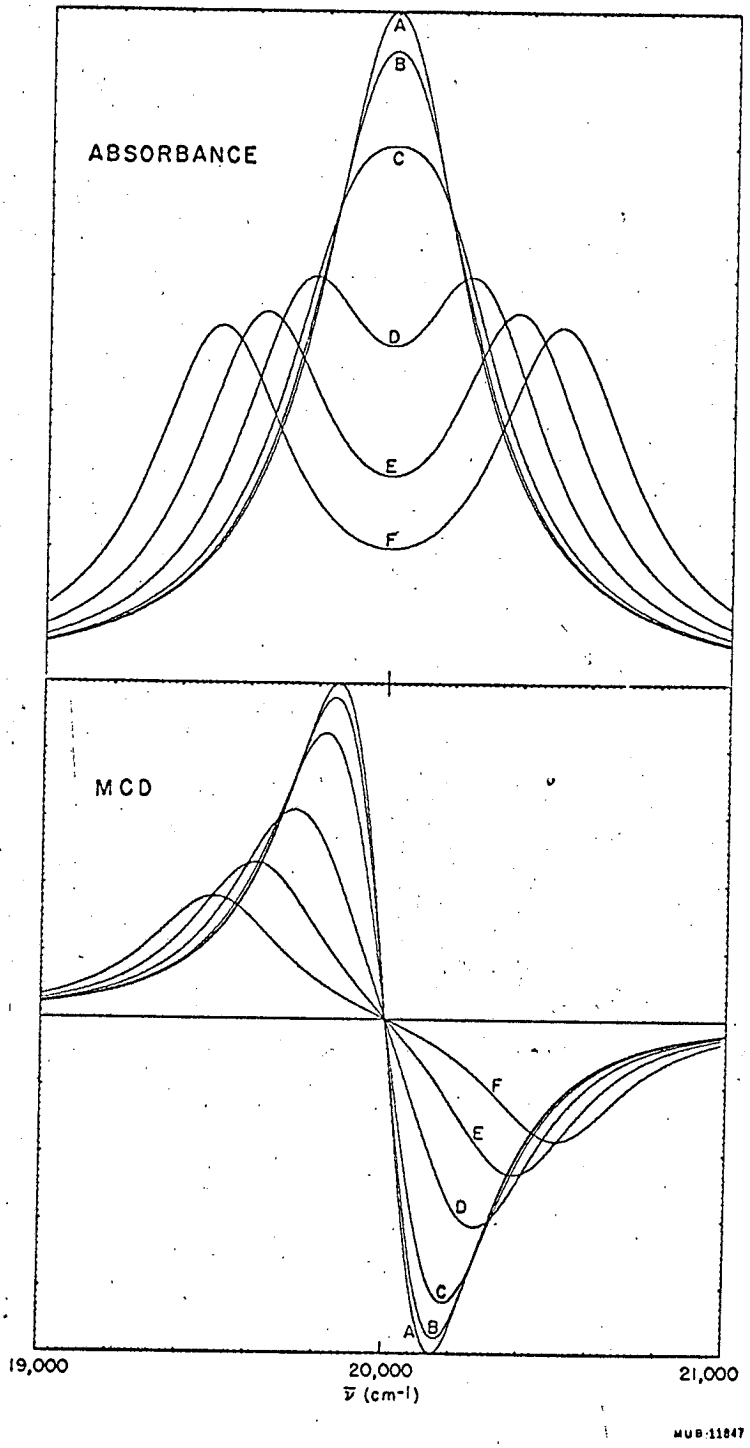
ABSORBANCE
A
B
C
D
E
F
MCD
F
E
D
C
A
B
19,000
20,000
21,000
$\bar{\nu}$ (cm-1)
MUB:11847

An oscillator strength, f, has already been inserted to account for the idea that net charge displacement during excitation of a molecular oscillator may be much less than one electronic charge. However, the detailed charge distribution of the "x" and "y" oscillators may couple slightly differently than the net linear components. This effect can be explicitly included classically, but will not add much here and will be clarified more simply in the semi-classical derivation. We may account for this effect in the classical derivation by inserting a dimensionless variable ("g") factor in the preceding expressions for MCD. If we make the well known identification of the oscillator strength, f_a, with the quantum mechanical electric dipole transition moment, $\underset{\sim}{\mu}^2_{oa}$ (e.g., Sandorfy, 1964),

$$f_a = \frac{8\pi^2 m \omega_o c}{3he^2} |\underset{\sim}{\mu}_{oa}|^2 \qquad \text{III-(71)}$$

and also put in the ("g") factor discussed above, the same expressions for MCD and absorption result as are derived by quantum mechanical arguments (e.g., Stephens, 1966). We will not go through this here because the purpose of the classical viewpoint is mainly heuristic.

It is hoped that the classical derivation, even though it is complicated algebraically in the general case, is much easier to understand than the quantum mechanical derivation. The classical derivation is intended to give a gross understanding of the phenomena. To be able easily to incorporate factors that depend on the detailed electron distribution of molecules, we will now derive the MCD from a semi-classical point of view.

B. Semi-classical MCD

The arguments given in this section are closely related to those made by Gouterman in unpublished work. Consider a three-state system, a diamagnetic ground state $|o\rangle$, an x polarized excited state $|x\rangle$ and a y polarized excited state $|y\rangle$. We will be interested in the electric dipole operator, $\mu = \sum_i e_i r_i$ between the above ground and excited states, where e_i and r_i are the charge and position of electron i. The electric dipole transition moments μ_x and μ_y are defined:

$$\langle o|\mu|x\rangle = e\mu_x \hat{i} \qquad \text{III-(73)}$$

$$\langle o|\mu|y\rangle = e\mu_y \hat{j} \qquad \text{III-(74)}$$

where $\hat{i}$ and $\hat{j}$ are perpendicular unit vectors fixed to the molecule.

The normal quantum mechanical derivation of absorption in unpolarized light for random systems has been presented in many books[1] (e.g., Sandorfy, 1964) with the result (which we have rearranged slightly):

$$\alpha = \frac{16}{3}\frac{\pi^2}{n_o}\frac{e^2 N}{h}\,|\mu|^2 f(\omega, \omega_o, \gamma) \qquad \text{III-(75)}$$

n_o is the refractive index, N, Avogadro's number, h, is Planck's constant over 2π. $f(\omega,\omega_o,\gamma)$ is a dimensionless shape function of unit area that could be a Gaussian, a Lorentzian or some other shape. The Lorentzian was found in the classical derivation, and is found experimentally for some optical lines. A dimensionless Lorentzian of unit area is:

$$f(\omega,\omega_o,\gamma) = 1/\pi(\gamma/2)/[(\omega_o - \omega)^2 + \gamma^2/4] \qquad \text{III-(76)}$$

where γ is the full width of the line at one-half maximum absorption

---

[1] The more familiar decadic molar extinction coefficient, $\epsilon = \dfrac{\alpha}{2303\,\lambda}$ where λ is in cm.

The absorption in circular light is given by the transition operator:

$$\mu_{\pm} = \mu_x \pm i\,\mu_y \qquad \text{III-(77)}$$

where $i = \sqrt{-1}$. The absorption coefficient for left circularly polarized light for the transition $|o\rangle \rightarrow |a\rangle$ is:

$$\alpha_l = \frac{16\pi^2}{3n_o}\frac{Ne^2}{\hbar}\langle o|\mu_-|a\rangle\langle a|\mu_+|o\rangle f(\omega,\omega_o,\gamma) \qquad \text{III-(78)}$$

(e.g., Bohm, 1951). For right light, μ_+ and μ_- are interchanged. In the absence of a magnetic field, for the $|o\rangle \rightarrow |x\rangle$ transition:

$$\langle o|\,\mu_{\pm}\,|x\rangle = \langle x|\,\mu_{\pm}\,|o\rangle = \mu_x \qquad \text{III-(79)}$$

and $\alpha_l = \alpha_r$ in the absence of the magnetic field; this argument applies for the y transition as well.

The magnetic field is introduced and if electron spin is neglected for the present, the new term in the Hamiltonian is the interaction of the orbital angular momentum, L, with the H field. If we restrict the discussion to systems with at least two planes of symmetry, we can show by symmetry arguments that the only nonzero angular momentum operator matrix element ($\underset{\sim}{L} = \sum_i \ell_i = \sum_i r_i \times p_i$) between the states $|o\rangle$, $|x\rangle$ and $|y\rangle$ is:

$$\langle x|\,L_z|y\rangle \equiv iM_z\hbar = \langle y|\,L_z\,|x\rangle^* \qquad \text{III-(80)}$$

where M_z is real and the * indicates a complex conjugate. If an integral like $(\phi_i|Op|\phi_j)$ is to be nonzero, the direct product of the symmetry species of $\phi_i \times \phi_j \times Op$ must contain the totally symmetric representation A_{1g} (e.g., Wilson, Decius and Cross, 1953; Eyring, Walter and Kimball, 1944). The x and y states transform like the x and y translations under symmetry operations, and $|o\rangle$ is totally symmetric. For common molecular point groups, with at least two planes of symmetry (C_{2v}, C_{3v}, D_{2h}, D_{4h},

D_{6h}, etc.), we can show that the only nonzero orbital angular momentum matrix element is the angular momentum about the axis perpendicular to the molecular plane, L_z. Table I contains the symmetry species for C_{2v}, a common molecular point group.

Table I

C_{2v}	E	C_2	$\sigma(xz)$	$\sigma(yz)$		
A_1	1	1	1	1	z	
A_2	1	1	-1	-1		L_z
B_1	1	-1	1	-1	x	L_y
B_2	1	-1	-1	1	y	L_x

For example, in C_{2v}, x is B_1, y is B_2 and the direct product of x and y is A_2. Since L_z is A_2, it is the only nonzero matrix element between x and y.

The Hamiltonian between the x and y states in the presence of the field is:

	$\|x\rangle$	$\|y\rangle$
$\langle x\|$	$\hbar\omega_x$	$iM_z\beta H_z$
$\langle y\|$	$-iM_z\beta H_z$	$\hbar\omega_y$

III-(81)

where $\beta = e\hbar/2mc$ = the Bohr magneton.

Nondegenerate case

The magnetic field mixes some $|y\rangle$ character into the $|x\rangle$ state and some $|x\rangle$ character into the $|y\rangle$ state. The physical basis of this statement was explained in terms of a molecular Hall effect in the

classical derivation (p. 131). We define the frequency difference between x and y as $\Delta\omega = \omega_x - \omega_y$. By first order perturbation theory, we get the new states $|x'\rangle$ and $|y'\rangle$ in the presence of the magnetic field.

$$|x'\rangle = |x\rangle + \frac{iM_z\beta H}{h\Delta\omega}|y\rangle \qquad \text{III-(82)}$$

$$|y'\rangle = |y\rangle + \frac{iM_z\beta H}{h\Delta\omega}|x\rangle \qquad \text{III-(83)}$$

We may now evaluate the transition moments for the $|x'\rangle$ and $|y'\rangle$ states in left and right circularly polarized light:

$$\mu_{\pm} = \mu_x \pm i\,\mu_y \qquad \text{III-(84)}$$

$$\langle o|\mu_{\pm}|x'\rangle = e[\mu_x \mp \frac{M_z\beta H_z}{h\Delta\omega}\,\mu_y] \qquad \text{III-(85)}$$

$$\langle o|\mu_{\pm}|y'\rangle = e[i\,\mu_y \pm \frac{M_z\beta H_z}{h\Delta\omega}\,\mu_x] \qquad \text{III-(86)}$$

The absorption intensities for the x polarized transition in right and left circular light are proportional to:

$$\begin{aligned} &X(\text{right}): \quad \langle o|\mu_+|x'\rangle\langle x'|\mu_-|o\rangle = e^2[\mu_x - \lambda\,\mu_y]^2 \\ &X(\text{left}): \quad \langle o|\mu_-|x'\rangle\langle x'|\mu_+|o\rangle = e^2[\mu_x + \lambda\,\mu_y]^2 \end{aligned} \qquad \text{III-(87)}$$

where $\lambda = \beta M_z H_z / h\Delta\omega$. The expression for the y polarized transitions are analogous, but the signs of the λ terms are reversed for left and right light. The resulting difference in absorption for right and left circular light can be written for the x transition:

$$(\alpha_l - \alpha_r)_x = H\left(\frac{32\pi^2}{3mo}\right)\left(\frac{Ne^3}{mhc}\right)\frac{\vec{\mu}_x M_z \vec{\mu}_y}{h\Delta\omega}\left(\frac{2}{\pi}\right)\left(\frac{\gamma_x/2}{(\omega-\omega_x)^2 + \gamma^2/4}\right) \qquad \text{III-(89)}$$

The expression for the y transition is exactly analogous, but is multiplied by a minus sign. This is an important result—that the MCD due to the interaction of an x and y polarized pair of transitions will occur

at both ω_x and ω_y and that the MCD at x exactly cancels that at y. In general, all the nondegenerate contributions to the MCD will cancel in pairs. Perpendicularly polarized transitions that are close in energy will give large contributions to the MCD because of the $1/\Delta\omega$ dependence on MCD amplitude. A factor of two correction must be applied in eq. III-(89) to account for random orientation of the molecules. This factor of two correction was derived in the classical section (p. 146).

Expressions for other line shapes can be given by replacing the Lorentzian shape function used above with another shape function of unit area. The result above agrees with the classical one developed earlier. Now, however, specific molecular transition moments (μ_x, μ_y and M_z) that are sensitive to the details of the electronic distribution of the molecule have been introduced. This result also agrees with the more general derivations of magnetic optical activity (e.g., Stephens, 1966b).

Degenerate case

For the degenerate case, $\omega_x = \omega_y = \omega_o$, and we can define new states in the presence of the field:

$$|\pm\rangle = 1/\sqrt{2}(|x\rangle \pm i\,|y\rangle) \qquad \text{III-(90)}$$

with energies:

$$E_{\pm} = \hbar\,\omega_o \pm M_z\beta H_z \qquad \text{III-(91)}$$

and transition moments:

$$\begin{aligned} \langle o|\mu_+|\pm\rangle &= 1/\sqrt{2}\; e(\mu_x \mp \mu_y) \\ \langle o|\mu_-|\pm\rangle &= 1/\sqrt{2}\; e(\mu_x \pm \mu y) \end{aligned} \qquad \text{III-(92)}$$

For the degenerate case $\mu_x = \mu_y = \mu_o$, and we find that the $|+\rangle$ state absorbs left circular light exclusively:

$$\begin{aligned} &\text{left:} \quad \langle o|\mu_-|+\rangle = \sqrt{2}\; e\; \mu_o \\ &\text{right:} \quad \langle o|\mu_+|+\rangle = o \end{aligned} \qquad \text{III-(93)}$$

and the $|->$ state absorbs right circular light exclusively:

$$\text{Left:} \quad \langle o|\mu_-|-\rangle = 0$$
$$\text{Right:} \quad \langle o|\mu_+|-\rangle = \sqrt{2}\, e\, \mu_o \qquad \text{III-(94)}$$

The $|+\rangle$ state absorbs left light as $E_+ = \omega_o + M_z\beta H_z$, and the $|-\rangle$ state absorbs right light at $E_- = \omega_o - M_z\beta H_z$. This is the orbital Zeeman effect. The M_z that appears above is the orbital angular momentum operator between the + or - states:

$$\langle +|L_z|+\rangle = 1/2[-i\langle y|L_z|x\rangle + i\langle x|L_z|y\rangle] = -M_z = -\langle -|L_z|-\rangle \qquad \text{III-(95)}$$

The absorption coefficients in right and left light are:

$$\alpha_L = 2\left(\frac{16\pi^2}{3n_o}\right)\left(\frac{Ne^2}{\hbar}\right)\mu_o^2 \quad f\left(\omega, \omega_o + \frac{M_z\beta H_z}{\hbar}, \gamma\right)$$

$$\alpha_R = 2\left(\frac{16\pi^2}{3n_o}\right)\left(\frac{Ne^2}{\hbar}\right)\mu_o^2 \quad f\left(\omega, \omega_o - \frac{M_z\beta H_z}{\hbar}, \gamma\right) \qquad \text{III-(96)}$$

For the Lorentzian shape function:

$$f(\omega, \omega_o \pm \delta, \gamma) = \left(\frac{1}{\pi}\right)\left(\frac{\gamma/2}{(\omega-\omega_o\pm\delta)^2+\gamma^2/4} \times \left[\frac{1}{\pi}\frac{\gamma/2}{(\omega-\omega_o)^2+\gamma^2/4} \pm \frac{2\delta(\omega-\omega_o)^{\gamma/2}}{\left[(\omega-\omega_o)^2+\gamma^2/4\right]^2}\right]\right) \qquad \text{III-(97)}$$

And the difference in absorption for left and right light is for a Lorentzian line:

$$\alpha_L - \alpha_R = \left(\frac{64\pi^2}{3n_o}\right)\left(\frac{Ne^2}{\hbar}\right)\mu_o^2 M_z \frac{\beta H_z}{\hbar}\left(\frac{2}{\pi}\right)\left\{\frac{(\omega\mp\omega_o)\ \gamma/2}{\left[(\omega-\omega_o)^2+\gamma^2/4\right]^2}\right\} \qquad \text{III-(98)}$$

This is the same relationship that is found by the more general quantum mechanical derivations and is usually called the A term (Stephens, 1966b). Other line shape functions, $f(\omega,\omega_o,\gamma)$ of unit area, [illegible], may be put into eq. III-(96) and similar expressions, III-(98), result. We are now in a position to consider the effect of electron spin. Multiplicity forbidden transitions from singlet ground state, and spin allowed transitions from paramagnetic ground states will be briefly considered.

Singlet-triplet transitions

There has been a good deal of speculation, as well as theoretical and experimental contention, that magnetic optical activity may be much more sensitive to multiplicity forbidden transitions than is absorption (Shashoua, 1960; Hameka, 1962; Foerhart and Renner, 1961). We shall give a brief argument here which indicates that this is not the case. According to the simple argument that follows, S → T transitions will occur with very nearly the same strength in MCD as they do in absorption.

We consider wavefunctions for a molecule as a product of an orbital and a spin part. This is analogous to the L-S or Russell-Saunders limit in atoms and is an excellent starting point for most molecules. We consider a transition in which an electron is promoted from a filled nondegenerate orbital a to an orbital b, with spin up, α, or spin down, β. The simplest excited states are a singlet = Ψ_S and a triplet = Ψ_T

$$\Psi_S = {}^1O \cdot {}^1S = [a(1)\, b(2) + a(2)\, b(1)][\alpha_1\beta_1 - \beta_1\alpha_2] \qquad \text{III-(99)}$$

$$\Psi_T = {}^TO \cdot {}^TS = [a(1)\, b(2) - a(2)\, b(1)] \begin{Bmatrix} \alpha_1\alpha_2 \\ \alpha_1\beta_2 + \beta_1\alpha_2 \\ \beta_1\beta_2 \end{Bmatrix} \qquad \text{III-(100)}$$

where O is the orbital part and S is the spin part, and the electrons are indicated as 1 and 2. We have seen in the previous section, for example, in eq. III-(89), that we need a nonzero magnetic transition moment to get MCD. In the presence of spin the magnetic transition moment is L + 2S. Since the L operator does not act on spin and the spin operator does not act on the orbital angular momentum, the magnetic transition moment can be expanded:

$$\langle {}^1O{}^1S \mid L + 2S \mid {}^3O{}^3S \rangle = \langle {}^1O|L|{}^3O\rangle\langle {}^1S|{}^3S\rangle + \langle {}^1O|{}^3O\rangle\langle {}^1S|2S|{}^3S\rangle \qquad \text{III-101)}$$

This expression is identically equal to zero because the singlet spin and orbital functions are orthogonal to the triplet spin and orbital functions respectively.

$$\langle {}^1S|{}^3S\rangle = 0, \quad \langle {}^1O|{}^3O\rangle = 0 \qquad \text{III-(102)}$$

So for the simple product wavefunctions, III-(99), (100), we have zero MCD for singlet-triplet transition. We must invoke spin-orbit interactions in order to get MCD from singlet-triplet transitions. The spin-orbit interaction mixes a little triplet character into the singlet state and vice versa. In the presence of spin orbit coupling we can write the new states by first order perturbation theory:

$$\Psi_T^1 = \Psi_T^0 + \lambda \Psi_S^0 \qquad \text{III-(103)}$$

$$\Psi_S^1 = \Psi_S^0 + \lambda \Psi_T^0 \qquad \text{III-(104)}$$

where λ is the spin orbit coupling parameter. For nondegenerate systems we need an interaction between perpendicularly polarized transitions to get MCD. We consider an x polarized singlet and a y polarized triplet and define:

$$\langle o|\ x\ |\ \Psi_S^1\rangle \equiv {}^1R_x \neq 0 \qquad \text{III-(105)}$$

The absorption by the triplet will be proportional to:

$$\langle o|\ y\ |\ \Psi_T^1\rangle \equiv {}^3R_y = \lambda\ {}^1R_x \qquad \text{III-(106)}$$

In the previous section we saw that the z component of the angular momentum M_z contributes to the MCD. M_z in this case is proportional to the spin-orbit interaction:

$$\langle M_z\rangle = \langle \Psi_S^1|L + 2S|\Psi_T^1\rangle \propto \lambda \qquad \text{III-(107)}$$

The absorption in right circular light for terms linear in H will be given by:

$$\alpha_R \propto \langle o|m_+|y^1\rangle\langle y^1|m_-|o\rangle = \text{order}\ [\lambda R_x - \langle M_z\rangle \beta H\rangle^2] \approx R_x^2\lambda_x^2 - 2\lambda^2 R_x \beta H \qquad \text{III-(108)}$$

and similarly for left light:

$$\alpha_L = \text{order } [\lambda^2 R_x^2 + 2\lambda^2 R_{x\beta H}] \qquad \text{III-(109)}$$

We now get MCD, but both the MCD and the absorption are proportional to the spin orbit interaction squared, λ^2:

$$\text{Absn: } \frac{\alpha_R + \alpha_L}{2} \alpha \lambda^2 R_x^2 \text{ , MCD: } (\alpha_L - \alpha_R) \alpha \lambda^2 H \qquad \text{III-(110)}$$

For nondegenerate singlet-triplet transitions, MCD will have about the same strength relative to the absorption as for allowed singlet-singlet transitions. For the degenerate case the same conclusion is reached, but will not be given here. In summary, MCD is not expected to be any more sensitive to singlet-triplet (or other multiplicity forbidden) transitions than is absorption.

C. Effect of Spin on MCD

Zeeman effects in the presence of spin have been treated in great detail for atoms (Condon and Shortly, 1935), color centers in crystals (Henry, et al., 1965), ions in crystals (Sugamo and Tanabe, 1958) and diatomic molecules (Herzberg, 1950).

Nondegenerate electronic transitions

Nondegenerate transitions involving spin might occur in free radicals with symmetry less than 3-fold, triplet-triplet transitions or in transition metal complexes where the optical transitions involved metal d electrons and the orbital angular momentum of the metal electrons is quenched by the ligand field (e.g., Slichter, 1963).

The spin is quantized with respect to the external field and split into the various 2S+1, M_S components along the field. The important fact is that $\Delta M_S = 0$ for electric dipole transitions in non-spherical molecules (Herzberg, 1950; Sandorfy, 1964). We draw an example energy

level scheme for a doublet-doublet transition to an |x> polarized state in Figure III-2a. If we had drawn triplets or higher multiplets the same conclusion would obtain, but would severely complicate our diagram. We see that in the presence of the H field there is no energy shift of any component in the transition and no MCD with only the |x> level present. If we introduce a |y> state as shown in the level scheme in Figure III-2b there will be the normal small amount of |y> character mixed by the field into the |x> state, leading to the single dichroism band characteristic of a nondegenerate system, but no contribution attributable to spin. The small amount of circulation induced by the field will be able to couple with the spin and give the excited state, |x> state, a very slightly different g value (g') than the ground state which is exaggerated in the level scheme in Figure III-2b. There will be a small splitting of transitions 1 and 2 by $(g-g')\beta H$. However, transitions 1 and 2 will have the same amount of |y> character to first order in H: $|x> + \lambda|y>$. Therefore, there is no contribution to the MCD attributable to the spin in this circumstance.

Degenerate electronic transitions

The degenerate case corresponds to molecules with greater than 3-fold symmetry with spin, including metal complexes, if the orbital angular momentum is not quenched by the ligand field. In the cases of interest, the electronic ground state is $^{n}, \ldots\ldots 3,2\ A_{1g}$, which can also be called $^{n}, \ldots 3,2\ \Sigma$ for molecules, where n is the multiplicity. The discussion here is very similar to diatomic molecules with spin, where the angular momentum is strongly coupled to the molecular axis (Sandorfy, 1964; Herzberg, 1950). In diatomic molecules, the projection of the orbital

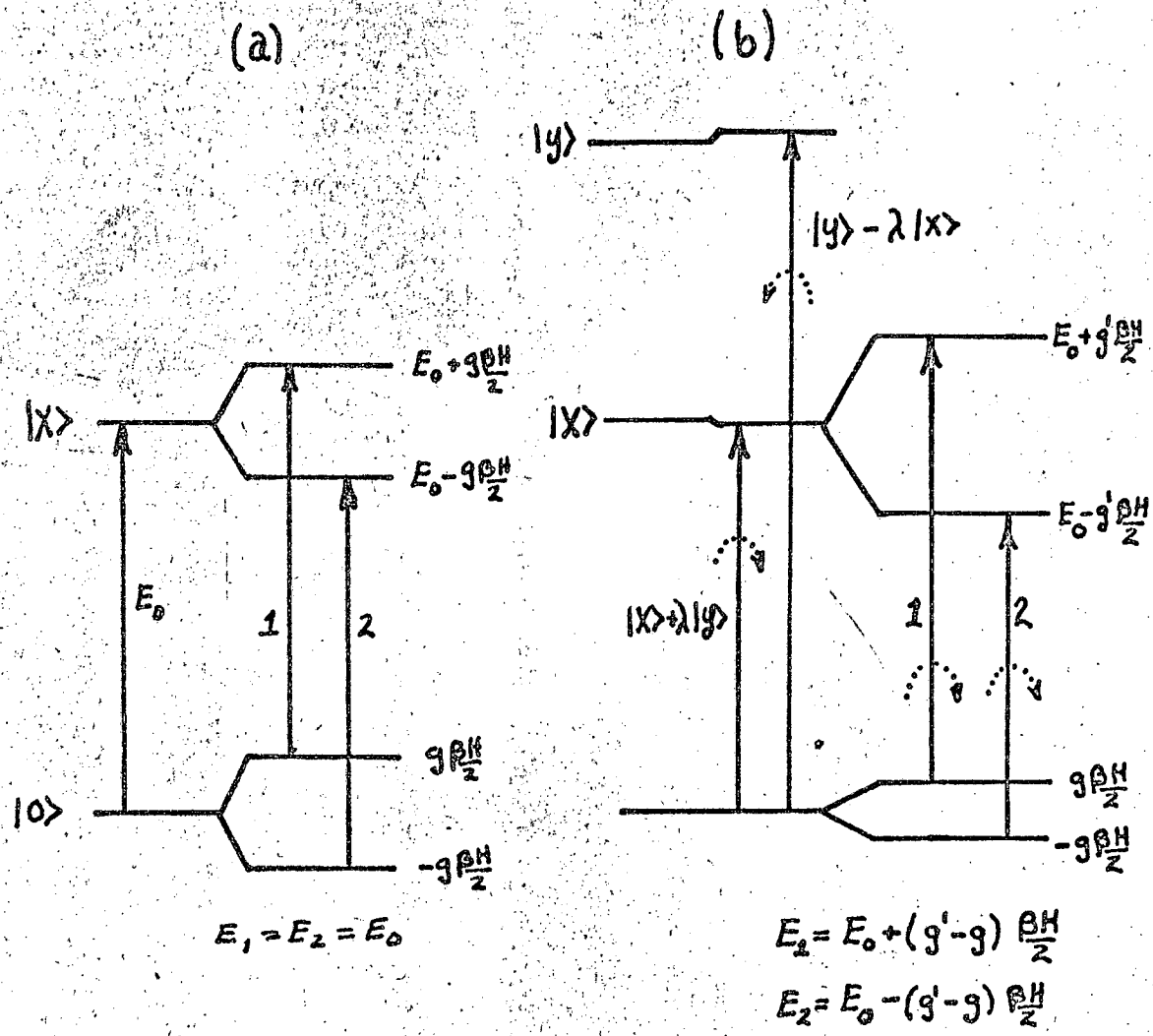

Figure III-2. Energy level diagram for S = $\frac{1}{2}$ orbitally non-degenerate state in the absence and presence of an external magnetic field. The electronic states are explained in the text.

angular momentum along the molecular axis, L_z, is a good quantum number and a selection rule $\Delta L_z = \pm 1$ holds for electronic transitions. In molecules with 3-fold axes or more, the orbitally degenerate states can have nonzero angular momentum along the figure axis, L_z, but it is no longer integral, and the electronic selection rule, $\Delta L_z = \pm 1$, is weak. For molecules containing atoms with nuclear charge, Z, less than 36 the coupling of the orbital angular momentum to the figure axis is generally much stronger than the coupling to the spin. Furthermore, the spin-orbit interaction is particularly weak in transition metal complexes with spin if the electronic transitions of interest are located predominantly on the ligands. The orbital angular momentum, L_z, involved in the electronic transition is due to a different set of electrons than the spin, and spin-orbit effects are expected to be much smaller than an electron spin interacting with its own orbital motion.

For electric dipole radiation the selectron rule for the spin is $\Delta M_S = 0$, as before (e.g., Sandorfy, 1964). We consider a ground state with $L_z = 0$ and an excited state with larger L_z. The field independently splits the $\pm L_z$ and $\pm M_S$ states because they are uncoupled by the strong molecular electric field. The only M_L values that occur are $\pm L_z$ because L_z is coupled so strongly to the molecular axis. Figure III-3 shows an example of an energy level scheme where the excited state has a large L_z (only because the diagram is clearer) and S=1/2. The g values for the spin splitting may be different for the ground and excited states; the difference in ground and excited state g value is called Δg. For $\Delta M_S = 0$ there are four possible transitions. The resulting right and left circularly polarized transitions show no energy shift due to the

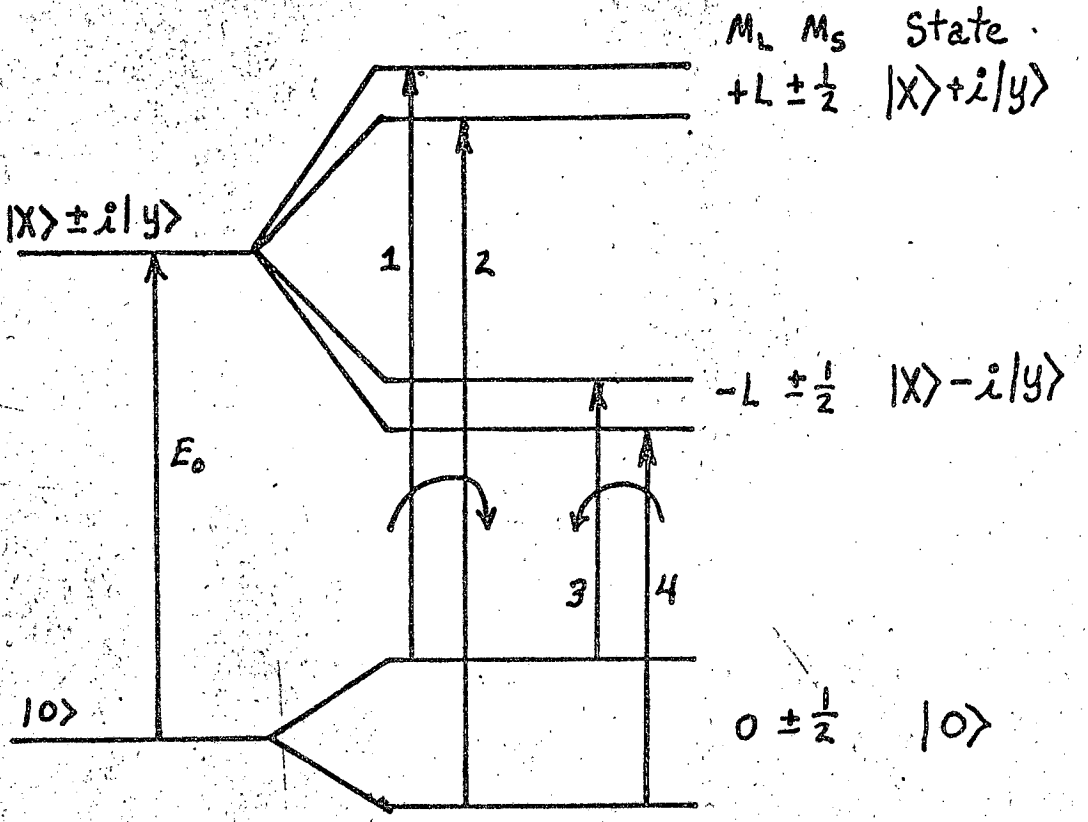

$$E_1 = E_0 + (L + \Delta g)\beta H \quad \left.\right\} \text{right polarized}$$
$$E_2 = E_0 + (L - \Delta g)\beta H \quad \left.\right\}$$
$$E_3 = E_0 - (L - \Delta g)\beta H \quad \left.\right\} \text{left polarized}$$
$$E_4 = E_0 - (L + \Delta g)\beta H \quad \left.\right\}$$
$$E_{right} = (E_1 + E_2)/2 = E_0 + L\beta H$$
$$E_{left} = (E_3 + E_4)/2 = E_0 - L\beta H$$

MUB-12639

Figure III-3. Energy level diagram of an orbitally degenerate excited state and $S = \frac{1}{2}$ with small spin-orbit coupling and the presence of an external magnetic field. The electronic states are described in the text.

spin, and again the presence of spin has no observable effect (particularly at normal temperature).

There are circumstances when the spin and orbital motion are strongly coupled. For example, such a situation obtains in rare earths and might obtain in metal complexes with organic ligands that form positive or negative ion radicals. In this case, the spin and orbital motion couple to give a resultant J value. For example, for an S=1/2 state we get only $J_z = \pm(L_z + 1/2), \pm(L_z - 1/2)$, because L_z is still coupled strongly to the molecular frame. In this case, we have the possibility of splitting of the different J_z values at zero field, and an energy level scheme such as that shown in Figure III-4 results. The possible transitions are drawn for $\Delta M_S = 0$ for electric dipole radiation.

The four transitions give a right-left pair at $E_{\pm} = E^o + D \pm (L_z + \Delta g)\,\beta H$ and at $E'_{\pm} = E^o - D \pm (L_z - \Delta g)\,\beta H$, where 2D is the zero field splitting. The Δg value is usually no larger than 0.02-0.05 and is small compared to the L_z value which is usually greater than 1. If L_z were small or Δg were large, for some reason, one might see a different splitting factor for E and E' (we are already dealing with an unusual case so the preceding circumstance would be a doubly rare case). In any event, the $E_{\pm}$ and $E'_{\pm}$ right-left pairs occur 2D apart. If we make the assumption that $L_z - \Delta g \tilde{=} L_z + \Delta g$ for simplicity (this is by no means necessary to our argument), we can simply investigate the effect of zero field splitting. There will be two double MCD curves separated by 2D. The MCD line shape equations are complicated in closed form, but an example will be adequate for our purpose. Figure III-5 shows the resulting MCD curves for a series of values of 2D/1/2 width (γ) for the

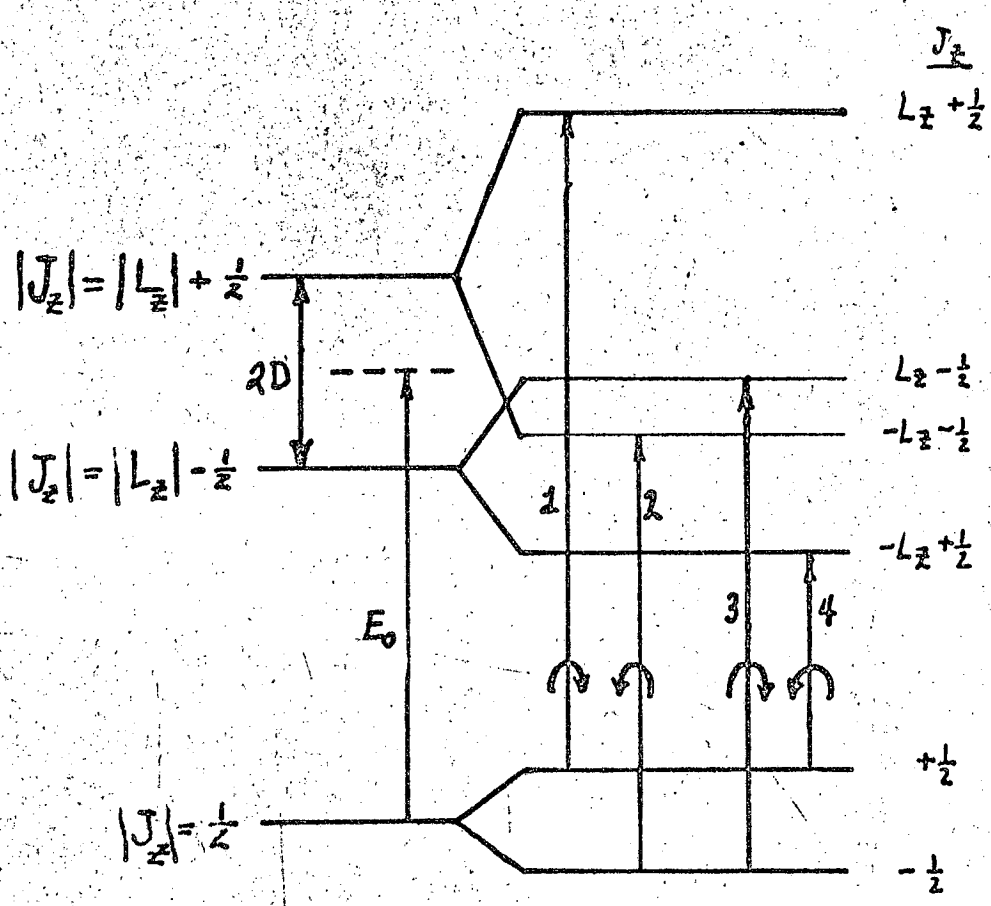

$E_1 = E_o + D + (L_z + \Delta g)\beta H$
$E_2 = E_o + D - (L_z + \Delta g)\beta H$
} right-left pair at $E_\pm = E_o + D \pm (L_z + \Delta g)\beta H$

$E_3 = E_o - D + (L_z - \Delta g)\beta H$
$E_4 = E_o - D - (L_z - \Delta g)\beta H$
} right-left pair at $E'_\pm = E_o - D \pm (L_z + \Delta g)\beta H$

MUB-12650

Figure III-4. Energy level diagram for S=1/2 ground state, orbitally degenerate excited state with strong spin-orbit coupling and zero field splitting (2D). The states are described more fully in the text.

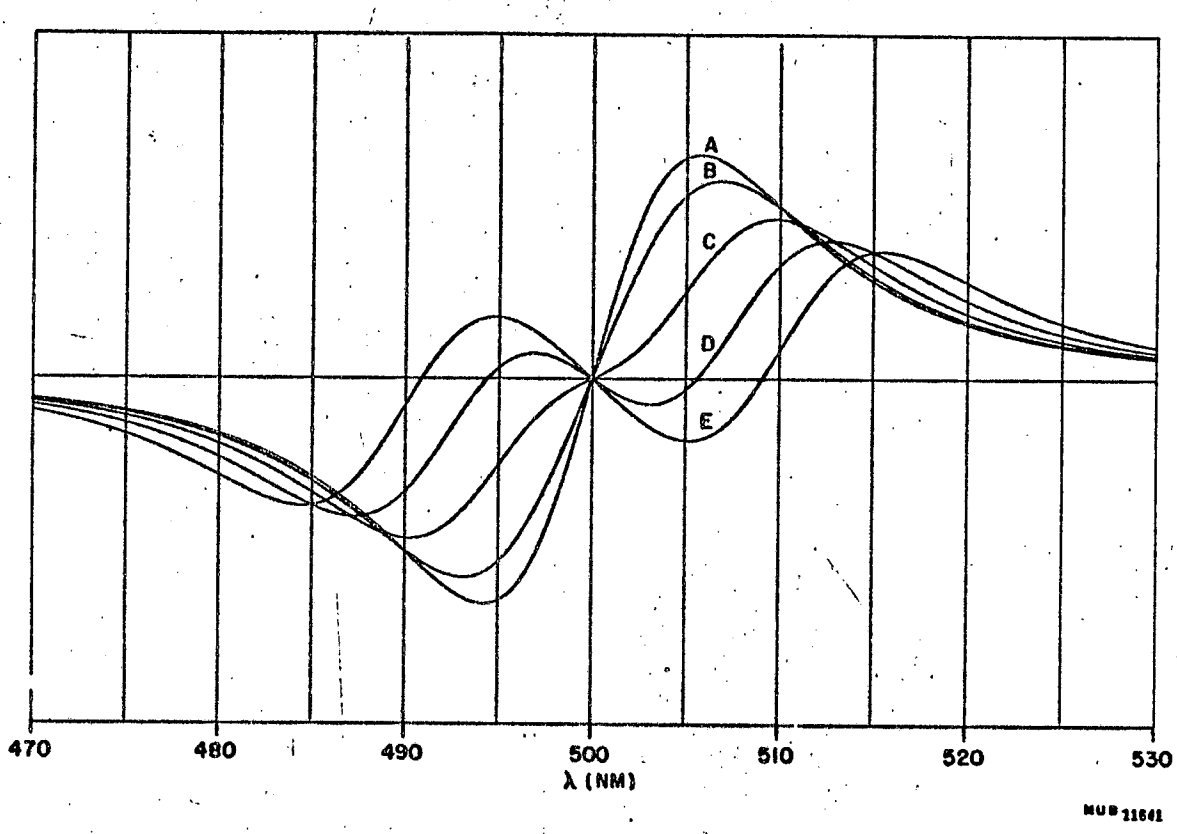

Figure III-5. Calculated MCD curves for an orbitally degenerate transition corresponding to the level scheme for Figure III-4 with various amounts of zero field splitting. The parent absorption bands are Lorentzian with γ = 20 NM full width at half-height. The values of zero field splitting for the various curves are: A, 2D = 0; B, 2D = 5 NM; C, 2D = 10 NM; D, 2D = 15 NM; E, 2D = 20 NM, and F, 2D = 25 NM.

Lorentzian shape. The zero field splitting has a negligible effect on the shape or amplitude of the MCD curve if 2D is less than $\gamma/4$.

For 2D intermediate between $\gamma/4$ and $\gamma/2$ there is a slight decrease (10 to 20%) in amplitude and some broadening of the double MCD effect, but no striking shape change. For 2D greater than $\gamma/2$, the splitting becomes apparent in the absorption and MCD begins to exhibit a new shape. The intermediate case will have a very dramatic temperature dependence at moderately low temperatures because 2D is nearly temperature independent, but $\gamma/2$ is very temperature dependent for most materials. At very low temperatures the $E_{\pm}$ pair will disappear and the $E'_{\pm}$ pair will increase because of a thermal population of the lowest ground level. We can conclude that except for a very restricted set of circumstances the MCD does not respond to the spin of a molecule.

Data analysis

All the theoretical approaches to MCD (classical, semi-classical and quantum mechanical) tell us that there are two types of MCD curves, double and single. For allowed electronic transitions ($\varepsilon \gtrsim 1000$) the single MCD curves are expected to have the same shape as the parent absorption band. This has been shown for natural circular dichroism by Moffit and Moscowitz (1959) and is assumed true for MCD. The theories indicate that the double MCD curves have the shape of the derivative of the absorption bands if the magnetic splitting is less than 10% of the line width. The theoretical sections only dealt with the Lorentzian line shape explicitly, but the Taylor series argument given on page 138 indicates that the double MCD curve shape is given by the derivative of the absorption for all line shapes. The Taylor series approach further

indicates that for the narrowest bands usually found in optical absorption lines in solution, e.g., 200 cm^{-1}) and for the largest magnetic splittings that can ever be expected (e.g., 1-2 cm^{-1}) the first derivative fits the MCD to 0.01%. The above assumes a rigid magnetic shift for the Zeeman components of a line. If a rigid shift does not obtain, the derivative will not fit so well. We will examine the consequences of a rigid shift assumption in this section. Later we will attempt to test the validity of this assumption for particular experimental data.

Since the theory indicates such a close relation between absorption shape and MCD shape, we utilize the absorption data in fitting the MCD. This procedure allows the MCD data to be fit with a relatively small number of parameters.

The main simplification that we have made in most of the experimental section is to represent the absorption by some analytic shape. The symmetrical Lorentzian shape and the Gaussian shape are most often used. Experimental curves are usually more symmetrical if plotted in wavelength, rather than frequency, but either form may be used. We define a general shape function: $f(\lambda,\lambda_i,\theta_i)$ of maximum value unity, where λ_i is the center position of the band and θ_i is a width parameter, the absorption is represented as a sum of N bands.

$$\text{Absn}(\lambda) = \sum_{i}^{N} E_i \quad f(\lambda,\lambda_i,\theta_i) \qquad \text{III-(111)}$$

where E_i is the amplitude (e.g., peak optical density) of the i th component. Usually the absorption will be fit with N equal to the number of obvious peaks and shoulders on the spectrum. A standard computer program is used to fit the experimental curves to eq. III-(111) using a

least squares criteria. A modified Newton-Raphson method, that is analogous to the method of steepest descents, is employed to determine the best fit E_i, λ_i, θ_i parameters (Share Routines-ZOEOVARM and E2EOLSQV).

Each absorption band is characterized by an amplitude E_i, a position, λ_i, and a width, θ_i. These parameters are used to fit the experimental MCD. For each parent absorption band, we seek an MCD component with the shape of the absorption and one with the shape of the derivative of the absorption. The MCD is fit according to:

$$\text{MCD}(\lambda) = \sum_{i}^{N} A_i f'(\lambda,\lambda_i,\theta_i) + B_i f(\lambda,\lambda_i,\theta_i) \qquad \text{III-(112)}$$

where $f(\lambda,\lambda_i,\theta_i)$ is the shape function found from the absorption spectrum and $f'(\lambda,\lambda_i,\theta_i)$ is the derivative of that function. The N A_i and B_i amplitude parameters are the only variables, because the N λ_i and θ_i are fixed. In this way we can use a linear least squares fitting procedure (see Appendix II for CDLSQ program) that gives the exact best fit to the data for the given functions (e.g., Wilson, 1952). This procedure also gives a statistical measure of how well the A_i and B_i parameters are determined and gives the correlations between parameters. The correlation coefficient (Deming, 1943) between parameter i and j is defined:

$$C_{ij} = \frac{\sum_{k}^{m} f_{jk} f_{ik}}{\left(\sum_{k}^{m} f_{ik} f_{ik} \sum_{k}^{m} f_{jk} f_{jk}\right)^{1/2}} \qquad \text{III-(113)}$$

where f_{jk} is the value of the j th function at the k th data point and m is the number of data points. If C_{ij} is close to one, the two parameters are strongly correlated, and fewer parameters should be used to fit the data or a different function should be tried. The A_i parameters when combined with the E_i parameters allow us to determine the Zeeman splitting

of bands, assuming a rigid shift:

$$M_{z,i} = \frac{-2.0\ A_i}{E_i \cdot \beta H \cdot (\lambda_i)^2 \cdot 10^{-8}} \qquad \text{III-(114)}$$

where βH is in cm^{-1} and λ_i is in Angstroms (if the MCD curves are fit in Angstrom units). The factor of two comes from correcting for random orientation (p. 146). This expression assumes that the absorption and MCD are expressed in the same units. Convenient units are: the molar extinction coefficient for absorption and molar ellipticity for the MCD, or the absorption may be in observed optical density unit (for the concentration used for the MCD measurement) and the MCD in observed Δ OD units.

The linear least squares procedure is developed in many places (Wilson, 1952, or Deming, 1943), and we will not reproduce it here. When it can be used, the linear approach is superior to the nonlinear iterative fitting which was used for the absorption. The linear approach is faster and is free of the false minima uncertainties sometimes encountered in the nonlinear procedure. Further, the linear procedure yields statistical information about the resulting parameters in a straightforward way.

C. Magnetic Circular Dichroism: Experimental

Introduction

The magnetic circular dichroism (MCD) of metal porphyrins is described in detail in this section. Other compounds have been investigated less completely and will be mentioned in a general summary where we attempt to evaluate the prospects for MCD in biology and chemistry. We hope that evaluation of MCD will be clearer after detailed discussion of particular examples. The metal porphyrin experiments are discussed in the reverse order to that in which they were performed. Some of the early observations were that reduced cytochrome c gave an enormous MCD signal and that MCD was sensitive to ligands in the sixth coordination position of the iron in hemoglobin (the position that normally holds oxygen). To aid in an understanding of these observations, we undertook a study of metal porphyrins, free of protein, with different metal substitution. We hoped to understand the role of the metal in the porphyrin MCD, with the possibility of coordination alteration, without complications of possible protein configuration changes.

There are fairly recent reviews on porphyrin spectra (Gouterman, 1961) and on attempts at relating porphyrin spectra to biological function (Williams, 1961). The importance of metal porphyrins in biochemical reactions is well known (e.g., Fruton and Simmons, 1959). The electronic structure and chemistry of metal porphyrins is important for understanding the role of these compounds in photosynthesis and oxidative metabolism.

The experimental details unique to magnetic CD are presented first. Next the metal porphyrin MCD experiments and their interpretation are presented and discussed in some detail. The MCD of hemoglobin, methemoglobin and cytochrome c follow. Last, we briefly attempt to assess the probable future usefulness of MCD in biology and chemistry.

Instrumentation

The superior sensitivity of ORD measuremahts relative to CD (see Appendix I) lead us to start this research by building a magnetic ORD (MORD) instrument. One of the large problems with MORD measurements is that everything has magnetic optical activity. In most cases, the solvent and cells used for MORD measurements have rotations 100 times larger than the solute of interest. The instrument we constructed had two opposed electromagnetics in a line, one to contain the sample of interest (in a solvent) and the other to compensate for the solvent rotation with pure solvent. The two electromagnets in series made the instrument long and bulky, and we found that mechanical and thermal instabilities could not be reduced to the point where satisfactory compensation for solvent and cell rotation were reliable.

Magnetic circular dichroism (MCD) is only measurable in the region of absorption of a material. In MCD measurements the solvent and cell contribute to the signal only to the extent that they absorb in the region of interest. Nonabsorbing solvents and cells are normally used for absorption measurements so the MCD experiment can easily be made free of solvent interference. Further-

more, the MORD compensation difficulties mentioned above seem to put MCD and MORD sensitivity on more equal footing, and we proceedded to convert our apparatus to MCD measurements.

The instrumentation required for MCD is identical to that used for natural CD measurements. A magnetic field must be added parallel to the propagation direction of the light and the photomultiplier and amplifiers must be shielded from stray magnetic fields. The basic dichrograph we constructed was described in detail in Chapter II, and the modification details will be given here. A schematic drawing of the optical layout, including the magnet, is shown in Figure III-6. All of the optical components were previously described (Ch. II, p. 39).).

Magnetic optical activity depends linearly on field strength so the larger the magnet used, the larger the resulting signals. The magnet available to us was a water cooled, 1.8 kilogauss, air core solenoid with two inch inside diameter. (The magnet was designed and built at the University of California Lawrence Radiation Laboratory, LRL print number 9H3634.) The field strength was increased by inserting soft iron pole pieces into the solenoid bore (P 1 and P 2 in Figure III-6). The pole pieces were designed and built by Dr. J. Thorne (1966). A large soft iron return was fitted around the solenoid; one pole piece (P 2) and a portion of the return on one side (labeled R in Figure I-6) were removable. A brass sample cell holder, machined to fit between the pole pieces, was used to establish the magnet gap of 1.4cm. Cylindrical quartz sample

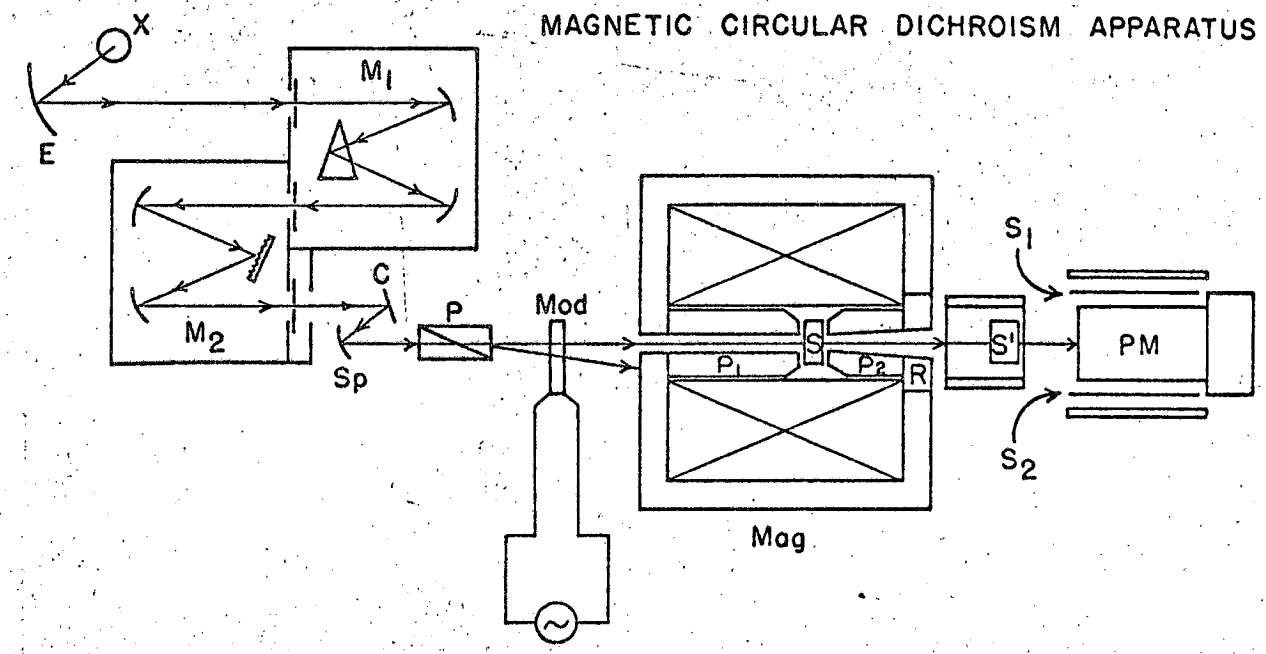

Figure III-6. Diagram of the optical components of the magnetic circular dichroism apparatus. The components are explained in the text.

cells (S in Figure III-6) of 22 mm o.d. were positioned against one pole piece by a gently compressed foam rubber washer. The average field strength, integrated over the volume of the light beam, was found to be 11.25 kilogauss (the magnet calibration is described later) and a field vs. magnet current curve indicated that the pole pieces were about 80% saturated at maximum field. The sample temperature was 30 ± 2° C when the magnet was at full field strength. S_1 and S_2 are mμ metal and soft iron cylindrical photo-multiplier shields, respectively.

Magnetic optical activity depends on the component of the field parallel to the propagation direction of the light and is not sensitive to perpendicular components. For this reason the magnetic field neednnot be homogeneous (ours varied about ± 20% over the sample volume as estimated with a Bell axial Hall effect probe). Extremely large perpendicular components can lead to orientation of molecules in the sdution. This perpendicular magnetic orientation, the Cotton-Mouton effect, is negligible for normal laboratory fields (a table of Cotton-Mouton constants has been given by Mouton (1930)). The Cotton-Mouton effect is similar to the Kerr effect, but is down in magnitude by about 10^4. (comparing electric fields in volts/cm to magnetic fields in gauss needed to produce the same effect). The possible presence of this effect can be checked by the field strength dependence of the MCD signal. The Cotton-Mouton effect depends on the square of the mag-

netic field strength, while the MCD depends on the first power of the field strength, so molecular orientation would cause the MCD signal to depart from a linear dependence on field strength.

The MCD signal responds to the average field intensity over the light beam area. Field calibration can be a problem for inhomogenous fields, so ease of calibration is the main virtue of homogeneous fields for this work.

An optical technique was used for field calibration which relies on the absolute calibration of a recording polarimeter. This procedure is very similar in concept to the previously described natural circular dichroism calibration (Chap. IIB). The Cary 60 polarimeter was fitted with a permanent magnet (Thorne, 1966) with a field strength of about 7 kilogauss for a 2 mm sample cell. The average field strength of the MCRD magnet is determined by measuring the Faraday rotation of water or benzene. The observed rotation is given by:

$$(\alpha) = V(\lambda)\ d\ H \qquad \text{III-(115)}$$

where λ is the wavelength of measurement, $V(\lambda)$ is the Verdet constant, $\alpha(\lambda)$ the observed rotation, d is the density times the path and H the average field strength. The Verdet constants of water or benzene are very precisely known at several visible wavelengths and are tabulated in several books (e.g., Waring and Custer, 1960). The empty cell in the magnet is used as a baseline for the water or benzene rotation measurement. The clean empty cell outside of

the magnet does not disturb the instrument baseline. The permanent magnet must be recalibrated each time it is used, since accidental jarring of the magnet reduces the field from the peak charge value of 8.5 kilogauss.

The first step in MCD field calibration is the measurement of the MCD of a suitable sample. The MCD spectrum is digitized and mathematically transformed to the MORD using the Kronig-Kramers relation (Moscowitz, 1960). (The Kronig-Kramers transform procedure is discussed in more detail in Chap. IIB and Appendix II.) The calculated MORD (using the calibrated magnet) to determine the field strength of the MCD magnet according to the simple relation:

$$H_{MCD} = \frac{MORD_{obs} \cdot H_{MORD}}{MORD_{calc}} \qquad \text{III-(116)}$$

A few comments on this procedure are necessary. First, it is not necessary to assume that calibration of the CD machine is precise, because the amplitude of the MCD signals depends on the product of the field strength and the CD calibration constant (see Chap. IIB, p. 48). If the CD calibration constant is set high or low by the previous procedure (Chap. IIB) the above field calibration will reflect this is a lower or higher value of the field, respectively. So we actually calibrate the product of the field strength and the CD calibration constant which is the experimentally important factor.

Second, the Kronig-Kramers transform is an exact procedure in the direction of MCD ——→ MORD, and no assumptions about

sample band shape or number of bands is required. The MORD due to the observed MCD is obtained and MORD tails from MCD bands that are not measured may be troublesome.

Several factors must be considered in the choice of a comparison sample, aside from the obvious stability requirement. The desired properties are:

1) A magnetic rotational strength large enough compared to oscillator strength to insure a favorable signal-to-noise ratio (>100).

2) The sample must have relatively isolated absorption bands, so that MORD tails from bands which cannot be measured in MCD do not contribute appreciably to the MORD.

3) Intense absorption, so that dilute solutions can be used and the solvent displacement correction (Shashoua, 1964) can be neglected in the MORD.

4) The material should be soluble in solvents that are transparent to at least 50-100 NM from the region of interest, so that refractive index corrections can be neglected in the Kronig-Kramers transform (Thiery, 1966).

5) The compound must have absorption bands sufficiently wide (greater than a few NM) so that MORD spectral resolution in the Cary 60 is not challenged.

Several different types of samples met most of the criteria rather well. Cobaltous chloride in H_2O is good, but solvent displacement corrections (3) must be made. Polycylic hydrocarbons

in $CHCl_3$, pyrene, acenaphthalene or phenanthrene are suitable, but accurate rotation amplitudes challenge the spectral resolution of the Cary 60. Metal porphyrins turned out to be ideal samples for this purpose. The particular type of MCD curves exhibited by these materials transform to MORD curves with nearly no tail. Figure III-7 shows an experimental MCD curve of Ni(II)-deuteroporphyrin dimethyl ester and the resulting calculated MORD. The experimental MORD of the same sample taken in the Cary 60, using the previously calibrated magnet, is shown in Figure III-8. The calculated MORD, suitably scaled, agrees with the observed MORD to within experimental error, and so this procedure is very accurate. It is also clear, from this agreement, that contributions of other absorption bands (not measured in the MCD) to the MORD in this region are entirely negligible. The large solvent baseline in the MORD is largely compensated with a concentrated sucrose solution, and the remaining baseline slope is removed with the Cary 60 multipots (which have a range of $\pm$ 0.2 degrees). This procedure is explained in detail by Thorne (1966).

In principle, an ideal MCD calibration standard (independent of the polarimeter) would be a crystal where the necessary electronic and magnetic data needed to calculate the expected MCD spectrum are known precisely from other measurements. Ruby, chromic ion in Al_2O_3, seems well suited to this purpose if it is viewed along the optic (c) axis. The ruby laser lines at 6936 (R_1) and 6925 Å (R_2)

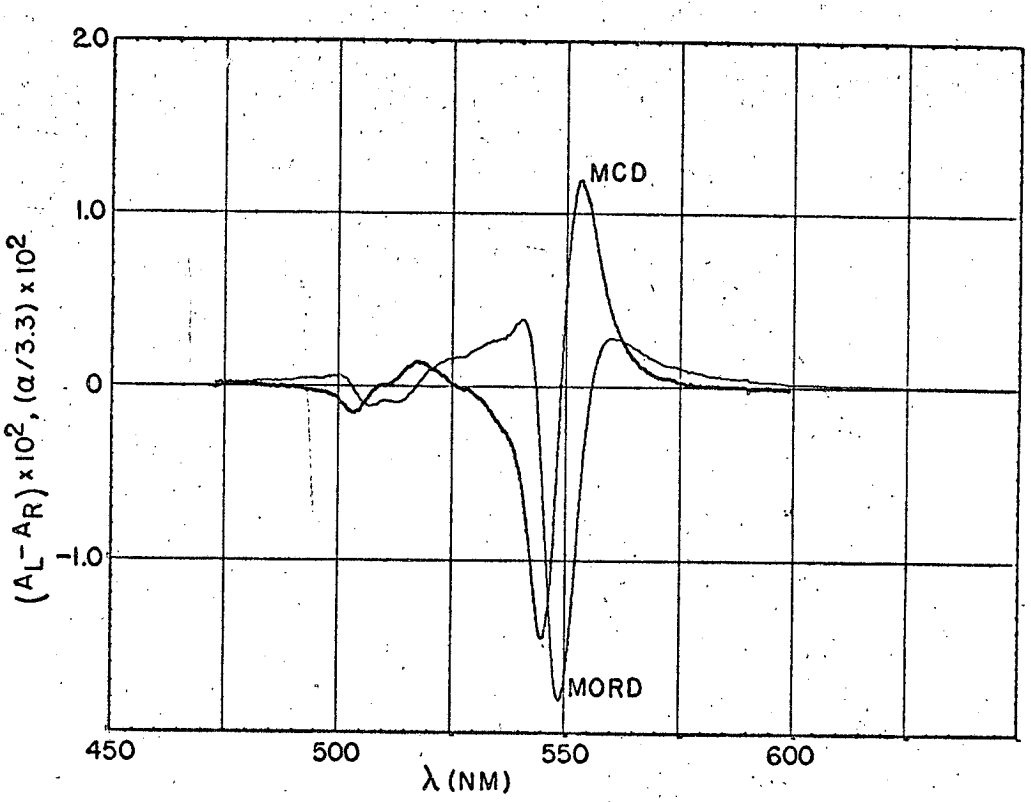

Figure III-7. Measured magnetic circular dichroism (MCD) in absorbance units of Nickel(II)deuteroporphyrin dimethyl ester, $5.76.10^{-5}$ moles/liter, chloroform, 1 cm path, darker curve. Calculated magnetic optical rotatory dispersion (MORD) (in degrees) due to the observed MCD. Peak optical density = 1.709.

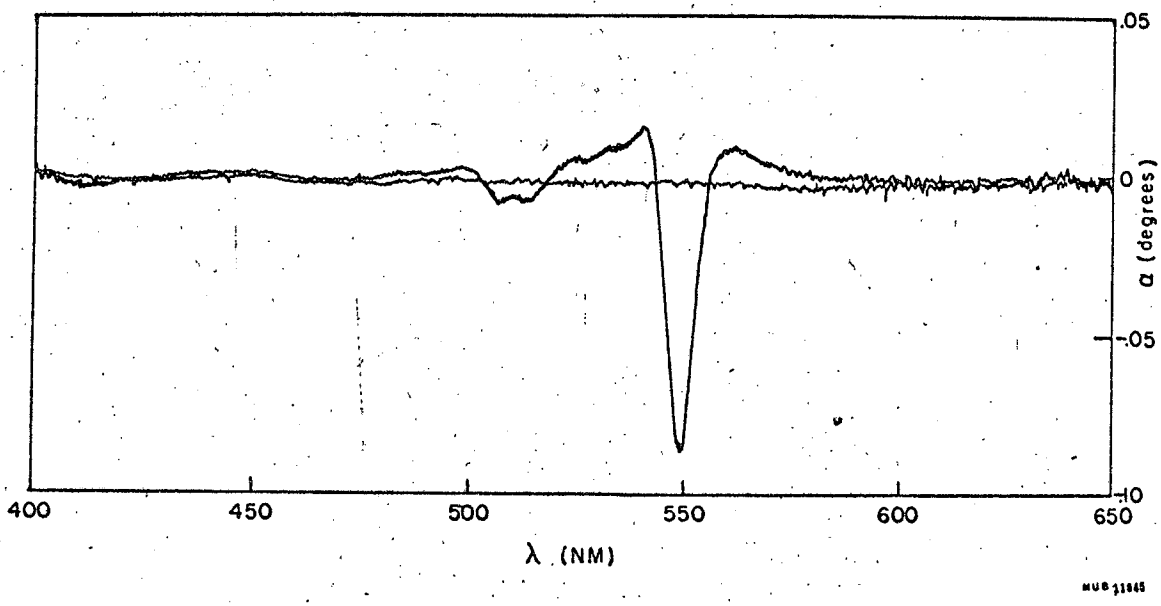

Figure III-8. Magnetic optical rotatory dispersion (MORD) of nickel(II)deuteroporphyrin dimethyl ester, 5.76×10^{-5} moles/liter, chloroform, 0.20 cm cell. Measured in the Cary 60 recording polarimeter using a 7.0 kilogauss permanent magnet as described in the text. Peak optical density = 0.372.

are precisely characterized from magnetic resonance and optical experiments and the MCD spectrum may be calculated by simply summing the Zeeman components. These lines are exceedingly sharp, with about 1 NM full width at $\frac{1}{2}$ height at room temperature. Accurate intensity measurements require a spectral bandwidth less than 0.05 NM and tax the resolution of our instrument. Experimental MCD measurements agree well with the predicted MCD spectrum for the R_1 line (to 5%, assuming the preceding calibration is correct), but are too large (50%) for the R_2 line. The relative intensities of the R_1 Zeeman components have been found to agree with the theoretical predictions (Sugano and Tanabe, 1958) by fluorescence measurements (Varsanyi, Wood and Schawlow, 1959). It is possible that there is something amiss in the theory of the R_2 ruby line intensities, but, on the other hand, we cannot be absolutely confident of our results under resolution limiting conditions.

In summary, consideration of the probable errors involved, the MCD calibration (field/sensitivity ratio) is accurate to about 1%; however, the precision may be somewhat less than this. The procedure adopted is a very satisfactory solution to the calibration problem, if a bit indirect. The average field strength calibration found (assuming the CD sensitivity found previously was correct) was 11.25 kilogauss.

Much of the MCD data requires computer analysis (Kronig-Kramers transforms, fitting, etc.) so a means for digital readout was devised. The spectra were in digital form in the Enhancetron memory (Nuclear Data, ND-800, see Chap. II, page 56) and it

was a relatively simple matter to build an interface to drive a Model 33 Teletype. The teletype prints an octal number record of the digical data while simultaneously punching (7 line and parity) paper tape. The interface uses Digital Data Corp. "Flip-Chip" logic modules to accomplish binary-to-octal conversion and parallel-to-serial readout. The interface was built by the Data Processing Group at the Lawrence Radiation Laboratory, Berkeley, and the schematic is available as LRL print number 10V8634.

The Teletype keyboard can be used to enter experiment identification, sensitivity and wavelength range information on the paper tape and printed record. The paper tape is converted to magnetic tape for further computation by standard methods. The program that interprets the data (ODTRAN) and does some of the processing is describediin more detail in Appendix II. Suffice it to say that, at this point, the essential ODTRAN output is a magnetic tape, or card deck, that includes a title (80 BCD characters), number of data points (N) and N values of ΔOD ($\Delta\varepsilon$ or $\Delta]$) and wavelength.

Spectra can be either added or subtracted from the Ehhancetron memory. The magnetic CD signals reverse sign when the electromagnet field polarity is reversed, while any natural CD or instrumental baseline is not affected by field polarity. If an equal number of spectra are added with positive field polarity and subtracted with negative field polarity, the MCD signal is doubled while the natural CD is cancelled out. The measurements are routinely done

in this way to subtract an instrumental baseline, even if the sample has nonnatural optical activity.

Absorption spectra were recorded in a digital form with a Cary 14 spectrophotometer fitted with a Cary retransmitting slidewire accessory. The voltage on the slidewire (linearly related to absorbance) was read with a digital voltmeter which drove an IBM Model 26 summary card punch. The Cary 14 wavelength is driven with the standard synchronous motor and the card punch was triggered by a separate synchronous motor fitted with a cam and a microswitch. The digital data cards were converted to absorbance vs. wavelength by a computer program (PROCESS) which is described in Appendix II. This primitive digitizing apparatus was largely satisfactory, but would "drop" occasional data points. The PROCESS program was written to detect most of these dropped points, and to set them equal to the arithmetic mean of the nearest neighbor points. Occasional bad points remain in the data that follows, that do not depart very far from the true curve, and therefore could not easily be corrected. The data point interval was small enough so that occasional bad points do not significantly effect the data.

D. Metal Porphyrins

Sample preparation

Zinc(II), Copper(II), Nickel(II), Cobalt(II), Silver(II), Vanadyl(II) and metal-free deuteroporphyrin IX dimethyl esters were a gift from Dr. Winslow Caughey, Johns Hopkins Medical School, Baltimore, Maryland.

These materials were highly purified and checked by IR, NMR, and elemental analysis (Caughey, 1966). The porphyrins were dissolved in analytical reagent grade chloroform which contained 0.5% ethanol. The chloroform was stored over solid calcium oxide and freshly filtered with 100 Angstrom millipore filters before use. Small quantities of solid porphyr were weighed into 5 ml volumetric flasks on a Mettler microbalance, solvent added and the flasks reweighed on a larger capacity Mettler balance. The volume of the solution was calculated from the density of chloroform (1.446 g/ml). The sdutions were kept in the dark and measured 2-3 hours after preparation to be sure that the porphyrin was completely dissolved. Zinc(II)coproporphyrin I and III tetramethyl ester samples in frozen dioxane were obtained from M. Malley, University of California, San Diego.

Hemin chloride was purchased from California Biochemicals Corp. and used without further purification. This material contained about 5-10% protoporphyrin free base impurity as judged from the absorption spectrum. Independent measurements of the MCD of protoporphyrin established that this impurity was

not important for our measurements. The hemin was dissolved in 0.1 M phosphate buffer (pH 8.0) or pH 12.0, sodium hydroxide. The iron(II)protoporphyrin IX was prepared from the hemin solution by addition of small amounts of solid dithionite. The Fe(II)protoporphyrin solution tended to reoxidize in air to Fe(III) quite rapidly at the higher pH, but the pH 8.0 solution was found to be sufficiently stable in a stoppered cuvette for several hours as judged by the constancy of the Fe(II) protoporphyrin absorption spectrum. Pyridine was sometimes added in large excess to the iron protoporphyrin solutions.

Bovine Hemoglobin (Hb) was purchased from California Biochemicals Corp. (Grade A and Grade C) and was once recrystallized by the method of Beychok (1964) and dissolved in pH 6.8 phosphate buffer (0.01 M). Some samples of human Hb were gifts from Dr. Lubert Stryer. The different samples gave equivalent MCD results for equivalent absorption intensity. The various hemoglobin derivatives were prepared by standard methods (Lemberg and Legge, 1949). We were not able to deoxygenate hemoglobin sufficiently well with N_2 bubbling without extensive denaturation of the sample by the bubbles, and the oxygen was removed with a tiny amount of solid dithionite. The carbonmonoxy derivative was formed by slow bubbling of hemoglobin solution with 100% CO gas in a fume hood for about six hours. The pyridine derivatives were formed by addition of small amounts of pure pyridine to the aqueous solutions until the spectrum showed no further change. The methemo-

globin Fe(III) hemoglobin, or Hi, was prepared from a pH 7.4 solution of Hb by addition of a four-fold excess of potassium ferricyanide. The azide or cyanide derivatives were formed by addition of a ten-fold excess of sodium azide, or potassium cyanide, in 0.01 M pH 7.4 phosphate buffer.

Horse cytochrome c (Grade A) was obtained from California Biochemicals Corp. and was dissolved in 0.1 M phosphate buffer pH 7.0. The reduced form was prepared by addition of solid dithionite.

Description of the porphyrin spectra

The structures of the metal coproporphyrin I, coproporphyrin III, deuteroporphyrin IX and protoporphyrin IX are shown in Figure III-9. These are, with the exception of coproporphyrin I, naturally occurring porphyrin isomers. The side group relationships can best be compared in tabular form:

Compound	1	2	3	4	5	6	7	8
Coproporphyrin I	M	P	M	P	M	P	M	P
Coproporphyrin III	M	P	M	P	M	P	P	M
Deuteroporphyrin IX	M	H	M	H	M	P	P	M
Protoporphyrin IX	M	V	M	V	M	P	P	M

where M is a methyl group, H is hydrogen, V is vinyl and P is propionic acid. The compounds we have studied are all propionic acid methyl esters, so the P symbol actually stands for:

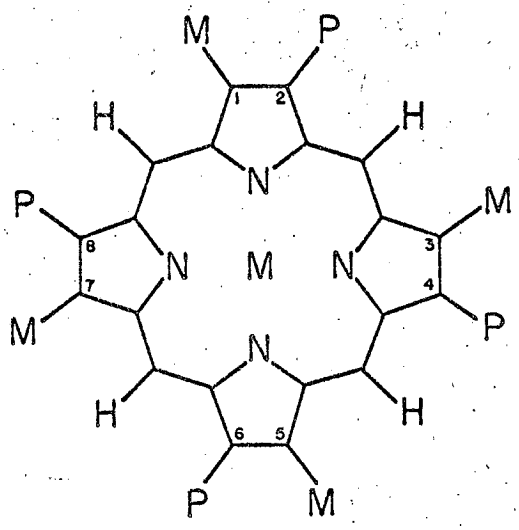

METAL COPROPORPHYRIN I

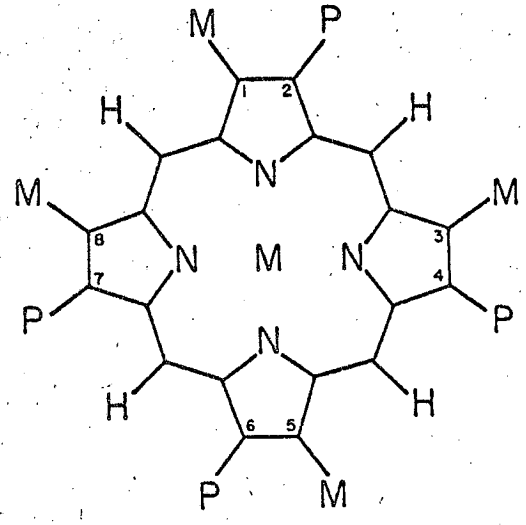

METAL COPROPORPHYRIN III

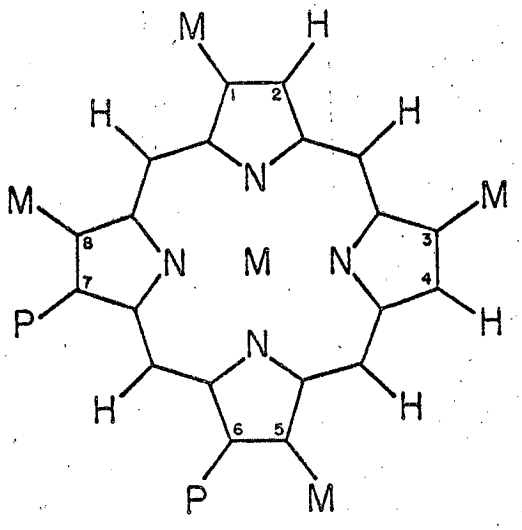

METAL DEUTEROPORPHYRIN IX

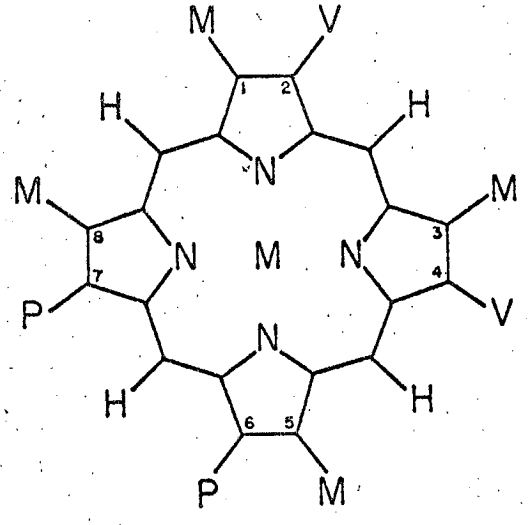

METAL PROTOPORPHYRIN IX

MUB 12084

Figure III-9. The chemical structure of the metal porphyrins used in this study. The central M stands for any one of a number of metals. The peripheral substituent symbols are identified in the text.

$$P = -(CH_2)_2-\overset{O}{\overset{\|}{C}}-O-CH_3$$

The absorption and MCD spectra of all of the metal porphyrin complexes are qualitatively very similar. The absorption and MCD spectra of zinc(II)deuteroporphyrin dimethyl ester are shown in Figures III-10 and III-11 as examples of the general features of these spectra. These compounds all have a very intense single band, called the Soret or UV band, near 4000 Angstroms as can be seen in Figure III-11. The metal porphyrin complexes have a pair of bands in the visible region (5000-6000 Angstroms) generally called the red bands. Note that the concentration is ten times higher for the visible spectrum in Figure III-10 and that the red bands are 10-20 times weaker than the Soret band. This large intensity difference turns out to be very significant for the theory of the porphyrin spectrum so it should be emphasized at this point. Some of the iron complexes have a few extra bands, but all the compounds show the basic three-banded spectrum with occasional shoulders. There are also a pair of weak absorption bands on the blue side of the Soret band (not shown here) which have recently been studied (Caughey, Deal, Weiss, Kobayashi and Gouterman, 1965). We investigated the MCD of these weak UV bands, but found very small, nondescript MCD spectra in this region, so very little mention will be made of these bands.

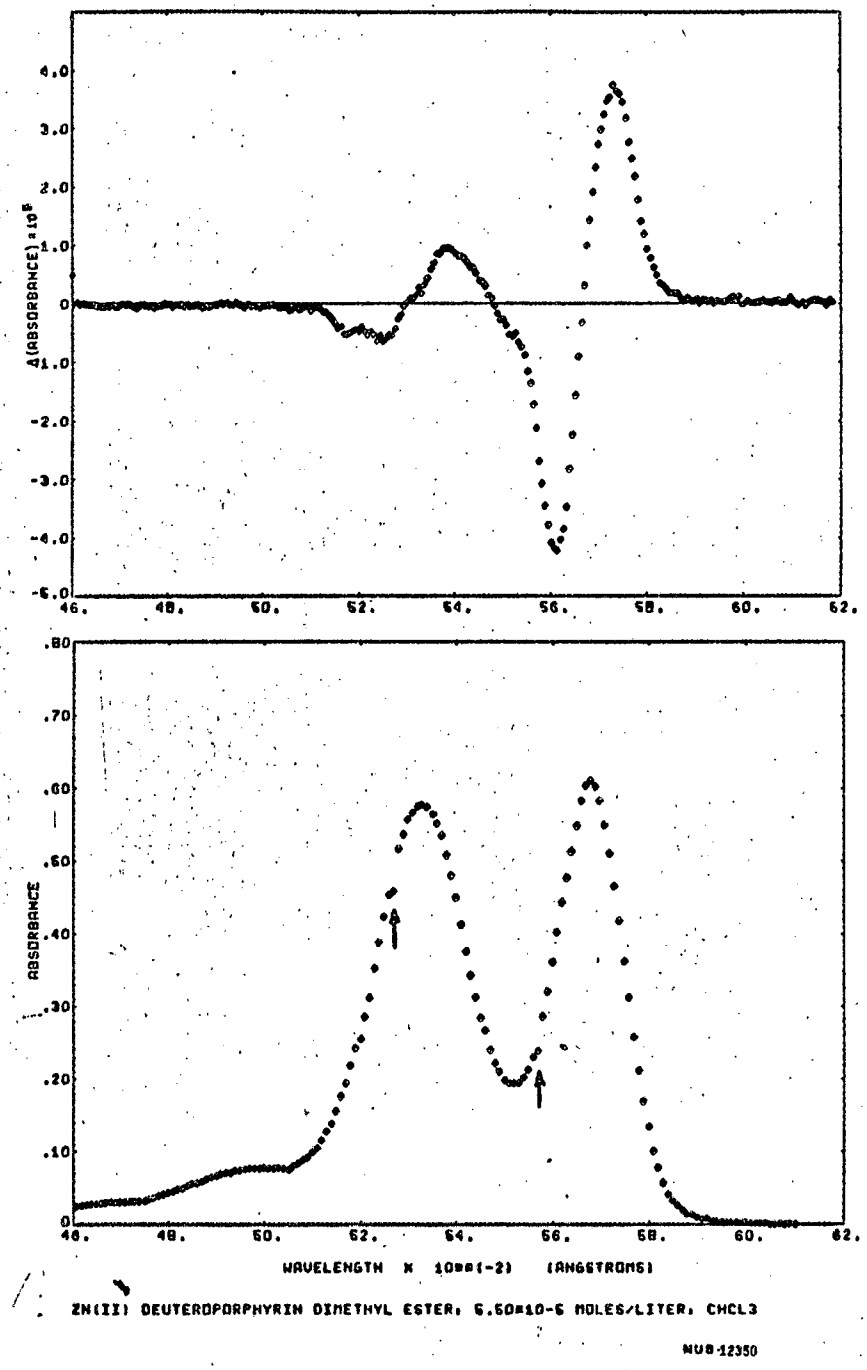

Figure III-10. The absorption (below) and MCD (above) in the visible region of Zinc(II)deuteroporphyrin dimethyl ester, $5.50.10^{-5}$ moles/liter, chloroform, 1 cm path. Some of the digital absorption spectra have bad points that should fit smoothly on the curve. An example of two of these points are marked on the absorption curves. These occasional slight departures from the true spectra have a negligible effect on the following experiments.

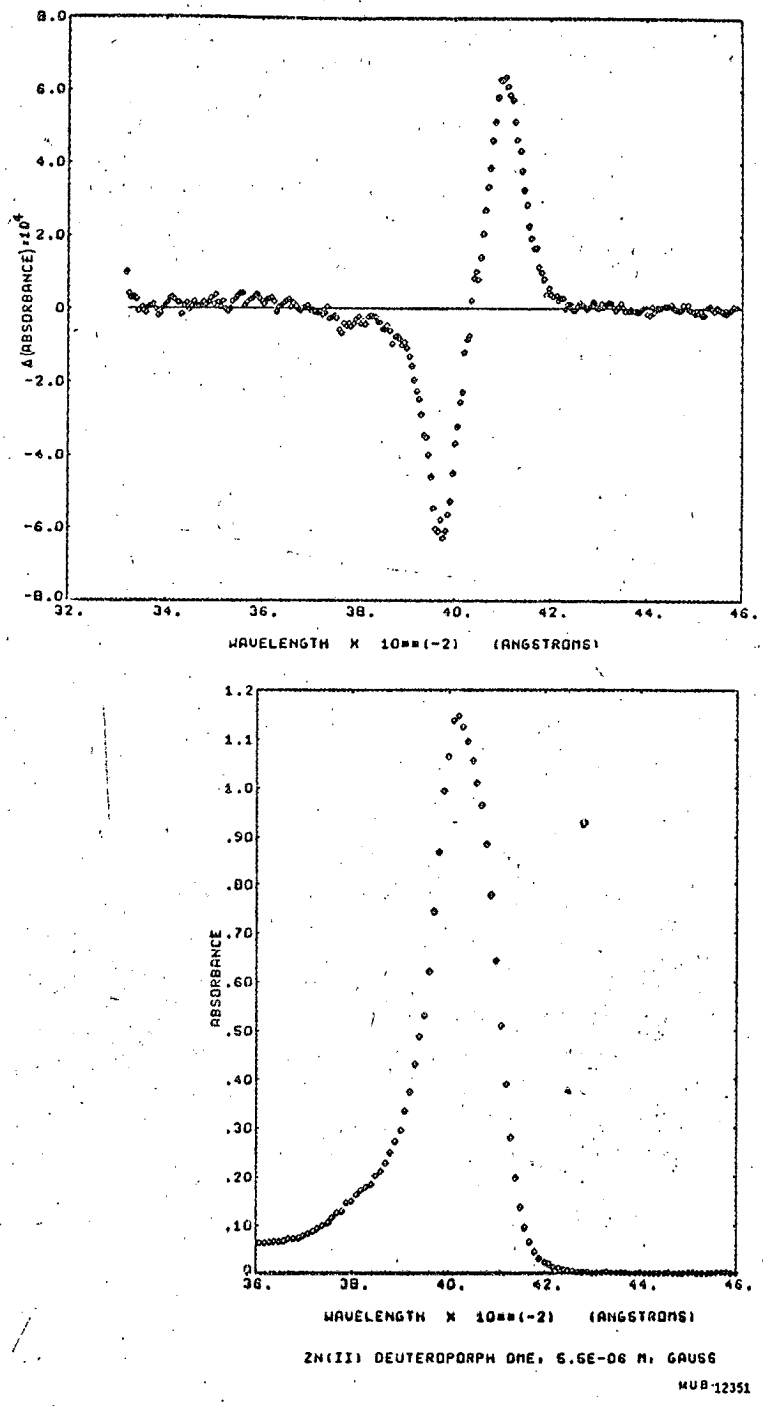

Figure III-11. The absorption(below) and MCD (above) of zinc(II)deuteroporphyrin dimethyl ester, $5.5.10^{-6}$ moles/liter, chloroform, 1 cm path.

A more convenient nomenclature for the prominent three bands of the metal porphyrin spectrum, due to Platt (1956), is the Q_{o-o} band for the longest wavelength peak at about 5700 Angstroms in Figure III-3, the Q_{0-1} (vibrational overtone) for the next peak at about 5300 Anstroms in the sample spectrum,and the B band for the intense Soret band in the 4000 Angstrom region. The exact peak positions of these three bands changes with metal substitution, solvent and side chain substitution. The above Q,B shorthand nomenclature is unambiguous for all cases of interest, and will be used throughout thesis to save writing out the peak wavelength each time a band is referred to.

The MCD spectra showed pronounced double MCD curves for the Q and B bands for all the compound studied, and the MCD curves in Figures III-10,11 are typical. While the MCD spectra are qualitatively similar for all the porphyrin metal complexes studied, we do observe a systematic variation in MCD amplitude with metal substitution. These effects will be discussed later. The Q_{0-1} region is very complex in the MCD and Figure III-10 shows evidence for 2-4 relatively small MCD components in the Q_{0-1} region. The room temperature absorption in the Q_{0-1} region shows a reasonably symmetrical single band for all these compounds, with occasional hints of shoulders. Zn Coproporphyrin(III) tetramethyl ester, in dioxane, has a nearly identical absorption spectrum to Figure III-10, but offers the best resolution of the several MCD components in the Q_{0-1} region. The MCD of the Zn coproporphyrin III is shown in Figure III-12, where at least three components are

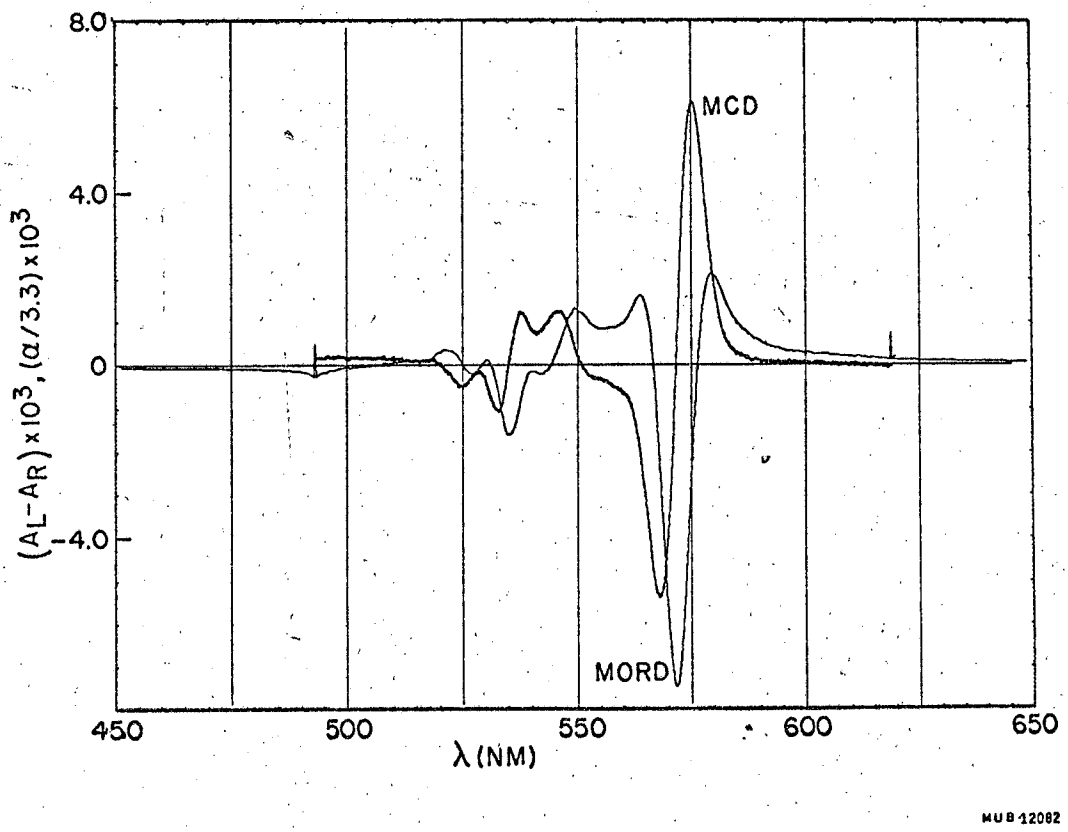

Figure III-12. Observed MCD (darker curve) and calculated MORD (lighter curve) of zinc(II)coproporphyrin III tetramethylester, dioxane, $6.3.10^{-5}$ moles/liter, 1 cm path. The peak optical density of this solution is 1.260.

clear in the Q_{0-1} region near 5300 Angstroms. It should be noted that the MCD of Zn coproporphyrin I is indistinguishable from III in shape and magnitude under the same conditions, indicating that the MCD is not markedly sensitive to the details of side chain isomerization. The MCD offers much more resolution in the Q_{0-1} region than does absorption, but the component bands are still rather confused. Since our room temperature absorption spectra do not resolve this region, we will not attempt a detailed analysis of the Q_{0-1} MCD, although it seems useful to pursue in the future. The Zn coproporphyrin III also shows the best resolution in the B region. Figure III-13 shows the MCD of this compound, the small single MCD peak on the short wavelength side of the main B band is the most distinctive minor peak seen on the high energy side of the B band.

With this introduction, we will concentrate on the main B and Q_{0-0} bands in what follows. Unless otherwise stated, we subsequently will take the Q band to be Q_{0-0}. We present, first, the general interpretation proposed for the main features of the metal porphyrin MCD spectraa. Next, we present a detailed numerical analysis of the spectra, and, finally, we investigate the more detailed theory of the porphyrin spectra as it relates to the systematic variations found in the observed MCD. Finally, the somewhat special case of the iron porphyrins and heme proteins is presented.

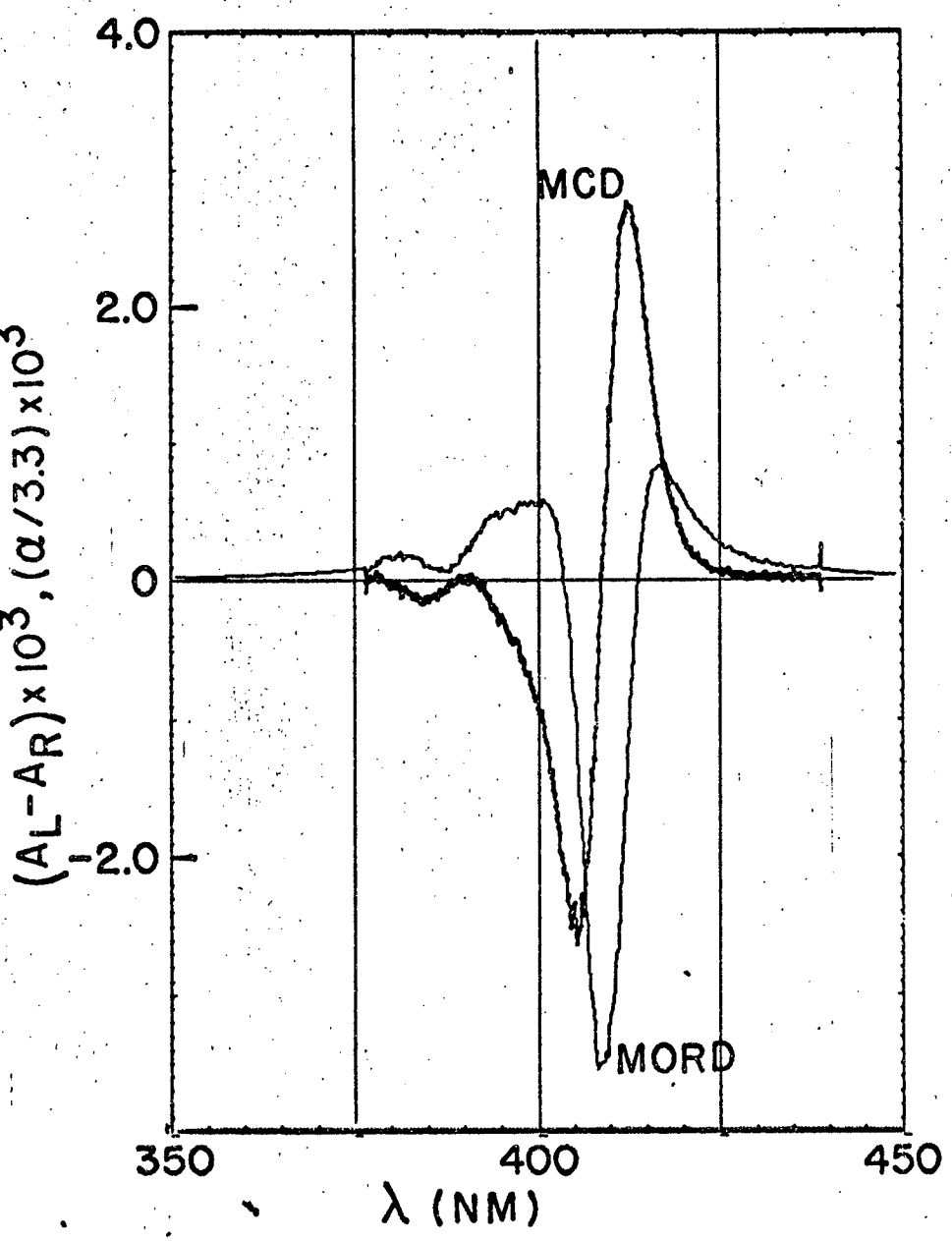

MUB 12080

Figure III-13. The observed MCD (darker curve) and calculated MORD (lighter curve) of zinc(II)coproporphyrin III tetramethylester, approximately $4 \cdot 10^{-6}$ moles/liter, solvent dioxane, 1.0 cm path. The peak optical density of the solution is 1.950.

Zn coproporphyrin I has full square symmetry, which means that the x and y directions in the molecular plane are equivalent. Some of the metal porphyrins studied have less symmetric side chain substitution than the Zn coproporphyrin I and so do not have a rigorous x-y degeneracy. We mentioned that the slightly less symmetric Zn coproporphyrin III shows an identical MCD and absorption spectrum to the I isomer. The MCD and absorption are apparently not very sensitive to the details of the side chains. The metal deuteroporphyrins (Zn spectrum given in Figure III-10) and metal protoporphyrins have qualitatively similar MCD spectra, so the asymmetry of side chain substitution does not alter the general double MCD curve features of the MCD spectra in the Q and B region.

In the metal-free porphyrin, however, two central nitrogens on opposite sides of the ring are occupied by hydrogens, making the x and y directions strongly non-equivalent. The central hydrogens split each of the two visible bands, previously x-y degenerate in the metal porphyrin, into x and y polarized components of different energy. The absorption and MCD spectra of metal-free protoporphyrin are shown in Figure III-14. Four absorption bands are found in the visible region; the B (Soret) band splitting resulting from the central hydrogens is not large enough to be seen at room temperature. However, the B band splitting of 250 cm^{-1} is resolved at low temperature (Rimington, Mason and

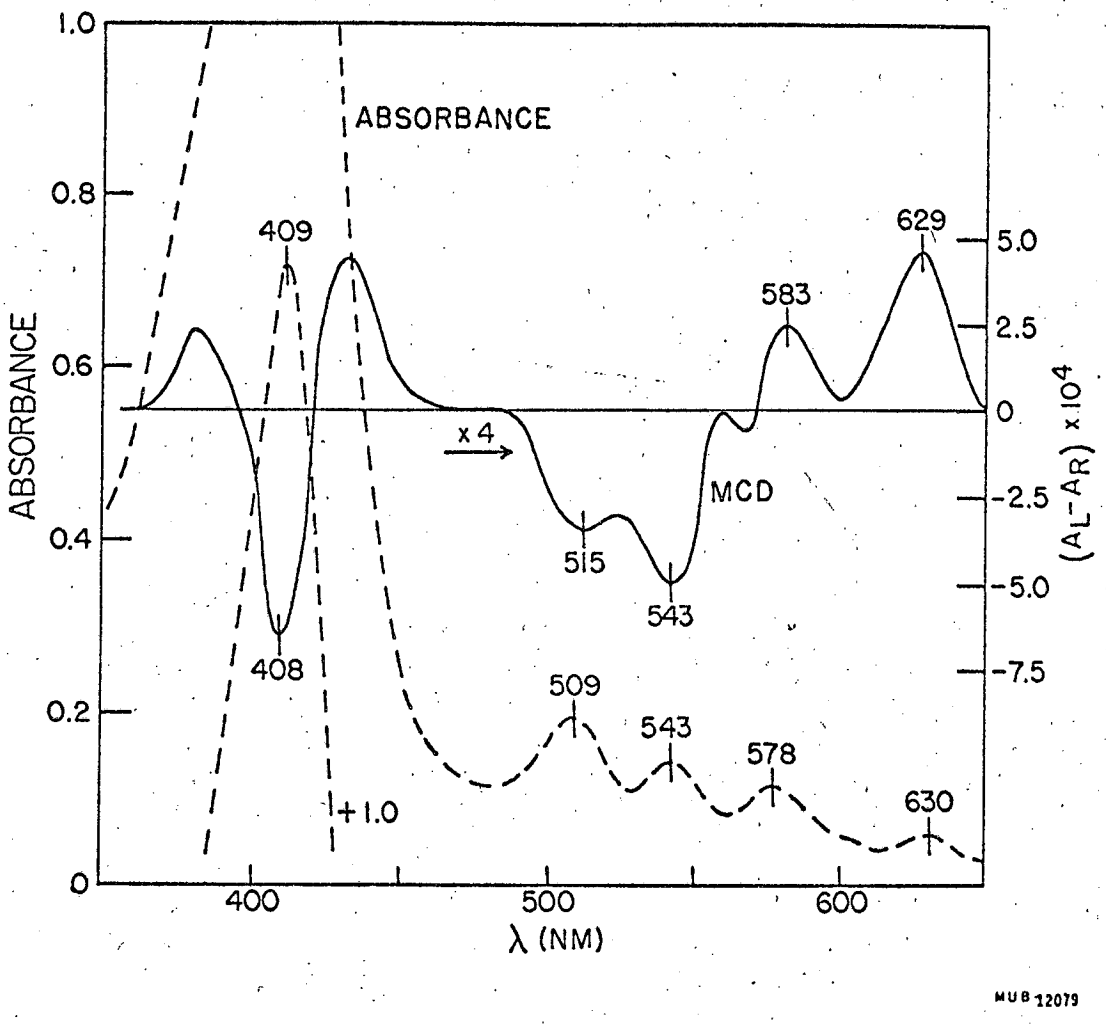

Figure III-14. MCD (solid curve) and absorbance (dashed curve) of metal-free protoporphyrin, 2.10^{-5} moles/liter, solvent, water, pH 8.0, 1 cm path.

Kennard, 1959). The MCD of the metal-free porphyrin is drastically different than the metal compounds shown above. Instead of the double MCD bands centered close to the absorption peaks, as in the metal porphyrins (Figure III-10), the metal-free compounds show single MCD bands. This is an example of the magnetic coupling of non-degenerate x,y transitions treated in the theoretical section. The porphyrins offer a nice confirmation of the general ideas of MCD spectra put forward in the theory section. The non-degenerate transitions of the metal-free porphyrins give single MCD bands, while the x,y degenerate metal porphyrins give double MCD bands.

Evidence for the B band splitting in the metal-free case, while not found in absorption at room temperature, is seen in the MCD (Figure III-14). A negative MCD peak at 408 NM is very close to the absorption peak at 409 NM, while in the metal complex the MCD crosses zero at the absorption peak. The MCD amplitude is down by about 10-20 times in the metal-free porphyrin compared to degenerate metal complex case, as is expected for non-degenerate magnetic coupling (p. 139), further evidence of x,y splitting in the B region.

The red region shows positive MCD peaks at 629 NM and 583 NM and negative MCD peaks at 543 NM and 510 NM. The Q band region shows approximate local conservation of MCD (the positive MCD area = the negative MCD area) indicating that the Q_x bands are coupling almost exclusively with the Q_y's. The same conservation

is found in the B region. The sign of the MCD allows the relative polarizations of the transitions to be assigned for the O-O bands as in Table I; band 3 ($Q_{y\ o-o}$) is perpendicular to band 1 ($Q_{x\ o-o}$), band 5 ($B_{x\ o-o}$) is perpendicular to band 6 ($B_{y\ o-o}$), and apparently parallel to band 1. The assignment of these polarizations agrees with that found by fluorescence polarization experiments with similare metal-free compounds (Gouterman and Stryer, 1962, Wiegel, 1957). The fluorescence polarization experiments indicate that the polarizations of the o-1 bands are mixed x and y. It has been assumed that some of the excited state vibrations which take part in the o-1 transitions mix x into y polarization and y into x polarization. Examination of the symmetry species of the porphyrin free base (neglecting substituents, it is D_{2h}) indicates that only totally symmetric A_g vibrations and B_{1g} vibrations are allowed in the o-1 bands. Q_{o-1} transitions with A_g vibrations will not have altered polarization, but B_{1g} vibrations convert x polarized transitions into y polarized transitions and vice versa. If we consider, for example, the $Q_{x\ o-1}$ band (which is made up of A_g and B_{1g} components) the A_g components must give positive MCD as does the $Q_{x\ o-o}$. The part of the $Q_{x\ o-1}$ band which is made up of B_{1g} vibrational components is actually y polarized and will have negative MCD, which partially cancels the positive A_g part. Apparently the A_g vibrational components occur predominantly on the long wavelength side of the band and are somewhat stronger than the B_{1g} components. The B_{1g} components are almost entirely cancelled

and are evidenced only by a red shift of the MCD peak compared to the absorption and by a small negative peak at ca. 572 mμ. In a similar manner, the $Q_{y\ o-1}$ band is predominantly A_g on the long wavelength side and has negative MCD like the $Q_{y\ o-o}$ band. Some B_{1g} component with positive MCD must be present on the short wavelength side of the $Q_{y\ o-1}$ band because the MCD peak is red-shifted from the absorption peak. These conclusions are summarized in Table I.

Table I. Relative polarizations of the transitions in free base protoporphyrin. (We have no information on the absolute polarizations, but for the purposes of presenting the results in this table we adopt Gouterman's convention, that the $Q_{x\ o-o}$ band lies at longest wavelength (Gouterman, 1961). The A_g and B_{1g} vibrational components are discussed in the text.)

	Assignment	ABSN(NM)	MCD(NM)	pol.
1.	$Q_{x\ o-o}$	630	629	∥
2.	$Q_{x\ o-1}$	578 (A_g + B_{1g})	583 (≈ Ag)	∥ Ag part
3.	$Q_{y\ o-o}$	543	543	⊥
4.	$Q_{y\ o-1}$	509 (A_g + B_{1g})	515 (≈ Ag)	⊥ Ag part
5.	$B_{x\ o-o}$	ca.412	412	∥
6.	$B_{y\ o-o}$	ca.409	409	⊥
7.	$B_{x\ o-1}$ (L_x?)	ca.390	390	∥

The assignment of band polarizations in the visible region as well as in the B region appears to be unambiguous, although the exact

positions of the B region components cannot be determined from these experiments. We have assumed for the band positions in Table I a $B_{x\ o-o} - B_{y\ o-o}$ separation as found by Rimington, et al. (1959) for porphyrin free base. The parallel component on the short wavelength side of the B peak could be either $B_{x\ o-1}$ or an independent higher transition (L_x?).

Simple interpretation of metal porphyrin MCD spectra

The remainder of this chapter will be devoted to understanding the double MCD spectra of the metal porphyrins. We saw in the previous theoretical section that an x-y degeneracy results in an orbital Zeeman splitting in the magnetic field. The electrons can circulate in the metal porphyrin plane much like a loop of wire. In the absence of the magnetic field, the direction of the electron circulation is not important; however, the field introduces a handedness to the system and one sense of circulation increases in energy while the other sense of circulation decreases in energy. This orbital Zeeman splitting leads to the differential absorption of circularly polarized light and to the double MCD curve as is observed for both the Q and B bands of the metal porphyrins.

Perhaps the most striking thing about the metal porphyrin MCD spectra is that the MCD amplitude of the Q band is approximately 8-10 times as large as the MCD amplitude of the B band, for equal peak absorption. We recall from the theory section that for equal peak absorption and band width, the relative amplitude of the MCD

is a measure of the relative Zeeman splitting. The Q and B band have nearly the same width so it is clear that the weak Q band has 8-10 times the Zeeman splitting of the strong B band. Figure III-15 shows a simplified energy level scheme for the metal porphyrins, with the relative magnetic splittings of the low energy Q and high energy B bands shown. The widths of the arrows to the levels are proportional to the intensities of absorption and the size of the magnetic splitting relative to the energy of the transition is greatly exaggerated. For our field direction convention, the Zeeman component that decreases in energy in the field absorbs left circular light.

A simple free electron model of the metal porphyrin put forward by Simpson (1949) explains the MCD spectra surprisingly well. The molecule is treated as a circular box with electrons completely free to move inside the box. Simpson's model considers the porphyrin as a 18-membered cyclic polyene, where the highest filled electronic states have symmetry $e^{\pm i14\phi}$ and the lowest empty electronic states have symmetry $e^{\pm i15\phi}$. The angle ϕ is the angular coordinate of the electron of interest in the molecular plane, and $i = \sqrt{-1}$. We are interested in the angular momentum of the electron about an axis (z) perpendicular to the molecular (xy) plane, which is given by the expectation values of the operator $\hbar/i \; \partial/\partial\phi$ (Herzberg, 1950), where $\hbar$ is Planck's constant divided by 2π. Electrons in the filled orbitals have angular momentum of $\pm 4\hbar$, while those promoted to the lowest empty orbital have angular momentum $\pm 5\hbar$.

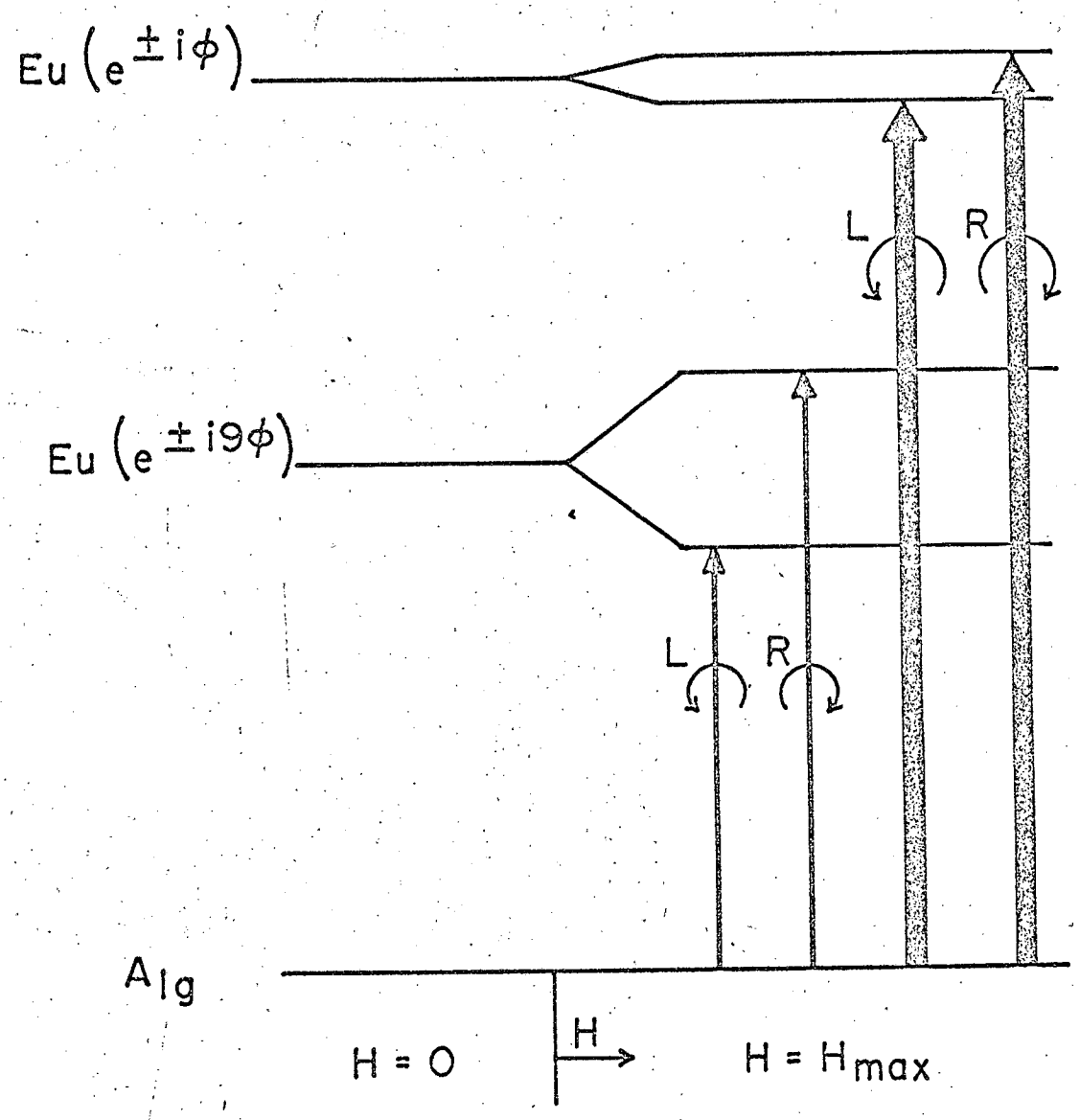

MUB 11451

Figure III-15. Simplified energy level diagram for the metal porphyrins in the absence (left) and presence (right) of the external magnetic field. The symbols that label the states are explained in the text. The intensities of the transitions are proportional to the widths of the lines between the states. The relative magnetic splittings of the low and high energy states are shown, but the absolute splittings relative to the transition energy is exaggerated.

The ground state of the metal porphyrin has four electrons in the highest filled orbital and no net orbital angular momentum. Transitions between the highest filled and lowest empty orbitals correspond to changes in angular momentum of $\pm\hbar$ (a state of $e^{\pm}$ 1ø symmetry) or changes in angular momentum of $\pm 9\hbar$ (a state of $e^{\pm}$ 19ø symmetry). The selection rule for orbital angular momentum is that the $\pm\hbar$ change is fully allowed (Platt, 1953) so the $e^{\pm}$ 1ø state corresponds to the strong B (Soret) band. The $\pm 9\hbar$ transition is forbidden and lies at lower energy because of its high multiplicity (e.g. Platt, 1964) and so corresponds to the Q (red) band.

The two values of angular momentum for a state (e.g. $\pm 9\hbar$) correspond to opposite senses of charge circulation about an axis perpendicular to the molecular plane. In the absence of the external magnetic field, the two directions of charge circulation have the same energy. In the presence of the external field the Q and B bands are split,

$E_{Q\pm} = E^{\circ}_{Q} \pm 9 \frac{\hbar e H}{2 mc}$ and $E_{B\pm} = E^{\circ}_{B} \pm \frac{\hbar e H}{2 mc}$, where $\frac{\hbar e}{2 mc}$ is the Bohr magneton. We see that treating the porphyrin as a free electron (wire loop) system gives the result that the magnetic splitting of the Q band is 9 times that of the B band. This is very close to what is seen in the MCD experiments (8-10 times), an astonishing result. More precisely, the free electron model (FEM) predicts a value of the magnetic splitting (the expectation value of orbital angular momentum about the axis perpendicular to

the molecular plane) $\langle L_z \rangle_Q = M_{zQ} = 9$ for the Q band and $\langle L_z \rangle_B = M_{z,B} = 1$ for the B band.

We anticipate the results of the next section by noting that the experimentalmmagnetic splitting observed for the zinc porphyrin is $\langle L_z \rangle_Q = 6.5$ for the Q band and $\langle L_z \rangle_B = 0.8$ for the B band. The ratio of the Q to B values is about 8. The metal porphyrin MCD is not exactly described by a circular box (FEM), but it is surprisingly close. The FEM predicts essentially zero intensity for the Q band while a small intensity is observed. These departures of the absorption and MCD of the metal porphyrin from the FEM predictions can be understood in terms of the elegant four orbital model of Gouterman (1959,1961). More elaborate theoretical explanation of the metal porphyrin MCD will be preceded by a discussion of the method used to extract the values for the magnetic splitting from the MCD spectra.

MCD and absorption data analysis

The logic of the data analysis procedure was presented in an earlier section. We fit the absorption spectrum of the compound of interest to a sum of component Gaussian or Lorentzian absorption bands. The computer fitting procedure is guided by the least squares criteria; that is, that the differences between the observed and calculated absorption is squared and summed over all the experimental points to get a $(Chi)^2$. The best fit to the spectrum is the one which minimizes $(Chi)^2$. An example of the results of the absorption fitting procedure is shown in Figures III-16 and III-17, which

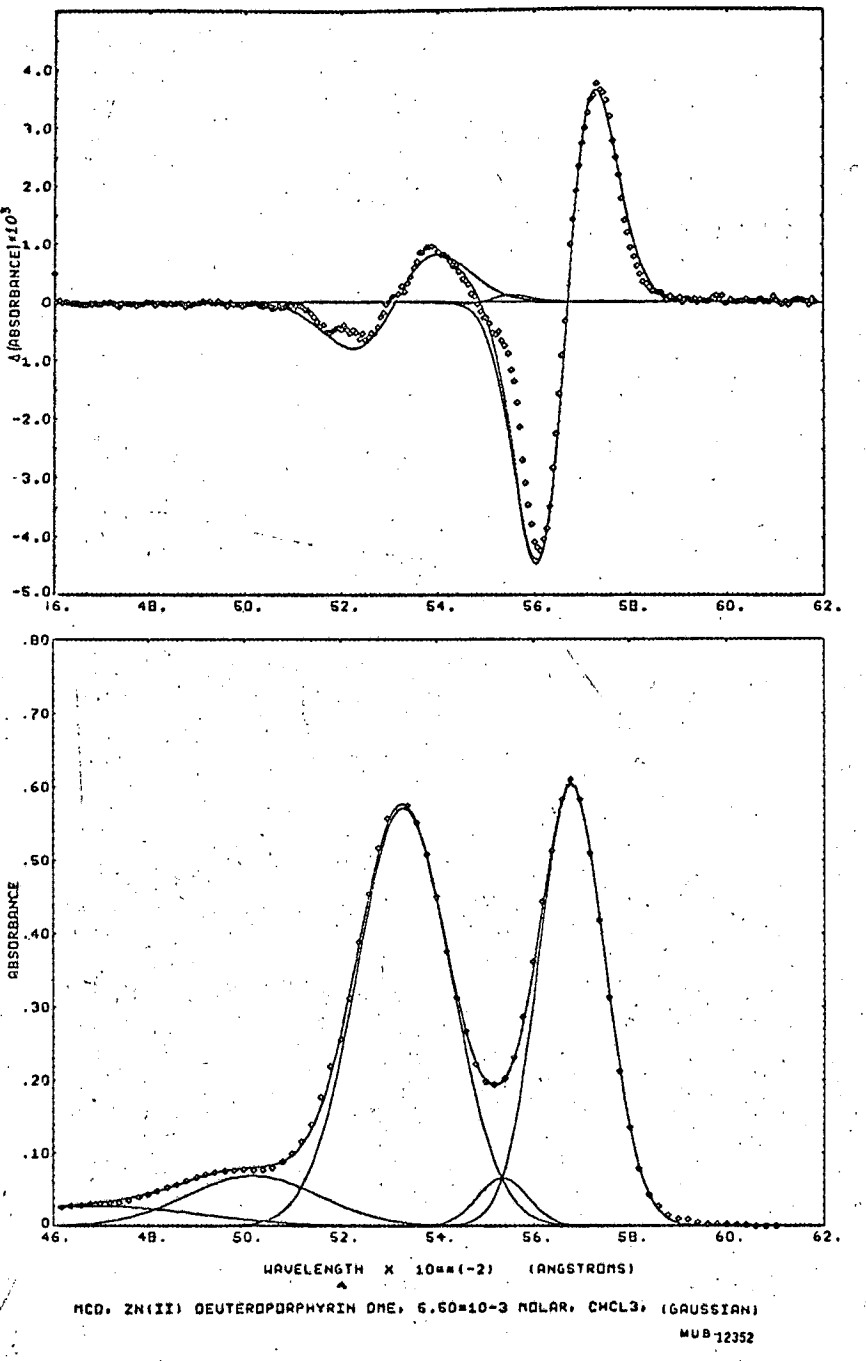

Figure III-16. Decomposition of the absorption (below) and MCD (above) of zinc(II)deuteroporphyrin dimethyl ester into symmetrical Gaussian components. The sum of the components is the line that runs close to the data points. The data points are shown as open diamonds, and every other data point is plotted.

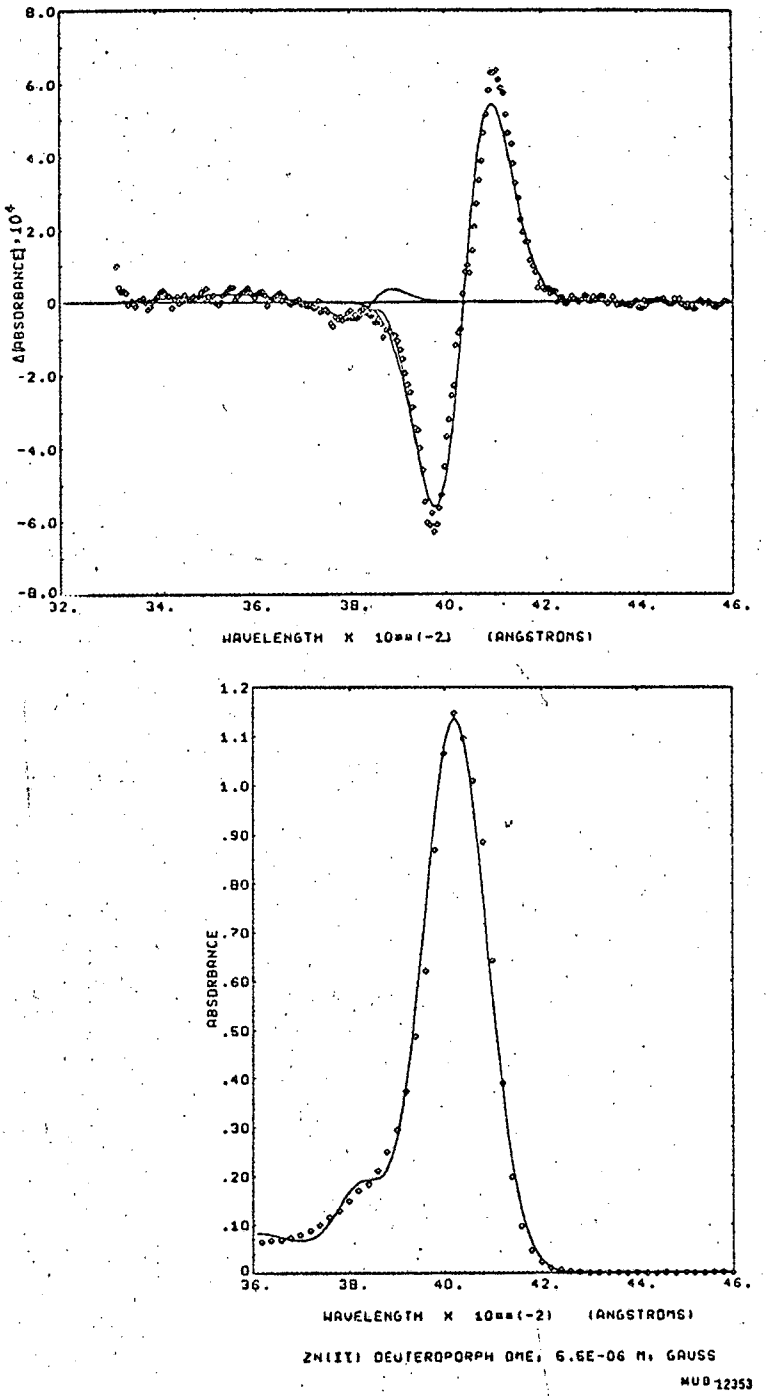

Figure III-17. Decomposition of the absorption (below) and MCD (above) of zinc(II)deuteroporphyrin dimethyl ester into symmetrical Gaussian components. Three bands are used for the absorption, but only one contributes appreciably to the main band. Every other data point is plotted.

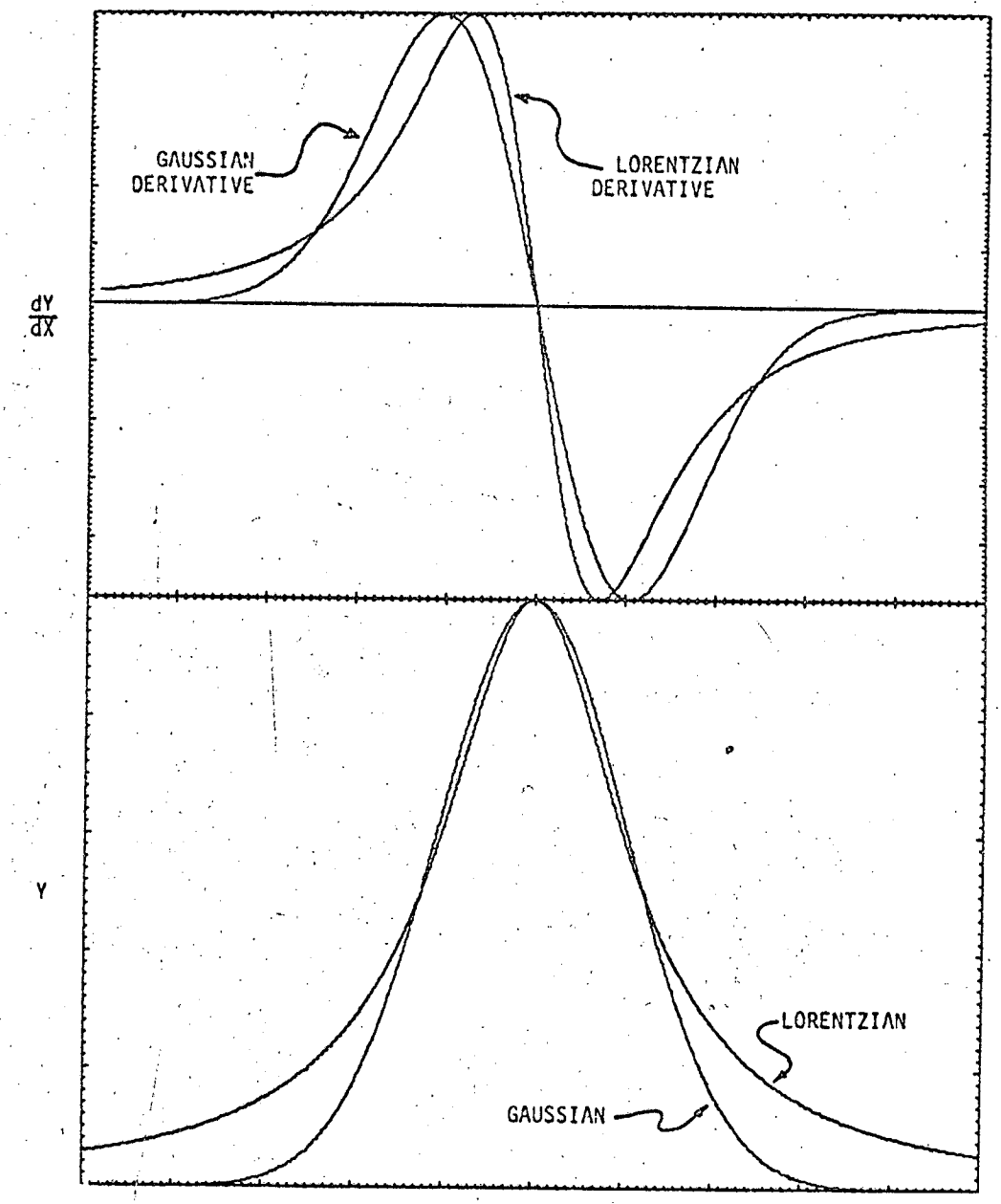

Figure III-18. Comparison of a Gaussian and Lorentzian of unit amplitude and identical width at half-height. The derivatives have been normalized to the same height, the Lorentzian derivative actually about 10% larger in amplitude.

show the absorption spectrum of zinc deuteroporphyrin fit to 5 Gaussian bands in the visible and 3 in the UV. One band is used for each obvious peak in the spectrum and occasionally other small bands are used to reproduce shoulders or pronounced tails on absorption peaks. We have used symmetrical Gaussians and Lorentzians systematically; however, absorption components with a different half width on the long and short wavelength side would have occasionally given slightly better fits to the spectra, or equivalent fits with fewer adjustable parameters.

For a given choice of band shape function, there seems to be a unique set of bands that describe the main peaks in the spectrum, the small shoulders are obviously not unique, but are not very important for our purpose. The main problem with this procedure is the choice of band shape function.

The Lorentzian function has much more tail than the Gaussian function as is illustrated in Figure III-18. The Gaussian and Lorentzian functions seem to represent extremes, within which the experimental spectra fall. For most spectra, the Lorentzian function has too much tail, while the Gaussian has too little. Some of the spectra, however, approach the extremes quite closely. For example the Zn porphyrins are fit rather well by Gaussian functions, as shown in Figure III-16. The Ni deuteroporphyrin, at the other extreme, is fit quite well by the Lorentzian function, as shown in Figures III-19 and III-20. For these extreme cases, the opposite extreme fits quite poorly. For an intermediate case like cobalt,

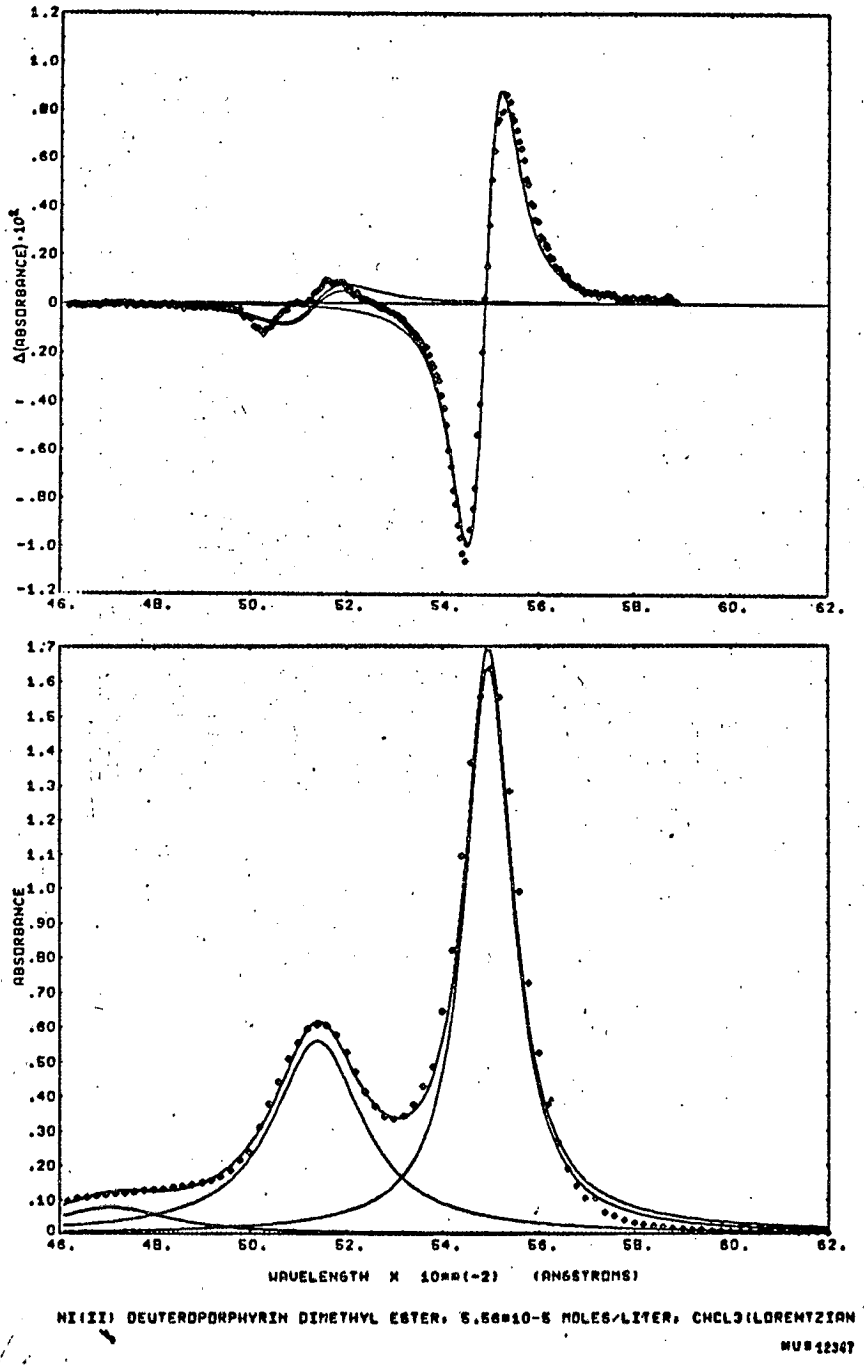

Figure III-19. Decomposition of the absorbance (below) and MCD (above) of nickel(II)deuteroporphyrin dimethyl ester, into symmetrical Lorentzian components. The sum of the components is the line that runs close to the experimental points. Every other experimental point is plotted.

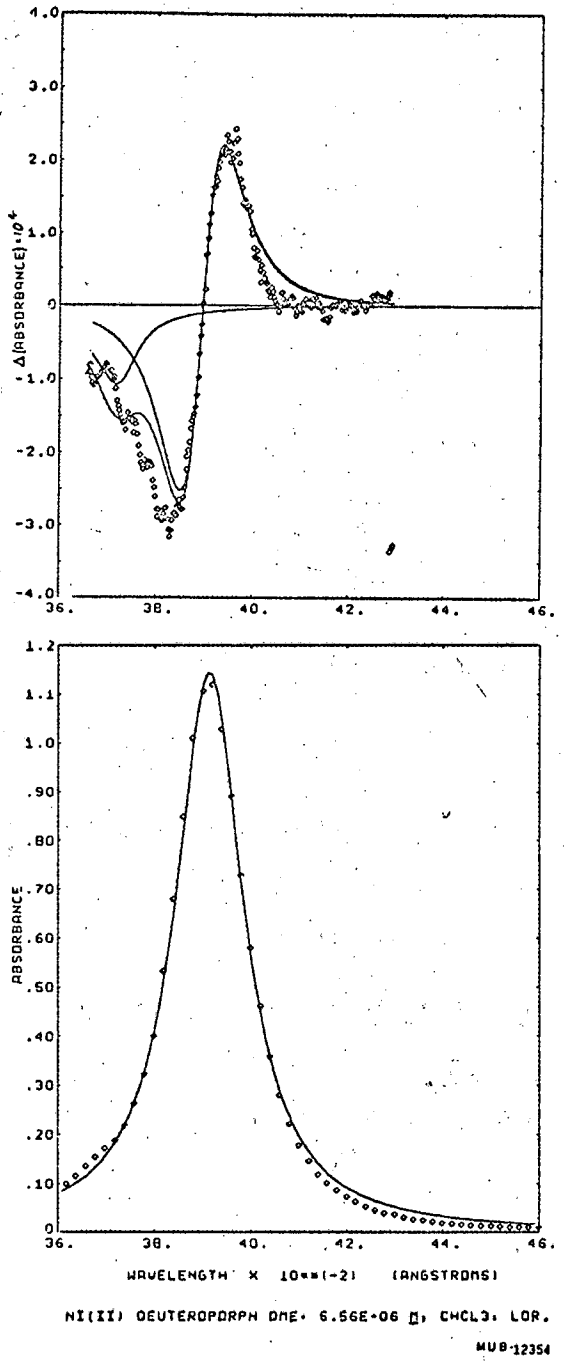

Figure III-20. Decomposition of the absorbance (below) and MCD (above) into symmetrical Lorentzian components. Two bands are used for the absorbance, but only one contributes to the main peak, and a second is on the short wavelength side.

deuteroporphyrin both functions give a satisfactory fit. The Lorentzian is shown in Figures III-21 and III-22. Table II gives the best fit parameters for Gaussian and Lorentzian shapes for some of the metal porphyrins studied. The absorption spectra can be fit in a largely satisfactory way by these procedures.

The position and width parameters of the best fit absorption band components are fixed and are used to fit the MCD spectra by the least squares criteria. Since the double MCD curves have a first derivative shape (p. 166), the line shape problems discussed above for absorption are somewhat more severe for MCD. The first derivative is always very sensitive to the details of curve shape. For example, shoulders that are barely discernible in absorption show up clearly in the first derivative curves (e.g. Brown and French, 1959).

We used symmetrical Gaussians and Lorentzians in our fitting procedure. The experimental absorption curves are not quite symmetrical on either a wavelength or frequency scale, although they are the most symmetrical on a wavelength scale. This slight asymmetry in the absorption also appears in the MCD spectra. Fitting a double MCD curve that is not quite symmetrical, with a symmetrical function by the procedure of section IIIB, p. 166, introduces a small, single MCD component. We could have used asymmetrical shape or functions with some complication; however, this was not judged to be necessary. From a mathematical, curve fitting point of view, a bell shaped curve and its first derivative are zero

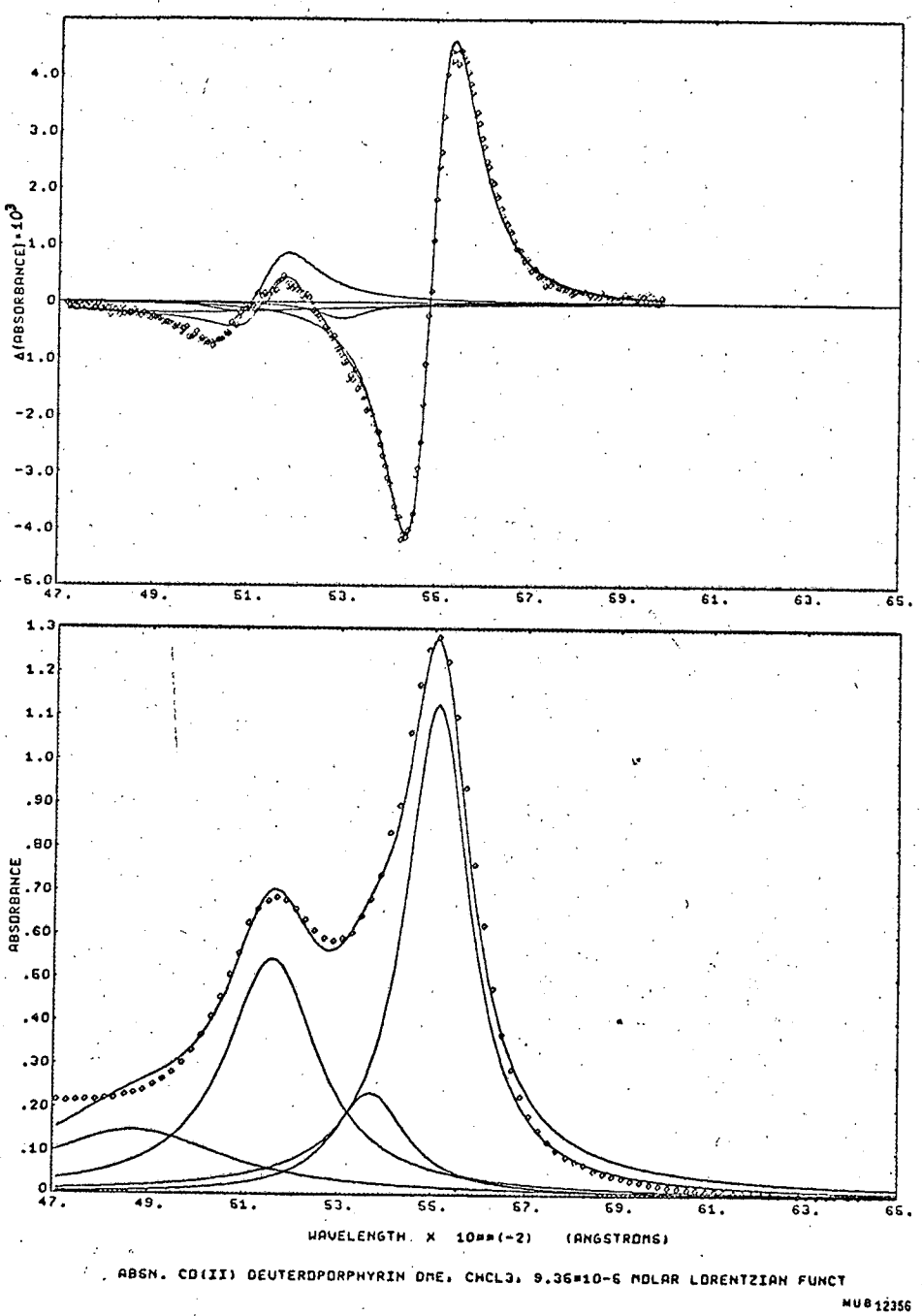

Figure III-21. Decomposition of the absorbance (below) and MCD (above) of cobalt(II)deuteroporphyrin dimethyl ester into symmetrical Lorentzian components. The sum of the components is the line that runs close to the data points. Every other data point is plotted.

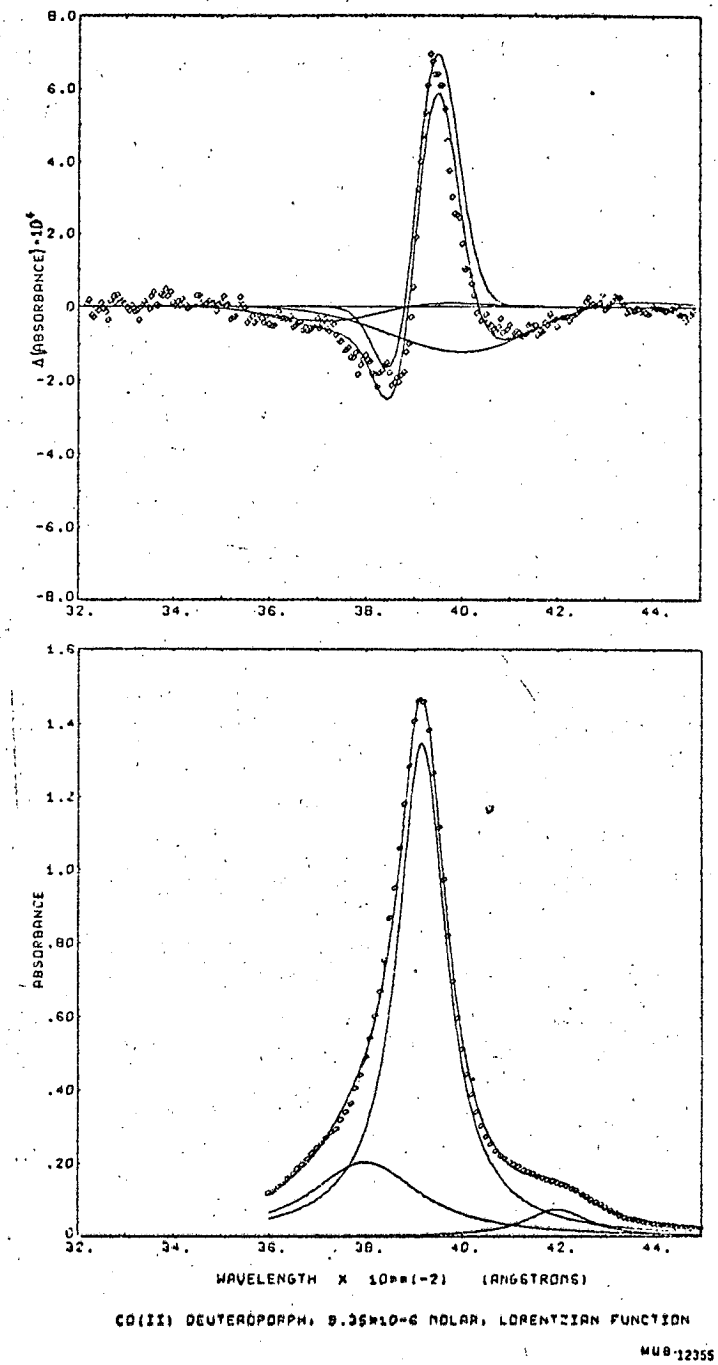

Figure III-22. Decomposition of the absorption (below) and MCD (above) of cobalt(II)deuteroporphyrin dimethyl ester into symmetrical Lorentzian components. The sum of the components is the line that runs close to the data points. Every other data point is plotted.

Table II. Metal deuteroporphyrin IX dimethyl ester best fit absorption band parameters. Solvent, chloroform; 1 cm path length. Wavelength in Angstroms. Gaussian width, θ_i = half width at 1/e height. Lorentzian width, γ_i = full width at half height.

Metal	Concentration (moles/liter) $.10^6$	Shape	OD_1	λ_1	θ_1, γ_1	OD_2	λ_2	θ_2, γ_2	OD_3	λ_3	θ_3, γ_3	OD_4	λ_4	θ_4, γ_4
Zinc(II)	55.0	G	0.603	5680	98.6	0.066	5535	74	0.571	5330	138	0.069	5017	196
	5.50	G	1.37	4020	94.3	0.159	3824	70.9	0.083	3600	174			
Copper(II)	39.0	G	0.869	5597	92	0.093	5443	79	0.444	5235	121	0.113	5065	650
		L	0.910	5597	135				0.510	5235	204	0.067	4758	176
	3.90	G	1.400	3973	51	0.313	3891	172						
		L	1.630	3975	70.2	0.302	3919	68.2	0.120	3801	102			
Nickel(II)	55.6	L	1.643	5495	120.8				0.560	5140	228	0.079	4711	294
	5.56	L	1.147	3913	170.2									
Cobalt(II)	93.5	G	1.109	5510	116.5	0.236	5334	97	0.466	5160	137	0.230	4870	805
		L	1.170	5510	168	0.234	5370	190	0.542	5160	238	0.147	4870	470
	9.35	G	0.185	4105	238	1.250	3915	71	0.345	3800	175.5			
		L	0.075	4200	164	1.347	3915	122	0.203	3800	272			
Silver(II)	130	G	1.147	5585	90.4	0.445	5403	342	0.884	5241	110	0.266	5008	674
		L	1.479	5581	156.4				1.403	5244	236	0.172	4785	418
	6.48	G	1.530	4085	64	0.370	3993	200						
		L	1.334	4085	84	0.300	4009	175						
Vanadyl(II)	50.0	G	0.961	5699	74	0.180	5427	338	0.385	5323	85	0.065	4834	544
		L	1.050	5699	108				0.565	5318	188	0.059	4830	382
	5.00	G	1.10	4070.5	50	0.200	3975	105						
		L	1.252	4068	96	0.146	3994	216						

correlated (linearly independent) (Biltonen, 1966; Deming, 1943) if considered on both sides of the peak. That is to say, the value of one component (e.g. the derivative) is not affected by the presence (or omission) of the other component (e.g. bell shape) when a best fit to an observed spectrum is sought. The correlation coefficients were indeed very small between the double and small single MCD components in the MCD spectrum fitting.

The asymmetry problem is a very minor one; however, a more serious shape problem is the choice of a basic shape function itself. As mentioned in the absorption fitting discussion, the metal porphyrins we have studied seem to be intermediate between Gaussian and Lorentzian. The most esthetically pleasing MCD fits can be derived by widening the best fit absorption Lorentzian or by narrowing the best fit absorption Gaussians. The reason for this can be seen in Figure III-18 where the derivative of a Gaussian and a Lorentzian of the same half width (γ) and height are shown. The Lorentzian derivative peaks at

$$\lambda_o \pm \frac{\gamma}{\sqrt{3}} = \lambda_o \pm \frac{\gamma}{1.732}$$

while the Gaussian derivative peaks at

$$\lambda_o \pm \frac{\gamma}{\sqrt{2\ln 2}} = \lambda_o \pm \frac{\gamma}{1.12}$$

So, the Gaussian derivative peaks considerably further from the center

of the band than the Lorentzian derivative. Unfortunately, these altered line widths, if used to fit the MCD spectra, have no significance other than as a measure of the"Gaussianness" or"Lorentzianness" of a line; they just indicate that we are dealing with an intermediate line shape, not exactly described by the functions we have chosen. The cases which closely approach the Gaussian or Lorentzian limit are straightforward. For example, Zn porphyrins are close to pure Gaussian bands as shown by the MCD fit in Figure III-16. The Ni porphyrin bands are close to pure Lorentzians as can be seen from the MCD fit shown in Figure III-19.

Fortunately, the intermediate shape cases give satisfactory fits with either function and very nearly the same result for the magnetic splitting for either the Gaussian or Lorentzian shape function to within about 5%. The detailed shape used does not seem to be important for the basic result we desire. We have not attempted to fit the complex MCD in the Q_{0-1} bands, but have concentrated on the more clear-cut Q_{0-0} and B bands.

Table III shows the magnetic splitting value $\langle L_z \rangle = M_z$ found by the above procedure (see p. 169 for basic relationship between fitting constants and magnetic splitting) for both Gaussian and Lorentzian line shapes. If one of the line shapes gave a very poor fit it was not considered; for example, the Lorentzian was not considered for the Zn case. Figures III-23 and III-24 show the experimental MCD and absorption of copper deuteroporphyrin not previously shown, and the fit obtained. The other spectra of silver(II) and

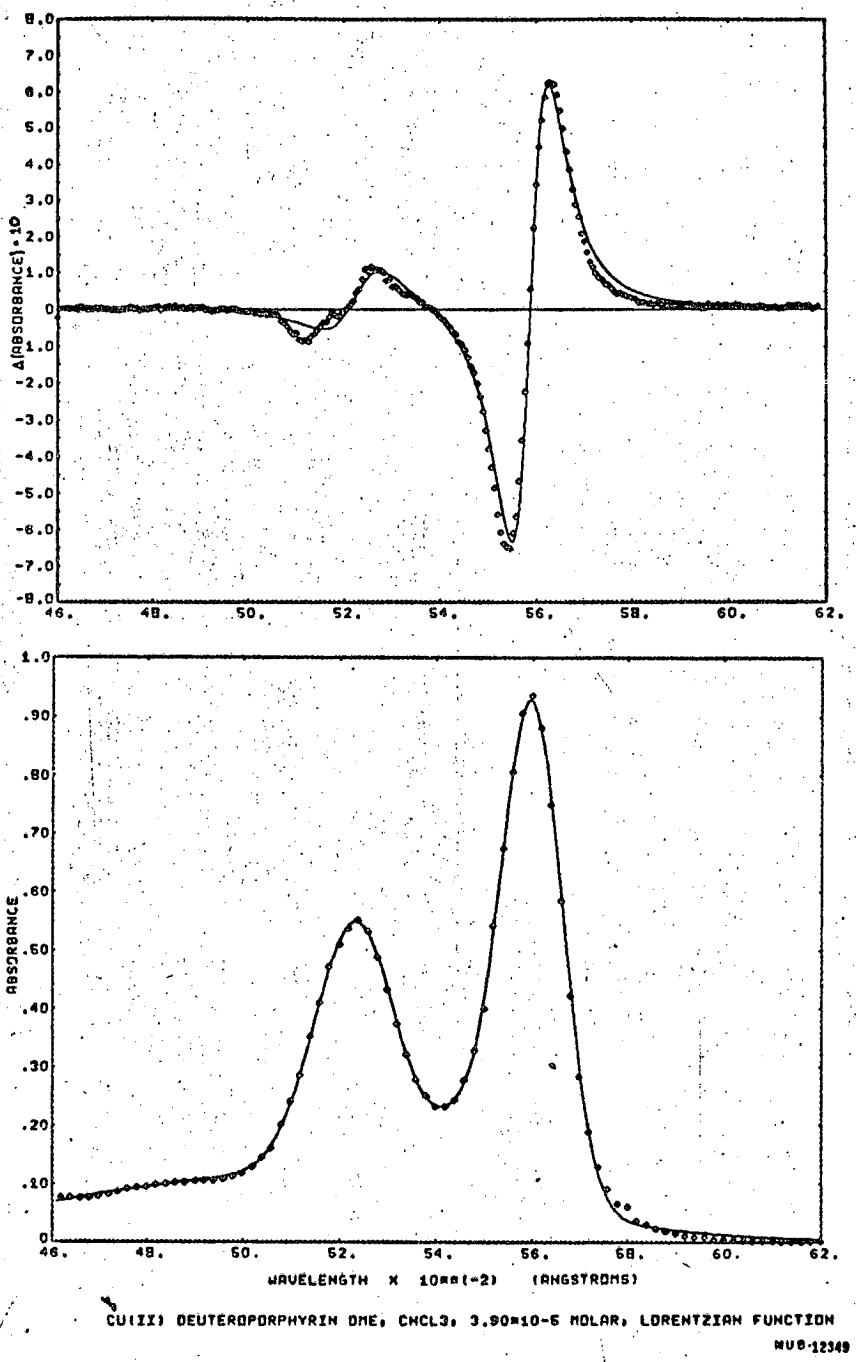

Figure III-23. Decomposition of the absorption (below) and MCD (above) of copper(II) deuteroporphyrin dimethyl ester into symmetrical Lorentzian components. Four components are used for the absorption and their sum is shown as the fine line that runs close to the data points. Only the two largest components contribute appreciably to the MCD.

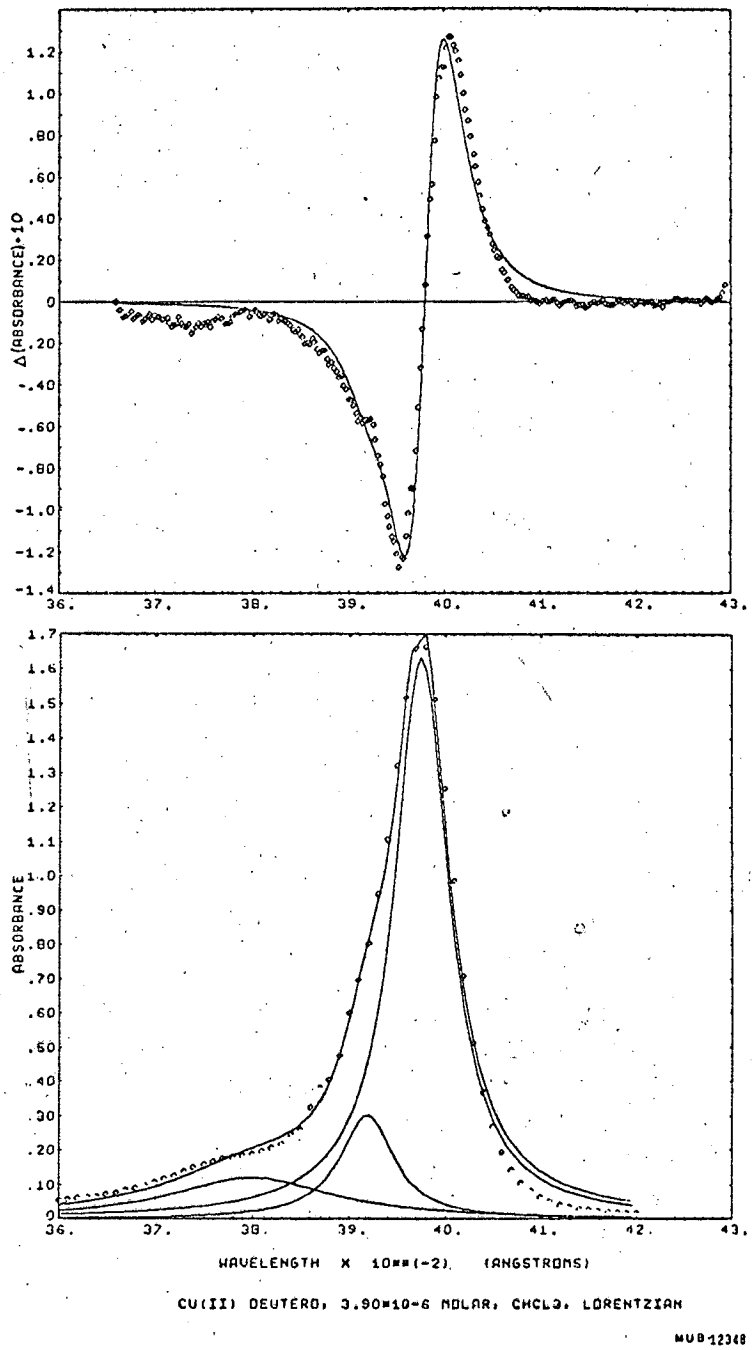

Figure II-24. Decomposition of the absorption (below) and MCD (above) into symmetrical Lorentzian components. The sum of the components is shown for the MCD. Every other data point is plotted.

Table III. Best fit magnetic splittings for the metal deuteroporphyrin dimethyl esters in chloroform. The magnetic splitting factor, M_Z, is defined by $\Delta\gamma = M_Z \beta H$ where $\Delta\gamma$ is the magnetic splitting (in cm^{-1}) and βH is the Bohr magneton times the magnetic field (in cm^{-1}). The magnetic splitting is calculated according to equation III-114 on p.169 .

Metal	Shape	M_Z, Q_{o-o}	Std. error ± , %	M_Z,B	Std. error ± , %
Zinc	Gaussian	6.52	9.3	0.82	6.6
Copper	Gaussian	6.05	15	0.65	4.8
Copper	Lorentzian	6.09	4.3	0.65	5.5
Nickel	Lorentzian	4.65	4.3	0.46	15
Cobalt	Gaussian	4.63	16.2	0.39	12
Cobalt	Lorentzian	4.44	5.0	0.40	16
Silver	Gaussian	5.24	8.4	0.50	5.5
Vanadyl	Gaussian	5.65	10.3	0.44	4
Vanadyl	Lorentzian	5.90	5.2	0.50	5

vanadyl(IV) are similar. The statistical uncertainty, the standard error, of the magnetic splitting value is of the order of ± 5%, about equal to the uncertainty introduced by the intermediate line shapes being fit with a Gaussian or a Lorentzian.

The data in Table III show that all the Q bands have a splitting greater than $M_{Z,Q} = 4$ and the B bands are all split less than $M_{Z,B} < 0.8$. The metal porphyrin is basically similar to the free electron circular box for all the metals studied, although the Zn porphyrin is the closest in absolute value to the free electron model predictions. The Zn deuteroporphyrin IX gives the same magnetic splitting as the more symmetrical Zn coproporphyrin III and I, to within the uncertainties involved. There seems to be a systematic decrease in the magnetic splitting as the number of d electrons is decreased. The M_Z value is plotted vs. the number of d electrons in the metal for the Q band in Figure III-25 and for the B band in Figure III-26.

The MCD of all these compounds is basically similar, and, therefore, must be due to the heterocyclic porphyrin ring. The MCD of the porphyrin ring seems to be quite sensitive to perturbations by the metal; as the d orbitals of the metal become empty the porphyrin departs more and more from the free electron model. Qualitatively, we might propose that as the d orbitals of the metals become empty, the electron promoted to the excited state may reside more and more on the metal. If the electron circulation is pulled towards the center of the ring, the angular momentum of the circulating electron is smaller.

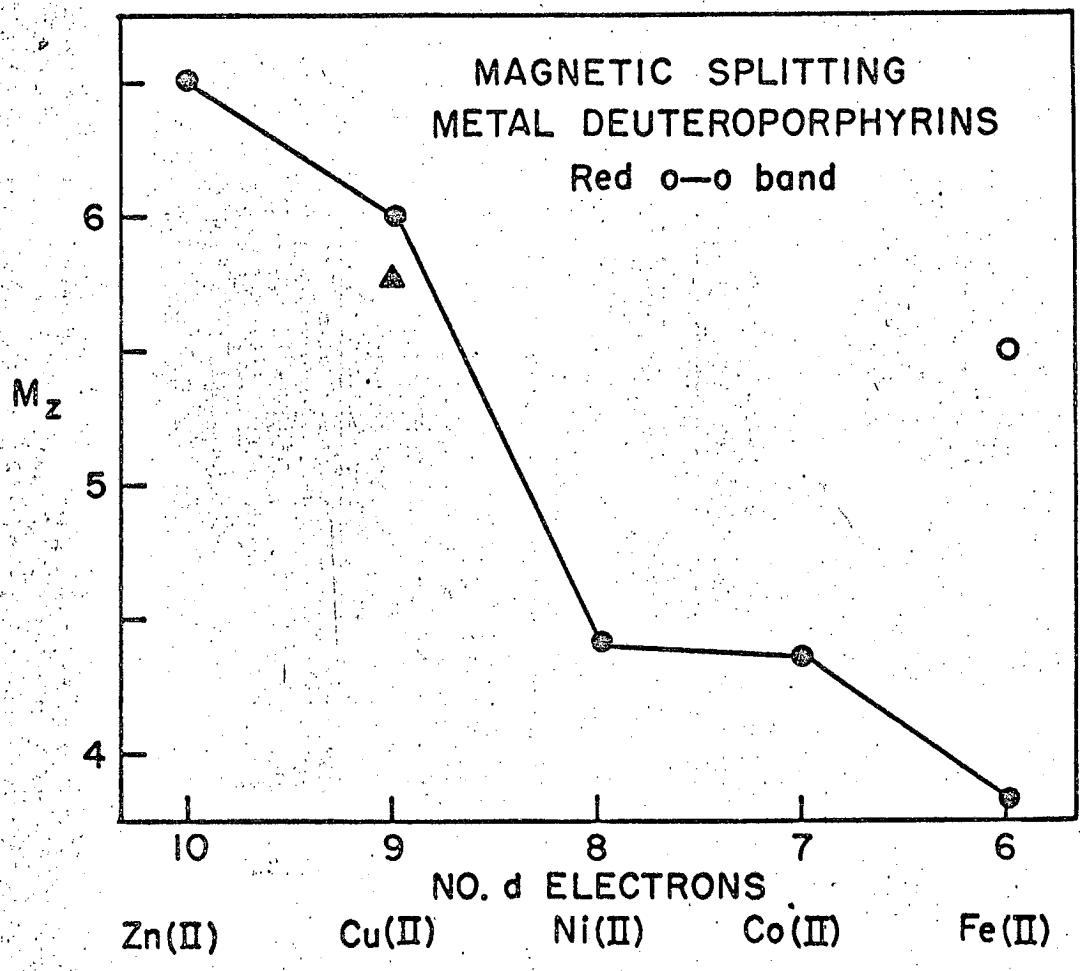

MUB 12089

Figure III-25. Summary of the magnetic splitting of the Qo–o band of the metal porphyrins. The diamond point is silver(II). All the complexes are deuteroporphyrins in chloroform, except for the Fe(II) complex which is protoporphyrin in H_2O (pH 8.0) • and in pyridine o .

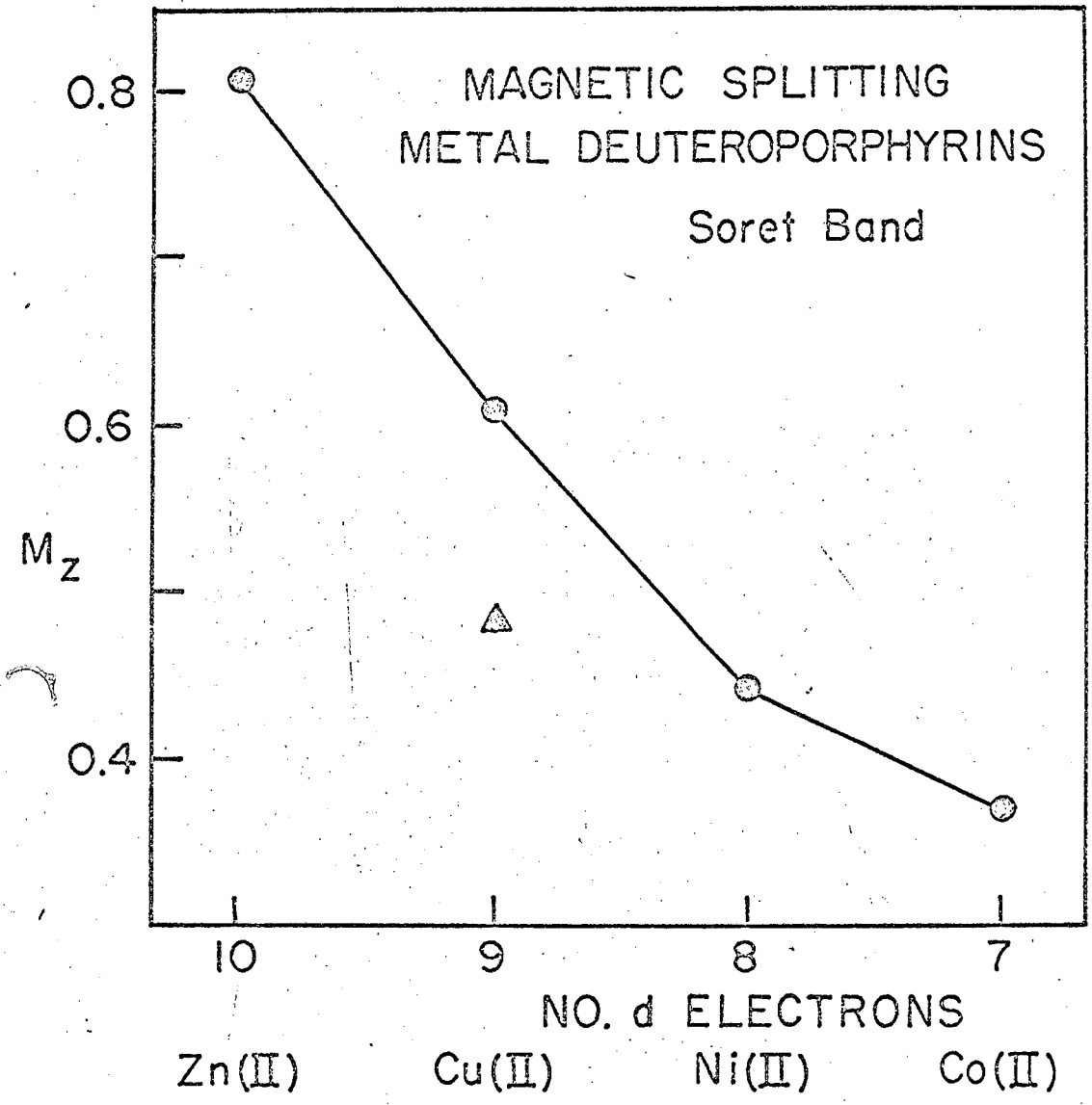

MUB-12088

Figure III-26. Summary of the magnetic splitting of the B band of the metal deuteroporphyrins in chloroform. The △ point is silver(II).

Specific paramagnetic effects were ruled out in the theoretical section, and we see that this prediction is confirmed empirically. There is a relatively smooth decrease in M_z values as the number of d electrons decreases, yet the metals alternate in diamagnetic and paramagnetic character across this series. In the porphyrin ligand field, Zn(II), Ni(II) and Fe(II) are diamagnetic, while the metals Cu(II) and Co(II) are paramagnetic. The silver (II) magnetic splitting is represented by triangles below the Cu(II) point in Figures III-25 and III-26. Silver(II) is $4d^9$ which is a very similar electronic structure to Cu(II), $3d^9$. The slightly lower (M_z) value of silver compared to Cu(II) may be due to the large size of the silver(II) which allows more overlap with the ring orbitals, facilitating the metal-ring interaction.

Feher, Malley, and Mauzerall et al. (1966) have recently measured the Zeeman splitting of the Q bands of Zn coproporphyrin I,III directly at 100 kilogauss. Their spectrum is reproduced in Figure III-27. They find a magnetic splitting of $M_z = 9 \pm 1$, significantly larger than we calculate from our data for the same compounds ($M_z = 6.5 \pm 0.5$). In view of the disagreement, we measured the identical samples and recalibrated our instrument to try to make our results agree, without success. The Feher et al. technique is, in principle, more precise than ours, although it is much less accurate. We cannot ascribe much of the disagreement to line shape problems in this case, because the Zn compounds are almost pure Gaussians. There remain three explanations for the disagreement: (A) The Feher et al. experiment shows some disturbing

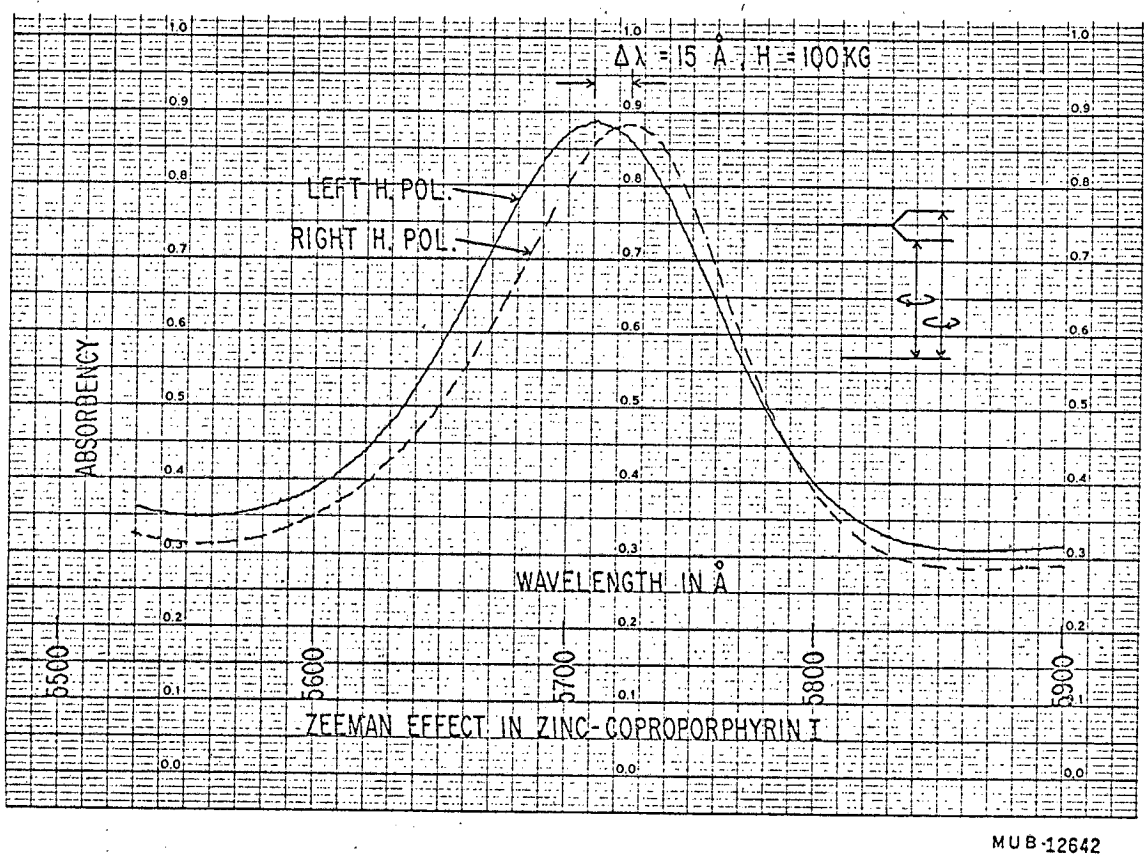

Figure III-27. Direct observation of the Zeeman splitting of the Qo-o band. (After Feher et.al., 1966)

base line problems which could change their value somewhat. Inspection of their data suggests this effect may be a minor one, however. (B) There could be a systematic error in our calibration. This is possible, but it seems that in the light of accumulated agreement between our CD and MCD measurements with the more absolute ORD and MORD measurements that this could not be a major source of disagreement. (C) The assumption implicit throughout our analysis, of a rigid magnetic shift of the porphyrin absorption lines, may not be correct. Feher et al. look only at the shift of the absorption peak in the magnetic field. Our measurements consider the entire line, but concentrate on the region of maximum slope of the line. Two tests of the rigid shift assumption are to, first, compare the observed MCD with the analytical derivative of the observed absorption line shape; or, second, to compare the shape of the line Malley et al. observed before and after applying the magnetic field. It is difficult to follow through the second method because of the base line uncertainties in the Feher et al. experiments, although retracing their lines in the presence of the field and superimposing them suggests that the center of the line may shift more than the wings. It is also difficult to take the derivative of the observed absorption line to use the first mentioned test of the rigid shift assumption. It turned out that our digital absorption spectra were too noisy to give a useful derivative directly. We have estimated the slope of the observed absorption for the Zn coproporphyrin III on the

long wavelength side of the Q_{o-o} band by drawing tangents to the absorption band. The observed MCD and the derivative estimated from the observed absorption line shape are plotted in Figure III-28. The calculated derivative has a relatively large uncertainty; however, it seems to agree very well in the region of the MCD peak. However, in the long wavelength wings of the line, the MCD seems to be significantly less than the absorption line derivative.

This observation suggests that the porphyrin bands do not shift as much in the wings of the line as they do in the center. The apparent lack of a rigid shift may explain some of the disagreement between our results and those of Feher, et al. If the center of the line shifts the most in the magnetic field and the shift becomes less as the wings are approached, we would expect to derive a somewhat lower value for the magnetic splitting from our experiments. We have no good quantitative estimates of this non-rigid shift effect on the MCD, but it seems insufficient to make our results agree with the observations of Feher, et al. It seems probable that all of the above explanations are partially responsible for the disagreement of the splitting derived from the MCD with the direct observation of the Zeeman splitting.

Perhaps the largest contributor to the disagreement is the apparent lack of a rigid magnetic shift of the absorption line. Only explanation (C) above would clearly tend to make our results closer to Feher et al.; errors (A) and (B) could go either way. More accurate absorption line derivatives would help resolve

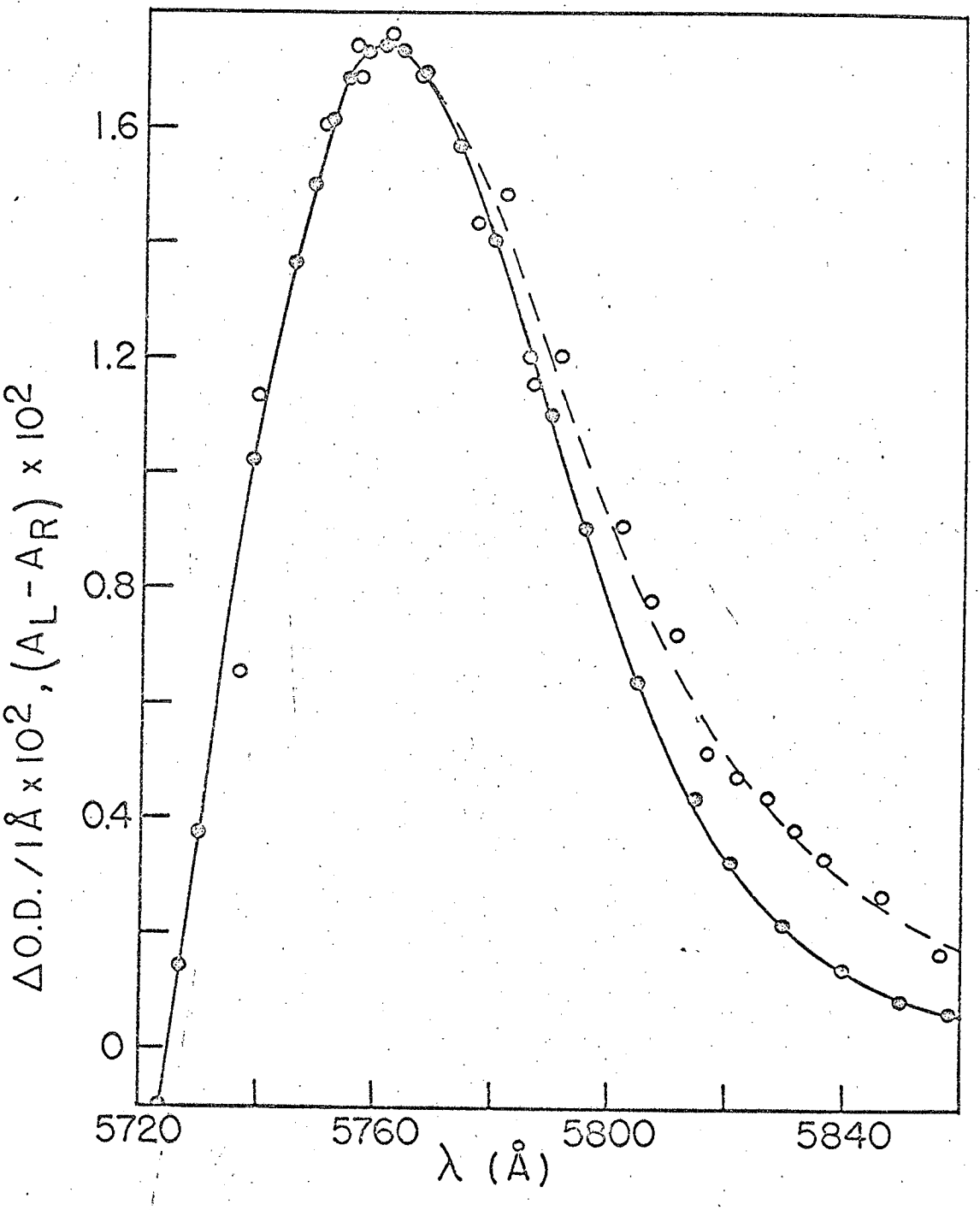

MUB 11876

Figure III-28. A comparison of the measured MCD, o—o—o and calculated absorption derivative, o---o---o , for zinc(II)coproporphyrin III in dioxane.

this rigid shift question as well as low temperature MCD measurements on a sharpened line. The wings of the lines tend to disappear as the lines narrow at low temperature, and the splitting calculated from the MCD would be expected to increase if the wings of the line do not shift as much as the center in the magnetic field.

We shall comment a bit further on the rigid shift problems in the theoretical section where we give some arguments that the Feher, et al. result is unreasonably high. We take our results to have relative validity, that is, the dependence of M_z number of d electrons is basically correct (Figure III-25), but, reserving the possibility that all the values may have to be adjusted upward if the magnetic splitting at the absorption peak is desired. The uncertainties that remain in this regard are subject to experimental test.

We have two further problems to discuss theoretically. The departure of the metal porphyrins from the free electron model and the origin of the metal dependence of the magnetic splitting.

Porphyrin electronic structure

The success of the simple free electron model (FEM) in explaining the essential elements of the absorption spectra (Simpson, 1949; Platt, 1956) and now the MCD spectra (see previous section, p. 202) of the metal porphyrins is quite striking. In comparison, the simple Hückel molecular orbital treatment (HMO) does rather poorly. The HMO treatment predicts electronic transitions of approximately the right energy (Longuet-Higgins, Rector and Platt, 1950). The two main

transitions of interest, Q, B, are predicted by HMO to have nearly equal intensity while experimentally the lowest energy transition (Q) is 10-50 times weaker than the strong B transition. The FEM model, although basically sound, predicts essentially zero intensity for the Q_{0-0} band and does not explain important features of the porphyrin spectra, such as the dependence of the absorption spectra on the metal and now the dependence of the MCD on metal. Gouterman combined the HMO and FEM in a very elegant way (1959, 1961) and was able to satisfactorily explain essentially all information on porphyrin absorption spectra. Significantly, the original, somewhat intuitive 4 orbital model has recently been justified by the most sophisticated pi-electron calculations presently available for large molecules (Weiss, Kobayashi and Gouterman, 1965). We shall show how Gouterman's 4 orbital model accounts for the MCD of these systems in a largely satisfactory way.

The HMO treatment (Longuet-Higgins, et al., 1950) of the square symmetric($D4_h$ in group theoretical notation) metal porphyrin finds a lowest empty, e_g, orbital pair, whose degeneracy is dictated by the symmetry of the system (Sponer, Teller, 1941), and two highest filled orbitals a_{1u} and a_{2u}. The relative energies of these HMO orbitals are shown in Figure III-29a. The free electron model (FEM) has the two highest filled orbitals ($e^{\pm i4\phi}$) exactly degenerate as shown in Figure III-29b. In order to force the more flexible HMO picture close to the basically correct FEM, Gouterman required that the a_{1u} and a_{2u} HMO orbitals be nearly (accidentally) degenerate, as shown in Figure III-29b.

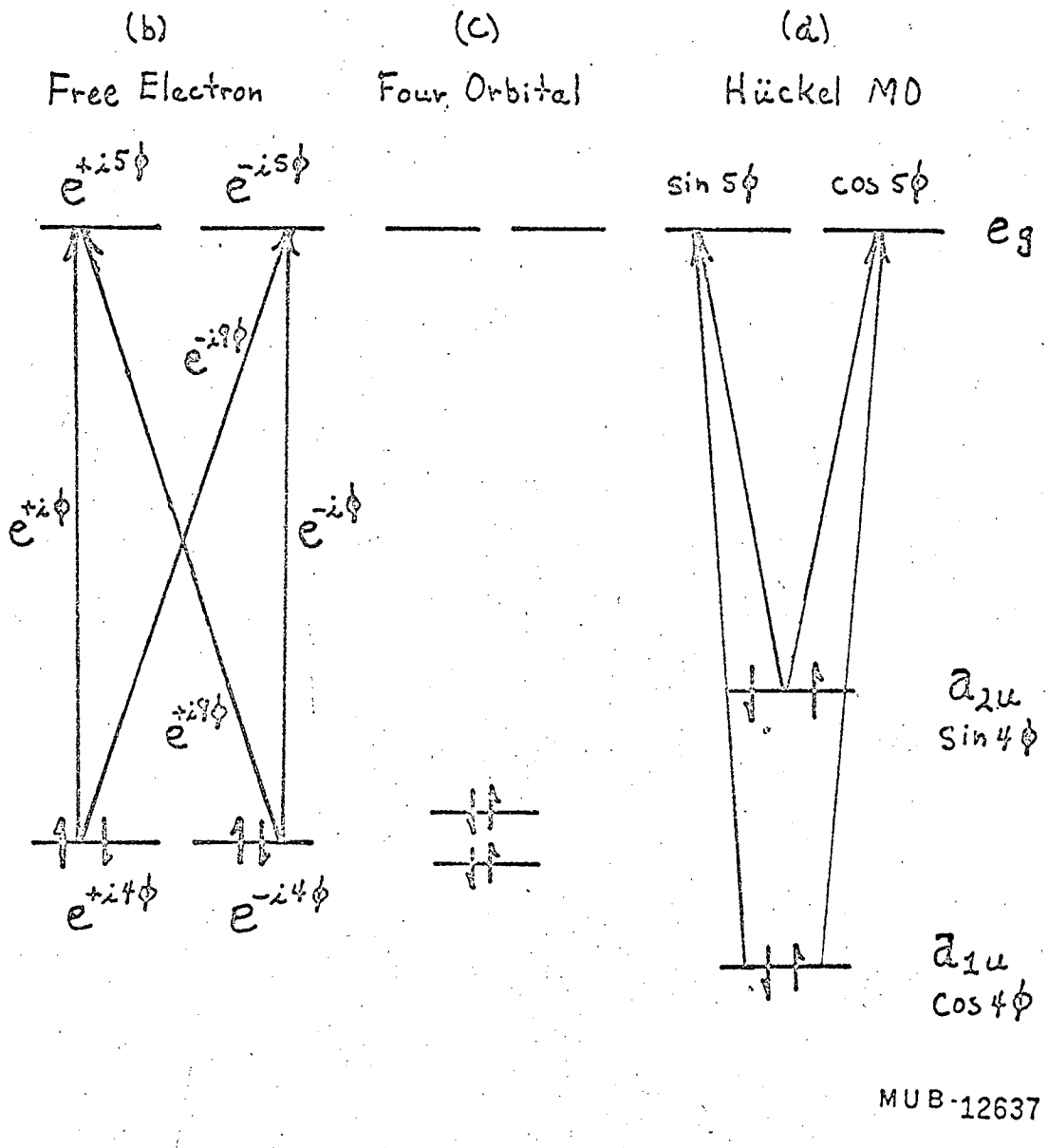

Figure III-29. Models of the metal porphyrin orbital energies.

Electronic transitions from the filled orbitals to the empty ones give two electronic configurations: $(a_{1u})^{-1} e_g = a_{1u} e_g$ and $(a_{2u})^{-1} e_g = a_{2u} e_g$. Gouterman's point of view was that these two electronic configurations, of the same symmetry, E_u, and nearly the same energy mixed strongly (Moffit, 1954) to give the observed Q and B states.

If we consider the x polarized state (y's behave identically) we have for strong mixing the symmetric and antisymmetric combinations of the two excited configurations:

States	Intensities
$Q_x^0 = \frac{1}{\sqrt{2}}\left[(a_{2u} e_{gx}) - (a_{1u} e_{gy})\right]$	$r^2 = \frac{1}{2}(R_1 - R_2)^2 \approx 0$
$B_x^0 = \frac{1}{\sqrt{2}}\left[(a_{2u} e_{gx}) + (a_{1u} e_{gy})\right]$	$R^2 = \frac{1}{2}(R_1 + R_2)^2 \approx 2R_1^2 \approx 2R_2^2$

III-(117)

The R's used to find the intensities are the electronic dipole transition moments:

$$R_{ix} = \int (a_{iu}\, e_{gy}) \,|\, x \,|\, \Psi_o \, d\tau \qquad \boxed{i = 1,2} \qquad \text{III-(118)}$$

where Ψ_o is the ground state wave function and x is the electronic coordinate in the x direction. We see that the Q intensity is close to zero and the B intensity is very strong for complete mixing, a result like that of the free electron model, but starting with the more flexible HMO orbitals.

If the configurations are mixed more weakly, or not at all, the Q band becomes stronger and we go back to the HMO limit of nearly equal Q and B intensity. The details of this 4 orbital picture are given by Gouterman (1959, 1961).

The porphyrin Hückel molecular orbitals under consideration are shown in Figure III-30. Note that the two highest filled orbitals, a_{1u} (b2) and a_{2u} (b1) differ in their nodal properties. The a_{1u} orbital has a node through the central metal position, so it cannot interact with a metal in the center. The a_{2u}, however, has no central node and can interact with a central metal and it will be expected to shift its energy with metal substitution. As the energy of the a_{2u} is raised or lowered relative to the a_{1u} by metal substitution, the configuration interaction will be altered. This means that the closeness of the metal porphyrin to the free electron model will be expected to be metal dependent. As a result, the Q band intensity is expected to change with metal substitution. (The B band intensity dependence on metal expected will be lost in experimental error), and that the magnetic splitting of the Q band and B band will also be altered by metal substitution. We will briefly develop the 4 orbital model predictions for these phenomena.

The four orbital model

The four orbital model is not limited to porphyrins, but applies to molecules with at least two planes of symmetry. Most of the

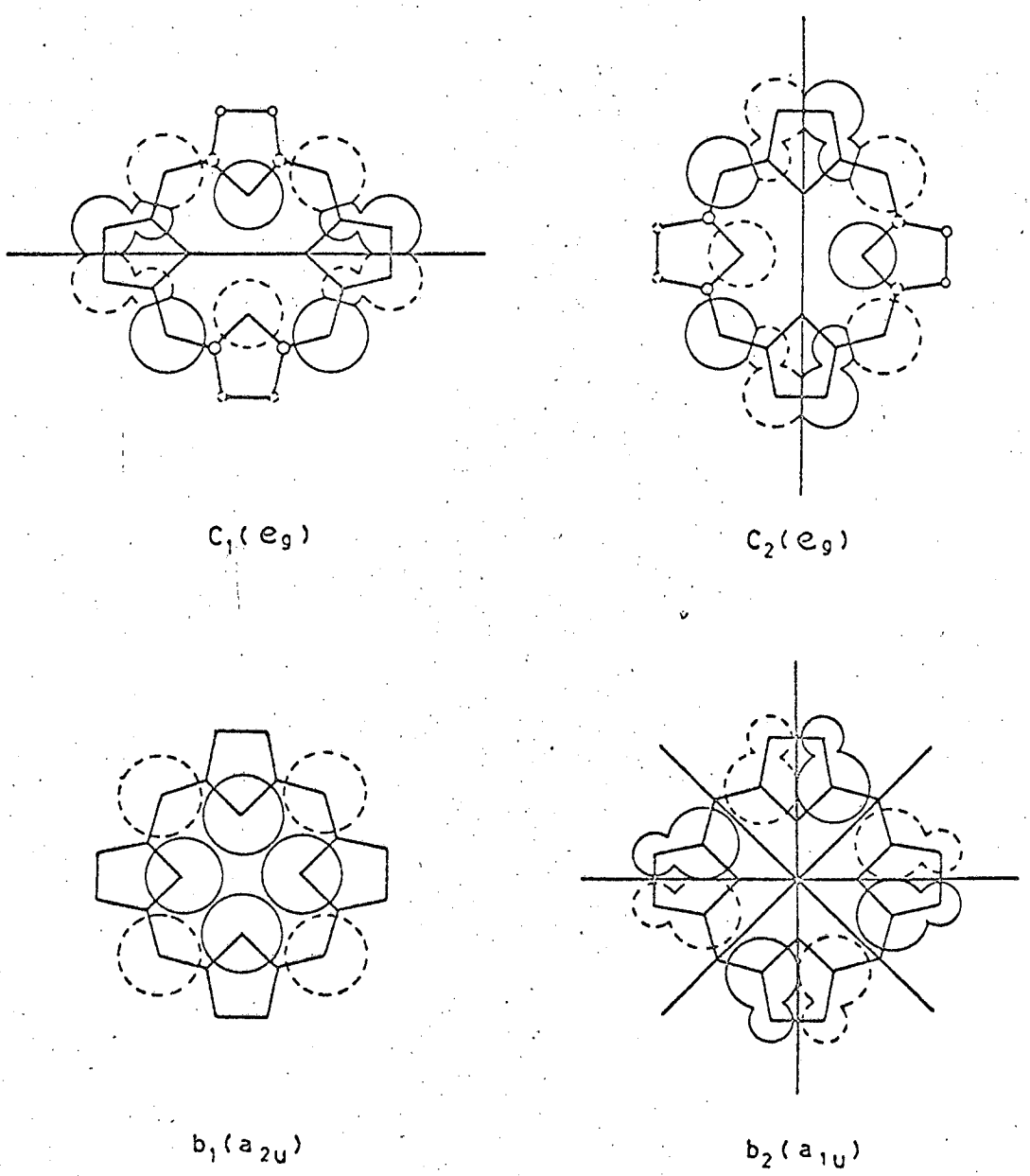

Figure III-30. Highest filled (a_{2u}, a_{1u}) and lowest empty (e_g) porphyrin molecular orbitals. The atomic orbital coefficients are proportional to the size of the circles, with positive coefficients drawn as solid circles and negative coefficients drawn as dashed circles. Symmetry nodes are drawn as heavy lines. After Gouterman (1961).

development of the model is very general and is based on symmetry arguments only. However, we will make simplifying assumptions appropriate to the porphyrin systems, quite early in the development.

The four possible transitions from two ground orbitals, b_1 and b_2, to two excited orbitals, c_1 and c_2, are considered to mix pairwise, where θx and θy are mixing parameters (Gouterman, 1959). The new singlet states, $Q_{x,y}$ and $B_{x,y}$, are given below:

$$\begin{aligned} Q_y &= \cos\theta_y \psi(b_1c_1) - \sin\theta_y \psi(b_2c_2) \\ Q_x &= \cos\theta_x \psi(b_1c_2) - \sin\theta_x \psi(b_2c_1) \\ B_y &= \sin\theta_y \psi(b_1c_1) + \cos\theta_y \psi(b_2c_2) \\ B_x &= -\sin\theta_x \psi(b_1c_2) + \cos\theta_x \psi(b_2c_1) \end{aligned} \qquad \text{III-(119)}$$

The $\psi(b_ic_j)$ are wave functions for excited singlet electronic configurations made by exciting one electron from a filled orbital b_i to an empty orbital c_j. The electric dipole and angular momentum transition moments are defined:

$$(b_1|x|c_1) \equiv R_{11}\hat{i} \qquad (b_2|y|c_1) \equiv -R_{21}\hat{j} \qquad \text{III-(120)}$$

$$(b_1|y|c_2) \equiv R_{12}\hat{j} \qquad (b_2|x|c_2) \equiv R_{22}\hat{i}$$

$$(b_1|L_z|b_2) \equiv -i\hbar m_b \qquad (c_1|L_z|c_2) \equiv -i\hbar m_c$$

where i and j are unit vectors parallel to the x and y molecular axes, respectively, x and y are the electronic coordinates and $L_z = l_z = i\hbar (x\, \partial/\partial y - y\, \partial/\partial x)$, the angular momentum operator, is purely imaginary one electron operator. Gouterman (1959) has shown that these are the only relevant (non-zero) matrix elements for the electric dipole transition moments.

That the L_z angular momentum transition moments are the only ones for systems with two planes of symmetry was discussed earlier (p. 152). We treated the molecular point group C_{2v} earlier, so here we will work out the present case of interest, the point group D_{4h}. An integral like $(\phi_i/Op/\phi_i)$ is non-zero is the direct product of the symmetry species of $\phi_i \times \phi_i \times Op$ contains the totally symmetric representatinn A_{1g} (e.g. Wilson, Decius and Cross, 1955). Table IV contains the relevant symmetries of the translations T (x,y,z) and rotations $R_x = L_x$, $R_y = L_y$, $R_z = L_z$) for D_{4h}, the point group of interest.

Table V. Symmetry of orbitals and operators in D_{4h}, appropriate for metal porphyrins.

Symmetry Species	Translations, Rotations	Orbitals	Operators
A_{1g}			
A_{2g}	R_z		L_z
B_{1g}			
B_{2g}			
E_g	R_x, R_y	c_1, c_2	L_x, L_y
A_{1u}		b_1	
A_{2u}	T_z	b_2	
B_{1u}			
B_{2u}			
E_u	T_x, T_y		

We take the direct products of the symmetries of the orbitals of interest:

$$b_1 \times b_2 = A_{2u} \times A_{1u} = A_{2g}$$

$$c_1 \times c_2 = E_g \times E_g = A_{2g} + A_{1g} + B_{1g} + B_{2g}$$

Since L_z is A_{2g}, which is contained in both direct products, the L_z matrix element between $b_1 - b_2$ and $c_1 - c_2$ is non-zero. However, L_x and L_y are E_g, which is not contained in either direct pro-

duct, therefore, the L_x and L_y matrix elements between these states are identically zero.

By combination of equations III-92,95,96, in the previous theoretical section, the MCD is found to be proportional to the following relation:

$$MCD \propto i/\hbar \langle 0|R_x|x\rangle\langle x|L_z|y\rangle\langle y|R_y|0\rangle \qquad \text{III-(121)}$$

Since x is equivalent to y in the metal porphyrins, we can make the following simplification in the four orbital equations:

$$\Theta_x = \Theta_y = \Theta$$
$$R_{11} = R_{12} = R_1$$
$$R_{22} = R_{21} = R_2$$

So, we can give some relatively simple formulas for the Q and B band MCD.

$$MCD_Q \propto \frac{1}{2}\left[-\left(\frac{R_1^2+R_2^2}{2}\right)+\left(\frac{R_1^2-R_2^2}{2}\right)\cos 2\theta + R_1R_2\sin 2\theta\right]\left[-m_c - m_b \sin 2\theta\right] \qquad \text{III-(122a)}$$

$$MCD_B \propto \frac{1}{2}\left[\left(\frac{R_1^2+R_2^2}{2}\right)+\left(\frac{R_1^2-R_2^2}{2}\right)\cos 2\theta + R_1R_2\sin 2\theta\right]\left[m_c - m_b \sin 2\theta\right] \qquad \text{III-(122b)}$$

Analogous expressions for the intensities have been given by Gouterman (1959).

For the metal porphyrins, the intensity difference between the Q and B bands is very large, so the configuration interaction is nearly complete, and, therefore, $\Theta \approx \pi/2$. From Gouterman's (1965) work we can make the approximation that $R_1 \cong R_2 = R$, so that the further simplified expressions for the four orbital predictions for absorption and MCD of the metal porphyrins:

Intensities: $R_Q^2 \cong R^2(1-\sin 2\theta)$, $R_B^2 \cong R^2(1+\sin 2\theta)$ III-(123)

Splittings: $M_{z,Q} \cong m_c + m_b \sin 2\theta$, $M_{z,B} \cong m_c - m_b \sin 2\theta$ III-(124)

The predictions of this model are now clearly seen for the metal porphyrins, the Q/B intensity ratio indicates that sin 2θ is almost 1, and, further, $m_c \approx m_b$ (Gouterman, 1965). The intensity of the Q band, R_Q^2, and the magnetic splitting of the B band, $M_{Z,B}$, are very small. The magnetic splitting of the Q band is large, $M_{Z,Q} \approx m_c + m_b$ compared to the Q band as is observed experimentally. The four orbital model accounts for the general features of the metal porphyrin MCD as well as the absorption. We saw previously, from examination of the nodal properties of the relevant orbitals, that metal substitution changes the level of the $b_1(a_{2u})$ orbitals, (Figure III-30), and, therefore, the configuration interaction parameter θ. So we now see that the four orbital model predicts that $M_{Z,Q}$ will vary with metal substitution, and, further, that the intensity of the Q

band, $R_Q^2 \propto f_Q$ (the oscillator strength) increases, the magnetic splitting is expected to decrease.

Figure III-31 shows the magnetic splitting of the metal porphyrin Q_{o-o} band, plotted vs. the intensity (oscillator strength) of the band. The fit is far from perfect, but for compounds as highly colored as these the absolute intensities are poorly known. Small amounts of these compounds were available, so weighing errors are large, and, further, small impurities can be quite significant. The magnetic splitting, M_z, depends only on the ratio of the MCD signal to the observed absorption intensity and the absolute intensity is not important for the MCD M_z number. For these reasons, there is considerable scatter expected in the oscillator strength direction, and we assume that Figure III-31 is acceptable fit.

The four orbital model seems to explain satisfactorily the metal dependence of the metal porphyrin MCD. Further, the four orbital model explains the departure of the zinc porphyrins from the FEM predictions. Note in Figure III-31 that extrapolation to zero oscillator strength, the free electron limit, we get the free electron magnetic splitting, $M_z = 9$.

Figure III-31 makes the previously mentioned experiments of Feher et al. (1966) extremely hard to understand. If M_z for zinc porphyrin is 9 at the peak of the bank as Feher et al. indicate and if all the other values in Figure III-31 were scaled up by the same factor as the zinc compound (9/6.5) the value of the magnetic splitting at zero oscillator strength (the free electron limit) would be $M_z \approx 12.5$, which seems unreasonably large. It is

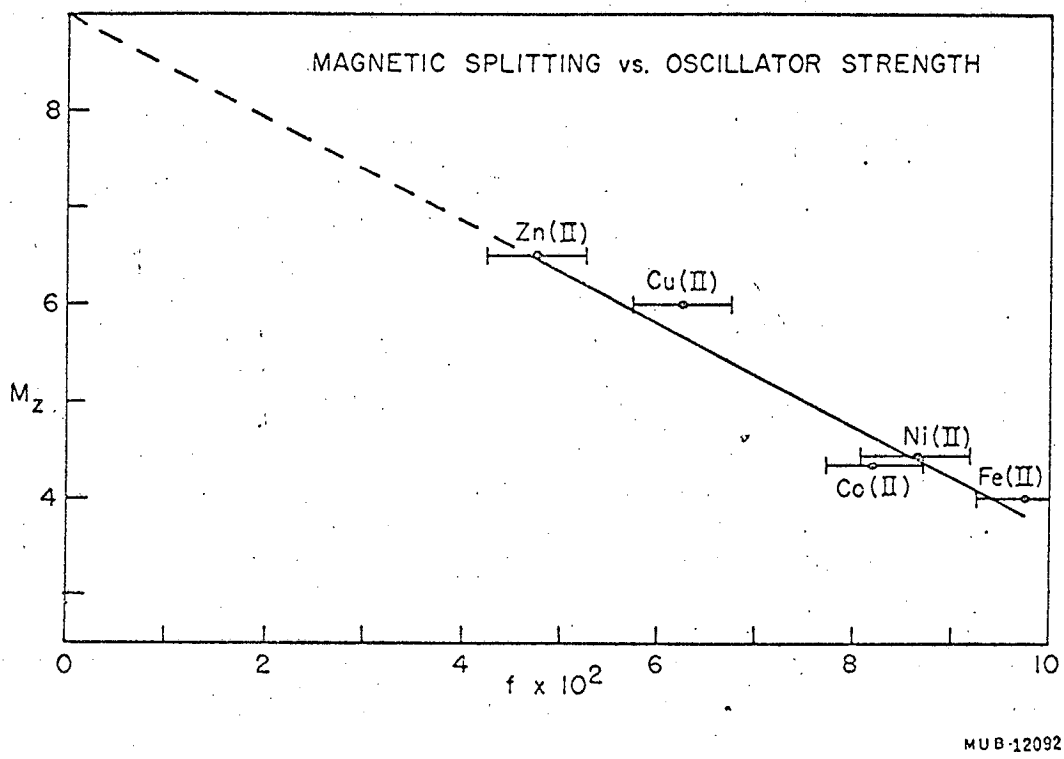

Figure III-31. Magnetic splitting of the metal porphyrin Qo-o bond plotted versus the Qo-o bond oscillator strength. The complexes are all deuteroporphyrins in chloroform except the Fe(II) point which is protoporphyrin in H_2O (pH 8.0). The horizontal bars are estimates of the uncertainty in the oscillator strength.

possible that the magnetic splitting at the absorption peak is not as strongly dependent on metal. However, it seems clear that the zinc porphyrins should not be exactly described by the free electron limit, as this predicts that the Q_{0-0} band should have zero intensity. The perturbations which give some intensity to the Q_{0-0} band must also decrease the magnetic splitting from the free electron value if the four orbital model (which had had every success in all other applications) has validity in this case. Further experiments are necessary to clear up this disagreement.

The four orbital model predicts that the B band splitting will increase as the Q band splitting decreases with metal substitution. We do not observe this; in fact, the B band splitting decreases in parallel to the Q band splitting, as can be seen by comparing Figures III-25, 26. We conclude that the four orbital model accounts for the MCD of the Q band satisfactorily, but does not work at all for the B band. A similar conclusion has been reached by other considerations. Self-consistent field molecular orbital calculations (Weiss, Kobayashi and Gouterman, 1965) show that Q bands are described extremely well by the four orbital model while the B band is described inadequately by this model. The B band can mix with many other nearby transitions, but the Q band is made up entirely (97%) of the two lowest states, as was assumed above.

Some other, quite different, theoretical calculations have been made by Zerner and Gouterman (1965), which specifically include the metal orbitals as well as all of the porphyrin valence orbitals. These calculations predict that the porphyrin excited states take

on progressively more metal d character as the metal loses d electrons. We expect qualitatively that if the electrons in the excited state go closer to the center of the ring (on the metal) and away from the periphery of the ring, their angular momentum would be reduced. Figure III-32 shows a plot of the observed M_z value vs. the $d\pi$ coefficient of the porphyrinhitrogens calculated by Zerner and Gouterman for the porphyrin excited state. The observed porphyrin magnetic splitting correlates surprisingly well with the calculated d character of the excited state. The large range of the iron(II) Mz value is due to the strong ligand dependence of the M_z value in this case (which is discussed in somewhat more detail later). Figure III-32 suggests that there are specific d orbital-ring orbital mixing effects not considered by the four orbital model that are responsible for at least some of the dependence of the magnetic splitting on metal substitution. We can formulate the metal dependence of the magnetic splitting as:

$$M_{z,Q} = m_b + m_c \text{ (metal) } \sin 2\theta \text{ (metal)} \qquad \text{III-(125)}$$

We saw in considering the four orbital model that θ is affected by the metal, and now we have added a dependence of m_c (the orbital angular momentum integral) on the metal through the specific d orbital interactions described above. Qualitatively, the copper wire loop model of the excited state is perturbed by putting charge in the center of the molecule. The details of the d-π electron interaction, and its effect on the orbital splitting, have not been worked out, but would seem feasible theoretically.

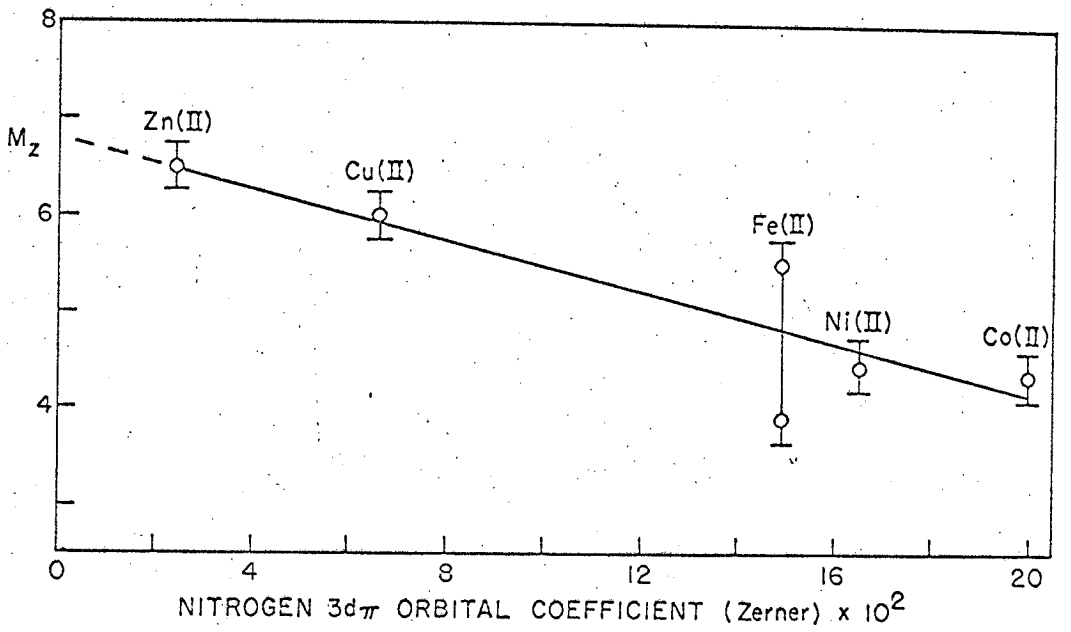

Figure III-32. The magnetic splitting of the Qo-o band of the metal porphyrins plotted versus the calculated d character of the porphyrin excited state (Zerner and Gouterman, 1965). The compounds are all metal deuteroporphyrins in chloroform, except the Fe(II) value which is protoporphyrin in H_2O (pH 8.0) (lower extreme) and pyridine (upper extreme).

To test more rigorously the applicability of the four orbital model for the MCD of the metal porphyrins, a series of metal derivatives are needed that have widely different Q band intensity but which do not have the possibility of specific metal d orbital interactions. A series of closed shell metals, like magnesium(II), zinc(II), cadmium(II) and perhaps calcium(II), would do the trick quite nicely. Except for the zinc compound, we have not yet been able to obtain the compounds in this series, and it is hoped that these measurements will be possible in the near future. A test of the four orbital model for this application has some importance. If the specific four orbital contribution to the M_z metal dependence can be extracted from the experimental results, it may be possible to deal with the specific d orbital-ring interactions apparently present in the open shell compounds.

The metal phthalocyanine MCD offers a further qualitative confirmation of the four orbital model. The metal phthalocyanines show a symmetrical double MCD in the Q band. The Q band absorption is very intense in these compounds. In terms of the four orbital model, this means that the configuration interaction is very small. The reason for this can be understood in a simple way. The phthalocyanines have nitrogens at the methine bridge positions where the a_{1u} orbital, Figure III-30, has nodes so it will not be affected by nitrogen substitution. However, the a_{2u} orbital has electron density peaks on the methine positions, and it will be strongly perturbed and shifted in energy by nitrogen substitution. We

saw that the configuration interaction required near degeneracy in the two filled orbitals, which no longer obtains, so small configuration interaction ($\theta \approx 0$) and an intense red (Q) band results ($R_Q^2 \approx R^2$), equation III-(123).

The four orbital equations, III-(124), predict that the magnetic splitting of the metal phthalocyanine Q band will be much reduced compared to the metal porphyrins. We find, for example, that copper phthalocyanine has $M_{z,Q} = 2.5$ (compared to copper porphyrin $M_{z,Q} = 6.0$), so the four orbital prediction is confirmed.

Dr. Gouterman has calculated the m_c and m_b matrix elements for the porphyrins (Gouterman, 1965) and we will discuss these calculations briefly as they are of interest in relation to our experimental results. The molecular orbitals ϕ_p are defined as a sum of atomic orbitals, χ_m, centered on atom m.

$$\phi_p = \sum_m C_{pm} \chi_m \qquad \text{III-(126)}$$

where the C_{pm} are molecular orbital coefficients determined by some standard procedure. For the porphyrin states of interest, the χ_m's are atomic 2p orbitals perpendicular to the molecular plane. Slater p functions will be used (Slater, 1930):

$$\chi_m = Nre^{-kr} \qquad \text{III-(127)}$$

where N is the angular p function (including normalization), r is a radial electronic coordinate, and k is an empirical exponent that determines the radial expanse of the orbital and represents the shielded effective nuclear charge of the atom. The coordinates of atom m

are defined as ξ_m, η_m, ζ_m and electronic coordinates are defined relative to atom m as $r_m = \sqrt{x_m^2 + y_m^2 + z_m^2}$, where $x_m = x - \xi_m$, $y_m = y - \eta_m$ and $z_m = z - \zeta_m$ for electronic coordinates x, y and z. The angular momentum integrals can be written:

$$(\phi_p | l_z | \phi_q) = \frac{\hbar}{i} \sum_{m<n} (C_{pm}^* C_{qn} - C_{qm} C_{pn}^*) \left[\frac{\xi_n \eta_m - \eta_n \xi_m}{R_{nm}^2} \right] T_{mn}$$

III-(128)

$$T_{mn} = R_{mn} \left(\chi_m \left| \frac{\partial}{\partial x'} \right| \chi_n \right)$$

III-(129)

where x' is measured along the m-n interatomic axis and R_{mn} is the distance between atoms.

There are several interesting aspects about this seemingly complex expression. With the exception of the T_{mn} integrals, the angular momentum depends only on the geometry of the molecule. The obvious geometrical part of eq. III-(128) contains the atomic coordinates, $\xi_n, \eta_n, R_{mn}, \xi_m, \eta_m$. It is not obvious that the part of eq. III-(128) that contains products of the molecular orbital coefficients, C_{mn}, depends only upon geometry. Gouterman found, however, that the sum over the products of molecular orbital coefficients in expression III-(128) was very insensitive to the detailed choice of coefficients. This particular expression seems to be largely independent of theoretical

model, and varied less than 10% for any reasonable set of molecular orbital coefficients. So, everything in eq. III-(128) except the T_{mn} integrals, is essentially determined by the geometry of the system.

The d/dx' operator (eq. III-(129)) when applied to the x_m p function gives a function similar to a d function, so the T_{mn} integrals are essentially overlap integrals between a p function on atom m and a d function on atom n. These T_{mn} integrals determine how freely the electron is allowed to move through the molecule, a subject of some interest to us.

Gouterman first set all the nearest neighbor T_{mn} overlap integrals to one. This gives the maximum freedom for the electron, and gives the geometry determined, upper limit angular momentum for the electron in the porphyrin excited state. The resulting angular momentum, using the best MO coefficients (Weiss, Kobayashi and Gouterman, 1965) available was found to be $8.75 = m_b + m_c$, very close to the free electron limit. Gouterman also calculated all the T_{mn} integrals explicitly considering all the atoms in the porphyrin as carbons, and using the Slater orbital exponent, k_n, found best for benzene. The T_{mn} integrals found with these assumptions average about 0.6, so the resulting angular momentum calculated is $m_b + m_c = 4.75$.

Experimentally, we find $m_b + m_c \sin 2\theta = 6.5$ for the zinc porphyrins and $\sin 2\theta = 0.9 - 0.95$, so the value of $m_b + m_c$ derived

from the experiment is approximately 7. The theoretical calculation gives amazingly good agreement with experiment, considering no adjustable parameters were used. The experimental value indicates that the T_{mn} values calculated by Gouterman do not give the porphyrin electrons enough freedom. Expansion of the Slater orbital coefficient by the maximum reasonable amount will give more overlap and more electron freedom and bring the theoretical number very close to the experimental value.

These theoretical considerations make the magnetic number of 9 ± 1 found by Feher et al. (1966) rather hard to justify. The factors determined by the geometry of the porphyrin would require an overlap integral of near unity to give Feher et al.'s result and this seems unreasonable.

Iron porphyrins and heme proteins

The iron porphyrins show the same type of double MCD spectra in the Q band (visible) that were discussed previously for the other metal porphyrins. However, one further feature is that the magnetic splittings of the iron porphyrins appear to be quite sensitive to ligand coordination above and below the porphyrin plane. Our data on these materials is somewhat preliminary but suggest several interesting conclusions. If $(H_2O)(^-OH)$ coordination is substituted by $(pyridine)_2$, the magnetic splitting of the Q band of Fe(II) protoporphyrin increases from M_z = 3.2 to 4.8. The MCD curves of these two complexes are shown in Figures III-33 and III-34, and are seen to be qualitatively similar.

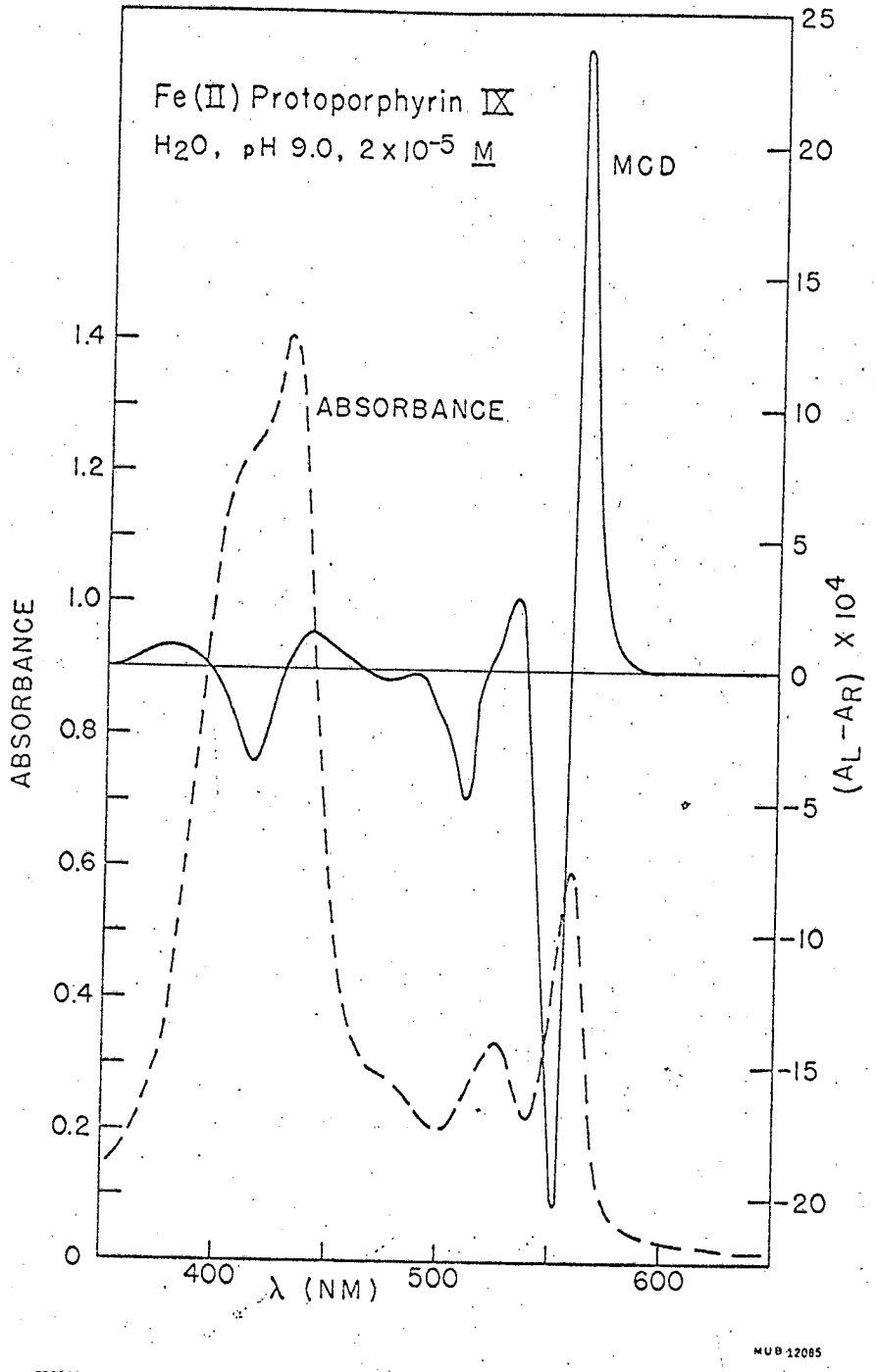

Figure III-33. MCD (solid curve) and absorbance (dashed curve) of iron(II)protoporphyrin IX in H_2O, pH 9.0, 2.10^{-5} moles/liter, 1 cm path.

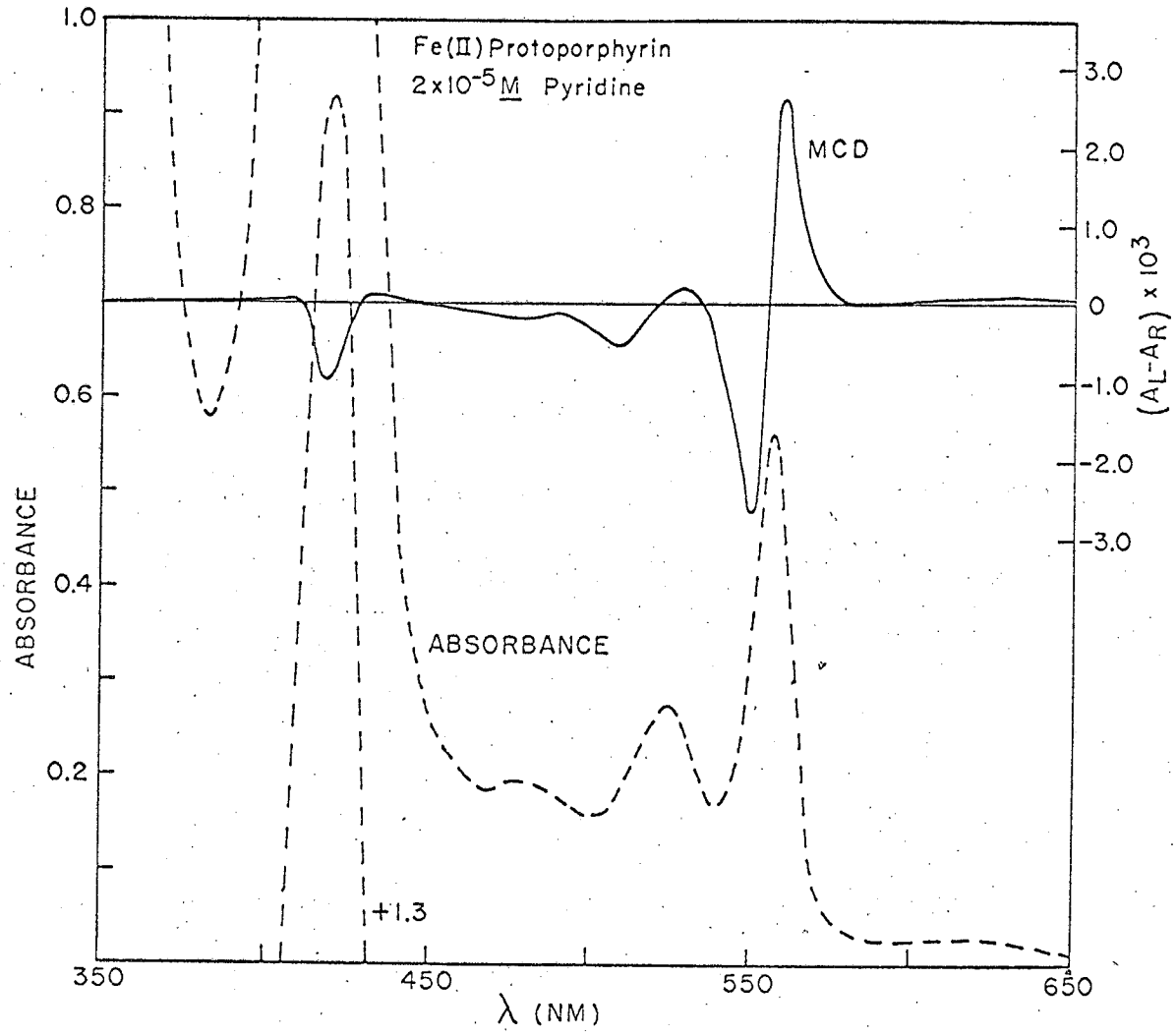

MUB 12078

Figure III-34. MCD (solid curve) and absorbance (dashed curve) of iron(II)protoporphyrin IX, 2.10^{-5} M in pyridine, 1 cm path. The small peak at ca. 630 NM is due to a free base impurity.

We realized long after completion of these exploratory experiments that the Fe(II) protoporphyrin shown in Figure III-33 is probably a mixture of low spin (S = 0) and high spin (S = 2) complexes and may be polymeric. It is extremely difficult to prepare pure S = 2 (high spin) monomeric iron porphyrins except in some heme proteins (e.g. myoglobin fluoride). The Fe(II) protoporphyrin $(pyridine)_2$ complex shown in Figure III-34 is undoubtedly pure low spin. The MCD and absorption of the low spin derivative in the red (Q) region is similar to the other metal porphyrins studied.

In the case of Fe(III) protoporphyrin, pyridine substitution causes a more drastic change, sharpening the absorption and markedly increasing the MCD as is shown in Figures III-35 and III-36. The magnetic splitting increases from $M_z = 4.0$ to 8.2 for Fe(III) protoporphyrin when $(pyridine)_2$ replaces the $(H_2O)(-OH)$ ligands.

The Fe(III) protoporphyrin shown in Figure III-35 is the high spin (S = 5/2) form and the pyridine derivative shown in Figure III-36 is the low spin ($S = \frac{1}{2}$) form. The MCD and absorption of the low spin form in the red (Q) region is similar to the other metal porphyrins studied. However, the MCD and absorption of the high spin Fe(III) protoporphyrin (Figure III-35) in the red (Q) region is anomalous compared to the other metal porphyrins. The Q region absorption is much broader than the usual metal porphyrin spectrum, and the Q region MCD is quite small and crosses zero to the red of the main absorption band (by ca. 12 NM). Per-

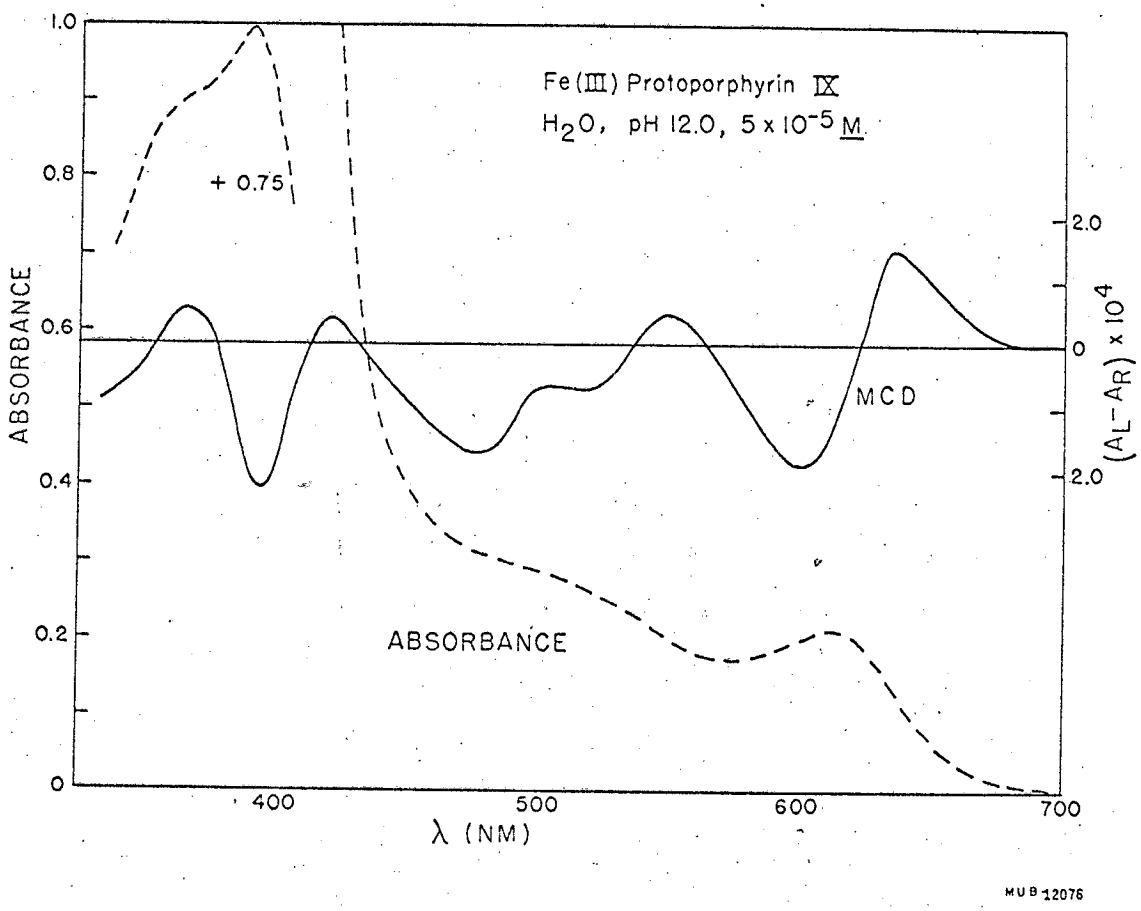

Figure III-35. MCD (solid curve) and absorbance (dahsed curve) of iron(III)protoporphyrin IX (hemin chloride) in H_2O, pH 12.0, 5.10^{-5} moles/liter, 1 cm path.

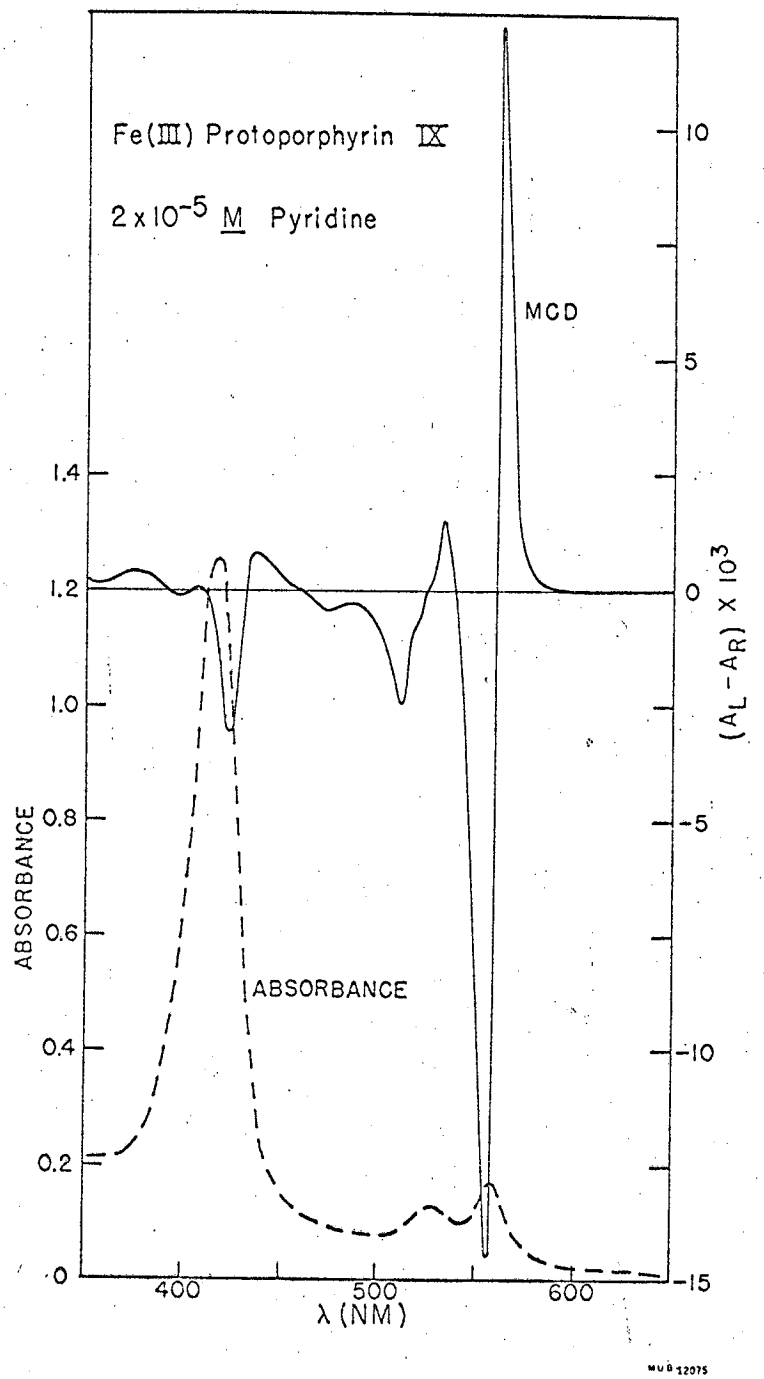

Figure III-36. MCD (solid curve) and absorbance (dashed curve) of iron(III)protoporphyrin IX in pyridine, 2.10^{-5} moles/liter, 1 cm path.

haps the Q band orbital degeneracy is strongly lifted in this complex and the M_z number may then be much larger than estimated above (where we assumed orbital degeneracy) if one of the absorption components were relatively weak (cf. p. 147). We cannot derive a precise estimate of the possible magnitude of the proposed lifting of the Q band degeneracy, but it could be as large as 1000 cm^{-1} and still be consistent with our data. It may also be that charge transfer transitions are present in this complex which are complicating (and broadening) the spectrum (e.g. Day, Scragg and Williams, 1964) and that the MCD of these charge transfer bands are partially cancelling the MCD of the Q bands. Perhaps low temperature MCD and absorption spectra would offer more resolution of these bands and allow a decision between the alternatives discussed above.

We find analogous ligand dependent MCD of the iron porphyrins in heme proteins. We have investigated the MCD of hemoglobin derivatives, which have various ligands in the sixth coordination of the iron porphyrin. Histidine coordinates the fifth position of the iron protoporphyrin in hemoglobin. Figure III-37 shows the experimental and calculated absorption of oxyhemoglobin; the calculated spectrum uses six Gaussian bands. Figure III-38 shows the experimental and calculated MCD spectra of oxyhemoglobin using five of the Gaussians found from fitting the absorption. The MCD fit to the Gaussian shape is very satisfactory

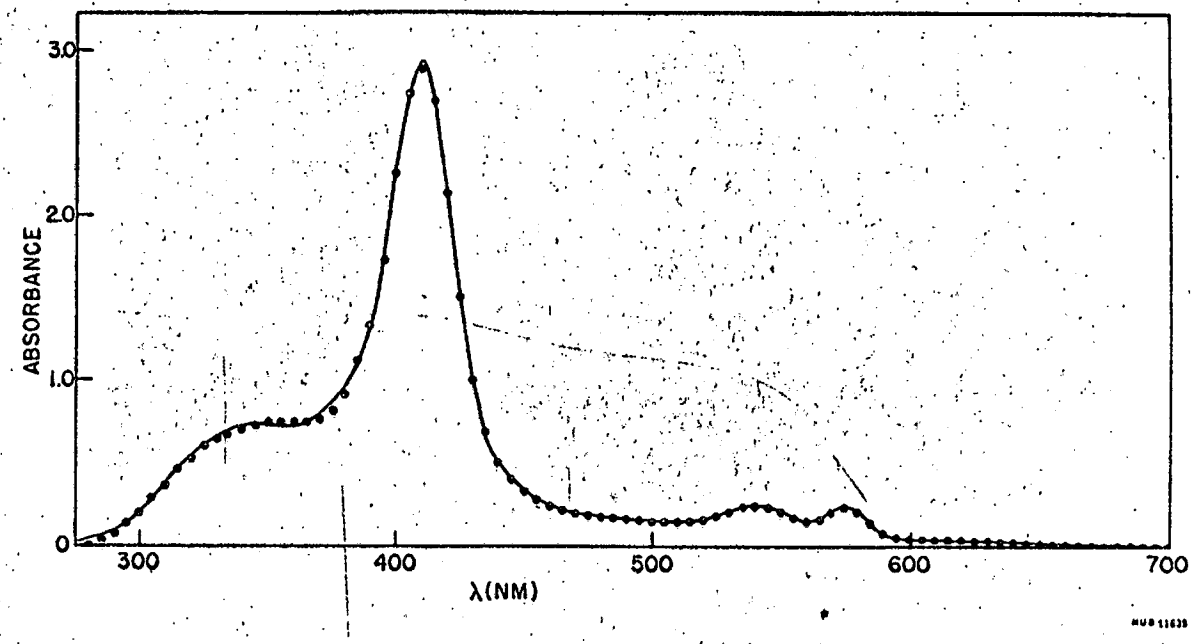

Figure III-37. Experimental (....) and calculated (_____) absorbance of bovine oxyhemoglobin in pH 6.8 phosphate buffer (0.1 M). Exact concentration unknown due to apparent contamination with colorless protein. The observed spectrum rose sharply below 300 NM and was smoothly truncated somewhat arbitrarily as shown. Six symmetrical Gaussian components used to fit the spectrum (including a tiny peak in the 625 mμ region which was not used in fitting the MCD).

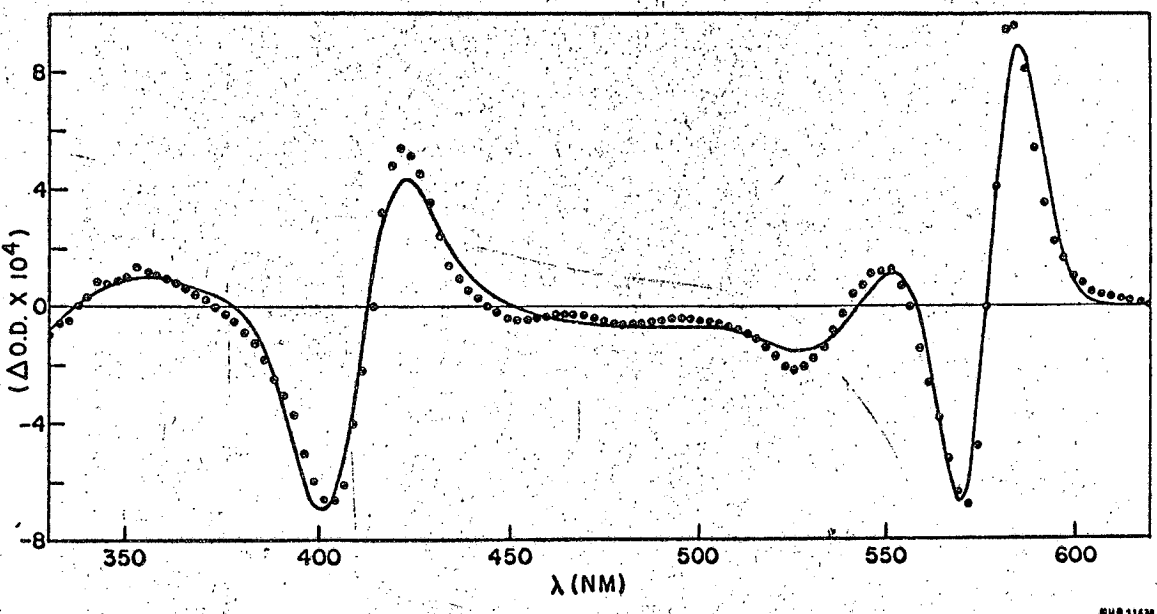

Figure III-38. Experimental (....) and calculated (———) MCD of bovine oxyhemoglobin in pH 6.8 phosphate buffer (0.1 M). The sample was the same as used for the absorption spectrum fit shown in Figure III-37. Five Gaussian components (omitting the small 625 mμ peak) from the absorption spectrum were used to fit the MCD.

for oxyhemoglobin. The Q band splitting is found to be $M_z = 3.8$ and the B band splitting is $M_z = 0.75$. The Q band splitting for the iron(II) coordinated with O_2-histidine (in oxyhemoglobin) is intermediate to that previously found for $(H_2O)(^-OH)$ and $(pyridine)_2$ coordination. Table IV gives the magnetic splitting found for other hemoglobin and methemoglobin (oxidized to Fe(III)) derivatives. The absorption and MCD spectra change somewhat upon forming these derivatives, but are qualitatively similar to the spectra shown in Figures III-33 to 36.

The MCD and absorption of reduced, Fe(II), cytochrome c is shown in Figure III-39. The MCD in the Q band is very large and the magnetic splitting found is $M_z = 7.5$. The iron in cytochrome c is thought to be coordinated with either two histidines or with one histidine and an ϵ-amino group of lysine. The magnetic splitting found is large compared to the other similar coordinations we have studied, Fe(II) protoporphyrin $(pyridine)_2$ and hemoglobin (pyridine). The cytochrome c porphyrin is derived from protoporphyrin (Figure III-9) but the vinyl groups on positions 2 and 4 have been replaced by thioether linkages to the protein. The sulfurs in the thioethers are two methylene groups away from the porphyrin ring, so they must have a very small effect on the ring. The effect of replacing vinyl with thioether is essentially to replace the vinyl groups with methyl or ethyl. We are not able to assess empirically the importance for the MCD of removing the

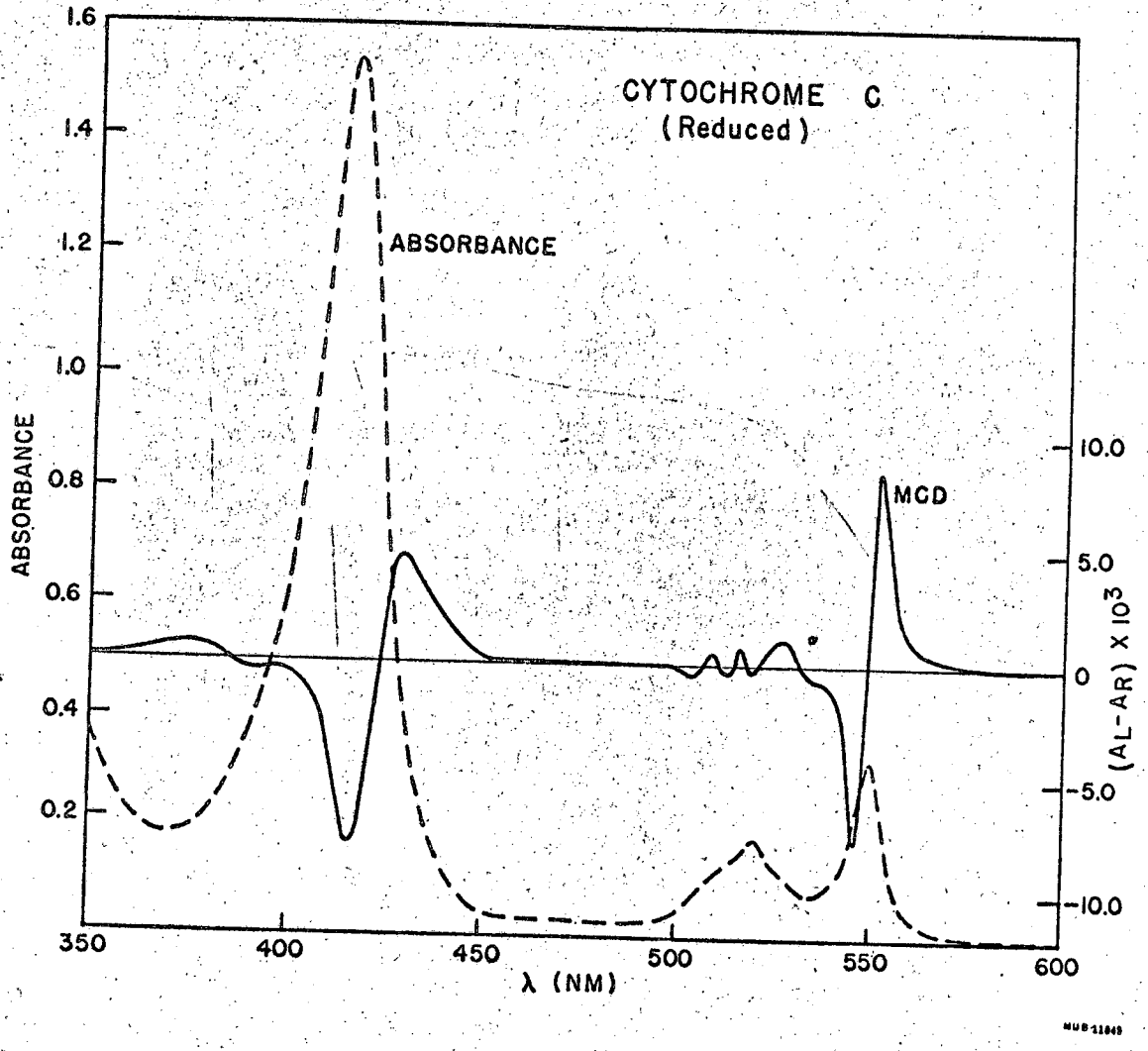

Figure III-39. MCD (solid) and absorbance (dashed) of reduced horse cytochrome c in pH 6.0 phosphate buffer (0.1 M). This is the same sample as shown oxidized inFigure III-40.

Table IV. Magnetic splittings for iron porphyrin complexes, assuming orbital degeneracy. Hb stands for hemoglobin and Hi for oxidized Fe(III) hemiglobin. Only compounds that show a simple symmetrical double MCD in the B band have $M_{z,B}$ splitting listed.

Fe(II) Complex	$M_{z,Q}$	$M_{z,B}$	Fe(III) Complex	$M_{z,Q}$	$M_{z,B}$
Fe(II) protoporphyrin ($^-OH,H_2O$)	3.2		Fe(III) protoporphyrin ($^-OH,H_2O$)	1.5	
Fe(II) protoporphyrin (pyridine)$_2$	5.0		Fe(III) protoporphyrin (pyridine)$_2$	8.2	
Hb(pyridine)	4.3		Hi(pyridine)	6.2	
Hb(H_2O)	3.4		Hi(OH)	1.15	0.88
Hb CO*	1.67	0.85	Hi(CN)	1.4	1.0
Hb O_2	3.8	0.75			
Cytochrome c	7.8				

* CO complex may not have been 100% formed, so this result may be questionable.

vinyl groups of this material. Theoretical considerations (Gouterman, 1959) would say that the vinyl groups split the Q band degeneracy very slightly, much less than the band width of the Q band. So, we expect that removal of the vinyl groups in itself will not affect the Q band MCD, and the large MCD found for reduced cytochrome c must be due to the iron coordination.

The relative effect of the various ligands on the magnetic splitting of the Fe(II) porphyrin Q band is:

ammine-histidine > pyridine-histidine > $(\text{pyridine})_2$ > θ_2-histidine > H_2O-histidine > $(H_2O)(^-OH)$

Many of the Fe(III) complexes have very broad absorption bands and the magnetic splittins are poorly determined in these cases (e.g. see Figure III-35). Ligand-dependent variations in magnetic splitting of the Q bands are apparent, but low temperature MCD and absorption measurements are needed to sharpen the bands and try to separate the contributions of the various broad bands.

Oxidized (Fe(III)) cytochrome c (Figure III-40) shows a broad absorption in the visible and essentially no double MCD. This is the only iron porphyrin where no Q band magnetic splitting was found. Recall that the reduced cytochrome c showed a larger splitting thahn Fe(II) protoporphyrin $(\text{pyridine})_2$, indicating that the iron environment in cytochrome c was favorable for a large magnetic splitting of the Q band. The other work with the Fe(III) complexes indicated the ligand dependence of the

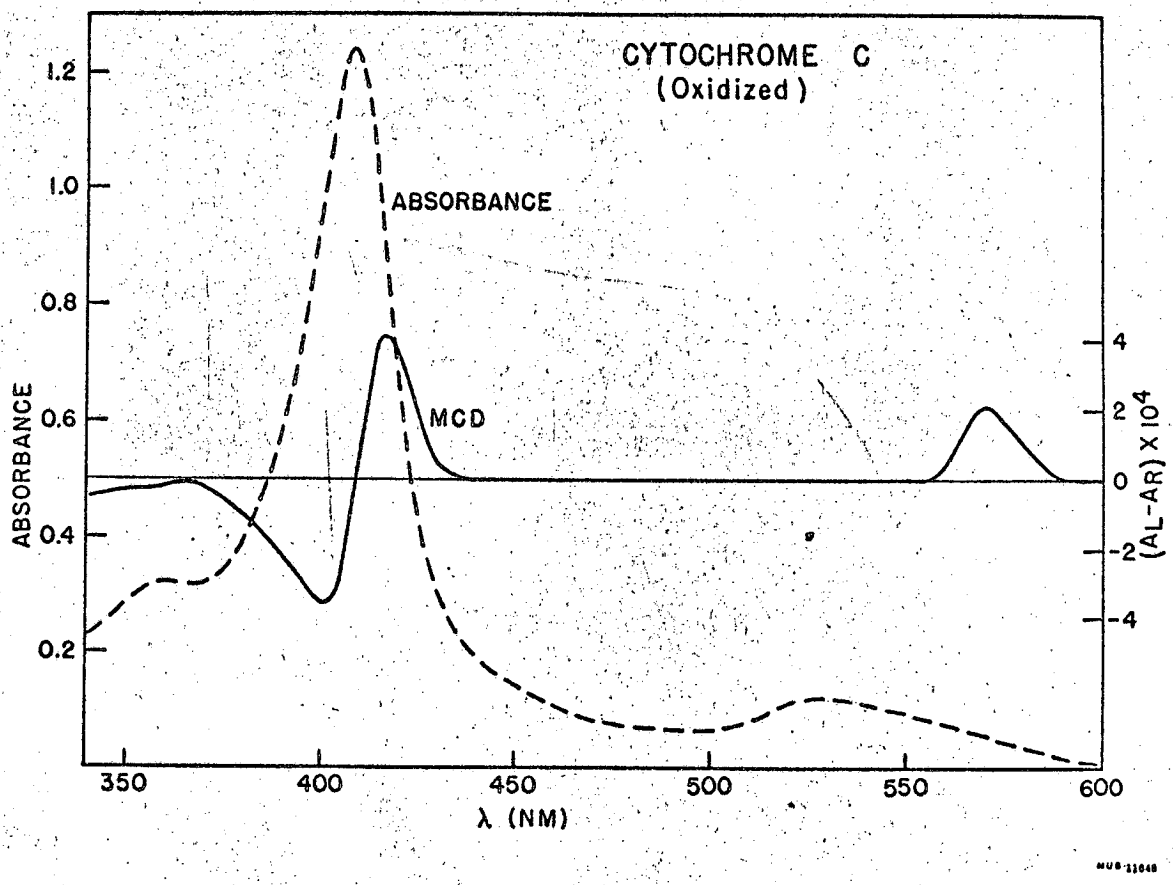

Figure III-40. MCD (solid) and absorbance (dashed) of oxidized horse cytochrome c in pH 7.0 phosphate buffer (0.1 M). This is the same sample as shown reduced in Figure III-39.

Fe(III) MCD is very similar to Fe(II); for example, $(pyridine)_2$ coordination gives a much larger MCD than $(H_2O)(^-OH)$ coordination for both Fe(II) and Fe(III). The observation that the magnetic splitting is large in reduced cytochrome c and very small in oxidized cytochrome c suggests that the iron coordination in cytochrome c is altered upon oxidation. Other experiments have indicated a conformational change in cytochrome c which is dependent on and linked to the state of oxidation-reduction (Urry and Doty, 1965). Our experiments, although incomplete, suggest that the conformation change causes a drastic change in iron coordination in cytochrome c.

A more extensive investigation of the MCD of a wide variety of iron porphyrin complexes may yield an empirical scale of ligand environment vs. magnetic splitting. This scale could be useful for determination of the iron coordination in many heme proteins. For example, there are very many cytochromes known, but the iron coordination is unknown in most of them. The coordination of the heme seems to be the key factor in determining the redox potential of the cytochromes (e.g. Falk and Perrin, 1961).

The Soret (B) region of the iron protoporphyrin MCD (Figures III-33,34,35,36) is very complicated and does not show the simple double MCD band found in the other metal porphyrins studied. The complex MCD suggests that there are extra transitions in the B region of the iron protoporphyrins. We have not done the MCD of

other metal protoporphyrins so we do not know whether this anomalous behavior should be attributed to the iron or the vinyl groups on the protoporphyrin (see Figure III-9). Cytochrome c, with the vinyl groups removed, has a normal B region MCD, but this is a rather complex model compound. Molecular orbital calculations (Sauer, 1966) indicate that dicarbonyl or divinyl substituents such as are on protoporphyrin add two strong transitions in the B region (with essentially no effect in the Q region). For these reasons we tentatively attribute the complicated MCD in the B region of the protoporphyrins to four overlapping transitions. Iron porphyrins free of conjugated substituents and zinc, or other closed shell metal protoporphyrins, can be studied to test this hypothesis. Most of the hemoglobin derivatives showed the anomalous MCD in the B region similar to Figures III-33,34,35,36. A few show normal metal porphyrin MCD in the B region (e.g. HbO_2, Figure III-34, HbCO). However, we are unable to judge at this point whether these cases are normal or abnormal for iron porphyrins.

Some of the iron porphyrins, as well as some manganese porphyrins, have obvious extra absorption bands in the visible and near IR, compared to all other metal porphyrin spectra. It has been proposed that these extra bands are due to "charge transfer" transitions from ring orbitals to metal orbitals (Day, Scragg and Williams, 1964; Gouterman, 1965; Offenhartz, 1964). We were

not aware of this hypothesis when these measurements were made, and the most clearly identified of these extra bands are in the 650-750 region which was not investigated. Some of these bands have been tentatively assigned to transitions to e_g metal orbitals. These transitions would be expected to give distinctive double MCD spectra.

There are obviously many unanswered questions on the electronic structure of the iron porphyrins. The theory is just being developed (Zerner and Gouterman, 1966b) and combined with further experimental work. We may look forward to progress in understanding these important molecules.

E. Closing Comments on Magnetic Circular Dichroism

Miscellaneous molecules

In the course of this research we investigated the MCD of many different types of molecules. Most of the other materials we studied had lower than three-fold symmetry and showed single MCD bands. Various organic molecules show weak (e.g. ketones) to fairly strong (e.g. polycyclic aromatic hydrocarbons) single MCD bands. Materials with large natural optical activity, such as chlorophyll crystal and several proteins with optically active chromophoric groups, tended to have small MCD. Various stable free radicals were investigated and no MCD effects attributable to spin were found. Aggregation of molecules (e.g. chlorophylls, phthalocyanines and other dyes) produced no striking effects on the MCD. There are indications, however, that formation of very symmetrical aggregates can produce a large MCD. For example, some helical polymers have an x-y degeneracy perpendicular to their helix axis which may be split by the magnetic field. Some of these polymers have been investigated in a preliminary manner and the results suggest that conformation dependent MCD of polymers may be useful in some cases.

Prospects for MCD in chemistry and biology

The MCD responds most markedly to the orbital Zeeman effect, where the magnetic field splits a degenerate level. If this degeneracy is to be expected, very symmetrical systems must be studied. There is the tendency, then, for the MCD to be the largest in

very symmetrical systems. However, small perturbations to lower than the minimum three-fold symmetry do not alter the expected MCD (P. 147). In this regard, the MCD is complementary to natural CD, where the most asymmetrical materials give the largest effects. High symmetry systems such as metal complexes and polymers may be studied profitably with MCD. The MCD method extends the very powerful Zeeman effect to wide line spectra in solution.

In molecules of less than three-fold symmetry, perpendicularly polarized transitions will couple strongly in MCD if they are close in energy. MCD methods will be useful in showing the relative polarizations of transitions (particularly for nonfluorescent materials) and in finding previously hidden weak transitions, if they are perpendicular to nearby strong ones. This type of spectroscopy will undoubtedly have a role in the future study of molecular electronic structure relevant to both chemistry and biology.

REFERENCES

Beychok, S., Biopolymers 2, 575 (1964).

Biltonen, R., unpublished.

Bohm, D. (1951), Quantum Theory (Prentice-Hall, Inc., Englewood Cliffs, N. J.).

Brown, J. S., and C. S. French, Plant Physiol. 34, 305 (1959).

Buckingham, A. D., and P. J. Stephens, Ann. Rev. Phys. Chem. (1966), in press.

Caughey, W. (1966), to be published.

Cotton, M., and M. Scherer, Helv. Phys. Acta 3, 459 (1930).

Day, P., G. Scregg and R. J. P. Williams, Biopolymers Symposia 1, 271 (1964).

Deming, W. E. (1943), Statistical Adjustment of Data (John Wiley, N. Y.).

Djerassi, C. (1960), Optical Rotatory Dispersion (McGraw-Hill Company, N. Y.).

Drude, P. (1900), The Theory of Optics (Dover Publications, Inc., N.Y., 1959).

Eberhart, W. H., and H. Renner, J. Mol. Spectr. 6, 483 (1961).

Eyring, H., J. Walter and G. E. Kimball (1944), Quantum Chemistry (J. Wiley and Sons, Inc., N. Y.).

Falk, J. E., and D. D. Perrin (1961), in Haematin Enzymes, J. E. Falk, R. Lemberg and R. K. Morton, eds. (Pergamon Press, N. Y.), p. 56.

Faraday, M. (1845), Diary, Sept. 13, 1845, Bell's Edition (1932), p. 264.

Faraday, M. , Phil. Trans. 136, 1 (1846).

Feher, G., M. Malley and D. Mauzerall (1966), Int. Conf. on Magnetic Resonance in Biological Systems, Stockholm, Sweden, June 14-16, 1966.

Foss, J. G., and M. E. McCarville, J. Am. Chem. Soc. 87, 228 (1965).

Fruton, J. S., and S. Simmonds (1959), General Biochemistry (John Wiley and Sons, Inc., N. Y.), 2nd Ed.

Gouterman, M. (1965), unpublished.

Gouterman, M. (1966), personal communication.

Gouterman, M., J. Chem. Phys. 30, 1139 (1959).

Gouterman, M., J. Mol. Spectry. 6, 138 (1961).

Gouterman, M., and L. Stryer, J. Chem. Phys. 37, 2260 (1962).

Groenewege, M. P., Mol. Phys. 5, 541 (1962).

Hameka, H. F., J. Chem. Phys. 37, 2207 (1962).

Henry, C. H., S. E. Schnatterly and C. P. Slichter, Phys. Rev. 137, A583 (1965).

Herzberg, G. (1950), Spectra Diatomic Molecules (D. Van Nostrand Company, Inc., Princeton, N. J.), p. 212.

Holzwarth, G., and P. Doty, J. Am. Chem. Soc. 82, 218 (1965).

Kramers, H. A., Proc. Acad. Sci. Amst. 33, 959 (1930).

Lemberg, R., and J. W. Legge (1949), Hematin Compounds and Bile Pigments Interscience Pub., Inc., N. Y.) p. 214-222.

Longuet-Higgins, H. C., G. W. Rector and J. R. Platt, J. Chem. Phys. 18, 1174 (1950).

Lowry, T. M. (1964), Optical Rotatory Power (Dover Publications, Inc., N. Y.).

Margenau, H., and G. M. Murphy (1956), The Mathematics of Physics and Chemistry, 2nd Ed. (D. Van Nostrand Co., Princeton, N. J.), p. 289.

Mason, S. F., Quarterly Revs. (London) 17, 20 (1963).

Moffitt, W., J. Chem. Phys. 22, 320, 1820 (1954).

Moffitt, W., and A. Moscowitz, J. Chem. Phys. 30, 648 (1959).

Moscowitz, A. (1960), Ch. 12 in Optical Rotatory Dispersion by C. Djerassi (McGraw-Hill Book Company, Inc., N. Y.).

Mouton, H. (1930), in International Critical Tables, Vol. I (McGraw-Hill Book Company, Inc., N. Y.), p. 109.

Offenhartz, P. O'd., J. Chem. Phys. 42, 3566 (1964).

Partington, J. R. (1953), An Advanced Treatise on Physical Chemistry (Longmans, Green and Co., London), 4.

Perkin, W. H., J. Chem. Soc. 69, 1025 (1896); ibid. 45, 421 (1884).

Platt, J. R. (1956), in Radiation Biology, A. Hollaender, ed., Vol. III, Ch. 2 (McGraw-Hill Book Company, N. Y.).

Platt, J. R. (1964), Free Electron Theory of Conjugated Molecules, J. R. Platt, ed. (Univ. of Chicago Press), p. 1.

Rimington, C., S. F. Mason and O. Kennard, Spectrochim. Acta 12, 65 (1959).

Rosenfeld, R., Z. Physik. 57, 835 (1929).

Sandorfy, C. (1964), Electronic Spectra and Quantum Chemistry (Prentice-Hall, Inc., Englewood Cliffs, N. J.).

Sauer, K. (1966), unpublished.

Schooley, D. A., E. Bunnenberg and C. Djerassi, Proc. Nat. Acad. Sci. 53, 579 (1965).

Serber, R., Phys. Rev. 41, 489 (1932).

Shashoua, V. E., J. Am. Chem. Soc. 82, 5505 (1960).

Shashoua, V. E., J. Am. Chem. Soc. 86, 2109 (1964).

Shashoua, V. E., J. Am. Chem. Soc. 87, 4044 (1965).

Simpson, W., J. Chem. Phys. 17, 1218 (1949).

Slater, J., Phys. Rev. 36, 57 (1930).

Slichter, C. P. (1963), Principles of Magnetic Resonance (Harper and Row, N. Y.).

Sponer, H., and E. Teller, Rev. Mod. Phys. 13, 75 (1941).

Stephens, P. J. (1966), Ph.D. Thesis, Oxford University.

Stephens, P. J., W. Suetaka and P. N. Schatz, J. Chem. Phys. (1966), in press.

Stone, J. M. (1963), Radiation and Optics (McGraw-Hill, N. Y.).

Sugano, S., and Y. Tanabe, J. Phys. Soc. Japan 13, 880 (1958).

Thiery, J. M. (1966), unpublished.

Thorne, J. M. (1966), Ph.D. Thesis, University of California, Berkeley.

Tinoco, I., Jr., and C. A. Bush, Biopolymers Symposia 1, 235 (1964).

Tobias, I., and Kauzman, W., J. Chem. Phys. 35, 538 (1961).

Urry, D. W., and P. Doty, J. Am. Chem. Soc. 87, 2756 (1965).

Van Vleck, H. J., and W. G. Penny, Phil. Mag. 17, 961 (1934).

Varsanyi, F., D. L. Wood and A. L. Schawlow, Phys. Rev. Letters 3, 544 (1959).

Velluz, L., M. Legrand and M. Grosjean (1965), Optical Circular Dichroism (Academic Press, Inc., N. Y.).

Verdet, Ann. chim. et phys. 69, 415 (1863); ibid. 41, 370 (1854); ibid. 43, 37 (1858); ibid. 52, 129 (1860).

Waring, C. E., and R. L. Custer (1960), Technique of Organic Chemistry I(III), 3rd Ed., A. Weissberger, ed., pp. 2497-2552 (Interscience, N. Y.).

Weigl, J. W., J. Mol. Spectr. 1, 133 (1957).

Weiss, C., H. Kobayashi and M. Gouterman, J. Mol. Spectr. 16, 415 (1965).

Williams, R. J. P. (1961), in Haematin Enzymes, J. E. Falk, R. Lemberg and R. K. Morton, eds. (Pergamon Press, N. Y.), p. 41.

Wilson, E. B., Jr. (1952), An Introduction to Scientific Research (McGraw-Hill Book Company, N. Y.).

Wilson, E. B., J. C. Decius and P. C. Cross (1955), Molecular Vibrations (Maple Press Co., York, Pa.).

Zerner, M., and M. Gouterman, Theoret. Chim. Acta (Berlin) 4, 44 (1966a).

Zerner, M., and M. Gouterman (1966b), in press.

Appendix I: The Relative Sensitivity of Circular Dichroism (CD) and Optical Rotatory Dispersion (ORD)

The ultimate limitation on the signal to noise ratio in an optical measurement is the statistical fluctuation in detected light quanta (commonly called shot noise). Other factors such as amplifier noise, vibrations or light source instability can be very important, of course, but we will assume that the instruments under consideration are designed so that these "removable" noise sources are negligable. We examine the consequences of the unavoidable shot noise limitation for optical activity measurements.

We have selected the state of the art optical methods for CD and ORD as a basis of comparison of the techniques. It is possible that fundamentally more sensitive methods could be devised. Any new proposed technique can be analyzed and evaluated in a manner analogous to the following.

First we consider the CD measurement. The method of Pockels' cell modulation of the polarization and detection was described in detail in Chapter II p. 44. We make the assumption that all amplification after the photomultiplier (PM) cathode is noise free (this can be realized to about 90%). And that the noise spectrum is white (constant noise power with frequency). The light intensity falling on the PM cathode was found to have a DC term and an AC term which carries the CD information (cf. equation II-8). The DC term in light intensity (see equation II-8) is large compared to the AC part and contributes essentially all of the shot noise. The PM cathode current

due to the DC term in the presence of a sample is

$$i = q \phi (I_o/2) e^{-A} \text{ (amps.)} \qquad \text{A-1}$$

where q is the charge on the electron, ϕ is the fractional cathode quantum efficiency, I_o is the light intensity incident on the polarizer (quanta/sec) and A is the sample absorbance divided by 2.303. The noise current due to the statistical fluctuation in the detected quanta is:

$$i_{noise} = (2 q i \gamma)^{1/2} \text{ (amps.)} \qquad \text{A-2}$$

where γ is the bandwidth in Hz. Substitution of eq. A-1 into eq. A-2 yields:

$$i_{noise} = q e^{-A/2} (I_o \phi \gamma)^{1/2} \qquad \text{A-3}$$

The AC term which carries the CD information is derived from equation II-8 and may be written:

$$i_{signal} = q \Delta \phi (OD_l - OD_r)(I_o/4) e^{-A} \sin(\delta_o \sin \omega t) \qquad \text{A-4}$$

where Δ is the fractional circular polarization and δ_o is the peak phase retardation of the Pockels' cell ($\delta_o \approx 2$ radians) and $(OD_l - OD_r)$ is the difference in optical density in left and right circular light, respectively. This signal is amplified by the PM and other amplifiers, demodulated (synchronously rectified) and filtered to yield:

$$V_{signal} = q G R_l \phi \Delta (OD_l - OD_r)(I_o/2\pi) e^{-A} \qquad \text{A-5}$$

where R_l is the value of the PM load resistor and G is the net gain of the PM and other amplifiers. V_{noise} is found from eq. A-3 for the noise current by multiplying i_{noise} by R_l and G as above. The signal to noise ratio is, of course, given by the ratio of V_{signal} to V_{noise}.

$$(S/N)_{CD} = (A/2\pi)(OD_l - OD_r)\, e^{-A/2}\, (I_o \phi T)^{1/2} \qquad A-6$$

where $T = 1/\gamma$, the filter time constant in seconds. It should be noted that the signal to noise ratio is linearly related to the fraction of peak circular polarized light, A; and to the square root of the light intensity I_o, PM quantum efficiency ϕ, and to the filter time constant T.

The above result is useful in determining the key parameters for optimization of a shot noise limited instrument. A simple test for the shot noise limited condition is to see if the signal to noise ratio follows the $(I_o T)^{1/2}$ function. This result is perhaps the most interesting when compared to a companion result for ORD which will be derived next.

The polarimetric method we discuss appears to be the most sensitive yet devised. The method has been treated recently by Cary, et. al. (Applied Optics 3, 329, 1964) and this paper should be consulted for more details. We offer a somewhat simplified treatment.

The basic relation for polarimetry is law of Malus, which gives the intensity transmitted by a linear polarizer-analyzer pair with unpolarized incident light, I_o:

$$I = (I_o/2)\, (\sin^2\alpha + L) \qquad A-7$$

If some optically active sample is interposed between the polarizer and the analyzer, α may be conveniently defined as the angle between the analyzer extinction axis and the major axis of the light incident on the analyzer. L is the fractional light leak when $\alpha = 0$. The polarimetric method under consideration is a null method where α is set to zero. The $\sin^2\alpha$ function is very

flat near $\alpha = 0°$ or 90° so the plane of polarization is modulated by γ:

$$\gamma = \gamma_o \sin \omega t \qquad \text{A-8}$$

A photomultiplier is placed behind the analyzer and the cathode current is:

$$i = q \phi (I_o/2) e^{-A} \left[\sin^2 (\alpha + \gamma_o \sin \omega t) + L\right] \qquad \text{A-9}$$

In practice, α is close to zero and γ_o is usually only a small fraction of a radian. Since α and γ_o are small, equation A-9 can be expanded (e.g. $\sin x \approx x$) and the only significant terms are:

$$i = \phi q (I_o/4) e^{-A} \underbrace{(L + \gamma_o^2)}_{\text{D.C.}} \quad \underbrace{-8\gamma_o \alpha \sin \omega t}_{\text{A.C. at } \omega t} + \underbrace{2\gamma_o^2 \cos 2\alpha \cos 2\omega t}_{\text{A.C. at } 2\omega t}) \qquad \text{A-10}$$

The ωt AC term is linearly proportional to the rotation angle α. The 2 ωt AC term is essentially independent of α ($\cos 2\alpha \approx 1$), is strongly discriminated against by an amplifier tuned to ωt, and the 2 ωt term can be neglected. For reasonably good polarizers, and for samples which don't depolarize or cause ellipticity to any appreciable extent, $L \approx 10^{-4}$ and since $\gamma_o \approx 0.1$ radian, $\gamma_o^2 >> L$. The ωt AC component is selectively amplified, demodulated, and filtered and is used to null the polarizer-sample-analyzer system (to set $\alpha \approx 0$). If α departs from zero a signal results:

$$i_{signal} = (8/\pi) \alpha \gamma_o \phi q I_o e^{-A} \qquad \text{A-11}$$

The shot noise near ωt is predominently carried by the relatively large DC term, so the PM cathode noise current can be approximated:

$$i_{noise} \approx q \gamma_o e^{-A/2} \sqrt{(\phi I_o T)/2} \qquad \text{A-12}$$

When the polarimetric system is close to balance, $i_{noise} \approx i_{error\ signal}$.

so we may define a rotation angle uncertainty, $\delta\alpha_{min}$, by the relation:

$$i_{noise} \tilde{=} i_{signal} = \delta\alpha_{min}(4/\pi)\gamma_o \phi q I_o e^{-A} \qquad A\text{-}14$$

This may be rearranged with the incorporation of eq. A-13 to yield:

$$\delta\alpha_{min} = (180/\pi)(\pi/4)\, e^{A/2} \sqrt{2/(\phi I_o T)} \qquad A\text{-}15$$

where $(180/\pi)$ has been inserted to convert from radians to degrees. The rotation angle uncertainty is independent of γ_o, the peak modulation angle, under the assumption of a stable light source and as long as γ_o is large enough so that the $\gamma_o^2 >> L$ approximation holds. If β is defined as the rotation of the material under examination, the signal to noise ratio is:

$$(S/N)_{ORD} = \beta/\delta\alpha_{min} = \beta(\pi/180)(4/\pi)\, e^{-A/2} \sqrt{(\phi I_o T)/2} \qquad A\text{-}16$$

Apart from multiplicative constants, this expression has the same functional dependence on A, ϕ, I_o and T as does the companion result for CD (eq. A-6).

The relative signal to noise for CD and ORD can be found from the ratio of equations A-16 to A-6. In the case where identicle light sources, monochromators, photomultipliers and samples are compared, the relative signal to noise is simply:

$$[(S/N)_{ORD}]/[(S/N)_{CD}] = [4\sqrt{2}\ \beta]/[180A\ (OD_l - OD_r)] \qquad A\text{-}17$$

The $(OD_l - OD_r)$ and β observables are related by the Kronig-Kramers transform given in chapter II p. 49, and the exact numerical result for the A-17 ratio will depend on the shape of the CD and ORD curves. If we assume a single Gaussian CD shape, the minimum to maximum rotation and the zero to peak CD are approximatly:

$$\beta_{max} - \beta_{min} \tilde{=} 40(OD_l - OD_r)_{max} \qquad A\text{-}18$$

Other spectral shapes may depart somewhat from A-18, but it is useful to consider this example. Combination of equations A-18 and A-17 yields for a Gaussian:

$$[(S/N)_{ORD}]/[(S/N)_{CD}] = 4 - 6 \quad (\text{for } \Delta = 1 - 0.7) \qquad A\text{-}19$$

By this analysis, ORD has a substantial sensitivity advantage over CD for the methods of measurement assumed. Direct measurement of the angle of ellipticity would, in principle, be a more sensitive method of CD measurement. An automatic recording ellipticity measureing instrument would be quite complex and it may be extremely difficult to conceive a design which would approach ideal behavior.

CD methods have other advantages compared to ORD which tend to outweigh the lower inherent sensitivity. The CD spectra usually offer higher resolution because nearby bands do not overlap as strongly as in ORD. CD peaks are usually found on a low background, whereas ORD curves due to a single band are superimposed upon a monotonic backround due to other bands. Rotational strength data are therefore easier to extract from CD curves, and extraction of rotational strengths from ORD curves often introduces uncertainties which tend to nullify the ORD sensitivity advantage. In magnetic optical activity measurements the very large MORD backround (see chapter III where this is discussed in more detail) appears to put MCD sensitivity on a more equal footing with MORD.

Appendix IIA: KKTRAN, a Fortran IV program for evaluating the Kronig-Kramers transform of circular dichroism to optical rotatory dispersion.

The basic relationship is found in chapter II, equation II-10 (togeather with relevent definitions) and may be rewritten more conviently:

$$\phi(x) = \left(\frac{2}{\pi}\right)\int_0^{\infty} \frac{\Theta(y)\, y}{x^2 - y^2}\, dy \qquad \text{A-20}$$

We are interested in the ORD due to an observed CD band or bands and so the ellipticity $\Theta(y)$ will be considered zero outside of wavelength limits defined by $y \leq a$ and $y \geq b$. The integral in equation A-20 will be evaluated from a to b and will be considered zero elsewhere. Equation A-20 may be rearranged:

$$\phi(x) = \left(\frac{2}{\pi}\right)\int_a^b \frac{y\,\Theta(y) - x\,\Theta(x)}{x^2 - y^2}\, dy + \left(\frac{2}{\pi}\right)\int_a^b \frac{x\,\Theta(x)\, dy}{x^2 - y^2} \qquad \text{A-21}$$

The second integral can be evaluated exactly:

$$\int_a^b \frac{x\,\Theta(x)\, dy}{x^2 - y^2} = \frac{\Theta(x)}{2}\left[\ln\left(\frac{x+b}{x-b}\right) - \ln\left(\frac{x+a}{x-a}\right)\right] \qquad \text{A-22}$$

and the first integral can be evaluated approximatly by the trapezoid rule.

The simple program (KKTRAN) which follows, can be used to evaluate equation A-21. The limitations on the KKTRAN program are that the data points must be evenly spaced in wavelength and that the wavelength values are treated as integers. The relevant wavelength extremes must be entered as integers which are simply related to the experimental wavelength values.

First card:

N1 and N2 are integers related to the minimum and maximum values respectively of the range of the ellipticity data wavelengths (2I5). If Δ is the data point interval, N1 = λ_1/Δ and N2= λ_2/Δ.

FACTOR is a constant multiplied into input data (e.g. to change Δ OD to $\Delta\epsilon$ or to ellipticity)(F10.5).

N3 and N4 are integers related to the minimum and maximum values respectively of the range of wavelengths over which the rotation is to be calculated (2I5). They are defined analogous to N1 and N2. Note that N3 must be less than or equal to N1 and N4 must be greater than or equal to N2.

IEND = 0 if there is another data case following.

$\neq$ 0 if this is the last data case.

CONST is a constant to be added to the experimental data to introduce a baseline shift (usually zero)(F10.5).

Next cards: N2-N1+1 values of Δ OD, $\Delta\epsilon$ or [θ] follow, one value/card, in order of increasing wavelength.

FORTRAN SOURCE LIST KKTRAN

SOURCE STATEMENT

```
      DIMENSION THETA(1000),PHI(1000)
      READ (2,5) N1,N2,FACTOR,N3,N4
    5 FORMAT (2I5,F10.5,2I5)
      N1=N1-1
      N3=N3-1
      N=N2-N1
      NN=N4-N3
      M=N3-N1
      READ (2,10) (THETA(I),I=1,N)
   10 FORMAT (F10.5)
      DO 20 I=1,N
      THETA(I)=THETA(I)*FACTOR
   20 CONTINUE
      DO 100 J=1,NN
      TJ=0.0
      JM=J+M
      IF ((J+N3 .GE. N1+1) .AND. (J+N3 .LE. N2)) TJ=THETA(JM)
      PHI(J)=-0.5*((FLOAT(N3+J)*TJ-FLOAT(N1+1)*THETA(1))/FLOAT((N1+1)**2
     ++(N3+J)**2)+(FLOAT(N3+J)*TJ-FLOAT(N2)*THETA(N))/FLOAT(N2*N2-(N3+J)
     ***2))
      DO 90 I=1,N
      IF (N1+I .EQ. N3+J) GO TO 90
      PHI(J)=PHI(J)+(FLOAT(N3+J)*TJ-FLOAT(N1+I)*THETA(I))/FLOAT((N1+I)**
     *2-(N3+J)**2)
```

```
 90 CONTINUE
    IF ((J+M .EQ. 1) .OR. (N3+J .EQ. N2)) GO TO 95
    PHI(J)=PHI(J)+0.5*TJ*ALOG(ABS(FLOAT((N3+J+N2)*(J+M-1))/FLOAT((N3+J
   J-N2)*(N3+J+N1+1))))
 95 PHI(J)=PHI(J)*2.0/3.1415927
100 CONTINUE
    WRITE (3,110)
110 FORMAT (7H1LAMBDA,9X,5HTHETA,10X,3HPHI)
    DO 200 I=1,NN
    J=N3+I
    IF ((J .GE. N1+1) .AND. (J .LE. N2)) GO TO 150
    A=0.0
    WRITE (3,120) J,A   ,PHI(I)
120 FORMAT (I6,4X,2E13.5)
    GO TO 200
150 K=J-N1
    WRITE (3,120) J,THETA(K),PHI(I)
200 CONTINUE
    STOP
    END
```

Appendix IIB: ODTRAN, a Fortran IV program for processing (M)CD digital data.

The program transforms the digital data derived from the (M)CD apparatus into ΔOD, $\Delta\epsilon$ or $[\theta]$ vs. wavelength. The appropriate sensitivity factors are applied and the Kronig-Kramers transform is computed. There are a large number of options possible, some of the most important are printing a Cal-Comp plot of the CD and the Kronig-Kramers transform and printing an output tape or card deck of the CD data and the wavelength of each CD point (suitable for input to other programs, e.g. LSQVARMIT or CDLSQ).

The input tape (TAPE 7) is made from the paper tape punched by the (M)CD apparatus in the following format:

Two lines of title and identification (at least 67 characters).

LAMBDA MAX - LAMBDA MIN, FORMAT(I5,1H-,I5,10H ANGSTROMS).

Number of channels, FORMAT(I4,4HNCH.).

Amplifier gain factors, FORMAT(F5.3,1H*,F4.2,3H=LI).

Number of passes, FORMAT(I3,5H PASS).

Seconds/pass, FORMAT(I3,9H SEC/PASS).

Concentration, FORMAT(E10.2,12H MOLES/LITER)(here is).

Path length, FORMAT(F8.4,20H CM. CELL)(here is).

Where (here is) is a teletype key which enters 10 blanks.

A carridge return-line feed should not be entered after the path length.

The first data card is the number of data cases (I10).

The control cards may be placed in any order and therefore have an identification name in the first 10 columns (name left adjusted, A10).

CONTROL CARD IDENTIFICATION

TITLE Next card has an 80 character title.

LAMBDA LAMBDA MIN, LAMBDA MAX (10HLAMBDA ,2F10.0) range of values over which KKTRAN is to be performed.

SENS Sensitivity (10HSENS ,E10.3) This is a number derived by comparison with a standard sample. SENS usually equals $1.75*10^{-6}$ if Δ OD is desired. If ellipticity is desired SENS must be multiplied by 3300.

Option cards

WRITE TAPE(must also REQUEST TAPE 8. Blank for output-at beginning of program if this option is used). An end of file mark is put after every data case.

LDIV ΔOD's are divided by the path length.

CDIV ΔOD's are divided by the concentration.

PRINT-N The values of the CD are printed out.

CAL COMP The next card contains: XFACT,PFACT,XAXIS,YAXIS(2E10.3,2A20).
XFACT is an x axis scale factor, the wavelength range is $N3*XFACT \leq \lambda \leq N4*XFACT$.

PFACT The graph is (N4-N3+1)*PFACT*XFACT inches long.

XAXIS,YAXIS are 20 character axis labels

NO GRAPH Suppresses the Cal Comp plot.

SLICE The program operates on 1/N fraction of the data points.

NO PUNCH Suppresses punching of a data card deck. If this is omitted, certain cards must be placed after the program execution card;

```
REWIND, TAPE 14
ASSIGN CP, TAPE 15
COPYCR(TAPE14,TAPE15)
```

SHIFT The value of the baseline shift desired. The number entered is 8192 ± the actual shift desired (in decimal).

NOISE Maximum allowable noise levelfor bad point rejection routine if different from 500 (decimal).

The last card in each data case must be blank.

```
      PROGRAM CDTRAN(INPUT,OUTPUT,TAPE2=INPUT,TAPE3=OUTPUT,TAPE7,TAPE98,
     2TAPE99,TAPE14,TAPE15,TAPE8,TAPE20)

C
C
  501 FORMAT(12A6)
  502 FORMAT(I5,1X,I5,A10)
  503 FORMAT(I4,A4)
  504 FORMAT(F5.0,1X,F4.0,A3)
  505 FORMAT(I3,A5)
  506 FORMAT(I3,A9)
  507 FORMAT(E8.2,2A6)
  508 FORMAT(F8.4,2A10)
  509 FORMAT(06,708)
      INTEGER SHIFT,N
      REAL NLI,L,C
      DIMENSION LAMB(1100) ,BLAM(1100)
      DIMENSION CHAR(12),XAXIS(4),YAXIS(4),KTEMP(10)
      DIMENSION TITLE1(12),TITLE2(12),N(1100)
      DIMENSION THETA(1100),PHI(1100),X(1100),Y(1100)
      COMMON /CCPOOL/ XMIN,XMAX,YMIN,YMAX,CCXMIN,CCXMAX,CCYMIN,CCYMAX
      COMMON/CCFACT/FACTOR
      DATA NCOMP/10HTTTTTTTTTT /
      DATA COMP1/5HSHIFT/,COMP2/4HSENS/,COMP3,COMP4/4HLDIV,4HCDIV/
      DATA COMP5/10H          /,COMP6/6HLAMBDA/
      DATA COMP7/5HTITLE/,COMP8/7HCALCOMP/,COMP9/7HPRINT-N/
      DATA COMP10/5HSLICE/,NAME15/3HC12/,COMP11/8HNO GRAPH /
      DATA COMP12/10HWRITE TAPE/,COMP13/8HNO PUNCH/,COMP14/5HNOISE/
      CALL CCBGN
C     READ NUMBER OF PROBLEMS
      READ(2,601)NPROB
      DO 300 NPROC=1,NPROB
C     TAPE READ-IN
  700 READ(7,501)(TITLE1(I),I=1,12)
      IF (ENDFILE 7)700,701
  701 READ(7,501)(TITLE2(I),I=1,12)
      READ(7,502)NT2,NT1 ,NAME1

      READ(7,503)NCH,NAME2
```

```
      READ(7,504)Z2,Z1,NAME3
      READ(7,505)NPASS ,NAME4
      READ(7,506)NSEC ,NAME5
      READ(7,507)C   ,NAME6,NAME7
      READ(7,508)L  ,NAME8,NAME9
      P1=FLOAT(NT1)
      P2=FLOAT(NT2)
C     DATA OUTPUT
      WRITE(3,511)(TITLE1(I),I=1,12),(TITLE2(I),I=1,12)
  511 FORMAT(1H1,///20X,12A6/20X,12A6)
      WRITE(3,512)P1,P2,NCH,Z1,Z2,NPASS,NSEC,C,L
  512 FORMAT(///10X,3HP1=F10.3/10X,3HP2=F10.3/10X,4HNCH=I4/
     210X,3HZ1=E9.2/10X,3HZ2=E9.2/10X,6HNPASS=I3/10X,5HNSEC=I3/
     310X,2HC=E9.2/10X,2HL=E9.2)
      JM=NCH-7
      DO 530 J=1,JM,8
      I=NCH-J+2
  530 READ (7,509)(N(I-K),K=1,8)
  530 STORE1=L
      L=1.0
      STORE2=C
      C=1.0
 7777 FORMAT(8(5X,08))
      DO 517 I=1,12
  517 CHAR(I)=COMP5
      ASSIGN 554 TO NNN5
      ASSIGN 206 TO NNN7
      ASSIGN 590 TO NNN8
      ASSIGN 546 TO NNN9
      NOISE=500
      NCUT=0
      NLI=Z1*Z2
      SHIFT=00020000
      SENS=1.0
C     CARD READ-IN AND PRINT-OUT
      WRITE(3,566)
  566 FORMAT(1H1,20X,31H----------INPUT CARDS----------//)
  515 READ(2,510)TEMP1,TEMP2,TEMP3,TEMP4,TEMP5,TEMP6
  510 FORMAT(A10,5E10.0)
      WRITE(3,567)TEMP1,TEMP2,TEMP3,TEMP4,TEMP5,TEMP6
  567 FORMAT(5X,A10,5(5X,E11.3))
      IF(TEMP1.EQ.COMP1)SHIFT=IFIX(TEMP2)
      IF(TEMP1.EQ.COMP2)SENS=TEMP2
      IF(TEMP1.EQ.COMP3)L=STORE1
      IF(TEMP1.EQ.COMP4)C=STORE2
      IF(TEMP1.EQ.COMP6)GO TO 523
      IF(TEMP1.EQ.COMP7)READ(2,105)(CHAR(I),I=1,8)
      IF(TEMP1.EQ.COMP8)GO TO 521
      IF(TEMP1.EQ.COMP9)ASSIGN 536 TO NNN5
      IF(TEMP1.EQ.COMP10)NCUT=INT(TEMP2)
      IF(TEMP1.EQ.COMP11)ASSIGN 300 TO NNN7
      IF(TEMP1.EQ.COMP12)ASSIGN 588 TO NNN8
      IF(TEMP1.EQ.COMP5)GO TO 525
      IF(TEMP1.EQ.COMP13)ASSIGN 587 TO NNN9
      IF(TEMP1.EQ.COMP14)NOISE=TEMP2
      GO TO 515
  521 READ(2,205)XFACT,PFACT,XAXIS(1),XAXIS(2),YAXIS(1),YAXIS(2)
      GO TO 515
  523 P3=TEMP2
      P4=TEMP3
      GO TO 515
  525 CONTINUE
```

```
C      OCTAL NUMBER CONVERSION
       DO535 I=1,NCH
       IF(N(I).GE.0)N(I)=N(I)+000020000
  535 N(I)=IABS(N(I))
       N1=NCH-4
       DO 539 I=1,N1
  539  N(I)=N(I+2)
       NCH=NCH-4
       DO 537 I=1,NCH
  537 N(I)=N(I)-SHIFT
C
C      SOME BAD VALUES OF NDEC. CANNOT BE CORECTED BY THE NEXT PROCEDURE
C      SO THEY CAN BE FIXED MANUALLY BY INSERTING CARDS HERE THAT SET NEW VALUE
C      FOR NDEC FOR PARTICULAR POINTS.  COUNT FROM ONE IN TABLE OF NDEC
C      IN PRINT OUT AND USE THAT INDEX FOR NDEC. E.G. N(236) = 1028.0
C
C E.G. N(157)= 1019
C
C
C     BAD VALUES OF N(DEC.) CORRECTED AND PRINTED OUT
       WRITE(3,6666) NOISE
 6666 FORMAT(1H1// 10X, 55HVALUES OF N(DEC.) CORRECTED (REJECTION CRITER
      2ION= +OR-  ,I5, 1H)//// 10X, 3HROW,2X, 6HCOLUMN,4X, 7HN(I-1) ,3X,
      312HN(I)-N(I-1) ,2X, 5HN(I) ,3X, 12HN(I+1)-N(I) ,2X, 7HN(I+1) )
       NL=NCH-1
       DO 538 I=2,NL
       NM1=N(I)-N(I-1)
       NM2=N(I+1)-N(I)
       NM3=N(I+2)-N(I)
       IF(NM2.EQ.0.OR.NM3.EQ.0) GO TO 538
       BT=FLOAT(NM1)/FLOAT(NM2)
       GT=FLOAT(NM1)/FLOAT(NM3)
       NM1=IABS(NM1)
       NM2=IABS(NM2)
       IF(BT.GE.0.OR.GT.GE.0.OR.NM1.LE.NOISE.OR.NM2.LE.NOISE) GO TO 538
       NM1= N(I)-N(I-1)
       NM2=N(I+1)-N(I)
       NROW= ((I-1)/8)+1
       NCOLUMN= I-8*(NROW-1)
       WRITE(3,5555) NROW,NCOLUMN, N(I-1), NM1, N(I), NM2, N(I+1)
 5555 FORMAT(I13,I6,I10,I12,I10,I12,I10)
       N(I)=(N(I-1)+N(I+1))/2
       WRITE(3,4444) N(I)
 4444 FORMAT(41X,I10//)
  538 CONTINUE
       GO TO NNNS
  536 WRITE(3,550)
  550 FORMAT(/////10X,29HVALUES OF TRANSFORMED N(DEC.)  //)
       DO 551 J=1,JM,8
       I=J-1
  551 WRITE(3,552)(N(I+K),K=1,8)
  552 FORMAT(10X,8I10)
  554 XNPASS=FLOAT(NPASS)
       XNSEC=FLOAT(NSEC)
C      REDUCE THE NUMBER OF DATA POINTS
       IF(NCUT.EQ.0) GO TO  555
       I=1
       J=1
  565 N(I)=N(J)
       I=I+1
```

```
      J=J+NCUT
      IF(J.LE.NCH) GO TO 565
      NCH=I-1
  555 CONST1=SENS*6.4E-03/(XNPASS* NLI*XNSEC)
      CONST2=CONST1/(L*C)
      DO545 I=1,NCH
  545 THETA(I)=FLOAT(N(I))*CONST2
      GO TO NNN9
C      CARD PUNCHING ROUTINE
  546 WRITE(14,570)TITLE1,TITLE2
      WRITE(14,571)NT1,NT2,NAME1
      WRITE(14,572)NCH,NAME2
      WRITE(14,573)Z2,Z1,NAME3
      WRITE(14,574)NPASS,NAME4
      WRITE(14,575)NSEC,NAME5
      WRITE(14,576)C,NAME6,NAME7
      WRITE(14,577)L,NAME8,NAME9
      WRITE(14,578)NAME15,NT2,NT1,NCH
  570 FORMAT(12A6)
  571 FORMAT(I5,1H=,I5,A10)
  572 FORMAT(I4,A4)
  573 FORMAT(E9.2,1H*,E9.2,A3)
  574 FORMAT(I3,A5)
  575 FORMAT(I3,A9)
  576 FORMAT(E9.2,2A6)
  577 FORMAT(E9.2,2A10)
  578 FORMAT(A3,1X,I5,1X,I5,I5)
C      PUNCH-OUT OF THE THETA(I) VALUES
      WRITE(14,586)(THETA(I),I=1,NCH)
  586 FORMAT(6E13.4)
      DO 585 INN=1,5
  585 WRITE(14,570)COMP5
C      CALCULATE N1 AND N2
  587 DELLAM=(P2-P1)/FLOAT(NCH+3)
      N1=P1/DELLAM+1.0E-06+2
      N2=P2/DELLAM+1.0E-06-2
C      CALCULATE N3 AND N4
      N3=P3/DELLAM -1
      N4=P4/DELLAM +1
      N1=N1-1
      N3=N3-1
      N=N2-N1
      NN=N4-N3
      IF(N.GT.NN) GO TO 5678
      IF(NN.GT.1100.) GO TO 5678
      M=N3-N1
      DO 101 I=1,NN
      J=N3+I
  101 LAMB(I)=INT(DELLAM*FLOAT(J))
      BLAM(1)=P1
      DO 102 I=2,NCH
  102 BLAM(I)=BLAM(I-1)+DELLAM
      GO TO NNN8
C      TAPE WRITING ROUTINE
  588 WRITE(8,600)(CHAR(I),I=1,8)
      WRITE(8 ,601)NCH
      J6=N1-N3
      DO 605 I=1,NCH
  605 WRITE(8,602)THETA(I),BLAM(I)
      END FILE 8
```

```
  600 FORMAT(8A10)
  601 FORMAT(8I10)
  602 FORMAT(2E10.3)
  590 DO 100 J=1,NN
      TJ=0.0
      JM=J+M
      IF ((J+N3 .GE. N1+1) .AND. (J+N3 .LE. N2)) TJ=THETA(JM)
      IF ((J+N3 .EQ. N1+1) .OR. (J+N3 .EQ. N2)) GO TO 80
      PHI(J)=-0.5*((FLOAT(N3+J)*TJ-FLOAT(N1+1)*THETA(1))/FLOAT((N1+1)**2
     --(N3+J)**2)+(FLOAT(N3+J)*TJ-FLOAT(N2)*THETA(N))/FLOAT(N2*N2-(N3+J)
     ***2))
   80 DO 90 I=1,N
      IF (N1+I .EQ. N3+J) GO TO 90
      PHI(J)=PHI(J)+(FLOAT(N3+J)*TJ-FLOAT(N1+I)*THETA(I))/FLOAT((N1+I)**
     *2-(N3+J)**2)
   90 CONTINUE
      IF ((N3+J .EQ. N2) .OR. (J+1 .EQ. (-N3-N1))) GO TO 95
      IF ((J+M .EQ. 1) .OR. (-J .EQ. N3+N2)) GO TO 95
      PHI(J)=PHI(J)+0.5*TJ*ALOG(ABS(FLOAT((N3+J+N2)*(J+M-1))/FLOAT((N3+J
     J-N2)*(N3+J+N1+1))))
   95 PHI(J)=PHI(J)*2.0/3.1415927
C
C     THIS NEXT OPERATION IS JUST INTENDED TO TAKE CARE OF THE INDEFINITE
C     USUALLY OBTAINED AT THE FIRST AND LAST DATA POINT IN THE TRANSFORM
      IF(PHI(J).GT.1.0E+10) PHI(J)=PHI(J-1)
  100 CONTINUE
  105 FORMAT(8A10)
      WRITE (3,106) (CHAR(I),I=1,8)
  106 FORMAT(1H1/8A10)
      WRITE (3,110)
  110 FORMAT (7HOLAMBDA,9X,5HTHETA,10X,3HPHI,10X, 6H33*PHI, 10X,5HINDEX)
      DO 200 I=1,NN
      PPHI = 33.0* PHI(I)
      J=N3+I
      IF ((J .GE. N1+1) .AND. (J .LE. N2)) GO TO 150
      A=0.0
      WRITE(3,120) LAMB(I),A,PHI(I),PPHI,I
  120 FORMAT (I6,4X,3E13.5,I10)
      GO TO 200
  150 K=J-N1
      WRITE(3,120) LAMB(I),THETA(K),PHI(I),PPHI,I
  200 CONTINUE
  205 FORMAT(2F10.5,6A10)
      GO TO NNN7
  206 FACTOR=1024.
      CCXMIN=100./1024.
      CCYMIN=150./1024.
      CCYMAX=1050./1024.
      CCXMAX=CCXMIN+PFACT*XFACT*(P4-P3+2.0) /10.5
      INCX=IFIX((P4-P3+2.0)*XFACT)/50
      YM=PHI(1)
      YP=YM
      DO 210 I=1,NN
      X(I)=FLOAT(LAMB(I))
      IF (PHI(I) .GT. YP) YP=PHI(I)
      IF (PHI(I) .LT. YM) YM=PHI(I)
  210 CONTINUE
      DO 220 I=1,N
      Y(I)=FLOAT(LAMB(I-M))
      IF (THETA(I) .GT. YP) YP=THETA(I)

      IF (THETA(I) .LT. YM) YM=THETA(I)
```

```
  220 CONTINUE
      IF (YM .LT. 0.0) YM=-YM
      P=AMAX1(YM,YP)
      IM=ALOG10(P)
      IF (IM .LT. 0) IM=IM-1
      P=P/10.**IM
      IP=IFIX(P)+1
      WRITE (3,9999) IP,IM
 9999 FORMAT (4H0IP=,I5,4H IM=,I5)
      IF (IP .GT. 3) GO TO 230
      INCY=2*IP
      IY=10
      GO TO 250
  230 IY=IP
      INCY=2
  250 YMAX=FLOAT(IP)*10.**IM
      YMIN=-YMAX
      XMIN=P3-10.0
      XMAX=P4+10.0
      CALL CCGRID (INCX,5,10,6HLABELS,INCY,IY,10)
      CALL CCLTR (200./1024.,25./1024.,0,2,CHAR,72)
      CALL CCLTR (400./1024.,50./1024.,0,2,XAXIS,12)
      CALL CCLTR (50./1024.,400./1024.,1,2,YAXIS,24)
      CALL CCPLOT (X,PHI,NN,4HJOIN)
      CALL CCPLOT (Y,THETA,N,4HJOIN,1,1)
      IF(NPROC.NE.NPROB)CALL CCNEXT
      GO TO 300
 5678 PRINT 5566
 5566 FORMAT(103HLAMBDA RANGE ERROR OR THE MAXIMUM DIMENSION EXCEEDED,
     *TERMINATE THIS CASE AND GO ON TO THE NEXT       )
  300 CONTINUE
      CALL CCEND
      REWIND 8
      REWIND 7
      END FILE 14
      REWIND 14
      RETURN
      END
```

Appendix IIC: DIMER, Fortran IV program to calculate the point dipole exciton splittings, oscillator strengths and rotational strengths for dimers of planar molecules with two perpendicular oscillators in the molecular plane. Any number of dimer orientations may be calculated (see figure II-18 for a definition of the coordinate system used) by specifying the limits of DO loops. The results are printed out only if the exciton splittings of the transitions have close to a specified relative size and if the dipole strength ratios of the two transitions are within a specified range of values. These criteria for print out are not entered by control card, but are built into IF statements in the program. These criteria are simply altered for comparison of the calculation with any particular set of experimental data.

```
C     DEFINITIONS OF VARIABLES
C     D11 = DIPOLE STRENGTH OF LONG WAVELENGTH TRANSITION IN DEBYES**2
C     D12 = DIPOLE STRENGTH OF SHORTWAVELENGTH TRANSITION IN DEBYES**2
C     FRQ1 = FREQUENCY OF LONG  WAVELENGTH TRANSITION IN KAYSERS
C     FRQ2 = FREQUENCY OF SHORT WAVELENGTH TRANSITION IN KAYSERS
C     R = DISTANCE BETWEEN MOLECULAR CENTERS IN ANGSTROMS
C     WIA= ANGLE BETWEEN R(XY) AND X AXIS IN RADIANS
C     WIG= ANGLE BETWEEN R AND Z AXIS IN RADIANS
C     WIT= ANGLE BETWEEN MU2A CROSS MU2B AND Z AXIS IN RADIANS
C     WIP= ANGLE BETWEEN LINE OF NODES AND X AXIS IN RADIANS
C     WIS= ANGLE BETWEEN LINE OF NODES AND MU2A IN RADIANS
C     WFP= FRACTIONAL ANGLE INCREMENTS OF PI RADIANS FOR PHI
C     WFS= FRACTIONAL ANGLE INCREMENTS OF PI RADIANS FOR PSI
C     WFT= FRACTIONAL ANGLE INCREMENTS OF PI RADIANS FOR THETA
C     WFA= FRACTIONAL ANGLE INCREMENTS OF PI RADIANS FOR ALPHA
C     WFG= FRACTIONAL ANGLE INCREMENTS OF PI RADIANS FOR GAMMA
C
C     MR= NUMBER OF R VALUES CALCULATED
C     MA ,MG,MP,MS,MT ARE INTEGER INDEXES, RUNNING FROM 1 TO (EG.) MP
C     THAT DETERMINE THE NUMBER OF ANGLE INCREMENTS CALCULATED.
C     FOR S,P,T, ANGLES ARE CALCULATED FOR EG. (0,1/WFS,2/WFS,...(MS-1)/WFS)
C     *PI
C     FOR A AND G, ANGLES CALCULATED ARE (1/WFA,.....MA/WFA)*PI
C
```

```
C
C       IF THE EXCITON SPLITTING (V) IS POSITIVE, THE NU- COMPONENT GOES
C       TO LONGER WAVELENGTH,  THE VALUES THAT ARE COMPARED TO EXPERIMENT
C       ARE----  D(LONG WAVELENGTH EXCITON COMP.)/D(SHORT WAVE EXCITON )
C       AND R(LONG WAVELENGTH EXCITON COMPONENT),  HOWEVER,THE CALCULATED
C       VALUES ARE D+/D- AND R+.  SO A CONVERSION IS MADE FROM CALCULATED
C       TO OBSERVED BY TESTING THE SIGN OF THE EXCITON SPLITTING
C
C       V           D(LONG)/D(SHORT)              R(LONG)
C
C       -           (D+)/(D-)                      R+
C       +           1/((D+)/(D-))                 -R+
C
C       FIRST CARD IS THE NUMBER OF DATA CASES (IIC)
C
C
      DIMENSION R(5),CG(9),LIG(9),SA(9),CA(9),LIA(9),SP(19),CP(19),
     1LIP(19),SS(19),CS(19),LIS(19),ST(10),CT(10),LIT(10),AL1(19,19,10),
     2AL2(19,19,10),BE1(19,19,10),BE2(19,19,10),GA1(19,10),GA2(19,10),
     3RATIC(19,19,10),
     4RCTP1(19,19,10),ROTP2(19,19,10),DV1(19,19,10),DV2(19,19,10),
     5DR1(19,19,10),DR2(19,19,10),TITLE(14)
      READ(2,20) NPROB
   20 FORMAT(I10)
      DO 110 J = 1,NPROB
      READ (2,21) (TITLE(I), I = 1,14)
   21 FORMAT (14A6)
      WRITE (3,22) (TITLE(I), I = 1,14)
   22 FORMAT (1H1, 20X, 14A6////)
      READ (2,23) FNU1, DI1, FNU2, DI2
   23 FORMAT (4F20.8)
      READ (2,24) MR, MA, MG, MP, MS, MT
   24 FORMAT (6I5)
      READ (2,25) (R(I), I = 1, MR)
   25 FORMAT (4F20.8)
      READ (2,26) WFA, WFG, WFP, WFS, WFT
   26 FORMAT (5F10.2)
      LWFA = WFA
      LWFG = WFG
      LWFP = WFP
      LWFS = WFS
      LWFT = WFT
      WRITE (3,27) FNU1, DI1
   27 FORMAT (29H FIRST TRANSITION FREQUENCY =, F7.0,25H K,      DIPOLE S
     1TRENGTH =, F6.2,11H (DEBYE)**2 //)
      WRITE (3,28) FNU2, DI2
   28 FORMAT (30H SECOND TRANSITION FREQUENCY =, F7.0,25H K,      DIPOLE
     1STRENGTH =, F6.2, 11H (DEBYE)**2 ////)
      RCT1 = 1.5708E-08 * FNU1 * DI1
      RCT2 = 1.5708E-08 * FNU2 * DI2
      DO 113 IG = 1, MG
      WIG=3.416*IG/WFG
      CG(IG) = COS(WIG)
  113 LIG(IG)=180*IG/LWFG
      DO 112 IA = 1, MA
      WIA=3.146*IA/WFA
      SA(IA) = SIN(WIA)
      CA(IA) = COS(WIA)
  112 LIA(IA)=180*IA/LWFA
```

```
      DO 91 IP = 1, MP
      FIP = IP - 1
      WIP = 3.1416 * FIP / WFP
      SP(IP) = SIN(WIP)
      CP(IP) = COS(WIP)
   91 LIP(IP) =180 * (IP-1) / LWFP
      DO 92 IS = 1, MS
      FIS = IS - 1
      WIS = 3.1416 * FIS / WFS
      SS(IS) = SIN(WIS)
      CS(IS) = COS(WIS)
   92 LIS(IS) =180 * (IS-1) / LWFS
      DO 93 IT = 1, MT
      FIT = IT - 1
      WIT = 3.1416 * FIT / WFT
      ST(IT) = SIN(WIT)
      CT(IT) = COS(WIT)
   93 LIT(IT) =180 * (IT-1) / LWFT
      DO 103 IT = 1, MT
      DO 102 IS = 1, MS
      DO 101 IP = 1, MP
      AL1(IP,IS,IT) = CP(IP) * CS(IS) - SP(IP) * SS(IS) * CT(IT)
      AL2(IP,IS,IT) = - CP(IP) * SS(IS) - SP(IP) * CS(IS) * CT(IT)
      BE1(IP,IS,IT) = SP(IP) * CS(IS) + CP(IP) * SS(IS) * CT(IT)
  101 BE2(IP,IS,IT) = - SP(IP) * SS(IS) + CP(IP) * CS(IS) * CT(IT)
      GA1(IS,IT) = ST(IT) * SS(IS)
  102 GA2(IS,IT) = ST(IT) * CS(IS)
  103 CONTINUE
      DO 110 IR = 1, MR
      RR= R(IR)
      R3 =RR**3
      DVK1 = 5035.6    * DI1 / R3
      DVK2 = 5035.6      * DI2 / R3
      ROTK1 = ROT1 * RR
      ROTK2 = ROT2 * RR
      DO 110 IG = 1, MG
      DO 110 IA = 1, MA
      DO 111 IT = 1, MT
      DO 111 IS = 1, MS
      DO 111 IP = 1, MP
      DR1(IP,IS,IT) = (1. + AL1(IP,IS,IT))/ (1. - AL1(IP,IS,IT))
      DR2(IP,IS,IT) = (1. + BE2(IP,IS,IT))/ (1. - BE2(IP,IS,IT))
      ROTP1(IP,IS,IT) = ROTK1 * ( SA(IA) * GA1(IS,IT) - CG(IG) * BE1(IP,
     1IS,IT))
      ROTP2(IP,IS,IT) = ROTK2 * ( CG(IG) * AL2(IP,IS,IT) - CA(IA) * GA2(
     1IS,IT))
      DV1(IP,IS,IT) = DVK1 * ( AL1(IP,IS,IT) - 3. * CA(IA) * ( CA(IA) *
     1AL1(IP,IS,IT) + SA(IA) * BE1(IP,IS,IT) + CG(IG) * GA1(IS,IT)))
      DV2(IP,IS,IT) = DVK2 * ( BE2(IP,IS,IT) - 3. * SA(IA) * ( CA(IA) *
     1AL2(IP,IS,IT) + SA(IA) * BE2(IP,IS,IT) + CG(IG) * GA2(IS,IT)))
  111 CONTINUE
      WRITE (3,40)RR, LIA(IA), LIG(IG)
   40 FORMAT (23H1MOLECULAR SEPARATION =, F5.2,22H ANGSTROMS,     ALPHA =
     1, I4,2OH DEGREES,     GAMMA =, I4, 8H DEGREES ///)
      WRITE (3,41)
   41 FORMAT(100H                              DIPOLE STRENGTH                E
     1XCITON SPLITTING        ROTATIONAL STRENGTH    )
```

```
      WRITE (3,42)
   42 FORMAT(100H  ANGLE                          RATIOS
     1                          LONG WAVE SIDE        //)
      WRITE (3,43)
   43 FORMAT(100H  DEGREES                        D(LONG)/D(SHORT)
     1  KAYSERS                    CGS UNITS X 10**36     //)
      WRITE (3,44)
   44 FORMAT(100H PHI  PSI  THETA            LONG       SHORT                 L
     1ONG        SHORT                 LONG      SHORT     ///)
      DO 53 IP = 1, MP
      DO 53 IS=1,MS
      DO 53 IT=1,MT
C
C     SKIP VALUES THAT ARE OUT OF RANGE OF INTEREST
C
      RATIO(IP,IS,IT) = DV1(IP,IS,IT)/DV2(IP,IS,IT)
      IF (ABS(RATIO(IP,IS,IT)).GE.2.0.OR.ABS(RATIO(IP,IS,IT)).LE.0.5)
     1   GO TO 53
      IF(DR1(IP,IS,IT).GE.2.0.OR.DR1(IP,IS,IT).LE.0.5)  GO TO 53
      IF(DR2(IP,IS,IT).GE.2.0.OR.DR2(IP,IS,IT).LE.0.5)  GO TO 53
C
C     CONVERT CALCULATED PARAMETERS TO OBSERVED ONES
C
      IF(DV1(IP,IS,IT).LE.0) GO TO 99
      DR1(IP,IS,IT)  = 1/ DR1(IP,IS,IT)
      ROTP1(IP,IS,IT) = - ROTP1(IP,IS,IT)
   99 CONTINUE
      IF(DV2(IP,IS,IT).LE.0) GO TO 100
      DR2(IP,IS,IT) = 1/DR2(IP,IS,IT)
      ROTP2(IP,IS,IT) = -ROTP2(IP,IS,IT)
  100 CONTINUE
      WRITE (3,50)        LIP(IP), LIS(IS), LIT(IT),
     1                                              DR1(IP,IS,IT), DR2(IP
     2,IS,IT), DV1(IP,IS,IT), DV2(IP,IS,IT), ROTP1(IP,IS,IT), ROTP2(IP,I
     3S,IT)
   50 FORMAT( 3I4, 8X, 2F10.3, 10X, 2F10.2, 10X, 2F10.4)
   52 WRITE (3,51)
   51 FORMAT (1HO)

   53 CONTINUE
  110 CONTINUE
      STOP
      END
```

Appendix II-D: PROCES, A Fortran IV program for absorption data processing.

```
C*************************        PROCESS        ********************************
C
C      THIS PROGRAM CONVERTS A CARD DECK OF VOLTAGES PROPORTIONAL TO OPTICAL
C      DENSITY (PUNCHED BY A DIGITAL VOLTMETER) INTO A MAGNETIC TAPE
C      WITH OPTICAL DENSITY AND WAVELENGTH VALUES FOR THE GIVEN SPECTRUM.
C      IT TESTS ALL POINTS AND SETS THEM EQUAL TO THE ARITHMETIC MEAN OF THE
C      NEAREST NEIGHBOR PUNTS IF THREE CONDITIONS ARE SATISFIED***
C            (1) THE SLOPES ARE THE OPPOSITE SIGN.
C            (2) THE  SLOPES ARE LARGER THAN RNOISE (OD UNITS)
C            (3) THE POINT IS OUTSIDE OF AN EXCLUSION INTERVAL, AMIN-AMAX OR
C                BMIN-BMAX
C
C      1 ST. CARD
C         NUMBER OF SPECTRA TO BE PROCESSED (I10)
C      2 ND. CARD
C         TITLE  (8A10)
C      3 RD. CARD
C         MIN,MAX,N
C               MIN= MINIMUM WAVELENGTH
C               MAX= MAXIMUM WAVELENGTH
C               N= NUMBER OF DATA POINTS
C      4 TH. CARD (EXCLUSION INTERVALS)
C
C         AMIN,AMAX,BMIN,BMAX,RNOISE
C         E.G. AMIN-AMAX EXLUDED FROM BAD POINT CHECK
C      5 TH. CARD
C         ODMIN,ODMAX,VMIN,VMAX
C         ODMIN AT VMIN VOLTAGE AND  ODMAX AT VMAX VOLTAGE
C      N VALUES OF VOLTAGES, 10 VALUES PER CARD, INCLUDING RANGE OF SPECTRO-
C      PHOTOMETER (WHICH IS 0 OR 1)
C      N VALUES OF BASELINE VOLTAGE
C
C
C
C

      DIMENSION IR(1000),LAMBD(1000),OD(1000),IV(1000),IBASE(1000),
     2TITLE1(8),BOD(1000)
      REAL LAMBD
      READ(2,100)NPROB
      DO 300 NPROC=1,NPROB
      READ(2,105)TITLE1
      READ(2,100)MIN,MAX,N
      READ(2,2) AMIN, AMAX, BMIN, BMAX, RNOISE
    2 FORMAT(5(F10.0))
      WRITE(3,999) TITLE 1
  999 FORMAT(1H1,8A10////)
      WRITE(3,601) RNOISE,AMIN,AMAX,BMIN,BMAX
  601 FORMAT(    10X,43HCORRECTED POINTS (REJECTION CRITERION= +OR-,F9.4
     2,1CH OD UNITS)//59HWAVELENGTH INTERVALS EXCLUDED FROM CORRECTION P
     3ROCEDURE ARE//11HLAMBDAMIN1=,F10.0,9HANGSTROMS,10X,11HLAMBDAMAX1=,
     4F10.0,9HANGSTROMS/11HLAMBDAMIN2=,F10.0,9HANGSTROMS,10X,11HLAMBDAMA
     5X2=,F10.0,9HANGSTROMS//)
      PMIN=FLOAT(MIN)
      PMAX=FLOAT(MAX)
      READ(2,101)ODMIN,ODMAX,VMIN,VMAX
      READ(2,102)((IR(J),IV(J)),J=1,N)
      READ(2,103)(IBASE(J),J=1,N)
      DO 10 I=1,N
      OD(I)=(FLOAT(IV(I))-FLOAT(IBASE(I)))*(ODMAX-ODMIN)/(VMAX-VMIN)
```

```
      2+FLOAT(IR(I))
   10 BCC(I)=CC(1)
C     CALCULATE LAMBDAS
      NL=N-2
      NA=N-1
      CELLAM=(PMAX-PMIN)/FLOAT(NA)
      LAMBC(1)=PMAX
      DO 20 I=2,N
   20 LAMBC(I)=LAMBC(I-1)-CELLAM
C     REJECT BAD POINTS
      DO 15 I=2,NL
      IF(LAMBC(I).GE.AMIN.AND.LAMBC(I).LE.AMAX) GO TO 15
      IF(LAMBC(I).GE.BMIN.AND.LAMBC(I).LE.BMAX) GO TO 15
      R1=  CC(I) - CC(I-1)
      R2 = CC(I+1) - CC(I)
      R3=CC(I+2)-CC(I)
      IF(R2.EQ.0.OR.R3.EQ.0) GO TO 15
      RT = R1/R2
      GT=R1/R3
      R1=ABS(R1/RNOISE)
      R2=ABS(R2/RNOISE)
      IF(RT.GE.0.OR.GT.GE.0.OR.R1.LE.1.OR.R2.LE.1)  GO TO 15
      R1=CC(I)-CC(I-1)
      R2=CC(I+1)-CC(I)
      WRITE(3,400) CC(I-1),R1,CC(I),R2,CC(I+1)
  400 FORMAT(10X,5(F10.4))
      CC(I) = (CC(I-1)+CC(I+1))/2
      WRITE(3,500) CC(I), LAMBC(I)
  500 FORMAT(30X,F10.4,20X,F10.0//)
   15 CONTINUE
      CALL YGRAPH(N,LAMBC,BCC,CC)
      WRITE(3,600)
  600 FORMAT(// ,10X,40HPROGRAM PROCESS FEEDING INPUT TO LSQVMT )
      WRITE(8 ,105)TITLE1
      WRITE(8 ,100)N
      WRITE(8 ,104)((CC(I),LAMBC(I)),I=1,N)
      END FILE 8
      WRITE(3,700)
  700 FORMAT(// ,10X,22HDATA FED TO LSQVARMIT )
      WRITE(3,105)TITLE1
      WRITE(3,100)N
      WRITE(3,106)((CC(I),LAMBC(I)),I=1,N)
  100 FORMAT(8I10)
  101 FORMAT(8F10.0)
  102 FORMAT(3X,I2,I5,I2,I5,I2,I5,I2,I5,I2,I5,6X,5(I2,I5))
  103 FORMAT(3X,2X,I5,2X,I5,2X,I5,2X,I5,2X,I5,2X,I5,6X,5(2X,I5))
  104 FORMAT(2E10.3)
  105 FORMAT(8A10)
  106 FORMAT (1HX,10X,F10.4,F10.0)
  300 CONTINUE
      REWIND 8
      RETURN
      END
```

Subroutine YGRAPH (which is given with E:CDLSQ)

Appendix IIE: CDLSQ, Fortran IV program which finds the best parameters to fit a number of specified functions to an array of data points by a linear least squares procedure.

The version shown here uses Gaussian functions and their first derivatives (in the functional form shown in equation III-112) but the fitting function subroutine can be simply substituted for other purposes. When the program is used to fit MCD data a subroutine GVAL calculates the magnetic splitting according to equation III-114 and the associated standard errors. Subroutine YGRAPH prints a quick plot of the input data and the sum of the best fit functions.

The first card is the number of data cases (I10). The control cards may be put in any order and therefore have an identifying name in columns 1-10 (left adjusted), the control card format is A10,7E10.0.

CARD Input data is read from cards (otherwise data is read from magnetic tape (TAPE 8).

CURVES Number of functions used to fit the data.

WIDTHS The next cards have the values of the width and position parameters of the fitting functions; i.e. $\theta_1, \lambda_1, \theta_2, \lambda_2, \ldots$.

HEIGHTS Next cards have values of the amplitudes of the component functions in absorption (used only in magnetic splitting calculation-GVAL).

GAMMA Value of the Bohr magneton times the magnetic field strength in wavenumbers (used in GVAL).

SAME DATA The data from the previous problem is used again with the new fitting functions specified in this data case.

The last card in each data case must be blank.

```
      PROGRAM CDLSQ(INPUT,OUTPUT,TAPE8,TAPE2=INPUT,TAPE3=OUTPUT,TAPE9)
      REAL LAM
      DIMENSION CHAR(13),THETA(1000),BLAM(1000),R(20),A(20),LAM(20)
      DIMENSION ALPHA(20,20),H(20,1)  ,YCALC(1000),COR(20,20) ,OD(20)
      DIMENSION STD(20)
      DATA TEST1/4HCARD/,TEST2/4HTAPE/,COMP1/6HCURVES /
      DATA COMP2/6HWIDTHS/,COMP3/10H          /,COMP4/9HSAME DATA/
      DATA COMP5/5HGAMMA/,COMP6/7HHEIGHTS/
      COMMON/SET1/N1,R,BLAM,M,LAM
      COMMON/SET2/YCALC,A
      READ 11,NPROB
      DO 400 NPROC=1,NPROB
      JK=8
      ASSIGN 105 TO NNN1
  101 READ 13,TEMP1,TEMP2,TEMP3,TEMP4
      IF(TEMP1.EQ.COMP1)N1=IFIX(TEMP2)
      IF(TEMP1.EQ.COMP2)READ 14,(R(I),LAM(I),I=1,N1)
      IF(TEMP1.EQ.COMP3)GO TO 102
      IF(TEMP1.EQ.COMP4)ASSIGN 106 TO NNN1
      IF(TEMP1.EQ.COMP5) GAMMA= TEMP2
      IF(TEMP1.EQ.COMP6)  READ 15,(OD(I), I= 1,N1)
      IF(TEMP1.EQ.TEST1)JK=2
      GO TO 101
   14 FORMAT(8E10.0)
   15 FORMAT(8E10.3)
   10 FORMAT(8A10)
  102 GO TO NNN1
  105 READ(JK,10)(CHAR(I),I=1,8)
      IF(EOF,8) 105,104
  104 READ(JK,11)M
   11 FORMAT(8I10)
      READ(JK,12)(THETA(I),BLAM(I),I=1,M)
   12 FORMAT(2E10.3)
   13 FORMAT(A10,5E10.0)
      CALL CENTER(CHAR,8,CHAR,130)
  106 PRINT 1,CHAR,M,N1,   (K,R(K),LAM(K),K=1,N1)
    1 FORMAT(1H1//40X,47H----------PROGRAM CDLSQ----------
     2/////13A10////55X,20H.....INPUT DATA.....////
     320X,27HTHE NUMBER OF DATA POINTS =I4/
     420X,30HTHE NUMBER OF FITTING CURVES =I2////
     510X,10HCURVE SET ,8X,5HWIDTH ,9X,10HWAVELENGTH/
     6 (14X,I2,9X,E11.4,5X,E11.4))
C
C     CALCULATE THE MATRIX ELEMENTS
C
      CALL ELEM(ALPHA)
C
C     CALCULATE THE H-VECTOR
C
      DO 210 J=1,N1
      H(J,1)=0.0
      DO 209 I=1,M
  209 H(J,1)= H(J,1)+THETA(I)*F(J,I)
  210 CONTINUE
C
C     CALL MATINV TO INVERT THE MATRIX AND CALCULATE THE A-VECTOR
C
      CALL MATINV(ALPHA,N1,H,1,DETERM)
      DO 300 I=1,N1
  300 A(I)=H(I,1)
      CALL DCAL(THETA,CSQ)
```

```
      CALL PARAM(N1,ALPHA,A,COR,CSQ,STD)
      CALL GVAL(STD,OO,GAMMA)
      CALL YGRAPH(M,BLAM,THETA,YCALC)
  400 CONTINUE
      RETURN
      END)
```

This subroutine calculates the matrix elements.

```
      SUBROUTINE ELEM(ALPHA)
      COMMON/SET1/N1,R,BLAM,M,LAM
      DIMENSION ALPHA(20,20),R(20),BLAM(1000),LAM(20)
      REAL LAM
      DO 201 J=1,N1
      DO 201 K=1,N1
      ALPHA(J,K)=0.0
      DO 200 I=1,M
  200 ALPHA(J,K)=ALPHA(J,K)+F(J,I)*F(K,I)
  201 CONTINUE
      RETURN
      END
```

This function subroutine defines a Gaussian function and first derivative

```
      FUNCTION F(J,I)
      COMMON/SET1/N1,R,BLAM,M,LAM
      DIMENSION R(20),BLAM(1000),LAM(20)
      REAL LAM
      NCURV=N1/2
      TEMP=BLAM(I)- LAM(J)
      TEMP2=EXP(-(TEMP*TEMP)/R(J)**2)
      IF(J.GT.NCURV)TEMP2=(-2.0*TEMP2)*TEMP/R(J)**2
      F=TEMP2
      RETURN
      END
```

```
      SUBROUTINE DCAL(THETA,CSQ)
C     CALCULATE THE ORDINATES FROM THE COMPUTED A-MATRIX AND PRINT,ALONG
C     WITH THE EXPERIMENTAL DATA POINTS AND THE PERCENTAGE DIFFERENCES.
C     ALSO CALCULATE CHI SQUARE AND THE AVERAGE DEVIATION.
      COMMON/SET1/N1,R,BLAM,M,LAM
      COMMON/SET2/YCALC,A
      REAL LAM
      DIMENSION BLAM(1000),LAM(20),  THETA(1000),YCALC(1000),A(20),R(20)
      PRINT 306
  306 FORMAT(1H1//28X,8HBEST FIT,7X,12HEXPERIMENTAL,5X,
     210HPERCENTAGE/12X,6HLAMBDA,11X,5HTHETA,12X,5HTHETA,
     3 9X,10HDIFFERENCE//)
      SUM1=0.0
      SUM2=0.0
      DO 310 I=1,M
      YCALC(I)=0.0
      DO 308 J=1,N1
  308 YCALC(I)=YCALC(I)+A(J)*F(J,I)
      TEMP=ABS(YCALC(I)-THETA(I))
      FRACT=100.0*ABS(TEMP/THETA(I))
      PRINT 307,BLAM(I),YCALC(I),THETA(I),FRACT
  307 FORMAT(11X,F7.1,8X,E11.4,6X,E11.4,5X,E11.4)
      SUM1=SUM1+TEMP
      SUM2=SUM2+TEMP**2
  310 CONTINUE
      IF(M.GT.N1)CSQ=SQRT(SUM2/(M-N1))
      AVD=SUM1/M
      PRINT 200,AVD,CSQ
  200 FORMAT(///20X,22HAVERAGE DEVIATION..... E11.4/
     2  20X,22HCHI SQUARE.............. E11.4)
      RETURN
      END
```

This subroutine calculates the correlation coefficents and the standard errors.

```
      SUBROUTINE PARAM(N1,A,B,COR,CSQ,STD)
      DIMENSION A(20,20),B(20,1),COR(20,20),STD(20)
      PRINT 10
   10 FORMAT(///7X,11HCOEFFICIENT 8X,10HSTD.ERROR  ///)
      DO 20 I=1,N1
      STD(I) =A(I,I)*CSQ
   20 PRINT 30,I,B(I,1),STD(I)
   30 FORMAT(2X,2HC(I2,2H) ,2E15.8)
      PRINT 35
   35 FORMAT(//// 10X,18HCORRELATION MATRIX  ///)
      DO 40 I=1,N1
      DO 40 J=1,I
   40 COR(I,J)=A(I,J)/SQRT(A(I,I)*A(J,J))
      DO 50 I=1,N1
   50     PRINT 60, (COR(I,J), J=1,I)
   60 FORMAT (8F9.6)
      RETURN
      END
```

```
      SUBROUTINE GVAL(STD,OD,GAMMA)
C
C     THIS ROUTINE CALCULATES THE G VALUES FROM THE LEAST SQUARES COEFF.
C     AND DETERMINES THE ERROR, RANGE OF VALUES WITHIN THE STD ERROR
C     AND THE PERCENTAGE ERROR AND PRINTS ALL THIS
C
      DIMENSION STD(20),A(20),R(20),BLAM(1000),LAM(20),YCALC(1000)
      DIMENSION OD(20)
      COMMON/SET1/N1,R,BLAM,M,LAM
      COMMON/SET2/YCALC,A
      REAL LAM
      WRITE(3,110)
  110 FORMAT(//// 10X, 88H LAMDA(0)      G VALUE   +OR-(STDERROR)       RAN
     1GE OF VALUES  FROM - TO   PERCENT ERROR     )
      NPEAK = N1/2
      NPEAK = NPEAK + 1
      DO 100 I = NPEAK, N1
      G = -1.5* A(I)/( OD(I)* GAMMA* LAM (I)*LAM (I)* 1.0E-08)
      DELG = G * STD(I)/A(I)

      G1 = G + DELG
      G2 = G - DELG
      G3 = ( 100. * DELG)/G
      WRITE(3,120) LAM (I),G,DELG,G1,G2,G3
  120 FORMAT(10X,F10.1,5X,F7.4,5X,F10.5,20X,2(F8.4),5X,F5.1)
  100 CONTINUE
      RETURN
      END
C     SUBROUTINE CENTER COMPRESSED DECK.
```

This subroutine merely centers the title on the printer page and is non-essential for the function of the program.

```
      SUBROUTINE CENTER(NTEMP,N,NSAVE,M)
      DIMENSION NFMT (5),NMASK(10),NTEMP(15)
      DIMENSION NWORD(15),NSAVE(15),NHOLD(15),MASK(10)
      DATA (NFMT (I),I=1,5)/1H(,1H ,2HX, ,1H  ,4HA10) /,MASK1/1H  /
      DATA(NMASK(I),I=1,10)/00000055,000005500,000550000,055000000,
     205500000000,055000000000,055000000000000,055000000000000000,
     3055000000000000000,0550000000000000000  /
      DATA (MASK(I),I=1,10)/00000077,000007700,000770000,077000000,
     207700000000,077000000000,077000000000000,077000000000000000,
     3077000000000000000,0770000000000000000  /
      IF(N.GT.13.OR.N.LT.1.OR.M.LT.1.OR.M.GT.132)RETURN
      DO 110 I=1,N
  110 NWORD(I)=NTEMP(I)
      JM=N+1
      DO 111 J=JM,15
  111 NWORD(J)=MASK1
      DO 100 J=1,15
  100 NHOLD(J)=MASK1
      NCOUNT=0
      DO 10 I=1,N
      IF(NWORD(I).NE.MASK1) GO TO 20
   10 NCOUNT=NCOUNT+10
```

```
   20 DO 30 J=1,10
      NCOMP=NWORD(I).AND.MASK(11-J)
      IF(NCOMP.NE.NMASK(11-J)) GO TO 35
   30 NCOUNT=NCOUNT+1
   35 NSTORE=NCOUNT
      DO 40 I=1,N
      J=N+1-I
      IF(NWORD(J).NE.MASK1) GO TO 45
   40 NCOUNT=NCOUNT+10
   45 DO 46 I=1,10
      NCOMP=NWORD(J).AND.MASK(I)
      IF(NCOMP.NE.NMASK(I)) GO TO 50
   46 NCOUNT=NCOUNT+1
   50 NCHAR=10*N-NCOUNT
      IF(NCHAR.GT.112.OR.NCHAR.GT.M)RETURN
      NBL=(M-NCHAR)/2
      IM=NCHAR/10
      IF(MOD(NCHAR,10).NE.0)IM=IM+1
      IK=NSTORE+10*IM
      IF(NSTORE.EQ.0)GO TO 210
      ENCODE(10,70,NFMT(2))NSTORE
   70 FORMAT(I10)
      GO TO 220
  210 NFMT(3)=10H
  220 ENCODE(10,70 ,NFMT(4))IM
      DECODE(IK,NFMT,NWORD)(NHOLD(I),I=1,IM)
      DO 229 J=1,15
  229 NWORD(J)=MASK1
      NFMT(2)=1H)
      IF(NBL.EQ.0)GO TO 54
      IF(NBL.LT.10)GO TO 55
      ENCODE(10,3,NFMT)NBL
    3 FORMAT(1H(,I2,7HX,15A10)
      GO TO 231
   54 NFMT(1)=10H(15A10
      GO TO 231
   55 ENCODE(10,5,NFMT)NBL
    5 FORMAT(1H(,I1,7HX,15A10)
  231 IM=IM+2
```

```
      IK=NBL+10*IM-MOD(NBL,10)+10
      IF(MOD(NBL,10).NE.0)IK=IK+10
      ENCODE(IK,NFMT,NWORD)(NHOLD(I),I=1,IM)
      JM=M/10
      IF(MOD(M,10).NE.0)JM=JM+1
      DO 240 I=1,JM
  240 NSAVE(I)=NWORD(I)
      NFMT(1)=1H(
      NFMT(2)=10H
      NFMT(3)=2HX,
      NFMT(4)=10H
      NFMT(5)=4HA10)
      RETURN
      END
```

```
$IBFTC MATINV
C*     MATRIX INVERSION WITH ACCOMPANYING SOLUTION OF LINEAR EQUATIONS
C
       FORTRAN IV SUBROUTINE MATINV(A,N,B,M,DETERM)
C
       DIMENSION IPIVOT(20), A(20,20), B(20,1), INDEX(20,2), PIVOT(20)
       COMMON /LSP/ PIVOT,IPIVOT,INDEX
       EQUIVALENCE (IROW,JROW), (ICOLUM,JCOLUM), (AMAX, T, SWAP)
C
C      INITIALIZATION
C
    10 DETERM=1.0
    15 DO 20 J=1,N
    20 IPIVOT(J)=0
    30 DO 550 I=1,N
C
C      SEARCH FOR PIVOT ELEMENT
C
    40 AMAX=0.0
    45 DO 105 J=1,N
    50 IF (IPIVOT(J)-1) 60, 105, 60
    60 DO 100 K=1,N
    70 IF (IPIVOT(K)-1) 80, 100, 740
    80 IF (ABS(AMAX)-ABS(A(J,K))) 85, 100, 100
    85 IROW=J
    90 ICOLUM=K
    95 AMAX=A(J,K)
   100 CONTINUE
   105 CONTINUE
       IF(AMAX) 110,800,110
   110 IPIVOT(ICOLUM)=IPIVOT(ICOLUM)+1
C
C      INTERCHANGE ROWS TO PUT PIVOT ELEMENT ON DIAGONAL
C
   130 IF (IROW-ICOLUM) 140, 260, 140
   140 DETERM=-DETERM
   150 DO 200 L=1,N
   160 SWAP=A(IROW,L)
   170 A(IROW,L)=A(ICOLUM,L)
   200 A(ICOLUM,L)=SWAP
   205 IF(M) 260, 260, 210
   210 DO 250 L=1, M
   220 SWAP=B(IROW,L)
   230 B(IROW,L)=B(ICOLUM,L)
   250 B(ICOLUM,L)=SWAP
   260 INDEX(I,1)=IROW
   270 INDEX(I,2)=ICOLUM
   310 PIVOT(I)=A(ICOLUM,ICOLUM)
   320 DETERM=DETERM*PIVOT(I)
C
C      DIVIDE PIVOT ROW BY PIVOT ELEMENT
C
   330 A(ICOLUM,ICOLUM)=1.0
   340 DO 350 L=1,N
   350 A(ICOLUM,L)=A(ICOLUM,L)/PIVOT(I)
   355 IF(M) 380, 380, 360
   360 DO 370 L=1,M
   370 B(ICOLUM,L)=B(ICOLUM,L)/PIVOT(I)
C
C      REDUCE NON-PIVOT ROWS
```

```
  380 DO 550 L1=1,N
  390 IF(L1-ICOLUM) 400, 550, 400
  400 T=A(L1,ICOLUM)
  420 A(L1,ICOLUM)=0.0
  430 DO 450 L=1,N
  450 A(L1,L)=A(L1,L)-A(ICOLUM,L)*T
  455 IF(M) 550, 550, 460
  460 DO 500 L=1,M
  500 B(L1,L)=B(L1,L)-B(ICOLUM,L)*T
  550 CONTINUE
C
C     INTERCHANGE COLUMNS
C
  600 DO 710 I=1,N
  610 L=N+1-I
  620 IF (INDEX(L,1)-INDEX(L,2)) 630, 710, 630
  630 JROW=INDEX(L,1)
  640 JCOLUM=INDEX(L,2)
  650 DO 705 K=1,N
  660 SWAP=A(K,JROW)
  670 A(K,JROW)=A(K,JCOLUM)
  700 A(K,JCOLUM)=SWAP
  705 CONTINUE
  710 CONTINUE
  740 RETURN
  800 DETERM = 0.
      RETURN
      END
```

```
      SUBROUTINE YGRAPH(M,X,Y,YFIT)
      DIMENSION X(10,1),Y(1),YFIT(1)
      DATA IFFF,IBBB,IOOO,IPPP/1HF,1H ,1HO,1HP/
      YMIN=Y(1)
      YMAX=Y(1)
      DO 3 I=1,M
      IF(YMIN .GT.  Y(I))  YMIN=Y(I)
      IF(YMAX .LT. Y(I))  YMAX=Y(I)
      IF (YMIN .GT. YFIT(I)) YMIN=YFIT(I)
      IF (YMAX .LT. YFIT(I)) YMAX=YFIT(I)
    3 CONTINUE
      WRITE (3,1005) YMIN,YMAX
 1005 FORMAT (1H1,15X,E13.5,87X,E13.5/19X,101HIIIIIIIIIIIIIIIIIIIIIIIII
     1IIIIIIIIIIIIIIIIIIIIIIIIIIIIIIIIIIIIIIIIIIIIIIIIIIIIIIIIIIIIIIII
     1IIIIIIIII   )
      DO 1100 I=1,M
      IO=1.0+100.0*(Y(I)-YMIN)/(YMAX-YMIN)
      IO=MAX0(MIN0(IO,100),1)
      IP=1.0+100.0*(YFIT(I)-YMIN)/(YMAX-YMIN)
      IP=MAX0(MIN0(IP,100),1)
      IF (IO .NE. IP) GO TO 1030
 1008 IF (IO .NE. 1) GO TO 1020
```

```
      WRITE(3,1010)X(I),IFFF
 1010 FORMAT (1X,E13.5,6H     -,100A1)
      GO TO 1100
 1020 K=IO-1
      WRITE (3,1010) X(I),  (IBBB,J=1,K),IFFF
      GO TO 1100
 1030 IPP=IPPP
      IOO=IOOO
      IF (IP .GT. IO) GO TO 1040
      IPP=IOOO
      IOO=IPPP
      IDUMMY=IO
      IO=IP
      IP=IDUMMY
 1040 IF (IO .GT. 1) GO TO 1060
      K=IP-IO-1
      IF (K .GT. 0) GO TO 1050
      WRITE (3,1010) X(I),  IOO,IPP
      GO TO 1100
 1050 CONTINUE
      WRITE (3,1010) X(I),  IOO,(IBBB,J=1,K),IPP
      GO TO 1100
 1060 K1=IO-1
      K2=IP-IO-1
      IF (K2 .GT. 0) GO TO 1070
      WRITE(3,1010)X(I),(IBBB,J=1,K1),IOO,IPP
      GO TO 1100
 1070 CONTINUE
      WRITE (3,1010) X(I),  (IBBB,J=1,K1),IOO,(IBBB,J=1,K2),IPP
 1100 CONTINUE
      WRITE (3,1110) YMIN,YMAX
 1110 FORMAT (19X,101HIIIIIIIIIIIIIIIIIIIIIIIIIIIIIIIIIIIIIIIIIIIIIIIIII
     1IIIIIIIIIIIIIIIIIIIIIIIIIIIIIIIIIIIIIIIIIIIIIIIIIII  /16X,E13.5,87
     2X,E13.5)
      WRITE (3,1120)
 1120 FORMAT (33H0P REPRESENTS THE PREDICTED POINT/28H0O REPRESENTS THE
     1DATA POINT/73H0F REPRESENTS BOTH THE DATA AND THE PREDICTED POINTS
     2 IF THEY LIE TOGETHER)
      RETURN



      END
```